The observational consequences of primordial fields

Chiara Caprini
Oriel College

Astrophysics
Department of Physics
University of Oxford

Thesis submitted for the degree of Doctor of Philosophy
in the University of Oxford
- Trinity Term 2004 -

The observational consequences of primordial fields

Chiara Caprini
Oriel College

Astrophysics
Department of Physics
University of Oxford

Abstract

The research presented in this thesis concerns three main topics. First, we investigate the presence of large scale magnetic fields in the universe. We focus on the possibility that they have originated in the primordial phases of the evolution of the universe, and derive a strong constraint on the intensity of causally generated fields. We also analyse the imprint of a helical magnetic field in the cosmic microwave background radiation. Second, we study the observational consequences of a hypothetical electric charge asymmetry in the universe, and we deduce upper limits on the charge of some fundamental particles, improving the current limits obtained from laboratory experiments or astrophysical observations. Third, we consider the theory of inflation, and in the context of the slow roll approximation we derive a constraint on the fourth derivative of the inflaton potential. The common methodology at the basis of these three analyses is the use of the observational properties of the cosmic microwave background radiation to constrain the presence of different components in the universe, which can act as a source of perturbation in the background metric. Part of the thesis is dedicated to the review of the theoretical framework at the basis of the topics considered. This is mainly done in the first three chapters. We start with a summary of the standard cosmological model, introducing the covariant formalism which is used in the analysis of the model of a charged universe. The details and results of this analysis are presented in the fifth chapter. The second chapter contains a review of the basic properties of cosmic magnetic fields, and then focuses on the derivation of strong upper limits on their intensity. The third chapter is an overview on cosmological linear perturbation theory, and on the formalism of the microwave background temperature anisotropies and polarisation. It introduces the technical tools used in the fourth chapter, where we analyse the temperature and polarisation signal induced in the microwave background by a primordial, helical magnetic field. We conclude by presenting, in the sixth chapter, the derivation of an upper bound on the fourth derivative of the inflaton potential, obtained using the inflationary flow equations.

Thesis submitted for the Degree of Doctor of Philosophy
in the University of Oxford

· Trinity Term 2004 ·

Contents

Chapter 1

Standard cosmological model

The subject of this first chapter is an introduction to the standard cosmological model. The first part of the chapter is based on the cosmology lectures given by G. Ellis in [1–3]. The 1+3 covariant formalism is adopted, which will be useful in part of the following thesis. This formalism allows a coherent description of a wider class of universes than the standard Friedmann Robertson Walker (FRW) cosmology. In the second part of the chapter, the FRW model is derived as a particular homogeneous and isotropic case. In this thesis, unless otherwise specified, the units are such that $c = 8\pi G = 1$, and we use Heaviside-Lorentz electromagnetic units. We refer to appendix A of [4] for the units definitions and conversion relations. The signature of the metric is $(-,+,+,+)$, Greek indices run from 0 to 3, and Latin indices from 1 to 3.

1.1 Basis of the description

A cosmological model is the description of the global properties of the universe. On large scales, the dominant force is gravity, consequently we will assume that the structure of the universe is governed by general relativity. A cosmological model is defined by specifying:

- *the space-time geometry*, determined by the metric tensor $g_{\alpha\beta}$. Since the space-time is curved, $g_{\alpha\beta}$ is no longer the Minkowski metric, but has components $g_{\alpha\beta}(x^\gamma)$ which are functions of the position in space-time (for a set of coordinates x^γ). The Christoffel symbols $\Gamma^\alpha{}_{\beta\gamma} = \frac{1}{2}g^{\alpha\mu}(-g_{\beta\gamma,\mu} + g_{\beta\mu,\gamma} + g_{\gamma\mu,\beta})$, with $f_{,\alpha} \equiv \partial f/\partial x^\alpha$, determine the covariant derivative: $u_{\alpha;\beta} = u_{\alpha,\beta} - \Gamma^\gamma{}_{\alpha\beta}u_\gamma$.

- *the matter content and its physical behaviour*, represented by the energy-momentum tensor and an equation of state. The usual choices are a combination of: fluids (normally a perfect fluid), with specified equation of state; a set of particles, with a kinetic theory description; an electromagnetic field; a scalar field with given potential.

- *the interaction of the geometry and matter.* This is given through Einstein's field equations
$$R_{\alpha\beta} - \frac{1}{2}R\, g_{\alpha\beta} + \Lambda\, g_{\alpha\beta} = T_{\alpha\beta}\,, \tag{1.1}$$
where $R_{\alpha\beta}$ is the Ricci tensor, the contraction of the curvature Riemann tensor $R_{\alpha\beta} = R^{\mu}{}_{\alpha\mu\beta}$; R is the Ricci scalar; Λ is the cosmological constant; $T_{\alpha\beta}$ is the energy momentum tensor of all the matter fields present.

The Riemann tensor $R_{\alpha\beta\gamma\delta}$ represents the non-commutativity of the second covariant derivatives: for any vector field u^α, the Ricci identities are satisfied, $u^\alpha{}_{;\beta\gamma} - u^\alpha{}_{;\gamma\beta} = R^\alpha{}_{\delta\gamma\beta}u^\delta$. Furthermore, the Riemann tensor satisfies the Bianchi identities: $R_{\alpha\beta[\gamma\delta;\rho]} = 0$ [1]. Contracting these equations twice, one obtains $R^\alpha{}_{\beta;\alpha} = \frac{1}{2}R_{;\beta}$ which, together with Eq. (1.1), implies the conservation equations $T^{\alpha\beta}{}_{;\beta} = 0$ (provided that Λ is constant in time and space).

1.2 The covariant formalism

1.2.1 Space-time splitting

We proceed with the 1+3 covariant description of space-time. We assume that in a cosmological space-time there is a family of preferred world-lines representing the average motion of matter and radiation at each point. Consequently, a unique splitting of space-time into space and time is defined by this motion. The 4-velocity corresponding to this motion is taken to be the one defined by the vanishing of the dipole of the cosmic microwave background radiation (CMB). The 4-velocity vector field is normalised, $u^\alpha u_\alpha = -1$, and in terms of general coordinates x^α, is given by

$$u^\alpha = \frac{d\,x^\alpha}{d\,\tau}\,, \tag{1.2}$$

[1] We use the convention that round brackets denote symmetrisation, $S_{(\alpha\beta)} = \frac{1}{2}(S_{\alpha\beta} + S_{\beta\alpha})$, and square brackets denotes anti-symmetrisation $S_{[\alpha\beta\gamma]} = \frac{1}{6}(S_{\alpha\beta\gamma} + S_{\gamma\alpha\beta} + S_{\beta\gamma\alpha} - S_{\alpha\gamma\beta} - S_{\beta\alpha\gamma} - S_{\gamma\beta\alpha})$.

where τ is the proper time measured along the fundamental world-lines. Given the 4-velocity, one can define unique projection tensors:

$$U^{\alpha}{}_{\beta} = -u^{\alpha}u_{\beta}\,, \qquad U^{\alpha}{}_{\gamma}U^{\gamma}{}_{\beta} = U^{\alpha}{}_{\beta}\,,\ \ U^{\alpha}{}_{\alpha} = 1\,,\ \ U_{\alpha\beta}u^{\beta} = u_{\alpha} \tag{1.3}$$

$$h_{\alpha\beta} = g_{\alpha\beta} + u_{\alpha}u_{\beta}\,, \qquad h^{\alpha}{}_{\gamma}h^{\gamma}{}_{\beta} = h^{\alpha}{}_{\beta}\,,\ \ h^{\alpha}{}_{\alpha} = 3\,,\ \ h_{\alpha\beta}u^{\beta} = 0\,. \tag{1.4}$$

The first operator projects parallel to the 4-velocity vector u^{α}, and the second operator projects into the instantaneous rest-space of an observer moving with u^{α}. $h_{\alpha\beta}$ is effectively the spatial metric for such an observer: from Eqs. (1.4) it follows

$$ds^2 = g_{\alpha\beta}\,dx^{\alpha}dx^{\beta} = h_{\alpha\beta}\,dx^{\alpha}dx^{\beta} - (u_{\gamma}dx^{\gamma})^2\,. \tag{1.5}$$

The 4-dimensional volume element is given by the totally skew pseudo-tensor $\eta_{\alpha\beta\gamma\nu} = \sqrt{|g|}\,\delta^0{}_{[\alpha}\delta^1{}_{\beta}\delta^2{}_{\gamma}\delta^3{}_{\nu]}$. The volume element for the rest-space orthogonal to u^{α} is defined to be $\epsilon_{\alpha\beta\gamma} = \eta_{\alpha\beta\gamma\delta}u^{\delta}$.

Using the projection tensors (1.3) and (1.4), any physical tensor field can be separated into space and time parts, corresponding to the way an observer moving with u^{α} would measure these fields. A relevant tensor field is of course the *energy momentum tensor*, which takes the form

$$T_{\alpha\beta} = \rho\, u_{\alpha}u_{\beta} + p h_{\alpha\beta} + 2q_{(\alpha}u_{\beta)} + \pi_{\alpha\beta}\,, \tag{1.6}$$

where ρ is the energy density, p is the isotropic pressure, q^{α} is the energy flux, and $\pi_{\alpha\beta}$ the anisotropic pressure. In the case of a perfect fluid, one has $q^{\alpha} = \pi_{\alpha\beta} = 0$: the energy momentum tensor then reduces to the form

$$T_{\alpha\beta} = \rho\, u_{\alpha}u_{\beta} + p h_{\alpha\beta}\,, \tag{1.7}$$

and one further needs to specify the equation of state, $p = p(\rho)$, relating the relevant variables. It is normally required (with an exception in the case of scalar fields) that these variables obey the strong energy condition

$$\rho + 3p > 0\,, \tag{1.8}$$

and the causality condition that the isentropic speed of sound is smaller than the speed of light

$$0 \leq {c_s}^2 = \left.\frac{\partial p}{\partial \rho}\right|_{s=\mathrm{const}} . \leq 1 \tag{1.9}$$

The *electromagnetic field tensor* $F_{\alpha\beta} = -F_{\beta\alpha}$ can be split into electric and magnetic fields, as measured by an observer moving with u^α:

$$F_{\alpha\beta} = 2u_{[\alpha}E_{\beta]} + \epsilon_{\alpha\beta\gamma}B^\gamma , \tag{1.10}$$

where the electric and magnetic 3-vectors are given by

$$E_\alpha = F_{\alpha\beta}u^\beta \qquad E_\alpha u^\alpha = 0 , \tag{1.11}$$

$$B_\alpha = \frac{1}{2}\epsilon_{\alpha\beta\gamma}F^{\beta\gamma} \qquad B_\alpha u^\alpha = 0 . \tag{1.12}$$

A similar structure applies to the splitting of the Weyl tensor $C_{\alpha\gamma\beta\delta}$, the trace-free part of the curvature Riemann tensor. It is split irreducibly by the velocity field u^α into two symmetric, trace-free tensors, called the "electric" and "magnetic" parts:

$$E_{\alpha\beta} = C_{\alpha\gamma\beta\delta}u^\gamma u^\delta , \qquad H_{\alpha\beta} = \frac{1}{2}\epsilon_{\alpha\gamma\delta}C^{\gamma\delta}{}_{\beta\mu}u^\mu , \tag{1.13}$$

which are 3-tensors in the rest space of u^α.

With respect to the observer moving with u^α, also the covariant derivative of any tensor field splits into time and space derivatives:

$$\dot{S}^{\alpha\beta} = u^\gamma S^{\alpha\beta}{}_{;\gamma} \tag{1.14}$$

$$D_\gamma S^{\alpha\beta} = h_\gamma{}^\delta h^\alpha{}_\mu h^\beta{}_\nu S^{\mu\nu}{}_{;\delta} . \tag{1.15}$$

1.2.2 Kinematic quantities

The splitting of the covariant derivative of the 4-velocity field defines the kinematic quantities. It takes the form:

$$u_{\alpha;\beta} = D_\beta u_\alpha - \dot{u}_\alpha u_\beta , \quad D_\beta u_\alpha = \omega_{\alpha\beta} + \Theta_{\alpha\beta} , \quad \Theta_{\alpha\beta} = \sigma_{\alpha\beta} + \frac{1}{3}\Theta h_{\alpha\beta} , \tag{1.16}$$

where $\dot{u}^\alpha$ is the time derivative, and we have split the space derivative into its anti-symmetric and symmetric parts: $\omega_{\alpha\beta} = -\omega_{\beta\alpha}$, the *vorticity tensor*, and $\Theta_{\alpha\beta} = \Theta_{\beta\alpha}$, the *expansion tensor*. This latter gets further divided into its trace Θ, and a trace-free part $\sigma_{\alpha\beta} = \sigma_{\beta\alpha}$, called the *shear tensor*. The *acceleration vector* $\dot{u}_\alpha = u_{\alpha;\beta}u^\beta$ represents the effect of non-gravitational forces: it vanishes, when a particle moves following a geodesic. The tensor $D_\beta u_\alpha$ instead, represents the motion of neighbouring particles. In order to show this, one defines a relative position vector $X^\alpha_\perp = h^\alpha{}_\beta X^\beta$, where X^β is a deviation vector joining two world-lines at all times, and decomposes it into a relative distance and a unitary direction $X^\alpha_\perp = \delta\ell e^\alpha$. Then one obtains that the rate of change of relative distances, and the rate of change of directions are given by

$$\frac{(\delta\ell)^\cdot}{\delta\ell} = \frac{1}{3}\Theta + (\sigma_{\alpha\beta}\, e^\alpha e^\beta)\,, \tag{1.17}$$

$$h^\alpha{}_\beta(e^\beta)^\cdot = (\omega^\alpha{}_\beta + \sigma^\alpha{}_\beta - h^\alpha{}_\beta(\sigma_{\gamma\delta}\, e^\gamma e^\delta))e^\beta\,. \tag{1.18}$$

The first equation is a generalised Hubble law, allowing for possible anisotropic expansion; the second describes the change in direction, with respect to a Fermi transported vector basis. These equations elucidate the meaning of the kinematic variables. First of all, (1.17) shows that the effect of the *volume expansion* Θ alone is to induce a pure isotropic expansion, with no distortion or rotation. If one considers a representative length a (which will correspond to the scale factor in the FRW model), this describes completely the volume behaviour of the fluid, and from Θ one can define the *Hubble parameter*, and the *deceleration parameter*

$$H = \frac{\dot{a}}{a} = \frac{1}{3}\Theta\,, \qquad q = -\frac{\ddot{a}}{H^2\, a}\,, \tag{1.19}$$

which represent the slope and the curvature of the curve $a(\tau)$. From both Eqs. (1.17) and (1.18), one can see that the effect of the *shear* tensor is to cause a distortion, but leaving volumes invariant ($\sigma^\alpha{}_\alpha = 0$); it will change every direction, except the axes of shear. From Eq. (1.18), the effect of the vorticity tensor alone is to cause a change in orientation, leaving shape and volume invariant (it does not enter Eq. (1.17)): it represents therefore a rotation with respect to local inertial axes. The axis of this rotation is given by the vorticity vector

$$\omega^\alpha = \frac{1}{2}\epsilon^{\alpha\beta\gamma}\omega_{\beta\gamma}\,. \tag{1.20}$$

The present values of the kinematic quantities can be estimated, either directly, from observations of galaxies, or indirectly from measurements of the CMB. The estimation of the Hubble and deceleration parameters is a very debated issue. The present value of the Hubble parameter is in the range

$$H_0 = 100\,h \frac{\text{km}}{\text{sec Mpc}}\,, \qquad \text{with} \quad 0.45 < h < 0.8 \tag{1.21}$$

($h = 0.71 \pm 0.04$ from the WMAP satellite [5], $h = 0.71 \pm 0.07$ from the Hubble Space Telescope Key Project [6]). The observations of Type IA supernovae seem to indicate a negative value of the deceleration parameter $q_0 \simeq -0.5$ [7], although this value is still controversial. On the other hand, there is no uncertainties about the isotropy of the present universe: in [8] the CMB anisotropy data from the COBE satellite was used to find tight constraints on uniform shear and vorticity in the case of a flat universe:

$$\frac{\sigma_0}{H_0} < 3 \times 10^{-9}\,, \qquad \frac{\omega_0}{H_0} < 10^{-7} \tag{1.22}$$

(see also [9, 10] for other constraints, and [11] for a more general discussion).

1.2.3 Conservation of energy and momentum

The energy momentum tensor must satisfy the relativistic conservation equations $T^{\alpha\beta}{}_{;\beta} = 0$ (see the end of paragraph 1.1). This tensor equation can also be split with respect to the 4-velocity u^α, to give the conservation of energy along a world-line,

$$\dot{\rho} + (\rho + p)\Theta + \pi_{\alpha\beta}\sigma^{\alpha\beta} + D_\alpha q^\alpha + 2\dot{u}^\alpha q_\alpha = 0\,, \tag{1.23}$$

and the conservation of momentum

$$(\rho + p)\dot{u}_\alpha + D_\alpha p + D^\beta \pi_{\alpha\beta} + \dot{u}^\beta \pi_{\alpha\beta} + h_\alpha{}^\beta \dot{q}_\beta + (\omega_{\alpha\beta} + \sigma_{\alpha\beta} + \frac{4}{3}\Theta h_{\alpha\beta})q^\beta = 0\,. \tag{1.24}$$

These equations are completely general. In order to proceed, we need to specify the matter and radiation content of the universe. For the purpose of this brief review, we assume that we can approximate this latter with a *fluid description.* For other purposes, for example a detailed description of the thermal history of the universe, it is better to use the relativistic kinetic theory to describe matter and radiation, which can also account for out of equilibrium states. We assume instead that the fluid is always in a state of thermal equilibrium.

The 4-velocity u^α coincides with the average velocity of the matter and radiation fluids. If the fluid is given by non-relativistic particles of rest mass m, then one can define a conserved current density $j^\alpha = \mu u^\alpha$, where μ denotes the rest mass density. Conservation of rest-mass then implies the conservation of matter along the particles world-lines:

$$(\mu u^\alpha)_{;\alpha} = 0 \quad \rightarrow \quad \dot{\mu} + \Theta\mu = 0 \quad \rightarrow \quad \mu = \frac{\mu_0}{a^3}\,, \tag{1.25}$$

with μ_0 the integration constant, and we made use of the first of Eqs. (1.19). In the case of zero rest-mass particles, like photons or neutrinos, μ is substituted by the particle number density n, which is also conserved in general. Conservation of rest-mass and number density therefore hold independently from the characteristics of the fluid and the equation of state. However, the latter must be specified in order to complete the description, and connect the variables appearing in the conservation equations (1.23), (1.24) with the thermodynamic variables. The temperature T and entropy S of the fluid are given by

$$d\varepsilon + p\,dv = TdS\,, \tag{1.26}$$

where ε is the specific internal energy, $\rho = \mu(1+\varepsilon)$, and $v = \mu^{-1}$ is the specific volume. The usual assumption is that the cosmic fluid is a *perfect fluid*, with zero viscosity and no heat conduction. The energy conservation equation then becomes

$$\dot{\rho} + (\rho + p)\Theta = 0\,. \tag{1.27}$$

Together with Eq. (1.26), this implies that entropy is conserved during the fluid flow, and in turn that there is only one independent thermodynamic variable along each world-line. This can be chosen to be the rest-mass density μ: that implies, from Eq. (1.25), that the change of thermodynamic state along the flow lines is determined in this case by the average length $a(\tau)$ alone. We assume an equation of state of the form $p = w\,\rho$, where $0 \leq w \leq 1$ in order for the causality and energy conditions to be valid (see Eqs. (1.8), (1.9)). Then the energy conservation equation (1.27) can be integrated, to give

$$\rho = \frac{\rho_0}{a^{3(w+1)}} \,. \tag{1.28}$$

The limiting case $w = 0$ describes zero-pressure *non relativistic dust*; one then has $T_{\alpha\beta} = \mu\, u_\alpha u_\beta$, and from (1.28) one recovers the conservation equation (1.25). If $w = 1/3$, one has the case of *radiation*: in this case one has

$$\rho_{\rm rad} = \frac{\rho^0_{\rm rad}}{a^4} \,, \tag{1.29}$$

and $T = T_0/a$, given that $\rho \propto T^4$.

1.2.4 Electromagnetic fields

Electromagnetic fields are part of the energy content of the universe, and must appear as source for the Einstein's fields equations (1.1). For example, as well as the fluid description carried out in the previous paragraph, the radiation content of the universe can in principle be described by assigning an electromagnetic field to the radiation at each frequency travelling in each direction: the two description will be shown to be equivalent in the following. Moreover, there is the possibility of the presence of a large scale magnetic field in the universe, which will be analysed in details in the next chapters of this work; therefore, in order to complete the picture introduced so far, we need to include the presence of electromagnetic fields.

The splitting of the electromagnetic tensor field given by the definition of the time-like vector u^α, and the consequent definition of electric and magnetic fields have been presented in section 1.2.1. Maxwell's equations need also be decomposed with respect to the observer moving with u^α. We define the current density 4-vector j^α, where $q = -j^\alpha u_\alpha$ is the charge density, and $J^\alpha = h^\alpha{}_\beta j^\beta$ is the spatial current measured by u^α. Then, Maxwell's equations in the covariant form [12]

$$F^{\alpha\beta}{}_{;\beta} = j^\alpha \tag{1.30}$$

$$F_{\alpha\beta;\gamma} + F_{\gamma\alpha;\beta} + F_{\beta\gamma;\alpha} = 0 \,, \tag{1.31}$$

become [13]

$$D_\alpha E^\alpha + 2\omega_\alpha B^\alpha = q \tag{1.32}$$

$$D_\alpha B^\alpha - 2\omega_\alpha E^\alpha = 0 \tag{1.33}$$

$$h_{\alpha\beta}\dot{E}^\beta - \epsilon_{\alpha\beta\gamma}D^\beta B^\gamma = -J_\alpha + \epsilon_{\alpha\beta\gamma}\dot{u}^\beta B^\gamma + (\omega_{\alpha\beta} + \sigma_{\alpha\beta} - \frac{2}{3}\Theta h_{\alpha\beta})E^\beta \tag{1.34}$$

$$h_{\alpha\beta}\dot{B}^\beta + \epsilon_{\alpha\beta\gamma}D^\beta E^\gamma = -\epsilon_{\alpha\beta\gamma}\dot{u}^\beta E^\gamma + (\omega_{\alpha\beta} + \sigma_{\alpha\beta} - \frac{2}{3}\Theta h_{\alpha\beta})B^\beta \,. \tag{1.35}$$

The first two equations are the "time" projection of (1.30) and (1.31), obtained multiplying these with u^α; the second two are the "space" projection, obtained by multiplication with the space projection tensor $h_{\alpha\beta}$. It appears clearly here how the motion of the observer affects the form of Maxwell's equations: beside the usual spatial divergences, curls and time derivatives of the fields, one has the appearance of extra terms representing the motion of the family of fundamental observers moving with 4-velocity u^α. Moreover, the current conservation equation $j^\alpha{}_{;\alpha} = 0$ takes the form

$$\dot{q} + \Theta q + D_\alpha J^\alpha + \dot{u}_\alpha J^\alpha = 0 \,, \tag{1.36}$$

and the covariant form of Ohm's law is

$$j_\alpha + u_\alpha u_\beta j^\beta = \sigma F_{\alpha\beta}u^\beta \,, \tag{1.37}$$

where σ denotes the conductivity. Projecting into the instantaneous rest space of the fundamental observer, Ohm's law becomes $J_\alpha = \sigma E_\alpha$.

The electromagnetic energy momentum tensor is a symmetric and trace-free tensor of the general form

$$T_{\alpha\beta} = F_{\alpha\gamma}F_\beta{}^\gamma - \frac{1}{4}g_{\alpha\beta}F_{\gamma\delta}F^{\gamma\delta} \,. \tag{1.38}$$

Relative to a fundamental observer, this tensor can be written like

$$T_{\alpha\beta} = \frac{1}{2}(E^2 + B^2)u_\alpha u_\beta + 2u_{(\alpha}\epsilon_{\beta)\gamma\delta}E^\gamma B^\delta + \frac{1}{2}(E^2 + B^2)h_{\alpha\beta} - E_\alpha E_\beta - B_\alpha B_\beta \,, \tag{1.39}$$

where E^2 and B^2 are the magnitudes of the electric and magnetic fields. By analogy with the energy momentum tensor of a general fluid (1.6), there is a fluid description for the electromagnetic field. One finds:

$$\rho_{em} = \frac{1}{2}(E^2 + B^2)\,, \tag{1.40}$$

$$p_{em} = \frac{1}{6}(E^2 + B^2)\,, \tag{1.41}$$

$$q^{\alpha}_{em} = \epsilon^{\alpha\beta\gamma} E_\beta B_\gamma\,, \tag{1.42}$$

$$\pi^{\alpha\beta}_{em} = \frac{1}{3}(E^2 + B^2)h^{\alpha\beta} - E^\alpha E^\beta - B^\alpha B^\beta\,. \tag{1.43}$$

Eqs. (1.40) and (1.41) lead to the previously mentioned equation of state for radiation: $p = 1/3\,\rho$; Eq. (1.42) is the usual expression for the Poynting vector, and Eq. (1.43) suggest that the presence of an electromagnetic field in the universe gives rise to anisotropic pressures.

Eq. (1.39) seems to affect the validity of the fluid description adopted in the previous paragraph, where the radiation content of the universe was approximated by a perfect fluid. However, one should account for the fact that the main radiation component of the universe is *isotropic* about the fundamental observers moving with velocity u^α: it is in fact the cosmic microwave background radiation. To describe the radiation content of the universe, one assigns an electromagnetic field to the radiation at each frequency travelling in each direction, and then sums Eq. (1.39) over all components, to find the total radiation energy-momentum tensor. Because of isotropy, when one performs this sum, the anisotropic part in Eq. (1.39) vanish, and one is left with the energy momentum tensor of a perfect fluid.

1.2.5 Dynamic equations

The Einstein's field equations (1.1), together with the conservation equations (1.23), (1.24) and the equation of state for the fluid, form a complete set of equations, which determine the interaction between the matter and the geometry of space-time. This system of equations must as well be decomposed from the point of view of the fundamental observer, in order to find explicit equations connecting the kinematic and dynamic variables introduced in the previous paragraphs. The way this is carried on, is to project out the "space" and "time" parts of the Ricci and Bianchi identities (paragraph 1.1), and use Eqs. (1.1) to substitute for the Ricci tensor.

Eqs. (1.1) can be rewritten in the form

$$R_{\alpha\beta} = T_{\alpha\beta} - \frac{1}{2}Tg_{\alpha\beta} + \Lambda g_{\alpha\beta}\,, \tag{1.44}$$

so that

$$R_{\alpha\beta}u^\alpha u^\beta = \frac{1}{2}(\rho + 3p) - \Lambda \tag{1.45}$$

$$R_{\alpha\beta}u^\alpha h^\beta{}_\gamma = -q_\gamma \tag{1.46}$$

$$R_{\alpha\beta}h^\alpha{}_\gamma h^\beta{}_\delta = \left(\frac{1}{2}(\rho - p) + \Lambda\right) h_{\gamma\delta} + \pi_{\gamma\delta}\,. \tag{1.47}$$

Equipped with this form of the field equations, and with the splitting of the covariant derivative of u^α (1.16), one can proceed with the projection of the Ricci identities, applied to the 4-velocity vector: $u^\alpha{}_{;\beta\gamma} - u^\alpha{}_{;\gamma\beta} = R^\alpha{}_{\delta\gamma\beta}u^\delta$. The "time" projection gives rise to three propagation equations, while the "space" projection gives rise to three constraint equations.

The first propagation equation is *Raychaudhuri's equation*, which is a propagation equation for the variable Θ:

$$\dot{\Theta} + \frac{1}{3}\Theta^2 = -\frac{1}{2}(\rho + 3p) + \Lambda + 2(\omega^2 - \sigma^2) + D_\alpha \dot{u}^\alpha + \dot{u}_\alpha \dot{u}^\alpha\,. \tag{1.48}$$

Recalling the definitions (1.19), one can write $\dot{\Theta} + 1/3\,\Theta^2 = 3\,\ddot{a}/a$: it appears clearly, then, that this equation shows how the evolution of $a(\tau)$ is determined at each point by the matter content (including the relativistic pressure term), and how the different kinematic quantities affect it: $\Lambda > 0$ is a repulsive term, which tends to push matter apart; so does the vorticity (which is however not constant in general), while the effect of shear is to pull the world-lines together. The acceleration affects the average distance of the lines through its divergence. Raychaudhuri's equation also has two applications which are of fundamental importance when treating the FRW model: it shows the usefulness of the deceleration parameter, and proves the existence of a singularity for those models.

The second propagation equation is the *vorticity propagation equation*, which determines the rate of change of the vorticity vector:

$$h_{\alpha\beta}\dot{\omega}^\beta + \frac{2}{3}\Theta\omega_\alpha - \sigma_{\alpha\beta}\omega^\beta = -\frac{1}{2}\epsilon_{\alpha\beta\gamma}D^\beta \dot{u}^\gamma\,. \tag{1.49}$$

By substituting in the source term with the momentum conservation equation (1.24), one can study the effect of a given equation of state on the propagation of vorticity. In particular, if the fluid is perfect, it is easy to derive from (1.49) that vorticity is a conserved quantity, and is "frozen into" the fluid.

The third propagation equation is the *shear propagation equation*:

$$\dot{\sigma}_{\langle\alpha\beta\rangle} + \frac{2}{3}\Theta\sigma_{\alpha\beta} + \sigma_{\gamma\langle\alpha}\sigma_{\beta\rangle}{}^{\gamma} = D_{\langle\alpha}\dot{u}_{\beta\rangle} + \dot{u}_{\langle\alpha}\dot{u}_{\beta\rangle} - \omega_{\langle\alpha}\omega_{\beta\rangle} + \frac{1}{2}\pi_{\alpha\beta} - E_{\alpha\beta}\,, \qquad (1.50)$$

where we have introduced the notation $S_{\langle\alpha\beta\rangle}$ to denote the projected symmetric trace-free parts of vectors and rank two tensors [14]:

$$S_{\langle\alpha\rangle} = h_{\alpha}{}^{\beta}S_{\beta}\,, \qquad S_{\langle\alpha\beta\rangle} = [h_{(\alpha}{}^{\gamma}h_{\beta)}{}^{\delta} - \frac{1}{3}h_{\alpha\beta}h^{\gamma\delta}]S_{\gamma\delta}\,. \qquad (1.51)$$

The shear propagation equation shows that the effect of the free gravitational field, represented by $E_{\alpha\beta}$, and of the anisotropic pressure $\pi_{\alpha\beta}$, is to cause distortion in the fluid, inducing shear in the flow lines. Shear then in turns determines the vorticity, and also enters into the volume expansion equation.

The constraint equations come from the "space" projection of the Ricci identities, and do not involve time derivatives of the kinematic quantities. They have to be consistent with the evolution equations at all times. One can derive three of them: *the 0a components of the field equations*,

$$D^{\beta}\sigma_{\alpha\beta} - \frac{2}{3}D_{\alpha}\Theta - \epsilon_{\alpha\beta\gamma}(D^{\beta}\omega^{\gamma} - 2\omega_{\beta}\dot{u}_{\gamma}) = -q^{\alpha}\,, \qquad (1.52)$$

the *vorticity divergence* constraint,

$$D_{\alpha}\omega^{\alpha} - \dot{u}^{\alpha}\omega_{\alpha} = 0\,, \qquad (1.53)$$

and the $H_{\alpha\beta}$ *constraint*

$$H_{\alpha\beta} = 2\dot{u}_{\langle\alpha}\omega_{\beta\rangle} + D_{\langle\alpha}\omega_{\beta\rangle} + \epsilon_{\gamma\delta(\alpha}D^{\gamma}\sigma_{\beta)}{}^{\delta}\,. \qquad (1.54)$$

By putting these equations together with the energy and momentum conservations (1.23), (1.24), once the equation of state is given, we have a set of equations connecting all the dynamic and kinematic variables. However, the appearance of the electric component of the Weyl tensor in the shear propagation equation, suggests that we are still missing the propagation equations determining $\dot{E}_{\alpha\beta}$ and $\dot{H}_{\alpha\beta}$ from the matter distribution. These are obtained by the splitting of the Bianchi identities $R_{\alpha\beta[\gamma\delta;\rho]} = 0$, which give a set of two propagation and two constraint equations, very similar to Maxwell's Eqs. (1.32-1.35). We refer to [2] for these equations and don't derive them here, since they are trivially satisfied in the case of major interest for us, the FRW model.

1.3 FRW universe

1.3.1 FRW metric

The FRW model of the universe is characterised by a perfect fluid energy momentum tensor, and by the condition that the space-time is *homogeneous* and *isotropic* at every point. In terms of the covariant variables defined in the previous chapters, this translates into the conditions

$$\omega = \sigma = \dot{u}^{\alpha} = 0 \qquad \text{and} \qquad E_{\alpha\beta} = H_{\alpha\beta} = 0\,, \tag{1.55}$$

so that the space-time is also conformally flat. The homogeneity condition implies

$$D_{\alpha}\rho = D_{\alpha}p = D_{\alpha}\Theta = 0\,. \tag{1.56}$$

Setting $\omega = 0$ in Eq. (1.16) gives $u_{[\alpha}u_{\beta;\gamma]} = 0$: therefore, u_{α} must be proportional to a gradient. Defining the functions $f(x_{\alpha})$, $t(x_{\alpha})$, one has that $u_{\alpha} = -f\,t_{,\alpha}$: consequently, the 4-velocity is orthogonal to the surfaces $\{t = \text{constant}\}$, and the local rest spaces $h_{\alpha\beta}$ mesh together to form a set of 3-surfaces in space-time, which are surfaces of simultaneity for all the fundamental observers. Thus, t defines a cosmological time coordinate. Setting also $\dot{u}_{\alpha} = 0$, it follows that $u_{[\alpha;\beta]} = 0$: therefore, $u_{\alpha} = -t_{,\alpha}$, and t measures *proper time* along the fluid flow lines. Eqs. (1.56) then imply that $\rho = \rho(t)$, $p = p(t)$, $\Theta = \Theta(t)$; recalling the first equation in (1.19), one can set $a = a(t)$. It is possible to demonstrate [2] the existence, in this situation, of simple comoving coordinates, in terms of which the metric takes the form

$$ds^2 = -dt^2 + h_{ij}dx^i dx^j\,, \qquad u^\alpha = \delta^\alpha{}_0\,. \tag{1.57}$$

Moreover, the spaces $\{t = \text{constant}\}$ are 3-spaces of constant curvature

$$K(t) = \frac{^3R}{6} = \frac{1}{3}\left(\rho + \Lambda - \frac{1}{3}\Theta^2\right)\,, \tag{1.58}$$

where ^3R is the Ricci scalar of the 3-spaces. Setting $a^2(t)K(t) = \kappa$, one can rewrite the spatial part of the metric as $h_{ij} = a^2(t)\,\gamma_{ij}$, where γ_{ij} is given by

$$\gamma_{ij}\,dx^i dx^j = dr^2 + f^2(r)(d\theta + \sin^2\theta d\phi^2)\,, \tag{1.59}$$

and

$$f(r) = \begin{cases} \sin r & \text{if } \kappa = 1\,, \quad \text{spherical model} \\ r & \text{if } \kappa = 0\,, \quad \text{euclidean model} \\ \sinh r & \text{if } \kappa = -1\,, \quad \text{hyperbolic model}\,. \end{cases} \tag{1.60}$$

It is useful to define at this stage the *conformal time* η such that $dt = a(\eta)d\eta$, which will be widely used in the following of this work. In terms of the conformal time, the FRW metric becomes

$$ds^2 = a^2(\eta)(-d\eta^2 + \gamma_{ij}\,dx^i dx^j)\,, \qquad u^\alpha = \frac{1}{a}\delta^\alpha{}_0\,. \tag{1.61}$$

Derivatives with respect to conformal time will be denoted by $'$; therefore [15],

$$\dot{S}_\alpha = \frac{\partial S_\alpha}{\partial t} - \frac{\dot{a}}{a}S_\alpha = \frac{1}{a}\frac{\partial S_\alpha}{\partial \eta} - \frac{a'}{a^2}S_\alpha\,, \tag{1.62}$$

$$\dot{S}_{\alpha\beta} = \frac{\partial S_{\alpha\beta}}{\partial t} - 2\frac{\dot{a}}{a}S_{\alpha\beta} = \frac{1}{a}\frac{\partial S_{\alpha\beta}}{\partial \eta} - 2\frac{a'}{a^2}S_{\alpha\beta}\,. \tag{1.63}$$

The spatial derivative operator D and the covariant derivative in the 3-surfaces (denoted with a stroke) are related simply by $D_\gamma S^{\alpha\beta} = \delta_\gamma{}^\mu S^{\alpha\beta}{}_{|\mu}$.

A fundamental property of the FRW metric is the *cosmological redshift.* If one considers a light ray travelling on a geodesic from a galaxy G toward a comoving observer O, using the metric (1.57) it is easy to demonstrate that the wavelength of the detected light is related to the one of the emitted light by

$$\frac{\lambda_O}{\lambda_G} = \frac{a(t_O)}{a(t_G)} = 1 + z_G\,, \tag{1.64}$$

where z is called the redshift parameter. Observations show that $a(t_O) > a(t_G)$, so the universe is expanding and $z > 0$. If one imagines that the light ray has been emitted at the beginning of the universe, the total distance travelled by such a light ray up to a certain age t of the universe is called the *particle horizon*:

$$\ell_{\rm hor} = a(t)\int_0^t \frac{dt'}{a(t')} = a(\eta)\,\eta\,, \tag{1.65}$$

where we fixed the beginning of the universe at $t = 0$ (see the next paragraph).

1.3.2 Dynamic equations

The dynamics of the FRW model, once the equation of state $p = p(\rho)$ is given, is determined by three relevant equations: the energy conservation equation (1.27)

$$\dot\rho + 3H(\rho + p) = 0\,, \tag{1.66}$$

Raychaudhuri's equation

$$3\dot H + 3H^2 + \frac{1}{2}(\rho + 3p) - \Lambda = 0\,, \tag{1.67}$$

and expression (1.58)

$$H^2 + \frac{\kappa}{a^2} - \frac{1}{3}(\rho + \Lambda) = 0\,. \tag{1.68}$$

These equations are not independent; the last two are called the Friedmann equations. From Raychaudhuri's equation, it is possible to see that if the matter content of the universe obeys the strong energy condition $\rho + 3p > 0$, and $\Lambda \leq 0$, then $\ddot a < 0$: the expansion is decelerated, and there exists a time for which $a(t_s) = 0$, and $\rho(t_s) \to \infty$. One chooses the time coordinate such that this singularity corresponds to $t_s = \eta_s = 0$. The age of the universe is then $t_0 < H_0^{-1}$, with $t_0 = H_0^{-1} = 3.08 \times 10^{17} h^{-1}$ sec in the case of a non-accelerating universe.

Cosmological parameters

It is useful to define the *cosmological parameters*: for a given universe component X, one defines $\Omega_X = \rho_X/\rho_c$, where ρ_X is the energy density of X, and ρ_c is the *critical density*, corresponding to the total energy density of a flat universe with vanishing cosmological constant:

$$\rho_c = 3H^2\,, \qquad \rho_c(t_0) = 1.879\,h^2 \times 10^{-29}\frac{\mathrm{g}}{\mathrm{cm}^3} = 8.099\,h^2 \times 10^{-47}\mathrm{GeV}^4\,. \tag{1.69}$$

One has then

$$\Omega_f = \frac{\rho_f}{\rho_c}\,, \qquad \Omega_\Lambda = \frac{\Lambda}{\rho_c}\,, \qquad \Omega_\kappa = -\frac{\kappa}{a^2H^2}\,, \tag{1.70}$$

which represent the contributions of the cosmic fluid, cosmological constant and curvature, and are evaluated at $t = t_0$ if nothing else is specified. One normally sets $\Omega = \Omega_f + \Omega_\Lambda$, the total contribution from the universe content. Inserting these definitions in Eq. (1.68), one finds the relation

$$1 = \Omega_f + \Omega_\kappa + \Omega_\Lambda\,, \tag{1.71}$$

which shows that the cosmological parameters are not independent, and $\Omega > 1$ if the curvature is positive, $\Omega = 1$ if it is zero, and $\Omega < 1$ if it is negative. Eq. (1.67) can be rewritten at the present time in the form $q_0 = \Omega_f/2 - \Omega_\Lambda$, showing the connection between the universe geometry and the energy content. The actual values of the cosmological parameters are in the range of $\Omega_\kappa \simeq 0$, $\Omega_\Lambda \simeq 0.7$, $\Omega_f \simeq 0.3$. These are obtained by combining different experiments: type IA supernovae, which gives a measure of the deceleration parameter q_0; CMB measurements, which give the value of Ω, and tight constraints on Ω_Λ and Ω_f assuming a value for the Hubble constant; and constraints from the dynamics of galaxies and clusters, which provide estimations of Ω_f. The contribution of baryonic matter to this latter is $\Omega_B h^2 \simeq 0.02$, obtained from CMB experiments and from the theory of Big Bang nucleosynthesis. Therefore, the rest must be given by non-baryonic dark matter, $\Omega_{\mathrm{DM}} \sim 0.26$. Essentially every known particle in the standard model of particle physics has now been ruled out as a candidate for dark matter; apart from its abundance, the only known features of this component are that it should be very weakly interacting with ordinary matter, and that it must have been non-relativistic for a very long time.

Although the measurement of the cosmological parameters represents a substantial accomplishment in observational cosmology, this is tempered by the absence of a self consistent model to explain them. Dark matter has not been directly detected so far; the baryon density is mysterious due to the asymmetry between baryons and anti-baryons; the energy density of the cosmological constant differs by 120 orders of magnitude from what naturally expected, if it was associated with quantum fluctuations of the vacuum: $m_{\rm Pl}^4$.

Solution of the dynamic equations

The solution of the system of equations (1.23), (1.67), (1.68) is straightforward for an equation of state of the form $p = w\,\rho$, in the cosmologically interesting case of flat spatial sections, $\Omega_\kappa = 0$, and if one further assumes that $\Lambda = 0$. This is fully justified in the early universe, and can be extended up to the present epoch, in which the cosmological constant is not yet dominating the dynamics. In terms of conformal time η, and normalising the scale factor today to $a(\eta_0) = 1$, the solution is

$$a(\eta) = \left(\frac{\rho_0}{3}\right)^{\frac{q}{2}} \left(\frac{\eta}{q}\right)^q , \tag{1.72}$$

where $q = 2/(3w+1)$, and we made use of the energy scaling (1.28). In the standard cosmological picture, the universe is filled with two components, matter (baryonic and dark matter) with $w = 0$, and radiation with $w = 1/3$. Since the scale factor is growing, comparing Eqs. (1.25) and (1.29) shows that at sufficiently early times the radiation must have dominated the energy density of the universe. The transition epoch, when radiation and matter have the same energy density, corresponds to a scale factor

$$a(\eta_{\rm eq}) = \Omega_{\rm rad} , \qquad \Omega_{\rm rad} = \frac{\rho^0_{\rm rad}}{\rho_c} = 4.2\,h^{-2} \times 10^{-5} , \tag{1.73}$$

where we have taken $\mu_0 = \rho_c$ because of the spatial flatness of the present universe. From Eq. (1.72) one finds

$$\eta < \eta_{\rm eq} \qquad \longrightarrow \qquad a(\eta) = H_0 \sqrt{\Omega_{\rm rad}}\, \eta , \tag{1.74}$$

$$\eta > \eta_{\rm eq} \qquad \longrightarrow \qquad a(\eta) = \frac{{H_0}^2}{4}\, \eta^2 , \tag{1.75}$$

which give the age of the universe in conformal time, $\eta_0 \simeq 6\,h^{-1} \times 10^{17}$ sec, and the matter-radiation equality epoch, $\eta_{\rm eq} \simeq 8\,h^{-2} \times 10^{14}$ sec, corresponding to redshift $z_{\rm eq} \simeq 2h^2 \times 10^4$.

1.3.3 The thermal history of the universe

It is useful at this stage to proceed with a brief description of the early phases of the evolution of the universe, concentrating on the interactions between the different components of the cosmic fluid: baryons and leptons, photons, neutrinos. The presence of a possible magnetic field will be accounted for in the next chapters. The fundamental assumption is that radiation and matter are in thermal equilibrium. This is certainly the case as long as microscopic reactions are quicker than the universal expansion, but is no longer valid after the formation of stable hydrogen atoms. The following paragraphs are based on references [4, 16, 17].

Recombination and photon decoupling

As discussed in the previous sections, the universe undergoes an adiabatic expansion, and the temperature decays with time. Proceeding backward in time, the first relevant step (as far as we are concerned) in the evolution of the universe is *recombination*. At a temperature of about $T_{\rm rec} \simeq 4000$ K $= 0.34$ eV, corresponding to redshift $z_{\rm rec} \simeq 1400$, the number density of photons with energy above the hydrogen ionisation energy drops below the baryon density: electrons and protons start to combine into hydrogen. This occurs at a lower temperature than 13.6 eV, the temperature corresponding to the hydrogen ionisation energy, because of the huge number of photons with respect to baryons: $\eta = n_B/n_\gamma \simeq 3 \times 10^{-8}\,\Omega_B h^2$. The recombination process proceeds up to a temperature $T_{\rm F} \simeq 0.24$ eV, when the number of free electrons and protons has dropped enough, that the rate of the reaction $p + e \rightarrow {\rm H} + \gamma$ becomes smaller than the Hubble rate. Then, the reaction is no longer in thermal equilibrium, and the process stops, leaving a small fraction of free electrons (and protons): $n_e(\eta) \simeq 3 \times 10^{-10} a^{-3}(\eta)\,\Omega h$ cm^{-3}. The decrease of the electron density subsequent to the recombination process affects the interactions between electrons and the photons of the plasma. The last interaction process to freeze out is Thomson scattering, at a temperature $T_{\rm dec} \simeq 3000$ K $=$ 0.26 eV, corresponding to a redshift $z_{\rm dec} \simeq 1100$. This *decoupling phase* marks a fundamental transition in the evolution of the universe: the mean free path of photons becomes bigger than the Hubble scale, they propagate freely and the universe becomes transparent. The photons maintain their relativistic Bose-Einstein distribution, with effective temperature $T \propto a^{-1}(\eta)$ (affected only by the universe expansion): they constitute the *CMB radiation.* The CMB radiation has two fundamental properties. The first one, is that it follows with extraordinary precision a black body spectrum at the temperature $T_0 = 2.725 \pm 0.001$ K, which corresponds to the decoupling temperature redshifted to today. The black body spectrum is due to the fact that the Bose-Einstein distribution of photons is thermalised by Compton scattering and Bremsstrahlung before decoupling. The CMB is the principal source of radiation in the universe, so that T_0 is the temperature of the universe today: the number of photons is so high, that the hydrogen is not decoupled from them. The second relevant property, is that the CMB radiation is almost perfectly isotropic, once one subtracts the dipole anisotropy due to the Earth's movement, which is of the order of $\Delta T/T \simeq 10^{-3}$. It is characterised by small fluctuations in temperature on all angular scales, of the order

$$\left\langle \left(\frac{\Delta T}{T}\right)^2 \right\rangle^{\frac{1}{2}} \simeq 10^{-5} \,. \tag{1.76}$$

These fluctuations are of fundamental importance in modern cosmology; they are the imprint of the presence of small variations in the density of matter at the time of CMB decoupling. Their origin will be explained in details in chapter 3.

Neutrinos decoupling and nucleosynthesis

Proceeding backward in time, the next remarkable stage of the universe evolution after recombination is the *domination of radiation over matter*, occurring at a temperature of $T_{\rm eq} \simeq 5500\, h^{-2}$ K, and discussed in section 1.3.2. The radiation component of the universe at this stage is constituted by photons and three kinds of neutrinos. Electrons and positrons cease to be relativistic when the temperature of the universe drops below $T = m_e = 0.5$ MeV, and the annihilation of e^+e^- pairs starts. This annihilation process is complete, leaving only a small fraction of electrons, due the to matter-antimatter asymmetry of the universe. At a temperature of the order of 1.4 MeV, the *freeze out of the weak interactions* occurs, which maintained the neutrinos in thermal equilibrium. Neutrinos then decouple from the background, and keep a relativistic Fermi-Dirac distribution, with temperature $T_\nu \propto a^{-1}(\eta)$: today the universe is permeated not only by the CMB radiation, but also by a background of neutrinos. The temperature of this background is $T_\nu(\eta_0) = 1.95$ K: since the neutrinos decoupled before e^+e^- annihilation, their temperature hasn't been affected by the reheating that this latter process induces.

Another important stage of early universe evolution is the synthesis of light nuclei. The agreement between experimental results and the predictions of *primordial nucleosynthesis theory* constitutes a remarkable confirmation of the Big Bang model of the universe. The observed abundance of helium in the universe is $Y = \frac{n_{\rm He} m_{\rm He}}{n_{\rm H} m_{\rm H}} \simeq 0.24$, and this amount cannot be explained by helium fusion in stars: the majority of helium must have been formed in the primordial universe. The temperature at which the nucleosynthesis process takes place is about 1 MeV, despite the fact that the binding energy of light nuclei (^{2}H, ^{3}H, ^{3}He, ^{4}He, ^{7}Li) is of the order of a few MeV. The reason for this difference in temperature is, as in the case of recombination, the huge density of photons with respect to baryons; in addition, the baryon density is not high enough to allow more than two-body collisions. The synthesis of deuterium starts to occur at $T_{^2{\rm H}} = 0.085$ MeV, and freezes out at about 0.004 MeV. Once this process is started, the formation of helium also begins by a chain of secondary processes. Almost all deuterium gets converted in helium, which is most energetically favourable for nucleons. Therefore, one can estimate the total abundance of helium as given by half of the number density of neutrons present at $T_{^2{\rm H}} = 0.085$ MeV. The density of neutrons is calculated considering the freezing out of the weak interactions which maintain equilibrium between protons and neutrons, and after that, taking into account the β decay of neutrons. The value found in this way is very sensitive to the cosmological model: any extra form of energy which might slightly change the expansion rate of the universe affects the freeze-out temperature, and in turns the neutrons density and the prediction for helium abundance. Nucleosynthesis constitutes therefore an excellent probe of the characteristics of the cosmological model at the time it takes place. The value for the helium abundance eventually found is in remarkable agreement with observations: $Y \simeq 0.25$. The abundances of light elements evaluated from nucleosynthesis imply a value for the baryon fraction of $0.01 \leq \Omega_B h^2 \leq 0.022$, very much comparable to what is found from CMB measurements. Therefore, nucleosynthesis also provides an indication of the presence of non-baryonic dark matter in the universe.

Phase transitions and baryogenesis

The previous description already underlined the need to go beyond a simple perfect fluid approach, in order to model properly the behaviour of matter and radiation in the early universe. Moreover, at sufficiently high temperature the universe is a plasma of relativistic particles, quarks, leptons, gauge and Higgs bosons: it should be described using quantum field theory. The combination of cosmic expansion and the associated thermodynamics with a field theory approach yields to the phenomenon of *finite temperature phase transitions*. The picture is that, in the very early universe, the matter was described by a unified gauge field theory, and consequently at extreme temperatures, the vacuum state of the theory respected the full symmetry of the Lagrangian. As the universe cooled, the gauge theory underwent a series of spontaneous symmetry breakings, which should include: the GUT phase transition, at temperature of $10^{14} - 10^{16}$ GeV; the electroweak phase transition, at $T \simeq 300$ GeV; the quark/hadron phase transition, for $T \simeq 100 - 300$ MeV. A phase transition from a high temperature, symmetric vacuum to a low temperature, symmetry breaking one can be of two kinds: first or second order. In a second order phase transition, the transition occurs smoothly: a global minimum of the finite temperature effective potential becomes gradually a local maximum as the ambient cools. In the first case, instead, a local minimum develops in the potential as the temperature decays, and for a critical value of the temperature, the global and the local minima become degenerate. A potential barrier then develops between the two minima, which can be overcome only through quantum tunnelling. The transition between the false and true vacua is discontinuous, and occurs through the nucleation of bubbles of the energetically favoured asymmetric phase, which expand outward at the speed of light. The QCD phase transition, through which quarks and gluons condense into colourless hadrons, is almost certainly of first order. The nature of the electroweak phase transition, which gives masses to the W and Z gauge bosons and to fermions, is instead uncertain, depending on the value of the Higgs boson mass.

The importance of cosmological phase transitions for the following work lies in the fact that they might be at the origin of a primordial magnetic field (*cf.* section 2.3.3). Magnetic fields characterised by a helical component can be associated with the process of electroweak *baryogenesis*.

The conservation of the baryon number, well established by experimental particle physics, clashes with the observation that the universe is composed almost entirely of matter. The baryon density of the universe η is well constrained by CMB measurements and by nucleosynthesis, and there is no evidence for the presence of primordial antimatter. One should therefore look for a process responsible for the generation of this baryon asymmetry. Three conditions must be satisfied for the production of a baryon asymmetry: baryon number violation, C and CP violation, and departure from thermal equilibrium. The electroweak phase transition could in principle be an epoch where these three conditions are satisfied. If the transition is first order, then thermal equilibrium is naturally broken. The probability of baryon number non-conserving processes, which can arise at the non-perturbative level and are normally suppressed at low temperature, is increased during the phase transition. C symmetry is maximally broken in the standard model, and CP violation is observed experimentally in weak interactions. However, CP violation turns out to be too small in the standard model to generate a large enough baryon asymmetry; moreover, the mass of the Higgs boson appears to be too large for the phase transition to be first order (the current lower bound is 115 GeV, and the transition is second order for masses bigger than 100 GeV). Therefore, the question of the baryon asymmetry of the universe cannot be solved in the context of the standard model of particle physics: one needs to postulate some extension of it, or invoke other mechanisms such as leptogenesis.

Inflation

The standard cosmological model can explain remarkably well the history of the universe from the epoch of nucleosynthesis onward; however, it requires extremely improbable initial conditions. The theory of inflation provides an explanation for these initial conditions within the context of classical gravitation. It attempts to find a class of models, described by classical general relativity, for which the FRW cosmology is an attractor solution: so that, whatever the initial conditions, the cosmological model at low temperature $T \lesssim 1$ MeV will be the one we observe today: a homogeneous and isotropic FRW model, with small fluctuations $\delta g_{\alpha\beta} \sim 10^{-5}$. The only way for a homogeneous and isotropic solution to become an attractor, is to render gravitation "repulsive", and violate the strong energy condition $\rho + 3p > 0$. This is realised by the vacuum energy of a scalar field (or, equivalently, by a cosmological constant $\Lambda = \rho_V > 0$), for which $T_{\alpha\beta} = -\rho_V \, g_{\alpha\beta}$, $w = p_V/\rho_V = -1$ and therefore $\rho_V + 3p_V = -2\rho_V < 0$. The solution of Friedmann equations for a universe dominated by vacuum energy is such that the expansion is accelerated, $\ddot{a} > 0$ (see Eq. (1.67)), and in the case of flat spatial sections one finds

$$a(t) = a(t_i) \exp\left(\sqrt{\frac{\rho_V}{3}}\,(t - t_i)\right). \tag{1.77}$$

We will now see how this particular behaviour for the scale factor can provide solutions to the problems of standard Big Bang cosmology.

If one considers the size of the universe today, $H_0^{-1} \simeq 10^{28}$cm, and evolves it backward in time up to the Planck epoch, $t_{\rm Pl} = 5.39 \times 10^{-44}$ sec, one finds that at this time the universe had a size of about 10^{-3} cm: 10^{30} times bigger than the Planck scale, $\ell_{\rm Pl} = 1.62 \times 10^{-33}$ cm. Why was the universe so big when it started? Moreover, at the present time the universe is very flat: $1 - \Omega = \Omega_\kappa \simeq 0$, even though the curvature is growing with time in a FRW model, $\Omega_\kappa \propto a^{1+3w}$. In order to have $\Omega \simeq 1$ today, one needs to require $\Omega(t_{\rm Pl}) = 1$ with a precision of 60 orders of magnitude. Why was the universe so flat when it started? If one computes the total entropy of the universe, one finds $S = sa^3(\eta) \simeq H_0^{-3}T_0^3 \simeq 10^{88}$: once again, such a huge number seems unnatural. These three puzzling characteristics of the FRW model are known as the *size/flatness/entropy problems*. The *horizon problem* is connected with the homogeneity and isotropy of the spacetime. A region of the size of the horizon at the epoch of last scattering is seen today under an angle of approximatively 1.7°, so that two points on the sky at bigger angular distance have never been in causal contact; yet they are at the same temperature, for one part in 10^5. So, the observed isotropy of the CMB appears to be in contradiction with the existence of a particle horizon in the FRW model.

A sufficiently long inflationary phase in the early universe can account for all these problems. Suppose that inflation starts in a region of size $\ell_{\rm Pl}$; Eq. (1.77) shows that, at the end of inflation, this region would have grown exponentially, by a factor $a(t_e)/a(t_i)$. Adjusting this factor to be 10^{30}, one can easily account for the size problem. Moreover, during an inflationary phase, $\Omega_\kappa \propto \exp(2H(t_i - t))$, so the curvature would decay to zero with time. The particle horizon instead would grow exponentially, as can be seen from Eqs. (1.65) and (1.77), while H^{-1} would remain approximately constant: a long lasting inflation would allow the particle horizon to grow enough to put in causal contact the entire observable universe.

Whatever the initial conditions, a large, flat and young-looking universe will be the result after an inflationary phase: exponential expansion will make a small, smooth and causally coherent patch of size less than H^{-1} grow to such a size that it can easily encompass the comoving volume that becomes the observable universe today.

The basic idea is that inflation is driven by the vacuum energy of a scalar field, called the inflaton, which dominated the energy density of the universe in some early epoch of its evolution. Therefore, it involves the dynamical evolution of a weakly coupled scalar field, that was at one time displaced from its minimum. The inflaton dynamics in the expanding universe will be analysed in chapter 6. In general, it must be distinguished in two phases: a phase of "slow roll", when the field evolves toward the real vacuum, which induces the exponential expansion of the scale factor; and a phase of "reheating", in which the scalar field oscillates around the minimum of the potential, and can decay into lighter particles (radiation or massive fields). As these particles thermalise, the cold, empty universe which was the result of the first inflationary phase is reheated and enters the standard, hot Big Bang era. During this process, a massive entropy production takes place, that accounts for the entropy problem stated before.

A fundamental property of inflation is that it has the means to produce density perturbations on cosmologically interesting scales. In the standard model, the metric must be characterised by the presence of small perturbations of the homogeneous and isotropic state, which account for the small temperature fluctuations observed in the CMB, and which provide the seed for the formation of structure in the universe. In the inflationary theory, these perturbations are a result of quantum mechanical fluctuations of the inflation scalar field in the expanding space. The spectrum of these quantum fluctuations is characterised by the same power at each scale. The important point is that, even though quantum fluctuations on a given scale arise when the scale is sub-horizon sized, subsequently, the scale is stretched with the expansion of space, and soon becomes larger than the Hubble radius. When that happens, it decouples from the micro-physics, and "freezes in" as a classical, metric perturbation. When inflation ends, and the Hubble radius starts growing again, these fluctuations eventually re-enter the horizon as density perturbations with a scale-invariant spectrum. This property corresponds to what is observed in the measurements of CMB temperature fluctuations.

Chapter 2

Cosmic magnetic fields

This chapter concerns the origin, evolution and features of magnetic fields in the early universe. After first motivating the study of cosmic magnetic fields, we proceed with a brief review of the experimental evidence for the presence of large scale magnetic fields in astrophysical objects. The origin of the observed magnetic fields is still an open problem in cosmology; in particular, we will be concerned with the issue of whether the seed for these magnetic fields can be generated before the epoch of recombination. We present in this chapter a summary of the proposed creation mechanisms taking place in the primordial universe, and an analysis of the time evolution of the magnetic field after its generation. The last part of the chapter deals with stochastic magnetic seeds, and presents the results obtained in the original work of reference [18].

2.1 Motivation

Magnetic fields are ubiquitous in the observable universe. They exist in stars and planets, but there is also evidence for their presence in the Milky Way and in external galaxies, in clusters of galaxies, and in high redshift objects. Remarkably, in all the latter structures, the magnetic fields intensity is roughly of the same order of magnitude: $0.1 - 10\,\mu$G. This is one of the features that makes it so difficult to find an explanation for the origin of the magnetic fields, and strongly points toward a common generation mechanism. The preferred, although still very debated, theory for their formation is that they result from the amplification of weak seed fields by a dynamo mechanism, taking place during the formation of structures.

The dynamo is not mandatory: magnetic fields could also grow by adiabatic contraction of the field lines during the gravitational collapse of galaxies, but in that case the seed must be of much bigger amplitude, in order to account for the observed amplitudes. There have been several propositions for the explanation of the seed fields, and the alternative is whether they originated prior or after the epoch of recombination. The hypothesis of a primordial origin is particularly appealing, because it can provide the presence of seed magnetic fields on very large scales, and account for the ubiquity of the observed fields. A crucial aspect for the survival of magnetic fields from such remote epochs of the universe's evolution until today is the high electrical conductivity of the medium: a feature which is satisfied throughout the history of the universe, as will be clarified later on. Moreover, in the early stages of its evolution, the universe seems to possess favourable conditions for magnetogenesis, in particular during the period of phase transitions. Many primordial generation mechanisms have been proposed so far; however, it is still debatable whether they actually create magnetic fields which are strong enough to account for those observed today, after undergoing some sort of amplification during the formation of structure. The features of the subsequent time evolution of the magnetic field in the primordial plasma are probably determinant for the resolution of this question, particularly if the magnetic field is helical, that is, characterised by a non-zero component in the direction of the electric current. Moreover, the presence of a primordial magnetic field can affect a number of relevant processes which took place in the primordial universe, as well as the geometry of the universe itself. Therefore, the amplitude of the magnetic field cannot be too large: it could spoil the well-established development of the standard hot big bang model.

In conclusion, even though the presence of magnetic fields in the Galaxy has been known for fifty years [19], this issue is far from being solved, and the proposition that these magnetic fields could be of primordial origin has widened and enriched the discussion. Complete reviews on the subject are [20–23].

2.2 Magnetic fields observations

There are three main techniques for the observation of astrophysical magnetic fields: Zeeman splitting of spectral lines, intensity and polarisation of synchrotron radiation, and Faraday rotation. They can respond to different components of the field, either the plane-of-the-sky component $B_\perp$, or the line-of-sight component $B_\parallel$. The last two techniques necessitate an independent measure of the local electron density, which is not always easy to determine. In general the observed magnetic field is thought to have two components, a uniform and a random one.

Zeeman splitting: the energy levels of a hydrogen atom in the presence of a magnetic field are not degenerate, and this causes a splitting in the emission (or absorption) spectral lines, of the order

$$\Delta\nu = \frac{eB}{2\pi m_e}\,. \tag{2.1}$$

This measurement technique is sensitive to the uniform component of the magnetic field, and leads to a direct determination of the magnetic field strength from the estimate of the splitting. Unfortunately, the Zeeman effect is small compared to the Doppler broadening of the lines due to thermal motion of atoms and molecules in the interstellar medium. As a result, this technique can only be used to determine the magnetic field of the Milky Way.

Synchrotron radiation: electrons accelerated by a magnetic field radiate energy at a rate

$$I(\nu) \propto {B_\perp}^{(1+\alpha)/2}\nu^{(1-\alpha)/2} \tag{2.2}$$

per unit volume, time, frequency and solid angle, where α is the spectral index of the electron number density distribution as a function of energy, $n_e(E) = n_0 E^{-\alpha}$. This technique is sensitive to the plane-of-the-sky component of the magnetic field. Once the intensity of the emission has been estimated, the magnetic field can be derived only by specifying the electron density distribution of the source, which is in general not known. In cluster of galaxies it is sometime possible to deduce it from observations of X-ray emission from the very hot electron gas: the shape of the emission spectrum depends on the abundances and on the temperature [24]. Otherwise, the usual assumption is equipartition between the electrons and magnetic field energy densities. Synchrotron radiation is also polarised, with polarisation direction perpendicular to $B_\perp$ and polarisation strength dependent on the random component of the field.

Faraday rotation: the presence of a magnetic field in an ionised plasma sets a preferred direction for the gyration of electrons, and therefore a difference in the index of refraction for left versus right circularly polarised light crossing the medium. A linearly polarised wave can be seen as the superposition of two circularly polarised rays, and therefore its direction of polarisation will get rotated by this effect. The rotation angle ϕ for a wave of wavelength λ is

$$\frac{\phi}{\lambda^2} = 812 \int_0^{z_s} \frac{n_e}{\mathrm{cm}^{-3}} \frac{B_{\parallel}}{\mu\mathrm{G}}\, d\left(\frac{\ell(z)}{\mathrm{kpc}}\right) \frac{\mathrm{rad}}{\mathrm{m}^2}\,, \tag{2.3}$$

where z_s is the redshift of the emitting source. This measurement is sensitive to the line-of-sight component of the magnetic field, and since it is an integral over distances, the effect of large distances will reflect in high values of measurement. In this case as well, an independent knowledge of the electron density is required. For our galaxy, an estimation of the electron density can be achieved by observing the radiation emitted from pulsars, whose regular pulses are delayed if passing through the interstellar medium, since light travel faster in vacuum. Otherwise, the measurement of the magnetic strength in other objects is dependent on the model chosen for the electron density.

We proceed now with a brief description of the observational situation.

Galactic magnetic fields

Observations show that the magnetic field lines in spiral galaxies closely follow the spiral arms. The magnetic field is therefore predominantly toroidal, and galactic magnetic fields are classified according to the parity under rotation of an angle π about the galactic centre; galaxies with even parity fields are called axisymmetric spirals, with odd parity bisymmetric spirals (*cf.* Fig. 2.1). This distinction is of fundamental importance in order to assess the primordial nature of the observed fields: if the field has been generated by a dynamo mechanism, then the axisymmetric configuration is preferred, while primordial magnetic fields are associated with the bisymmetric configuration. Another distinctive feature is that a dynamo mechanism would lead to equipartition between the magnetic field and the kinetic energy densities. Connected to the field configuration is the observed reversal of the magnetic field direction. Observations of the Milky Way indicate the presence of three reversal in the solar circle, and possibly a fourth one near the Perseus arm: this seems to be consistent with a bisymmetric configuration. Moreover, the magnetic field of our galaxy is parallel to the

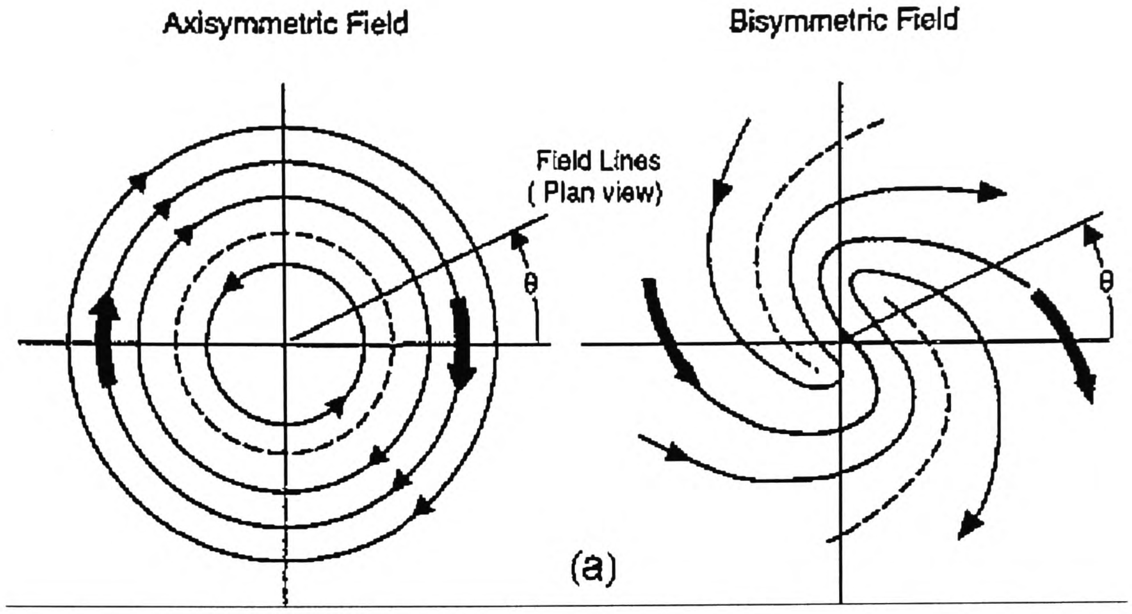

Figure 2.1: This figure shows the model of the axisymmetric and bisymmetric magnetic field configurations in a galactic disk [20] .

galactic plane and mostly toroidal, although a poloidal component has been detected in the centre, which is of the order 1/3 of the toroidal component. The strength of the regular field is 1.8 ± 0.3 μG, and equipartition between the magnetic field and relativistic particles energy densities appears to hold in our galaxy. The total field strength can reach as much as 6 μG, indicating the possible presence of a strong stochastic component [23].

The characteristics of galactic magnetic fields are not homogeneous: for some observed galaxies equipartition does not hold, with the magnetic field strength exceeding the equipartition value, and the geometrical structure is also varying from case to case. In general, one can assume that galactic magnetic fields are characterised by an intensity of the order of a few μG, and that they keep their orientation on the kpc scale (although attempts to find the typical length scale of the magnetic fields fluctuations have not yet produced a coherent picture). It is clear that this mixed observational situation does not help any conclusion about the possible origin of the observed fields.

Cluster magnetic fields

The existence of μG magnetic fields in clusters of galaxies appears well-established [25]: in spite of the necessary physical assumptions often connected with the different measurement techniques, all observational data are consistent with this order of magnitude estimate. Typical values of the reversal field length are $1 - 100$ kpc. Studies of the synchrotron emission from the radio halo of the Coma cluster indicate the presence of a magnetic field in the cluster of the order of $0.3 - 2$ μG. Beside synchrotron emission, a standard tool for measuring the field in clusters is Faraday rotation studies of cluster centre radio sources. Using this technique, a magnetic field of $2-10$ μG has been estimated in the cluster atmosphere enveloping the radio galaxy Cygnus A; for the radio galaxy Hydra A, a large scale field of 7 μG, and a tangled component of 40 μG have been found, with the large scale component ordered on 100 kpc scale. Faraday rotation can be observed also in the polarised emission from background radio sources, seen through a cluster atmosphere. The observation of radio sources behind 16 Abell clusters with X-ray emission, performed in [26], lead to magnetic fields of the order of μG, extending to 0.5 Mpc from the centre, in all the clusters. A very interesting tool is the use of cosmological magnetohydrodynamic simulations to study the evolution of magnetic fields in clusters, and make predictions about the magnetic field power spectrum [27]. The strength of the intra-cluster magnetic field and its power spectrum can be inferred by comparison between the simulations and the observed polarisations of the radio galaxies and halos within the cluster [28, 29]. The simulations seem to confirm that μG magnetic fields and Faraday rotation observations are well reproduced starting from an initial magnetic field of 10^{-9} Gauss. Moreover, it seems that the final magnetic field configuration is dominated by the cluster collapse: the initial configuration, homogeneous or stochastic, is lost after the collapse [30].

In conclusion, the observed strength of cluster magnetic fields is comparable to that of galactic fields: this strongly disfavours the possible explanation of the origin of cluster magnetic fields by simple ejection from galactic magnetic fields [22].

Magnetic fields in high redshift objects

Radio galaxies and quasars have been detected at redshifts $z > 2$. They emit polarised light which provides, through Faraday rotation observations, an ideal probe of their environment. It appears that these high redshift sources are situated behind dense Faraday screens of magnetised, ionised plasma. By analogy with lower-z radio galaxies, it has been proposed that the high-z sources might be embedded in magnetised proto-cluster atmospheres, with magnetic fields strength again of the order of μG [20, 25]. This observation poses a serious challenge to the galactic dynamo picture, since at that time galaxies should have rotated only few times.

2.3 The origin of magnetic fields

There have been several attempts to explain the presence of magnetic fields in astrophysical objects. The general picture is that, because of the high conductivity of the universe, magnetic fields lines follow the motion of the cosmic fluid. Magnetic flux is neither created nor destroyed in large amount in galaxies at present, so the existing field must have been formed at an earlier epoch. Indeed, a seed magnetic field on large scales can get amplified during the gravitational collapse of structures. The amplification factor can be of several orders of magnitude, assuming that a dynamo mechanism takes place during the collapse. Many models have been proposed to explain the generation of the pre-galactic seed, which can take place before or after recombination. The "cosmological" generation mechanisms, taking place before recombination, can be divided in two categories: *causal mechanisms*, for which the magnetic seeds are produced at a given scale inside the horizon, and *inflationary mechanisms*, for which correlations in the magnetic field are produced outside the horizon. In the following we will present a brief review of some of the generation models which have been proposed up to date. The cosmological ones are very interesting from the theoretical point of view, providing a fruitful connection between cosmology and particle physics: many of them are based on new ideas in particle theory. However, they are lacking in predictiveness: depending on the model, the predicted amplitude for the seed can vary from very tiny (10^{-65} Gauss) to surprisingly high (10^{-9} Gauss). The causal mechanisms are a bit more promising in this respect; however, in this case the seeds are produced on very small scale, and the fundamental issue is therefore how to extrapolate the correct amplitudes at the required galactic and clusters scales.

2.3.1 Adiabatic compression and dynamo mechanism

The simplest way to account for galactic magnetic fields is to assume that they result directly from seeds which get *adiabatically compressed when the proto-galactic clouds collapse.* Due to the large conductivity of the intergalactic medium, magnetic flux is conserved (*cf.* section 2.4.3). Therefore, the magnetic field increases like the inverse square of the size of the system, which decreases from about 1 Mpc to about 30 kpc. It follows that

$$B_s = B_g \left(\frac{\rho_c}{\rho_g}\right)^{\frac{2}{3}}, \tag{2.4}$$

where the ratio between the energy density in the proto-galactic patch of size 1 Mpc and the galaxy energy density is of the order 10^{-6}. To account for the observed μG magnetic field, the seed needed at the galaxy formation time, $z \sim 5$, adiabatically rescaled to the present time (*cf.* Eq. (2.35)), is

$$B_s = 10^{-10}\ \text{Gauss}\,. \tag{2.5}$$

The spatial structure of the field produced by this mechanism, followed by differential rotation of the disk, is bisymmetric spiral, with reversal along the galactic radius and no reversal across the galactic plane. Equipartition between the field energy and the kinetic energy is unexplained by this mechanism. The same consideration can be applied to clusters. To explain the observed value of about 10^{-7} Gauss by compression of an inter-galactic field, one requires a seed of 10^{-9} Gauss, given that the present day over-density in clusters is of about $\delta \sim 10^3$.

The other leading picture for the origin and maintenance of galactic magnetic fields is the *dynamo theory.* This is a mechanism responsible for the conversion of kinetic energy of an electrically conducting fluid into magnetic energy. As for the adiabatic compression, it is based on the feature of negligible magnetic diffusion; however in this case, the resistivity of the medium should be small, but not zero. A non-vanishing seed field is required to initiate the process, which is maintained by the presence in the structure of hydrodynamic turbulence, differential rotation, and fast reconnection of the magnetic field lines. If the conductivity is sufficiently high, the magnetic flux lines are stretched and twisted by the turbulent motion of the fluid. Turbulence and global rotation of the fluid can produce the twisting of closed magnetic flux tubes; if the resistivity is not zero, two twisted loops can merge together, changing the topology of the field and restoring the initial one-loop configuration, but with double flux [31]. The simplest theory is the mean field (or $\alpha - \Omega$) dynamo, which studies the evolution and amplification of the mean large-scale component of the magnetic field. This theory predicts an exponential amplification for the field, and the reaching of the equipartition value between the magnetic field energy and the kinetic energy of the fluid. When equipartition is reached, the amplification process stops. We proceed now to analyse the mean field dynamo in a bit more details. Note that the following equations are given in the context of flat space-time, and deal therefore with the "lab" magnetic field: *cf.* section 2.4.1. The mean field dynamo is based on the assumption that the magnetic field and the fluid velocity can be decomposed into an average part, varying only on the large scale, and a weak, small-scale fluctuating part:

$$\mathbf{B} = \langle \mathbf{B} \rangle + \mathbf{b}\,, \qquad \qquad \mathbf{V} = \langle \mathbf{V} \rangle + \mathbf{v}\,, \tag{2.6}$$

where the average is over an ensemble of many realisations of the turbulent velocity field. This averaging procedure is conceptually equivalent to average over scales and times exceeding the characteristic correlation scale and time of the turbulent velocity field (the scale of variation of the galactic turbulent motions is generally less than 100 pc, while the scale of variation of the mean component of the magnetic field is longer than a kiloparsec). $\langle \mathbf{V} \rangle = \mathbf{\Omega}(\mathbf{r}) \times \mathbf{r}$ is taken to be the differential rotation of the galactic disk, where $\mathbf{\Omega}(\mathbf{r})$ is the angular velocity, and $\mathbf{v}$ the turbulent motion generated by stars and supernovae. The magnetic field satisfies the diffusion equation [12] (*cf.* also section 2.4.1)

$$\frac{\partial \mathbf{B}}{\partial t} = \nabla \times (\mathbf{V} \times \mathbf{B}) + \frac{1}{\sigma} \nabla^2 \mathbf{B}\,; \tag{2.7}$$

in this picture, it is further assumed that the scale of variation of the turbulent motions is large in relation to the dissipative scales, so that the diffusion term on the right-hand-side can be dropped. One now breaks the above evolution equation into a mean part and a random part, aiming to derive an evolution equation for $\langle \mathbf{B} \rangle$ in terms of any statistics of the turbulence. Transforming to a moving coordinate system, one can temporarily set $\langle \mathbf{V} \rangle = 0$, and one obtains [32]:

$$\frac{\partial \langle \mathbf{B} \rangle}{\partial t} = \nabla \times \epsilon \tag{2.8}$$

$$\frac{\partial \mathbf{b}}{\partial t} = \nabla \times (\mathbf{v} \times \langle \mathbf{B} \rangle) + \nabla \times (\mathbf{v} \times \mathbf{b}) - \nabla \times \epsilon\,, \tag{2.9}$$

where $\epsilon = \langle \mathbf{v} \times \mathbf{b} \rangle$ denotes the average electric field generated by the small scale turbulence. In order to evaluate this quantity, one neglects the non-linear terms on the right-hand-side of Eq. (2.9), and re-expresses ϵ in terms of $\mathbf{v}$ and $\langle \mathbf{B} \rangle$ as [32]

$$\epsilon = \langle \mathbf{v}(t, \mathbf{x}) \times \int_{-\infty}^{t} dt' \, \nabla \times (\mathbf{v}(t', \mathbf{x}) \times \langle \mathbf{B} \rangle) \rangle \,. \tag{2.10}$$

On the assumption that the turbulent velocity field is statistically homogeneous and isotropic, and independent on $\langle \mathbf{B} \rangle$, ϵ is a linear function of $\langle \mathbf{B} \rangle$ and its first derivatives. The most general expression is given by [32]

$$\epsilon = \alpha \langle \mathbf{B} \rangle - \beta \nabla \times \langle \mathbf{B} \rangle \,, \tag{2.11}$$

and one finds

$$\alpha = -\frac{\tau_c}{3} \langle \mathbf{v} \cdot \nabla \times \mathbf{v} \rangle \,, \qquad \beta = \frac{\tau_c}{3} \langle \mathbf{v}^2 \rangle \,; \tag{2.12}$$

τ_c denotes the correlation time of the velocity field, α represents the mean helicity of the turbulence, and β the kinetic energy. The evolution equation for the mean component of the magnetic field (2.8) becomes then

$$\frac{\partial \langle \mathbf{B} \rangle}{\partial t} = \nabla \times \alpha \langle \mathbf{B} \rangle + \beta \nabla^2 \langle \mathbf{B} \rangle + \nabla \times (\langle \mathbf{V} \rangle \times \langle \mathbf{B} \rangle) \,, \tag{2.13}$$

where we have reintegrated the mean velocity term. In order to solve this equation, one introduces cylindrical coordinates (r, ϕ, z). In terms of the radial and azimuthal components of the galactic magnetic field, the above equation can be written, under certain assumptions, as [33]

$$\frac{\partial \langle B_\phi \rangle}{\partial t} = -\Omega \langle B_r \rangle \tag{2.14}$$

$$\frac{\partial \langle B_r \rangle}{\partial t} = -\frac{\partial \alpha \langle B_\phi \rangle}{\partial z} \,. \tag{2.15}$$

First of all one makes the assumption that the β-term in Eq. (2.13), describing the additional field dissipation due to the turbulent motion, can be neglected with respect to the α-term. Moreover, the r dependence of the angular velocity is taken to be $\Omega \sim r^{-1}$. The radial derivatives coming from the curl in Eq. (2.13) have been dropped with respect to the derivatives in z, and one can see that under these assumptions the evolution equation for the B_z component decouples from the ones above, and can be neglected [33]. The second equation

(2.15) illustrates the so-called α effect: conversion of the toroidal component of the field into a poloidal one; to complete the dynamo cycle, the amplification of the poloidal component is converted back into a toroidal one, by the differential rotation of the galactic disk: this is the Ω effect. To show that equations (2.14), (2.15) lead to a growing solution, one assumes $\langle B_\phi \rangle$ and $\langle B_r \rangle$ proportional to $e^{\gamma t}$, both independent on z. Furthermore, one needs an estimate for $\alpha(z)$; we follow the model of reference [33], $\alpha = \alpha_0 z/h$, with $-h < z < h$. Then, the solution becomes $\langle B_r \rangle = -(\alpha_0/h\gamma)\langle B_\phi \rangle$, $\langle B_\phi \rangle = -(\Omega/\gamma)\langle B_r \rangle$, so that the growth factor is $\gamma^2 = \Omega\alpha_0/h$. Using $\alpha_0 \sim 1\,\text{km/sec}$, $\Omega \sim 10^{-15}\,\text{sec}^{-1}$, $h \sim 300$ pc, R. Kulsrud [33] finds the approximative value of $\gamma^{-1} \sim 10^8$ years. A more precise estimation of γ is given for example in reference [34], in which G. Fields determines $\gamma = 2.5\,\text{Gy}^{-1}$. For a galactic age of $10\,\text{Gy}$, this gives an amplification factor of $e^{25} = 7 \times 10^{10}$: to account for the μG field observed, one needs a seed of about 10^{-17} Gauss, over a typical scale of $30 - 100$ kpc, right after the collapse of the galaxy. This gives an initial condition of

$$B \sim 10^{-21}\ \text{Gauss}\,,$$

over a scale of 1 Mpc. The actual effectiveness of the galactic dynamo, and consequently the required order of magnitude for the seed field amplitude, are still debated: one of the main problems seems to be that this picture neglects the amplification of small scale fields, which could reach equipartition and stop the process before the mean field is developed at galactic scales [33, 35]. The application of a dynamo mechanism to explain magnetic fields in clusters is also considered problematic, the reason being that clusters rotate less than galaxies; the same argument applies to the explanation of the presence of μG fields in high redshift galaxies.

2.3.2 Magnetogenesis after recombination

The mechanisms that can produce the required seed field in the epoch after matter-radiation decoupling all rely on charge separation processes. The principle is the Biermann battery mechanism [23]: the presence of a gradient in the pressure of electrons of the plasma gives rise to a thermoelectric current term $\nabla P_e/(en_e)$, whose curl appears as a source for the magnetic diffusivity equation (2.32). The magnetic field grows linearly in time, and the magnetic field intensity due to this process can be estimated as $B \sim (t/en_e^2)|\nabla n_e \times \nabla P_e|$. The Biermann battery alone can generate magnetic fields with strength 10^{-19} Gauss in the interstellar medium [36]. Several astrophysical mechanisms have been proposed that invoke some sort of Biermann battery and then evolve the seed obtained in different ways: for example, in [37] and [38], turbulence arising in the proto-galactic cloud is responsible for the amplification. These kinds of processes, however, can hardly be responsible for magnetic fields in galaxy clusters. In [39], a seed of 10^{-20} Gauss on galactic scales is formed at the re-ionisation epoch, $z \gtrsim 5$, by a thermally generated electric field at the ionisation fronts. The most interesting mechanism up to date is given in [40]; the model is based on charge separation by anisotropic radiation pressure at the epoch of re-ionisation, and provides a remarkably high seed of the order of $10^{-5}\mu$G, suitable for simple adiabatic collapse.

2.3.3 Magnetogenesis prior to recombination

Generation from primordial vorticity

Seed magnetic fields can be created out of nothing during the radiation dominated epoch, provided that vortical motions are present in the primordial plasma. The generation mechanism is also based on charge separation, caused by the fact that electrons and protons have the same charge but very different masses. This mechanism was first proposed in [41, 42], where it is claimed that it can produce an intergalactic magnetic field today of 10^{-8} Gauss on 1 Mpc scale. It is based on the fact that the ions and electrons rotational velocities should decrease differently with the scale factor in the pre-recombination era, because Thomson scattering couples the electrons to the photons of the plasma, whereas ions gets non-relativistic before. The differential motions of electrons and ions generate an electromotive force which gives rise to a magnetic field. The problem with this scenario is that vorticity is decaying: in order for this effect to be substantial at recombination, vorticity should dominate the universe at matter-radiation equality epoch, and this strongly affects the formation of structure [43]. Moreover, vector perturbations cannot be created in the very early universe as it happens for scalar and tensor perturbations, since vorticity must be conserved. A possible way out is given in [44], where the plasma vorticity is produced by cosmic strings after the beginning of structure formation. In this case vorticity does not decay with the expansion of the universe, and the mechanism described above can operate, provided that a sufficient amount of ionisation is generated by the turbulence. Vorticity driven by cosmic strings might generate a magnetic seed of 10^{-18} Gauss on scales $10-100$ kpc, suitable for amplification by galactic dynamo. The possibility of magnetogenesis at recombination via charge separation processes has been reanalysed more recently in [45, 46], which find however quite different amplitudes for the seed: 10^{-20} Gauss in the first case, 10^{-8} Gauss in the second case.

Generation from a phase transition

The first proposition that a cosmological phase transition may generate a magnetic field has been put forward by Hogan [47]. In this seminal paper he argues that an unspecified mechanism might operate at a first order phase transition, giving rise to a magnetic field coherent on a scale L of the order of the size of the bubbles, which is at most the size of the horizon at the epoch of the considered phase transition. The amplitude of the field on a bigger length scale λ is estimated by performing a volume average of the fields produced by $N = \lambda^3/L^3$ randomly oriented dipoles, to find

$$B_\lambda = B_L \left(\frac{L}{\lambda}\right)^{\frac{3}{2}} . \tag{2.16}$$

We will argue about the correctness of this claim in section 2.5.2; it is important to keep in mind that this result has been widely used in the literature for the estimation of the amplitude of magnetic fields generated at first order phase transitions. Indeed, a fundamental issue for primordial generation mechanisms is to model how the seed fields, which are characterised by a coherence length of at most the Hubble size at formation ($\eta_{\rm ew} \sim 10^{-4}$ pc in the case of the electroweak (EW) phase transition, for example) are transformed into macroscopic scale magnetic fields. Concerning the time evolution, it is normally assumed that the magnetic field energy density decays like radiation, as a^{-4} (*cf.* section 2.4.3).

In [48], Quashnock *et al.* considered the possibility of generating magnetic seeds at the QCD phase transition, by a mechanism similar to the Biermann battery: the formation of electric fields behind the shock fronts which precede the expanding bubbles, due to the different dynamical response of the baryonic and leptonic fluid. Small scale magnetic fields are formed by the currents induced by the electric field; however, these fields turn out to be too weak at the relevant galactic scales. Cheng and Olinto [49] analysed a different mechanism, based on charge separation at the boundaries between the quark and hadron phases when the broken and symmetric phases coexist, which can give stronger amplitudes for the field; using the scaling law (2.16), they found a seed of 10^{-20} Gauss at the present time, on a kpc scale. Other interesting values for a seed field created in this way are found by Sigl *et al.* [50], who also consider the formation of hydrodynamical instabilities at the bubble walls. These instabilities could give rise to turbulence in the plasma on scales of the order of the bubble size, and consequently the seed field could be amplified by magnetohydrodynamic effects up to equipartition level: this gives a field strength of 10^{-29} Gauss in the case of the EW phase transition, and 10^{-20} Gauss for the QCD phase transition, on the remarkably large scale of 10 Mpc. A similar mechanism was previously analysed by Baym *et al.* [51] in the case of the EW phase transition: small seed fields are created via the dipole electromagnetic charge layers that form on the surfaces of the bubbles, and are then amplified by the turbulence in the fluid given by the collision of the shock fronts preceding the bubbles. If there is time for reaching equipartition, the fields today can be of $10^{-17} - 10^{-20}$ Gauss on kpc scale. This value is found considering that the large scale field is a superposition of the fields at bubble size; however, instead of assuming a random walk of field dipoles like in [47], the authors used a continuum approximation for their distribution. More recently, Boyanovsky *et al.* [52] studied in more generality the issue of magnetogenesis during phase transitions in the radiation dominated epoch, and confirmed that large scale magnetogenesis is possible. They claim a seed of 10^{-14} Gauss on 1 Mpc at the QCD phase transition, and of 10^{-23} Gauss at the EW phase transition.

Concerning the generation of magnetic fields, the EW phase transition can be generally more interesting than the QCD, because the electromagnetic field can be directly influenced by the dynamics of the Higgs field which drives the transition. Indeed, before the EW phase transition it is not even possible to define the electromagnetic field, and this operation remains non-trivial until the transition is completed [22, 53, 54]. The issue is the need of a gauge-invariant definition of the electromagnetic field, which should reproduce the standard definition in the broken phase with a uniform Higgs background. The case of a first order transition has been analysed by Ahonen and Enqvist [55], giving rise to a field of 10^{20} Gauss and coherence length 10^4 GeV^{-1} at the end of the phase transition. Assuming turbulent enhancement of the field, and a volume average $B \sim 1/L$, they found the value 10^{-21} Gauss on scale 10 Mpc today. In [56], Vachaspati argued that magnetic fields can be generated at the EW phase transition even if it is second order. The formation process is similar to the formation of topological defects, and is based on the fact that the gradients in the Higgs field appear in the definition of the electromagnetic field. Two subsequent analysis [57, 58], have revised this work examining the definition of the electromagnetic field and the averaging procedure which were used (see section 2.5.2).

Generation of helical magnetic fields

Magnetic helicity is defined by

$$\mathcal{H} = \int_V d^3x \, \mathbf{A} \cdot \mathbf{B} \,, \tag{2.17}$$

where $\mathbf{A}$ is the vector potential. The properties and meaning of this quantity will be presented in section 2.4.3. In particular, magnetic helicity has the remarkable property of being conserved in a medium with sufficiently high conductivity. A magnetic field with non-vanishing helicity is very interesting for several reasons. First of all, the presence of a helical term can lead to an inverse cascade mechanism, in which the magnetic field undergoes a transfer of power to larger and larger scales: this could be of fundamental importance for causally created magnetic fields, which are normally coherent on too small scales compared to the ones observed today. Moreover, in field theory language, helicity coincides with a Chern-Simons term, which is related to the topological properties of the gauge fields; it is a P- and CP-odd function, so its presence is a macroscopic manifestation of violation of both these symmetries. There have been many propositions for the production of helical magnetic fields in the early universe starting from particle physics processes. The first work appears to be [59], in which Cornwall discussed the production of electromagnetic helicity associated with the generation of EW Chern-Simons number through non-conservation of baryon and lepton numbers. He found that the translation of EW helicity into magnetic helicity gives rise to a residual magnetic helicity after the EW transition of $\mathcal{H} = \alpha^{-1}(N_B + N_L)$, where α is the fine structure constant and N_B, N_L the baryon and lepton numbers today. A similar process was analysed more recently in [60, 61], where it is also claimed that EW baryogenesis creates a left-handed magnetic field with helicity density today of $10^2 \, N_B$. The helicity and baryon number are carried, in this scenario, by the twisting and linking of EW strings, arising at the phase transition. The time evolution of the helical seed with the expansion of the universe is also studied in these references. Another possibility for the creation of primordial helicity is through the coupling between the electromagnetic field and a cosmic pseudo-scalar field, which provides the necessary parity violation [62, 63]: such scalar fields appear in various extensions of the standard model. Finally, a different mechanism was proposed in [64], where Joyce and Shaposhnikov assumed that the variation in the Chern-Simons term is given by the presence of an excess of right-handed electrons over left-handed positrons. Again they found that this asymmetry, providing a macroscopic parity violation, plays a similar role to that played by the fluid vorticity in the dynamo mechanism, and can lead to amplification of magnetic fields.

Generation from inflation

Astrophysical magnetic fields have roughly the same amplitude on different physical scales, which is hard to explain in the context of causal creation mechanisms, but could be a feature of inflationary created fields. Inflation could provide the means to amplify electromagnetic quantum fluctuations that would appear today as large scale magnetic fields; moreover, during inflation the conductivity of the universe is very low, so magnetic flux is not conserved and the magnetic field energy density can grow. The main difficulty in this picture is that quantum fluctuations in the electromagnetic field cannot be amplified by the evolution of the background geometry, because electromagnetism is conformally invariant (*cf.* section 2.4.1). Therefore, in order to produce seed fields at inflation one has to find a way out of this obstacle, and several methods to break conformal invariance have been proposed. In reference [65], Turner and Widrow analysed a coupling between the electromagnetic vector potential and the Ricci scalar or the Ricci tensor. These terms break gauge invariance and give a mass to the photon; they can produce astrophysically interesting magnetic seed, but the result is very model-dependent. Breaking of conformal invariance can also be produced by gauge invariant coupling terms between the electromagnetic field and the curvature tensor, but their contribution leads to far too small magnetic seeds [65]. Another way is by introducing a coupling with a scalar field. This possibility has been analysed in several articles: for example, in [66] the coupling is directly to the inflaton field, in the case of an exponential inflaton potential; in the context of superstring cosmology, the scalar field is taken to be the dilaton [67,68]. More recently, in [69], Bamba and Yokoyama considered dilaton electromagnetism in the context of inflation and reheating; the model they propose is interesting, being the only one to date which could produce seeds with very red spectral index. Another mechanism that has been proposed is based on the presence during inflation of a charged scalar field, which leads to the creation of charged particles during reheating, and the creation of magnetic fields by the charged stochastic currents [70]. More recently, many works have studied the possibility of generating magnetic fields from the acquirement of a non-zero mass to the photon during inflation, given by vacuum polarisation from massless scalar electromagnetism: *cf.* [71, 72] and more recent works of the same authors. The general claim is that all these mechanisms are able to produce magnetic fields which are sufficiently high to be the seed for galactic dynamos. However, for many of them the results are strongly model dependent.

2.4 The evolution of primordial magnetic fields

The time evolution of the magnetic seed in the cosmic fluid is a fundamental issue in the study of primordial magnetic fields. The permanence of the large scale component of the field since the very early universe is guaranteed mainly by two conditions: the absence of magnetic monopoles which could screen the field, and the high conductivity of the universe, which causes the magnetic diffusion time to be much bigger than the Hubble time. On small scales, however, there is dissipation of magnetic energy due to radiative viscosity. Moreover, the presence of a helical component can play an important role in the field time evolution.

2.4.1 Electrodynamics in FRW space-time

The basis of the description of electromagnetic fields in a curved background has been given in section 1.2.4. The form of the energy momentum tensor, Eq. (1.39), implies that a general electromagnetic field cannot be supported in the case of a simple FRW background, since homogeneity and isotropy force a perfect fluid form for the energy momentum tensor. In the following sections we will be neglecting the back-reaction of the presence of electromagnetic fields upon the form of the metric: the assumption is that the electromagnetic energy density is largely sub-dominant with respect to the total energy density of the universe, and does not contribute enough to affect the FRW background (*cf.* chapter 3).

Under this assumption, one can re-express the equations of section 1.2.4 in a FRW background, where ∂_η denotes the partial derivative with respect to conformal time, a stroke denotes the derivative with respect to the spatial coordinates of metric (1.61), and now $\epsilon_{abc} = \delta^1{}_{[a}\delta^2{}_b\delta^3{}_{c]}$. Maxwell's equations become

$$E^c{}_{|c} = q \tag{2.18}$$

$$B^c{}_{|c} = 0 \tag{2.19}$$

$$a\,\partial_\eta E_c + a' E_c = a^3 \epsilon_{cde} B_{e|d} - a^2 J_c \tag{2.20}$$

$$a\,\partial_\eta B_c + a' B_c = -a^3 \epsilon_{cde} E_{e|d}\,, \tag{2.21}$$

and the conservation of charge $\partial_\eta q + 3\frac{a'}{a}q + a\,J^c{}_{|c} = 0$. It is possible to define a new set of variables in terms of which the above equations take the same form as in flat space-time. Rescaling

$$\mathcal{U}_\alpha = a\,u_\alpha\,, \qquad \mathcal{E}_c = aE_c\,, \qquad \mathcal{B}_c = aB_c\,, \qquad \mathcal{J}_c = a^2 J_c\,, \qquad Q = a^3 q\,, \qquad \tilde{\sigma} = a\,\sigma\,, \tag{2.22}$$

one finds simply

$$\mathcal{E}^c{}_{|c} = Q \tag{2.23}$$

$$\mathcal{B}^c{}_{|c} = 0 \tag{2.24}$$

$$\partial_\eta \mathcal{E}_c = \epsilon_{cde} \mathcal{B}_{e|d} - \mathcal{J}_c \tag{2.25}$$

$$\partial_\eta \mathcal{B}_c = -\epsilon_{cde} \mathcal{E}_{e|d}\,, \tag{2.26}$$

and $\partial_\eta Q + \mathcal{J}^c{}_{|c} = 0$, $\mathcal{J}_c = \tilde{\sigma}\mathcal{E}_c$ (note that the components of the spatial vectors defined above are such that, for example, $\mathcal{B}_c = \mathcal{B}^c$). This is the property of conformal invariance of electromagnetism: since the FRW metric (1.61) is conformally flat, all the results in electromagnetism obtained in the context of flat space-time can be straightforwardly transferred to FRW space-time, for scales such that the metric perturbations created by the electromagnetic anisotropies and the induced fluid motions are small [73, 74]. At this point, it is useful to perform a coordinate transformation from the FRW frame to the physical coordinates $dt = a\,d\eta$, $d\mathbf{r} = a\,d\mathbf{x}$. Covariant vectors transform according to $\bar{S}_\alpha = \frac{\partial x^\alpha}{\partial \bar{x}^\beta} S_\beta$, and accounting for the fact that the electric and magnetic fields and the current are purely spatial vectors, one has

$$\mathbf{B}_L = \frac{\mathcal{B}}{a^2}, \qquad \mathbf{E}_L = \frac{\mathcal{E}}{a^2}, \qquad \mathbf{J}_L = \frac{\mathcal{J}}{a^3}, \tag{2.27}$$

and $q_L = q$, $\sigma_L = \sigma$, where the subscript L denotes the variables in the "Lab" frame $(t, \mathbf{r})$ [73]. The set of Eqs. (2.23-2.26) now becomes

$$\nabla \cdot (a^2 \mathbf{E}_L) = a^2 q_L \tag{2.28}$$

$$\nabla \cdot (a^2 \mathbf{B}_L) = 0 \tag{2.29}$$

$$\partial_t (a^2 \mathbf{E}_L) = \nabla \times (a^2 \mathbf{B}_L) - a^2 \mathbf{J}_L \tag{2.30}$$

$$\partial_t (a^2 \mathbf{B}_L) = -\nabla \times (a^2 \mathbf{E}_L), \tag{2.31}$$

$\partial_t (a^3 q_L) = \nabla \cdot (a^3 \mathbf{J}_L)$, and $\mathbf{J}_L = \sigma \mathbf{E}_L$. In particular, we are interested in the time evolution law of the magnetic field in a conductive medium [12]. In the primordial universe one can apply the magnetohydrodynamics (MHD) description, based on the fact that the frequency of collisions between the fluid particles is high enough that the mechanical motion of the system can be described in terms of a single conducting fluid with the usual hydrodynamic variables of density, velocity and pressure. Consequently, in the MHD approximation there are no oscillations in the charge density, and it is customary to neglect the displacement current. Therefore, in the above "Lab" frame, the time evolution for the magnetic field takes the form [12]

$$\partial_t (a^2 \mathbf{B}_L) = \frac{1}{\sigma} \nabla^2 (a^2 \mathbf{B}_L), \tag{2.32}$$

so that the physical diffusion time is $t_{\rm d} = \sigma L^2$, where L is the characteristic length scale of the spatial variation of the field. In order to estimate whether an initial magnetic configuration in a cosmological setting will undergo relevant dissipation, one needs to estimate the conductivity of the universe.

2.4.2 Conductivity of the universe

The conductivity varies in the different epochs of the evolution of the universe, depending on the number of charge carriers and on the dominant scattering process. Three main phases can be distinguished: a phase in which the plasma is relativistic, before e^+e^- annihilation, a phase in which the plasma is ionised, before recombination, and the last phase in which the free charges are the residual electrons left by the decoupling process. The conductivity of the first phase has been evaluated in references [75,76], in which the authors considered a plasma in an electric field, and solved the Boltzmann equation accounting for all the relevant diffusion processes. The main role is played by leptonic interactions, and the conductivity is found to decay with temperature like $\sigma \sim T/(\alpha^2 \log(1/\alpha))$, where α is the fine structure constant. During the second phase, we consider the relevant scattering process to be Thomson scattering, as in [65]. From $\mathbf{J} = \sigma \mathbf{E} = e\, n_e\, \mathbf{v}$ and $\mathbf{v} = e\tau \mathbf{E}/m_e$, one finds $\sigma = e^2 n_e\, \tau/m_e$, where τ is the average time between collisions. Therefore, in this case $\tau = 1/(n_\gamma\, \sigma_T)$, and $\sigma_T = e^4/(2\pi\, m_e^2)$ is the Thomson cross section [12]. This gives a constant conductivity:

$$\sigma = 2\pi \frac{n_e}{n_\gamma} \frac{m_e}{e^2} \simeq 3 \times 10^{13}\, \mathrm{sec}^{-1}\,, \tag{2.33}$$

which corresponds roughly to the conductivity of copper at room temperature; the universe is therefore a good conductor during the radiation dominated epoch. A similar argument can be applied also to find the conductivity of the first relativistic phase, considering a relativistic scattering cross section $\sigma_\times \propto 1/T^2$ [77], which gives rise to the same behaviour $\sigma \propto T$ found in [75, 76]. During the matter dominated epoch, the dominant scattering process for the determination of the conductivity is again Thomson scattering of CMB photons with the residual free electrons, whose number density is $n_e = 3 \times 10^{-10} a^{-3} \Omega h\ \mathrm{cm}^{-3}$ [22]. Therefore, the conductivity is given by the same expression as in Eq. (2.33), apart from the fact that the density of electrons drops. Taking the number of photons today $n_\gamma = 422\ \mathrm{cm}^{-3}$, one has $\sigma \sim 3 \times 10^{10}\, \mathrm{sec}^{-1}$.

Knowing the conductivity, one can evaluate the diffusion time of a magnetic field of characteristic length L. In particular, it is meaningful to evaluate the minimal characteristic length which can survive diffusion, for a magnetic field generated at the beginning of the universe. Making the restrictive assumption that the conductivity always takes the same value as in the matter dominated regime, one has

$$L_0 = \sqrt{\frac{t_0}{\sigma}} \simeq 10^{14}\ \mathrm{cm} \simeq 10^{-5} \mathrm{pc}\,. \tag{2.34}$$

Therefore, magnetic diffusion is negligible on galactic and cosmological scales. This condition is valid during the entire evolution of the universe, since one can prove that it is always verified that $H(t)L(t) < 1$. The high conductivity of the medium has relevant consequences on the evolution of the magnetic field.

2.4.3 Infinite conductivity limit and large scale evolution

It appears from the last paragraph that when analysing the evolution of cosmological magnetic fields one can safely neglect diffusion due to the high conductivity of the cosmic medium. Therefore, the second term in Eq. (2.32) can be set to zero: this is known as the *ideal MHD or infinite conductivity limit* [12]. The physical magnetic field will then evolve as

$$\mathbf{B}(\mathbf{r},t) = \frac{\mathbf{B}_0(\mathbf{r})}{a^2(t)}\,, \tag{2.35}$$

where the normalisation is chosen such that $\mathbf{B}_0(\mathbf{r})$ indicates the value of the magnetic field today (we have omitted the subscript L). This field is said to be *frozen in the fluid*, in the sense that the flux through a surface moving with the fluid is constant. Therefore, the energetic properties of the large scale magnetic field are conserved throughout the fluid evolution. From Eq. (2.35) one deduces that the energy density of the magnetic field $\rho_B = B^2/2$ evolves like radiation, $\rho_B \propto a^{-4}$.

Another quantity which is conserved in the infinite conductivity limit is magnetic helicity $\mathcal{H}$, defined in Eq. (2.17). Although expressed in terms of the vector potential, in this limit this quantity is gauge invariant, since the integrating volume is chosen to be delimited by a flux tube: such that $\mathbf{B}\cdot\mathbf{n} = 0$, where $\mathbf{n}$ is the normal to the boundary ∂V [78]. In this case in fact, possible gauge dependent contributions arising from the integrand vanish. Using the diffusion equation (2.32) one can show that the time evolution of the helicity is determined by

$$\frac{d\mathcal{H}}{dt} = -\frac{1}{\sigma}\int_V d^3x\, \mathbf{B}\cdot\nabla\times\mathbf{B}\,. \tag{2.36}$$

Therefore, this quantity is constant in the ideal MHD limit $\sigma \to \infty$. The term $\mathbf{B}\cdot\nabla\times\mathbf{B}$, called magnetic gyrotropy, is a measure of the diffusion of $\mathcal{H}$; sometimes it is also referred to as magnetic helicity, since it is qualitatively equivalent to it, as will appear in the next section (and as discussed in [59]). While the conservation of magnetic flux is related to the energetic properties of the magnetic configuration, magnetic helicity is related to the topological properties of the flux lines: it is essentially a measure of the links and twists in the magnetic configuration. We have presented in section 2.3.3 some primordial generation mechanisms which can give rise to seed fields with non vanishing helicity.

2.4.4 Small scale evolution and inverse cascade

The scaling law (2.35) of the magnetic field amplitude with the expansion of the universe has been derived in a cosmological setting, assuming a FRW space-time and adopting the reference frame of observers comoving with the cosmic fluid. Therefore, it is certainly valid on super-horizon and generally large (in what sense will be specified in the following) scales. On small scales, however, one cannot neglect the fact that the magnetic field interacts with the particles of the primordial plasma, inducing density and velocity perturbations in the primordial fluid. One should therefore consider the MHD equations describing the coupled system of fluid and magnetic field, and investigate on which scales the magnetic field is actually affected by the interaction with the fluid. This has been performed in references [73,79], in which the authors studied the evolution of the field in an expanding fluid composed of non-relativistic matter and radiation. This description is therefore valid from the epoch of e^+e^- annihilation up to decoupling. The presence of the magnetic field generates MHD waves in the fluid [12], and because of radiation viscosity from photons and neutrinos, magnetic energy can be dissipated by the scattering of charged particles off radiation particles. However, the amplitude of the magnetic field must be small, in order not to affect the FRW background, and this implies that the radiation pressure of the cosmic fluid is much bigger than the magnetic pressure. Therefore, the fluid motions can be treated as largely incompressible, and the main effect is the excitation of Alfvén waves [12]. In [73], Subramanian and Barrow pointed out that the usual procedure of linearisation about a constant field carried out by Jedamzik *et al.* [79] to analyse MHD waves is not a good approximation for a primordially created magnetic field, which will be inhomogeneous with roughly the same power on a multitude of scales, as will be clarified in the next section. Therefore, Subramanian and Barrow concentrated on the study of *non-linear* Alfvén modes in a viscous plasma, shear viscosity being given by the presence of the radiation component, photons and neutrinos. They divided the magnetic field into two components, a homogeneous one and a tangled one, but did not put any restriction on the amplitude of the tangled one, so that it need not be a small perturbation. The time evolution for the Fourier modes of the tangled component is given by a damped wave equation, with driving term kV_A ($V_A \simeq 3.8 \times 10^{-4} B/(10^{-9}$ Gauss) being the Alfvén velocity dependent on the amplitude of the magnetic field) and with damping term directly proportional to the shear viscosity coefficient (and therefore to the mean free path of the diffusing particle, photons or neutrinos). For tangled magnetic modes on galactic scales or larger, they found that the corresponding Alfvén mode oscillates negligibly before recombination, and does not suffer damping. In fact, in the cosmological context, there is only a finite time for the Alfvén wave to develop once the magnetic mode enters the horizon. Only small scales magnetic inhomogeneities have the time to oscillate appreciably before recombination, and therefore suffer energy dissipation. Moreover, it is demonstrated in [73] that the Alfvén modes can become over-damped, when the diffusing particle mean free path becomes large enough for dissipation to overcome the oscillations. Because of strong viscosity, that prevents fluid acceleration by the magnetic force, the damping is inefficient for over-damped modes. Accounting for this, the authors found that the largest comoving scale which suffer appreciable damping at a given time η is $\lambda(\eta) \sim \ell_\gamma(\eta)/V_A$, where $\ell_\gamma(\eta) = 1/(\sigma_T n_e)$ is the photon mean free path for Thomson scattering. On scales larger than $\lambda(\eta)$, the dissipation of magnetic energy is negligible. One can therefore consider $\lambda(\eta)^{-1}$ as a time dependent upper cutoff for the magnetic modes of the tangled component [80]. This is valid up to when the photon mean free path increases above the wavelength of a given mode, and one enters the free-streaming regime. The Alfvén modes are already in the over-damped regime when they start to free-stream; the authors of [73] analysed their evolution, and found that the damping in this regime is similar to Silk damping, except that one has an extra factor given by the Alfvén velocity. In conclusion, the largest scale to be damped before recombination is of the order of the Alfvén velocity times the Silk scale: $\lambda(\eta_{\rm rec}) \sim V_A L_S(\eta_{\rm rec})$, with $L_S(T) \sim 6 \times 10^{25}(T/0.25 \text{ eV})^{-5/4}(\Omega_B h^2/0.0125)^{-1/2} h^{-1}$ cm. The transition between the two damping scales occurs at about the epoch of matter-radiation equality.

For epochs earlier than e^+e^- annihilation, the above analysis needs to be modified. The plasma electron population at that time is much larger, and the photon mean free path is much smaller. The consequent reduction in the viscosity ν increases the kinetic Reynolds number to $Re = vL/\nu \gg 1$, and one has the appearance of hydrodynamic turbulence in the primordial fluid. Because of the very high conductivity, also the magnetic Reynold number $Re_M = vL\sigma \gg 1$, and the transport of the magnetic lines with the fluid dominates over the diffusion. Hydrodynamic turbulence therefore gives rise to magnetic turbulence, and can produce substantial modifications in the scaling laws of the magnetic field: the magnetic energy can be redistributed in time from small to large scales, a phenomenon known as *inverse cascade* [81]. In particular, if the magnetic field is helical, conservation of helicity implies that the small scale modes cannot be simply dissipated by the turbulent decay, but their helicity must be transferred to large scale modes [82]. Together with magnetic helicity, also some magnetic energy is saved from the turbulent decay. Therefore, if the initial magnetic field configuration presents helicity, the frozen-in time evolution might have to be modified, and the initial correlation length can grow faster than simple FRW expansion. The scaling laws for the coherence length and the magnetic energy during the relativistic epoch have been evaluated in the literature both theoretically [63, 82] and using numerical simulations [83, 84]. These two analysis lead to different results: $L(\eta) \sim \eta^{2/3}$, $E_M(\eta) \sim \eta^{-2/3}$ is the theoretical result, while the conclusion drawn from simulations is $L(\eta) \sim \eta^{1/2}$, $E_M(\eta) \sim \eta^{-1/2}$. It is still controversial if in the helical case, turbulence may survive also after e^+e^- annihilation [82] or not [60]. The occurrence of inverse cascade in the presence of non-helical magnetic configurations, driven simply by hydrodynamical turbulence occurring prior to $\eta_{e^+e^-}$, has also been put forward [77,85], and the theoretical scaling law in this case should be $L(\eta) \sim \eta^{2/(n+5)}$ for an initial power law magnetic power spectrum, with spectral index n. However, it has been argued that in this case the above anomalous scaling law is not the consequence of a process of inverse cascade, but is induced by a mechanism of selective decay [82]. Also in this case of zero helicity numerical simulations give a scaling law which is not consistent with the mentioned one [83].

The time evolution of helical magnetic fields is still an open issue, and the determination of commonly accepted scaling laws, arising from both numerical and theoretical evaluations, has not yet been achieved. In [86, 87] it is claimed that accounting for inverse cascade from numerical simulations can lead to surprisingly strong magnetic seeds, $10^{-13} - 10^{-11}$ Gauss on coherence scales 100 pc $-$ 10 kpc. It should be pointed out, however, that in most of the works dealing with helical configurations, the magnetic field amplitude is evaluated directly from conservation of helicity, assuming a maximally helical configuration: this means, setting

$\mathcal{H} \sim \mathbf{A} \cdot \mathbf{B} \sim LB^2 = \text{const}$, which gives

$$B_\lambda = B_L \left(\frac{L}{\lambda}\right)^{1/2} . \tag{2.37}$$

This result corresponds to "line averaging", which gives a much larger amplitude than "volume averaging", for the same length scale λ [82]. The line averaging procedure has been contested in [58], and will be discussed also in the next section.

2.5 Stochastic magnetic fields

After dealing with the time evolution of a primordial magnetic field, we turn now to the description of its spatial structure. The simplest structure one can conceive is a homogeneous field: this has been considered in several works, among which for example [88–91]. There is no fundamental reason to discard the possibility of a homogeneous field; however, in the following we will concentrate on a stochastically distributed magnetic field, with no homogeneous term. We consider a stochastic distribution because the primordial generation mechanisms proposed to date, whether inflationary or from phase transitions, lead to the presence of stochastic fields. Our magnetic field configuration is then characterised by fluctuations on a wide range of scales. We assume that the time evolution for the magnetic field is the one given in Eq. (2.35), so we can decouple the spatial structure from the time dependence. We further assume that the spatial stochastic variable $B_i(\mathbf{x})$ is statistically homogeneous and isotropic, and is characterised by a gaussian distribution with zero mean $\langle B_i(\mathbf{x})\rangle = 0$. In the case of a gaussian distribution, the second moment of the distribution is enough to completely determine the statistic, and the higher moments can be obtained via Wick's theorem (*cf.* section 4.2). One then defines the two point correlation function

$$\langle B_j(\mathbf{x}) B_l(\mathbf{y})\rangle = \xi_{jl}(|\mathbf{x}-\mathbf{y}|) , \tag{2.38}$$

where the brackets represent the average over many realisations, and the second equality holds because of the hypothesis of statistical homogeneity and isotropy. Note that since there is only one realisation of the universe, it is assumed that the statistic average over many realisations appearing in the previous formula can be identified with a spatial average, by means of some "ergodic theorem". Therefore one can set $\xi_{jl}(|\mathbf{z}|) = V^{-1}\int_V d^3y B_j(\mathbf{y}+\mathbf{z})B_l(\mathbf{y})$, with $\mathbf{z} = \mathbf{x}-\mathbf{y}$. It is convenient to carry on the rest of the analysis in Fourier space, and we adopt the Fourier transformation convention

$$B_j(\mathbf{k}) = \int d^3x\, e^{i\mathbf{k}\cdot\mathbf{x}} B_j(\mathbf{x})\,,$$
$$B_j(\mathbf{x}) = \frac{1}{(2\pi)^3}\int d^3k\, e^{-i\mathbf{k}\cdot\mathbf{x}} B_j(\mathbf{k})\,.$$

The reality condition for the field implies $(B_j(\mathbf{k}))^* = B_j(-\mathbf{k})$. The Dirac function is defined as

$$\delta(\mathbf{k}) = \frac{1}{(2\pi)^3}\int d^3x\, e^{i\mathbf{k}\cdot\mathbf{x}}\,. \tag{2.39}$$

The following section presents the analysis performed in references [80,92].

2.5.1 Magnetic field power spectrum

The second moment of the magnetic field distribution in Fourier space is given by

$$\begin{aligned}
\langle B_j(\mathbf{k})B_l^*(\mathbf{q})\rangle &= \int d^3x \int d^3y\, e^{i\mathbf{k}\cdot\mathbf{x}}\, e^{-i\mathbf{q}\cdot\mathbf{y}}\, \xi_{jl}(|\mathbf{x}-\mathbf{y}|) \\
&= \int d^3z \int d^3y\, e^{i\mathbf{k}\cdot(\mathbf{z}+\mathbf{y})}\, e^{-i\mathbf{q}\cdot\mathbf{y}}\, \xi_{jl}(|\mathbf{z}|) \\
&= \int d^3z\, e^{i\mathbf{k}\cdot\mathbf{z}}\, \xi_{jl}(|\mathbf{z}|) \int d^3y\, e^{i(\mathbf{k}-\mathbf{q})\cdot\mathbf{y}} \\
&= \mathcal{P}_{jl}(\mathbf{k})\,(2\pi)^3\delta(\mathbf{k}-\mathbf{q})\,;
\end{aligned} \tag{2.40}$$

the delta function indicates that under the hypothesis of statistical homogeneity and isotropy the Fourier modes of the distribution evolve independently from each other. The quantity $\mathcal{P}_{jl}(\mathbf{k})$, which corresponds to the Fourier transform of the two point correlation function defined in (2.38), is the *power spectrum* of the magnetic field distribution. The power spectrum must be given by two terms, one representing the magnetic field energy, and one representing the helicity. Moreover, it must account for the fact that the magnetic field is a divergence-less quantity, $\mathbf{B}(\mathbf{k})\cdot\mathbf{k} = 0 \rightarrow k^j\mathcal{P}_{jl} = 0$, and it must satisfy the reality condition $\mathcal{P}_{jl}^*(\mathbf{k}) = \mathcal{P}_{jl}(-\mathbf{k}) = \mathcal{P}_{lj}(\mathbf{k})$. Therefore, it takes the form [93]

$$\langle B_j(\mathbf{k})B_l^*(\mathbf{q})\rangle = \frac{(2\pi)^3}{2}\delta(\mathbf{k}-\mathbf{q})[P_{jl}S(k) + i\epsilon_{jlm}\hat{k}_m A(k)]\,, \tag{2.41}$$

where $P_{ij} \equiv \delta_{ij} - \hat{k}_i \hat{k}_j$ is the transverse-plane projector, satisfying the conditions $P_{ij}P_{jk} = P_{ik}$, $P_{ij}\hat{k}_j = 0$, ϵ_{ijl} is the totally antisymmetric tensor, and $\hat{k}_i = k_i/k$. We define $S(k)$ and $A(k)$ respectively as the *symmetric and helical part of the magnetic field power spectrum*: from (2.41) one has

$$\langle \mathbf{B}(\mathbf{k}) \cdot \mathbf{B}^*(\mathbf{q}) \rangle = (2\pi)^3 \delta(\mathbf{k} - \mathbf{q}) S(k) \tag{2.42}$$

$$i \langle \mathbf{B}(\mathbf{k}) \cdot (\hat{\mathbf{k}} \times \mathbf{B}^*(\mathbf{q})) \rangle = k \langle \mathbf{A}(\mathbf{k}) \cdot \mathbf{B}^*(\mathbf{q}) \rangle = (2\pi)^3 \delta(\mathbf{k} - \mathbf{q}) A(k) \,, \tag{2.43}$$

where $\mathbf{A}(\mathbf{k})$ is the vector potential, and the first equality in the second line holds in the Coulomb gauge $\mathbf{k} \cdot \mathbf{A} = 0$. Within this gauge choice, the helicity diffusion or magnetic gyrotropy $i\langle \mathbf{B} \cdot (\mathbf{k} \times \mathbf{B}^*) \rangle$ is therefore equivalent to the magnetic helicity (*cf.* section 2.3).

The symmetric part of the power spectrum represents the energy density of the magnetic field. By Fourier transforming the definition of the energy density, and using (2.41) one has in fact

$$\rho_B = \frac{1}{2} \langle \mathbf{B}(\mathbf{x}) \cdot \mathbf{B}(\mathbf{x}) \rangle = \frac{1}{(2\pi)^2} \int_0^\infty dk\, k^2\, S(k) \,. \tag{2.44}$$

The magnetic field helicity instead is given by the antisymmetric part of the spectrum,

$$\mathcal{H} = \langle \mathbf{A}(\mathbf{x}) \cdot \mathbf{B}(\mathbf{x}) \rangle = \frac{2}{(2\pi)^2} \int_0^\infty dk\, k\, A(k) \,. \tag{2.45}$$

It is useful for the following of this work (*cf.* chapter 4) to introduce the orthonormal 'helicity basis' ($\mathbf{e}^+$, $\mathbf{e}^-$, $\mathbf{e}_3 = \hat{\mathbf{k}}$) (see also [93]), where

$$\mathbf{e}^\pm(\mathbf{k}) = -\frac{i}{\sqrt{2}} (\mathbf{e}_1 \pm i \mathbf{e}_2) \,, \tag{2.46}$$

and ($\mathbf{e}_1$, $\mathbf{e}_2$, $\mathbf{e}_3 = \hat{\mathbf{k}}$) form a right-handed orthonormal basis with $\mathbf{e}_2 = \hat{\mathbf{k}} \times \mathbf{e}_1$. Under the transformation $\mathbf{k} \to -\mathbf{k}$ we choose $\mathbf{e}_2$ to change sign while $\mathbf{e}_1$ remains invariant. The basis $(\mathbf{e}^+, \mathbf{e}^-, \hat{\mathbf{k}})$ has the following properties: $\mathbf{e}^\pm \cdot \mathbf{e}^\mp = -1$, $\mathbf{e}^\pm \cdot \mathbf{e}^\pm = 0$, and $\mathbf{e}^\pm(\mathbf{k}) = \mathbf{e}^\mp(-\mathbf{k})$, as well as $i\hat{\mathbf{k}} \times \mathbf{e}^\pm = \pm \mathbf{e}^\pm$. The components of a vector with respect to this basis will be indicated by a superscript $\pm$. An arbitrary transverse vector $\mathbf{v}$ can be decomposed as $\mathbf{v} = v^+ \mathbf{e}^+ + v^- \mathbf{e}^-$. Here v^+ is the positive helicity component and v^- is the negative helicity component.

With the definition (2.41), and the reality condition $(B^\pm(\mathbf{k}))^* = -B^\pm(-\mathbf{k})$, we obtain the connection between the power spectra $S(k)$, $A(k)$ and the magnetic field components in the new basis:

$$-\langle B^+(\mathbf{k})B^+(-\mathbf{q}) + B^-(\mathbf{k})B^-(-\mathbf{q})\rangle = (2\pi)^3 S(k)\delta(\mathbf{k}-\mathbf{q}), \tag{2.47}$$

$$\langle B^+(\mathbf{k})B^+(-\mathbf{q}) - B^-(\mathbf{k})B^-(-\mathbf{q})\rangle = (2\pi)^3 A(k)\delta(\mathbf{k}-\mathbf{q}). \tag{2.48}$$

In other words, $A(k)$ represents the difference of the expectation values of the positive and negative helicity field components, determining the net circular polarisation of the Fourier mode $\mathbf{B}(\mathbf{k})$. If $A(k)$ does not vanish, the left handed and right handed magnetic fields have different strength.

We assume that both the symmetric and helical terms of the magnetic field power spectrum (2.41) can be approximated by a simple *power law*, as is customary when working with primordial magnetic fields:

$$S(k) = \begin{cases} S_0\, k^{n_S}, & \text{for } k < k_D \\ 0 & \text{otherwise} \end{cases} \tag{2.49}$$

and

$$A(k) = \begin{cases} A_0\, k^{n_A}, & \text{for } k < k_D \\ 0 & \text{otherwise} \end{cases} \tag{2.50}$$

where S_0, A_0 are the normalisation constants, n_S, n_A the spectral indices of the symmetric and helical parts respectively, and we have introduced an upper cutoff $k_D(\eta)$. This accounts for the dissipation of magnetic energy due to radiation viscosity in the primordial fluid (*cf.* section 2.4.4). At a given time η every magnetic mode $k > k_D(\eta)$ has already been dissipated, while for every $k < k_D(\eta)$ the time evolution equation (2.35) holds.

One wishes to express the normalisation constants in terms of physical quantities. To this aim, we define, for the symmetric part of the spectrum, the averaged magnetic field energy density $B_\lambda{}^2 \equiv \langle \mathbf{B}(\mathbf{x})\cdot\mathbf{B}(\mathbf{x})\rangle|_\lambda$, smoothed over a sphere of comoving radius λ. To account for the helical part of the spectrum, we define a helicity parameter directly comparable to B_λ: the absolute value of the averaged helicity $\mathcal{B}_\lambda{}^2 \equiv \lambda|\langle \mathbf{B}(\mathbf{x})\cdot(\nabla\times\mathbf{B}(\mathbf{x}))\rangle||_\lambda$, also smoothed over a sphere of comoving radius λ. $\mathcal{B}_\lambda$ measures the amplitude of helicity on the given comoving scale λ: $\mathcal{H}_\lambda = \lambda\mathcal{B}_\lambda{}^2$. One can then choose the value of the parameter λ according to the physical problem under analysis; for example, $\lambda \sim 0.1$ Mpc if one wishes to estimate the magnetic field at cluster size. In order to calculate B_λ and $\mathcal{B}_\lambda$, and connect them to the normalisation constants, we convolve the magnetic field and its helicity with a 3D-Gaussian filter function, so that $B_i \to B_i * f_\lambda$, where $\hat{f}_\lambda(k) = \exp(-\lambda^2 k^2/2)$. The mean-square values B_λ^2 and $\mathcal{B}_\lambda^2$ are then given by the Fourier transform of the products of the corresponding spectra $S(k)$ and $kA(k)$ with the square of the filter function $\hat{f}_\lambda$:

$$B_\lambda^2 = \frac{1}{(2\pi)^3}\int d^3k\, S(k)\hat{f}_\lambda(k)^2 = \frac{S_0}{(2\pi)^2}\frac{1}{\lambda^{n_S+3}}\Gamma\left(\frac{n_S+3}{2}\right), \quad (2.51)$$

$$\mathcal{B}_\lambda^2 = \frac{\lambda}{(2\pi)^3}\int d^3k\, k|A(k)|\hat{f}_\lambda(k)^2 = \frac{|A_0|}{(2\pi)^2}\frac{1}{\lambda^{n_A+3}}\Gamma\left(\frac{n_A+4}{2}\right). \quad (2.52)$$

In order not to over-produce long range magnetic fields or helicity as $k \to 0$, we require for the spectral indices $n_S > -3$ and $n_A > -4$ (for $n_A \leq -3$ and $n_A \leq -4$ the integrals (2.51) and (2.52) diverge at small k).

Using (2.51), (2.52) and the definition of the magnetic field spectrum (2.41), we can rewrite expressions (2.47) and (2.48) in the form (see also [63, 93])

$$-\langle B^+(\mathbf{k})B^+(-\mathbf{q}) + B^-(\mathbf{k})B^-(-\mathbf{q})\rangle = (2\pi)^5 \frac{\lambda^3 B_\lambda^2}{\Gamma\left(\frac{n_S+3}{2}\right)}(\lambda k)^{n_S}\delta(\mathbf{k}-\mathbf{q}), \quad (2.53)$$

$$\langle B^+(\mathbf{k})B^+(-\mathbf{q}) - B^-(\mathbf{k})B^-(-\mathbf{q})\rangle = (2\pi)^5 \frac{\lambda^3 \mathcal{B}_\lambda^2}{\Gamma\left(\frac{n_A+4}{2}\right)}(\lambda k)^{n_A}\delta(\mathbf{k}-\mathbf{q}), \quad (2.54)$$

for $k < k_D$ and 0 for $k > k_D$.

2.5.2 Primordial magnetic fields and causality

This section is based on reference [18], and aims to clarify a point which is often missed when investigating stochastic magnetic fields: namely that, because they are divergence-free, they are suppressed stronger than white noise on large scales.

As presented in the previous section and in section 2.3, a primordial stochastic magnetic field is usually assumed to be generated with a certain comoving coherence scale L, by a random process which is statistically homogeneous and isotropic. If the field generation occurs during a non-inflationary phase of the universe evolution, L must be smaller than the horizon scale. During inflation, L may diverge and the arguments presented below do not apply. We further make the assumption that the field created by this causal process is a purely classical magnetic field satisfying Maxwell's equations, or that it might be considered to be such soon after its generation. Neglecting possible quantum mechanical fluctuations in the field, we can state that its amplitudes and directions must be uncorrelated for points which lay farther apart than L:

$$\langle B_j(\mathbf{x})B_l(\mathbf{y})\rangle = \xi_{jl}(|\mathbf{x}-\mathbf{y}|) = 0 \qquad \forall\ \mathbf{x},\mathbf{y} \text{ with } |\mathbf{x}-\mathbf{y}| > L\,. \tag{2.55}$$

In reference [47], C. Hogan has argued that the field averaged over a volume of size $\lambda^3 > L^3$ behaves like

$$B_\lambda \simeq B_0 \left(\frac{L}{\lambda}\right)^{3/2}, \tag{2.56}$$

where B_0 is the amplitude of the field averaged over a volume given by the correlation scale L, and B_λ is the field averaged over a volume V_λ of size λ^3. Hogan's argument leading to the above result is very simple: V_λ contains $N = (\lambda/L)^3$ uncorrelated volumes, and within each of them the magnetic field has an average value of B_0 pointing in an arbitrary direction; the amplitude of the field averaged over a volume of size V_λ is therefore reduced by a factor $\sqrt{N}$ (like for a random walk), leading to the result (2.56). However, in the following it is shown that this result is not correct and has to be replaced by

$$B_\lambda \simeq B_0 \left(\frac{L}{\lambda}\right)^{5/2}. \tag{2.57}$$

The fact that magnetic fields are divergence-free implies that the integral over an arbitrary closed surface of the normal component of $\mathbf{B}$ has to vanish. This shows that $\mathbf{B}$ cannot take arbitrary mean values in all boxes of size L. One can express this result in a more formal way. Since $\xi_{jl}(\mathbf{x})$ is a function with compact support, its Fourier transform, the power spectrum $\mathcal{P}_{jl}(\mathbf{k})$, must be analytic. Therefore, both the symmetric and helical terms must be analytic, and this implies that for sufficiently small values of k they can be approximated by power laws, as in Eqs. (2.49), (2.50). Concentrating for the moment on the symmetric part of Eq. (2.41), analyticity of $(\delta_{jl} - \hat{k}_j\hat{k}_l)S(k)$ then requires that

$$n_S \geq 2 \text{ is an even integer.} \tag{2.58}$$

Genericallv, if there are no additional constraints, we expect $n_S = 2$. The usually assumed value $n_S = 0$, corresponding to a white noise spectrum, is not allowed *because of the non-analytic pre-factor $\hat{k}_j\hat{k}_l$ which is required to keep the magnetic field divergence-free,* $\mathbf{k}\cdot\mathbf{B} = 0$. In other words, the divergence-free condition forces a blue spectrum on the magnetic field energy density, $\langle|\mathbf{B}(\mathbf{k})|^2\rangle \propto k^2$.

We want to estimate the average field on a given scale $\lambda \geq L$. As already presented in the previous section, to this aim we perform a *volume average* of the field on a region of size λ^3, convolving $\mathbf{B}$ with a Gaussian window function,

$$\mathbf{B}_\lambda(\mathbf{x}) = \frac{1}{(\lambda\sqrt{2\pi})^3}\int d^3y\,\mathbf{B}(\mathbf{y})\exp\left(-\frac{(\mathbf{x}-\mathbf{y})^2}{2\lambda^2}\right), \tag{2.59}$$

and obtaining for the magnetic energy density on λ, B_λ^2, Eq. (2.51). The reason why we choose a volume average of the field is that it is the only one which keeps information about the underlying magnetic field once the mean is performed, as explained by Hindmarsh and Everett in reference [58]. Other possibilities could be to consider a line average (as used by Enqvist and Olesen [57])

$$B_1 = \frac{1}{L}\int_C \mathbf{B}(\mathbf{x})\cdot\mathbf{d}\ell\,, \tag{2.60}$$

where C is a curve of length L, or an averaged flux

$$B_2 = \frac{1}{L^2}\int_S \mathbf{B}(\mathbf{x})\cdot\mathbf{dS}\,. \tag{2.61}$$

However, the line and surface averages always deliver the same behaviour with scales, regardless of the shape of the spectrum of the underlying magnetic field [58].

Going back to Eq. (2.51), we have for two different scales, λ_1 and λ_2

$$\left(\frac{B_{\lambda_1}}{B_{\lambda_2}}\right)^2 = \left(\frac{\lambda_2}{\lambda_1}\right)^{n_S+3},$$

and especially, for the generically expected value $n_S = 2$

$$\frac{B_\lambda}{B_0} \simeq \left(\frac{L}{\lambda}\right)^{5/2}, \tag{2.62}$$

as claimed in Eq. (2.57). For $n_S > 2$, the suppression with scale is even stronger.

To demonstrate the importance of this additional L/λ factor with respect to Eq. (2.56), we consider magnetic fields produced during the electroweak phase transition as it has been proposed by various authors, see section 2.3.3 and for example [52, 55, 56] (note that the authors of [52] found a magnetic field spectrum $\propto k^2$). Following these references, at the scale $L_c \sim 10^5$ cm, a magnetic field with amplitude $B_{\rm ew}(L_c) \sim 10^{-6}$ Gauss is produced (where we have scaled the field value to today). Now L_c is much smaller than the horizon scale, $\eta_{\rm ew} \sim 10^{15}$ cm. But in Ref. [55], it is argued that a field is induced also on large scales, scaling like λ^{-1}. As we have shown above, this scaling can only take place up to the horizon scale, and so we have at best a field of about $B_{\rm ew}(\eta_{\rm ew}) \sim B_{\rm ew}(L_c)(L_c/\eta_{\rm ew}) \sim 10^{-16}$ Gauss. As we have argued above, due to causality the field has to decay like $\lambda^{-5/2}$ on super-horizon scales. For $\lambda \sim 1$ Mpc $\sim 3 \times 10^{24}$ cm one can therefore have a field of only about $B_\lambda \sim 10^{-39}$ Gauss, and not 10^{-20} Gauss as inferred in Ref. [55] and also in Ref. [58], where the authors have set $n_S = 0$ for "frozen-in" magnetic fields.

We proceed to investigate the limits due to causality on the antisymmetric component of Eq. (2.41). Again, causality requires that the function $\epsilon_{jlm}\hat{k}_m A(k)$ must be analytic and featureless for $k < 1/L$, so that $A(k) = A_0 k^{n_A}\left(1 + \mathcal{O}((kL)^2)\right)$, where n_A has to be a positive odd integer (*cf.* Eq. (2.50)). However, there is an additional constraint on the helical part of the spectrum. From the inequality $\langle |(i\hat{\mathbf{k}} \times \mathbf{B}) + \mathbf{B}|^2\rangle \geq 0$, one can easily derive that [93]

$$|A(k)| \leq S(k) \tag{2.63}$$

(note that $S(k) \propto \langle |\mathbf{B}|^2\rangle$, and therefore $S(k) \geq 0$). Using Eqs. (2.49) and (2.50), this translates into

$$\mathcal{B}_\lambda{}^2 \leq B_\lambda{}^2 (\lambda\, k)^{n_S - n_A} \frac{\Gamma((n_A+4)/2)}{\Gamma((n_S+3)/2)}\,. \tag{2.64}$$

Therefore, for Eq. (2.63) to be valid for very small values of k, we must require

$$n_A \geq n_S\,. \tag{2.65}$$

Together with the causality limit from above and (2.58) this implies that

$$n_A \geq 3 \text{ is an odd integer.} \tag{2.66}$$

Again, generically we expect $n_A = 3$. Furthermore, applying Eq. (2.63) at the upper cutoff of the spectrum k_D we have

$$\mathcal{B}_\lambda{}^2 \leq B_\lambda{}^2 (\lambda k_D)^{n_S - n_A} \frac{\Gamma((n_A+4)/2)}{\Gamma((n_S+3)/2)} \,. \tag{2.67}$$

Since typically the cutoff scale is much smaller than the physical scale of interest λ, one can conclude that the helical component of the magnetic field is even more suppressed by causality than the non-helical one, for all scales $\lambda > k_D^{-1}$. To quantify this additional suppression, we recall definition (2.52), which gives, with the generic value $n_A = 3$,

$$\frac{|\mathcal{B}_\lambda|}{|\mathcal{B}_0|} \simeq \left(\frac{L}{\lambda}\right)^3 , \tag{2.68}$$

a factor $\sqrt{L/\lambda}$ more suppression than the non-helical component, which for a coherence length of $\eta_{\rm ew}$ translates into an additional suppression of the order of 10^{-5}. However, for helical magnetic fields an inverse cascade effect can take place in the early universe, as explained in section 2.4.4. This results in a larger coherence scale than the frozen in one, while the magnetic spectral index remains unchanged on larger scales [83, 87]. Given the disagreement between theoretical and numerical analysis for the determination of the time evolution of a helical field, we choose to follow reference [60], and account for our scaling law on the results presented in this reference. The primordial helicity is given by $\mathcal{H} \sim L_c \mathcal{B}_0^2 = -n_b/\alpha$, where n_b is the baryon density of the universe today, $n_b(\eta_0) = 3 \times 10^{-7}$ cm^{-3} [5], and α is the fine structure constant. Just as the magnetic field strength, we have also scaled the helicity, which evolves like a^{-3} to today and is a conserved quantity like the baryon number. L_c is the comoving coherence length, which in reference [60] is found to be $L_c = 0.1$ pc, after accounting for turbulent enhancement. On this coherence scale, the amplitude of the magnetic field today becomes $\mathcal{B}_0 = \sqrt{n_b/(\alpha\, L_c)} \sim 10^{-19}$ Gauss. Taking again a scale λ of 1 Mpc, we get a maximal helicity amplitude of $\mathcal{B}_\lambda = \mathcal{B}_0 (L_c/1 \text{ Mpc})^3 \sim 10^{-40}$ Gauss.

To summarise, causally produced magnetic fields cannot have a white noise spectrum on large scales as usually assumed, but have a blue spectrum with index $n_S = 2$. Moreover, a possible helical component of the field, having a spectral index $n_A = 3$, is even more suppressed on large scales. These spectral indexes are valid on scales larger than the coherence scale of the field. The helical component typically has a larger coherence scale than the frozen-in one, because of non-linear MHD processing which leads to an inverse cascade.

From the previous estimates of the amplitudes of the symmetric and helical components at $\lambda = 1$ Mpc, we can conclude that: a causal magnetic field which has evolved on large scales simply via flux conservation from its creation at the electroweak phase transition until today *is not sufficient to have seeded the large scale magnetic fields observed in clusters*, even if a dynamo mechanism could amplify it during the process of structure formation (see however reference [94] which argues that a seed of 10^{-30} Gauss or even less might suffice). The same conclusion can be drawn for a helicity component of the magnetic field, if accounting for MHD processing in the simple way as explained above.

Possible ways out are either that the magnetic fields observed in clusters are due to very small scale seed fields, coherent on scales of the order of a pc or less, or that the seed fields have been generated by a "non-causal" mechanism, *e.g.* during an inflationary phase (*cf.* section 2.3.3). But also in this latter case, a very red spectrum, $n_S < -2$, is needed for the magnetic fields to play the role of seed for large scale magnetic fields. The requirement of such red spectrum is based on the results of reference [80], which obtains the strongest constraints to date on the amplitude of a general primordial magnetic seed. The constraint is derived by computing the gravitational waves induced by the anisotropic stresses of a stochastic primordial magnetic field, and imposing the nucleosynthesis bound on gravitational waves, which translates into a bound on the amplitude of the field as a function of the spectral index. The results apply to any non-helical seed field created before nucleosynthesis, also by an inflationary mechanism. For a causally created field, the bound is of the same order of magnitude of the one derived in the above analysis. For an inflationary created field, and $\lambda = 0.1$ Mpc, one finds $B_\lambda \leq 10^{-39}$ Gauss for every $n_S \geq 0$, but the limit weakens for negative spectral indices: $B_\lambda \leq 10^{-16}$ Gauss for $n_S \sim -2$. Such a strong bound is due to the fact that a magnetic field on superhorizon scales converts most of its energy into gravitational waves, before it is dissipated by plasma viscosity: gravity wave production happens before and at horizon crossing, while viscosity damping is active only on scales which are well inside the horizon. Morevoer, the spectrum of the gravity wave energy density is always blue (k^{2n_S+6}, and recall the condition $n_S > -3$), and leads to stronger constraints on small scales than on the large scales probed by CMB anisotropies (*cf.* section 3.3).

In conclusion, our results strongly disfavour the hypothesis of primordial seeds for the large scale magnetic fields observed in galaxies and clusters at the present day, with the exception of inflationary created seeds with very red spectra. Such fields are not well motivated by current theoretical models, which mostly give rise to white noise, or much bluer spectra.

Chapter 3

Linear perturbation theory and the CMB

This chapter contains a review of the cosmological linear perturbation theory, and the formation of CMB temperature anisotropies and polarisation. The aim of this chapter is to present the derivation of some results that will be used in the original work that is the subject of the rest of this thesis (in particular in chapters 4 and 5). In the first part of this chapter we define the geometric and matter perturbation variables, which will act as sources for the formation of the CMB temperature and polarisation fluctuations. The second part review a way of connecting primordial perturbations with the observed CMB fluctuations, based on the total angular momentum method developed by Hu and White in reference [95]. A comprehensive review of this topic can also be found, for example, in reference [96]. The last part of the chapter presents a brief review of previous articles, which have analysed the effects of a primordial magnetic field on the CMB anisotropies and polarisation.

3.1 Cosmological linear perturbation theory

The observation of the extreme degree of isotropy of the CMB, and other observational and theoretical results (*cf.* chapter 1), lead to the conclusion that the overall structure of the universe is well described by the homogeneous and isotropic FRW model. Therefore, the observed large scale structure of the universe is believed to have grown from initially small density perturbations in a FRW background. It is assumed that these perturbations can be described using linear perturbation theory for sufficiently early times, $z \gtrsim 5$. There are two possible approaches to the relativistic theory of linear perturbations: a covariant one, based on the 1+3 splitting carried on in the first chapter, in which one takes the point of view of the observers comoving with the cosmic fluid [15,97,98]; and a coordinate-based one, in which a 3+1 arbitrary slicing of the spacetime is performed, and one takes the point of view of the observers sitting in the slicing [99–101]. These two approaches define two sets of perturbation variables which are equivalent to first order [15]. Although the covariant approach presents some advantages (for example it provides gauge invariant variables with a straightforward physical meaning), in the following we will be adopting the coordinate based approach, which will be useful for the aim of chapter 4.

In the standard approach to perturbation theory, one is dealing with two space-times: the physical, perturbed space-time and the background FRW one. The perturbation of a tensorial quantity T is defined as the difference between the value it takes at a point in the physical spacetime, and the value at the corresponding point in the unperturbed background: $\delta T = T - \bar{T}$. Consequently, a one-to-one correspondence between the points of the two space-times must be established, which carries the coordinates of the background over into the physical spacetime. A change in this correspondence, keeping the background fixed, is called a *gauge transformation*. A gauge transformation induces a coordinate transformation in the physical spacetime, but also changes the point in the background corresponding to a given point in the physical spacetime. Therefore, even if the perturbed quantity T is a scalar, the value of the perturbation δT will in any case depend on the gauge choice, unless $\bar{T}$ is constant or identically vanishes. This result is known as the Stewart & Walker lemma. The main example of this issue is given by the perturbation of the energy density $\delta\rho$: being the energy density in the background time-dependent, the value of the perturbation is modified by a gauge transformation which changes the correspondence between the hyper-surfaces of simultaneity in the two space-times. In order to overcome the issue of gauge dependence of the perturbation variables, Bardeen [99] found a set of gauge invariant quantities, constructed as linear combinations of the gauge dependent perturbation variables. The general covariance of general relativity guarantees a complete freedom in the choice of the gauge, which also means that only gauge invariant quantities have an inherent physical meaning. We proceed in the development of linear perturbation theory following references [99, 100].

3.1.1 Geometric and matter perturbations

The background spacetime is described by the FRW metric in conformal time $\bar{g}_{\alpha\beta}$, given in Eq. (1.61). The unperturbed energy momentum tensor, describing the matter, is that of a perfect fluid at rest relative to the coordinates of the metric; therefore, it is given by Eq. (1.7), with background velocity $\bar{u}^\alpha = a^{-1}\delta^\alpha{}_0$ and background energy density and pressure $\bar{\rho}$, $\bar{p}$. Following [99], we adopt the "energy frame" choice: we define the rest frame for the matter to be the frame in which the energy flux q^α vanishes. This choice is relevant when considering the perturbed form of the energy momentum tensor. The homogeneity and isotropy of the background allows a separation of the time and spatial dependence of the perturbation fields, and one can further perform a *decomposition in spatial harmonics* of the spatial perturbation fields on the surfaces of homogeneity. The basis functions of this decomposition are eigenfunctions of the laplacian operator of the spatial coordinates, and are classified as scalar, vector and tensor harmonics, according to how they transform under spatial coordinates transformation. The scalar harmonics $Q^{(0)}(x^a)$ are solutions of the scalar Helmholtz equation

$$Q^{(0)\,|i}{}_{|i} + k^2 Q^{(0)} = 0\,, \tag{3.1}$$

therefore are simply plane waves if the space geometry is flat. The wave number k sets the spatial scale of the perturbation relative to the background spatial coordinates. The scalar harmonics generate vector and symmetric tensor functions related to them,

$$Q^{(0)}{}_i = -\frac{1}{k}\,Q^{(0)}{}_{|i} \qquad \text{and} \qquad Q^{(0)}{}_{ij} = \frac{1}{k^2}\,Q^{(0)}{}_{|ij} + \frac{1}{3}\,\gamma_{ij}\,Q^{(0)}\,. \tag{3.2}$$

The vector harmonics $Q^{(1)}_i(x^a)$ are solutions of the vector Helmholtz equation

$$Q^{(1)\,i|j}{}_{|j} + k^2 Q^{(1)\,i} = 0\,, \tag{3.3}$$

and must satisfy the divergence-less condition $Q^{(1)\,i}{}_{|i} = 0$; the corresponding traceless symmetric tensor is

$$Q^{(1)}{}_{ij} = -\frac{1}{2k}[Q^{(1)}{}_{i|j} + Q^{(1)}{}_{j|i}]\,. \tag{3.4}$$

Tensor harmonics $Q^{(2)}{}_{ij}(x^a)$ are the transverse ($Q^{(2)\,ij}{}_{|j} = 0$) and traceless tensor laplacian eigenfunctions, such that

$$Q^{(2)\,ij|l}{}_{|l} + k^2 Q^{(2)\,ij} = 0\,. \tag{3.5}$$

In linear perturbation theory a general perturbation in the gravitational field can be written as a linear combination of the independent harmonics, with coefficients functions of time, and no coupling terms between different harmonics: scalar perturbations couple to perturbations in the energy density and isotropic pressure, in the irrotational part of the velocity field and in the traceless anisotropic stress; vector perturbations couple to the divergence-less, vortical part of the velocity field and to the traceless anisotropic stress; tensor perturbations to the transverse traceless part of the anisotropic stress only. Considering the perturbed metric $g_{\alpha\beta} = \bar{g}_{\alpha\beta} + \delta g_{\alpha\beta}$, one has at linear order, for scalar perturbations

$$\delta g_{00} = -2a^2 A(\eta) Q^{(0)} \tag{3.6}$$

$$\delta g_{0i} = -a^2 B^{(0)}(\eta) Q^{(0)}_i \tag{3.7}$$

$$\delta g_{ij} = 2a^2 [H_L(\eta) Q^{(0)} \gamma_{ij} + H_T^{(0)}(\eta) Q^{(0)}_{ij}]\,, \tag{3.8}$$

for vector perturbations

$$\delta g_{0i} = -a^2 B^{(1)}(\eta) Q^{(1)}_i \tag{3.9}$$

$$\delta g_{ij} = 2a^2 H_T^{(1)}(\eta) Q^{(1)}_{ij}\,, \tag{3.10}$$

and for tensor perturbations

$$\delta g_{ij} = 2a^2 H_T^{(2)}(\eta) Q^{(2)}_{ij}\,. \tag{3.11}$$

The unit vector field normal to the constant time hyper-surfaces is $n^\alpha = \bar{n}^\alpha + \delta n^\alpha$, with $\bar{n}^\alpha = a^{-1} \delta^\alpha{}_0$, and

$$\delta n^0 = -\frac{1}{a} A(\eta)\, Q^{(0)}\,, \qquad \delta n^i = \frac{1}{a}\,[B^{(0)}(\eta)\, Q^{(0)\,i} + B^{(1)}(\eta)\, Q^{(1)\,i}]\,. \tag{3.12}$$

Therefore, A is interpreted as the perturbation in the lapse function, which measures the ratio between the proper time distance (measured along the world-lines normal to the hyper-surfaces of constant time), and the coordinate time distance between two neighbouring constant time hyper-surfaces. B is interpreted as the perturbation in the shift vector, which measures the rate of deviation of a constant space-coordinate line from a line normal to a constant time hyper-surface. H_L represents the amplitude of perturbation of a unit spatial volume, and ${H_T}^{ij} = H_T^{(0)} Q^{(0)\,ij} + H_T^{(1)} Q^{(1)\,ij} + H_T^{(2)} Q^{(2)\,ij}$ the anisotropic distortion of each constant time hyper-surface.

The perturbations in the matter are given by the perturbed matter four-velocity and the perturbed energy momentum tensor. As stated before, we choose the energy frame, so we define the perturbed velocity of the matter $u^\alpha = \bar{u}^\alpha + \delta u^\alpha$ as the unitary time-like eigenvector of the perturbed energy momentum tensor, $T_{\alpha\beta} = \bar{T}_{\alpha\beta} + \delta T_{\alpha\beta}$, and the perturbed energy density $\rho = \bar{\rho} + \delta\rho$ by the corresponding eigenvalue:

$$T^\alpha{}_\beta \, u^\beta = -\rho\, u^\alpha \,, \tag{3.13}$$

and $u_\alpha u^\alpha = -1$. The energy density and the isotropic pressure are scalars, so we define their perturbations as

$$\rho = \bar{\rho}\,(1 + \delta(\eta) Q^{(0)}) \tag{3.14}$$

$$p = \bar{p}\,(1 + \pi_L(\eta) Q^{(0)})\,, \tag{3.15}$$

while the time and space components of the velocity perturbation take the form

$$\delta u^0 = -\frac{1}{a} A(\eta)\, Q^{(0)}\,, \qquad \delta u^i = \frac{1}{a}\,[v^{(0)}(\eta)\, Q^{(0)\,i} + v^{(1)}(\eta)\, Q^{(1)\,i}]\,. \tag{3.16}$$

The perturbed energy momentum tensor is then given by

$$\delta T^0{}_0 = -\bar{\rho}\,\delta(\eta)\, Q^{(0)} \tag{3.17}$$

$$\delta T^0{}_i = (\bar{\rho} + \bar{p})\,[v^{(0)}(\eta) - B^{(0)}(\eta)]\, Q_i^{(0)} \tag{3.18}$$

$$\delta T^i{}_0 = -(\bar{\rho} + \bar{p})\, v^{(0)}(\eta)\, Q^{(0)\,i} \tag{3.19}$$

$$\delta T^i{}_j = \bar{p}\,[\pi_L(\eta)\, Q^{(0)}\, \gamma^i{}_j + \pi_T^{(0)}(\eta)\, Q^{(0)\,i}{}_j] \tag{3.20}$$

for scalar perturbations,

$$\delta T^0{}_i = (\bar{\rho} + \bar{p})\,[v^{(1)}(\eta) - B^{(1)}(\eta)]\,Q_i^{(1)} \tag{3.21}$$

$$\delta T^i{}_0 = -(\bar{\rho} + \bar{p})\,v^{(1)}(\eta)\,Q^{(1)\,i} \tag{3.22}$$

$$\delta T^i{}_j = \bar{p}\,\pi_T^{(1)}(\eta)\,Q^{(1)\,i}{}_j \tag{3.23}$$

for vector perturbations, and

$$\delta T^i{}_j = \bar{p}\,\pi_T^{(2)}(\eta)\,Q^{(2)\,i}{}_j \tag{3.24}$$

for tensor perturbations. We have introduced the anisotropic stress perturbation $\pi^i{}_j = \pi_T^{(0)} Q^{(0)i}{}_j + \pi_T^{(1)} Q^{(1)i}{}_j + \pi_T^{(2)} Q^{(2)i}{}_j$. The perturbed isotropic pressure p is in general not related to the energy density in the same way as it is in the background. The entropy perturbation is defined as the difference between the fractional isotropic pressure perturbation $\pi_L(\eta)$ and what expected from the background pressure-energy density relation:

$$\Gamma(\eta) = \pi_L(\eta) - \frac{{c_s}^2}{w}\delta(\eta)\,, \tag{3.25}$$

with $w = \bar{p}/\bar{\rho}$ and ${c_s}^2 = \bar{p}'/\bar{\rho}'$.

The geometric and matter perturbation variables defined above are in general not gauge invariant. Always following [99], we now proceed to study their gauge transformation properties and construct gauge invariant combinations of them.

3.1.2 Gauge-invariant perturbation variables

As stated before, a gauge transformation corresponds to a change of coordinates in the physical spacetime. Since we are dealing with linear perturbation theory, it is necessary only to consider infinitesimal gauge transformations, which correspond to first order effects. They are classified into scalar type and vector type (there are no tensor type gauge transformations), and they are expanded with the corresponding harmonic functions, so that different modes are decoupled from each other. The most general scalar type gauge transformation is

$$\tilde{\eta} = \eta + T(\eta)\,Q^{(0)} \tag{3.26}$$

$$\tilde{x}^i = x^i + L^{(0)}(\eta)\,Q^{(0)\,i}\,, \tag{3.27}$$

and vector type is

$$\tilde{\eta} = \eta \tag{3.28}$$

$$\tilde{x}^i = x^i + L^{(1)}(\eta)\, Q^{(1)\,i}\,. \tag{3.29}$$

The corresponding change in the perturbed metric from a scalar type gauge transformation will therefore be

$$\tilde{g}_{\alpha\beta}(\eta, x^i) = \frac{\partial x^\mu}{\partial \tilde{x}^\alpha}\frac{\partial x^\nu}{\partial \tilde{x}^\beta}\, g_{\mu\nu}(\eta - TQ^{(0)},\, x^i - L^{(0)}Q^{(0)\,i})\,. \tag{3.30}$$

From this expression and the equivalent one for vector perturbations it is possible to evaluate the changes in the amplitudes of the metric perturbations at first order. One has for scalar modes

$$\tilde{A} = A - T' - \frac{a'}{a}T \tag{3.31}$$

$$\tilde{B}^{(0)} = B^{(0)} + L^{(0)\prime} + kT \tag{3.32}$$

$$\tilde{H}_L = H_L - \frac{k}{3}L^{(0)} - \frac{a'}{a}T \tag{3.33}$$

$$\tilde{H}_T^{(0)} = H_T^{(0)} + kL^{(0)}\,, \tag{3.34}$$

and for vector modes

$$\tilde{B}^{(1)} = B^{(1)} + L^{(1)\prime} \tag{3.35}$$

$$\tilde{H}_T^{(1)} = H_T^{(1)} + kL^{(1)}\,, \tag{3.36}$$

while the tensor mode amplitude $H_T^{(2)}$ is gauge invariant. A gauge transformation removes two scalar and one vector degrees of freedom, so that beside $H_T^{(2)}$ three further independent gauge-invariants can be constructed from the metric perturbations: the two Bardeen potentials from the scalar perturbations,

$$\Psi = A + \frac{1}{k}\frac{a'}{a}\left(B^{(0)} - \frac{1}{k}H_T^{(0)\prime}\right) + \frac{1}{k}\left(B^{(0)\prime} - \frac{1}{k}H_T^{(0)\prime\prime}\right) \tag{3.37}$$

$$\Phi = H_L + \frac{1}{3}H_T^{(0)} + \frac{1}{k}\frac{a'}{a}\left(B^{(0)} - \frac{1}{k}H_T^{(0)\prime}\right)\,, \tag{3.38}$$

and from the vector perturbations, the variable

$$\Sigma = B^{(1)} - \frac{1}{k} H_T^{(1)\prime} \,. \tag{3.39}$$

The physical and geometrical meaning of these gauge-invariants often emerges once a particular gauge choice has been performed. This will be discussed later on in the particular case of the longitudinal and vector gauges. As stated earlier, in reference [15] the authors defined a set of covariant and gauge invariant variables describing the curvature of the perturbed spacetime and the kinematic behaviour of matter and matter inhomogeneities, and then proceeded with a comparison between their and Bardeen's sets of variables. This procedure can provide insight for a gauge-independent significance of the Bardeen's variables defined in this paragraph. As an example, Eqs. (113-116) of [15] show how the variables Ψ, Φ, Σ and $H_T^{(2)}$ combine to give the electric and magnetic components of the Weyl tensor.

We now proceed to consider gauge invariant combinations of the matter perturbation variables. The energy density is a scalar quantity, therefore, it transforms simply like

$$\rho(\tilde{\eta}) = \rho(\eta + TQ^{(0)}) \simeq \rho(\eta) + \rho' \, T \, Q^{(0)} \,, \tag{3.40}$$

which, using Eq. (1.27) for the background energy leads to

$$\tilde{\delta} = \delta + 3(1+w)\frac{a'}{a} T \,, \tag{3.41}$$

and analogously one finds

$$\tilde{\pi}_L = \pi_L + 3(1+w)\frac{{c_s}^2}{w}\frac{a'}{a} T \,. \tag{3.42}$$

The effect of a gauge transformation on the velocity can be evaluated from the definition $v^i = a^{-1} dx^i/d\eta$; one has

$$\tilde{v}^{(0)} = v^{(0)} + L^{(0)\prime} \tag{3.43}$$

$$\tilde{v}^{(1)} = v^{(1)} + L^{(1)\prime} \,. \tag{3.44}$$

The amplitudes $\pi_T^{(0,1,2)}$ defined from the decomposition of the anisotropic stress perturbation are gauge invariant following the Stewart & Walker lemma. Also the entropy perturbation

Γ is gauge invariant, as it follows from the transformation rules for the energy density and the isotropic pressure. In order to construct gauge invariant quantities corresponding to the energy density perturbation and the velocity perturbation, one must combine them with the geometrical quantities. Starting with the velocity perturbation, one obtains the gauge invariant combination for the scalar modes combining Eqs. (3.43) and (3.34):

$$V_S^{(0)} = v^{(0)} - \frac{1}{k} H_T^{(0)\prime} \, . \tag{3.45}$$

Comparing instead Eq. (3.44) with (3.35) and (3.36), one finds that there are two possible gauge invariant combinations for the vector mode:

$$V_S^{(1)} = v^{(1)} - \frac{1}{k} H_T^{(1)\prime} \tag{3.46}$$

$$V_C = v^{(1)} - B^{(1)} \, . \tag{3.47}$$

The velocity perturbation amplitude $V_S(\eta)$ is related to the amplitude of the shear of the matter velocity field, as appears from Eq. (102) of [15]

$$\sigma_{ij} = a \, (-k \, V_S^{(0)} \, Q^{(0)}{}_{ij} - k \, V_S^{(1)} \, Q^{(1)}{}_{ij} + H_T^{(2)\prime} \, Q^{(2)}{}_{ij}) \, ; \tag{3.48}$$

the other gauge invariant possibility, $V_C(\eta)$, is instead related to the vorticity tensor:

$$\omega_{ij} = a \, V_C \, Q^{(1)}{}_{[i|j]} \, , \tag{3.49}$$

where brackets denote anti-symmetrisation (*cf.* Eq. (103) of [15]). Only scalar perturbations contribute to the amplitude of perturbation in the expansion rate of matter, given in Eq. (98) of the same reference,

$$\delta\Theta = \frac{3}{a} \left(H_L' - \frac{a'}{a} A + \frac{k}{3} v^{(0)} \right) Q^{(0)} \, ; \tag{3.50}$$

Eq. (99) of [15] shows instead that the potential Ψ can be seen as the relativistic analog of the Newtonian potential: its spatial derivative is in fact related to the gauge invariant acceleration of the matter field $a_i = \dot{u}_i$,

$$a_i = \left(-k\Psi + \frac{(aV_S^{(0)})'}{a} \right) Q_i^{(0)} + \frac{(aV_C)'}{a} Q_i^{(1)} \, . \tag{3.51}$$

Concerning the energy density perturbation, there are many choices of gauge invariant combinations. Bardeen [99] considered the two possibilities

$$\epsilon_m = \delta + 3(1+w)\frac{1}{k}\frac{a'}{a}(v^{(0)} - B^{(0)}) \tag{3.52}$$

$$\epsilon_g = \delta - 3(1+w)\frac{1}{k}\frac{a'}{a}\left(B^{(0)} - \frac{1}{k}H_T^{(0)\prime}\right), \tag{3.53}$$

apparently gauge invariant from Eqs. (3.32), (3.34), (3.43). Note that both reduce to the energy perturbation δ of Eq. (3.41) as soon as the perturbation enters the horizon, $k^{-1}(a'/a) \ll 1$, and that they are related through

$$\epsilon_m = \epsilon_g + 3(1+w)\frac{1}{k}\frac{a'}{a}V_S^{(0)}. \tag{3.54}$$

Again, comparing with Eq. (119) of [15] shows that these variables are related to the gauge invariant spatial gradient of the energy density. Another gauge invariant combination, which will be used in the following, is [100]

$$\Delta_g = \delta + 3(1+w)\frac{1}{k}\frac{a'}{a}\left(H_L + \frac{1}{3}H_T^{(0)}\right) = \epsilon_g + 3(1+w)\Phi. \tag{3.55}$$

The discussion in the next section 3.2 is based on reference [95], where Hu and White adopted the commonly used longitudinal and vector gauges. Therefore, we present here the details of these particular gauge choices. In order to specify a gauge for scalar perturbations, one has to impose two relations among the gauge-dependent variables, one for fixing the time coordinate and one for the space coordinates. The gauge condition for the time coordinate corresponds to the choice of a time slicing of the perturbed space-time, and is fixed by imposing a constraint on a gauge dependent variable whose change under a gauge transformation is expressed only in terms of $T(\eta)$ (*cf.* Eq. (3.26)). For each time slicing, one then eliminates the spatial gauge freedom by constraining a perturbation variable whose gauge transformation involves $L(\eta)$ only (*cf.* Eq. (3.27)). In the context of a longitudinal gauge, one first performs a "Newtonian" slicing of the spacetime. This corresponds to setting $k^{-1}H_T^{(0)\prime} - B^{(0)} = 0$, which completely eliminates the gauge freedom $T(\eta)$, as appears clearly from Eqs. (3.32) and (3.34). Given that $B^{(0)}$ represents the three velocity amplitude of world-lines normal to the constant time hyper-surfaces (*cf.* Eq. (3.12)), and remembering the definition of the shear in Eq. (3.48), one can deduce that within this gauge choice one picks the constant time hyper-surfaces corresponding to zero shear [100]. In this slicing, the gauge invariant geometrical perturbation variables have the most clear physical meaning: one has in fact $\Psi = A$, corresponding to the amplitude of perturbation in the gravitational potential, and $\Phi = H_L + (1/3)H_T^{(0)}$, corresponding to the scalar perturbation in the curvature of the hyper-surfaces. Moreover, from Eq. (3.53) one has that the suitable variable to describe the energy density perturbation is ϵ_g. The residual spatial gauge freedom is fixed in the longitudinal gauge by choosing $B^{(0)} = H_T^{(0)} = 0$. One therefore has that $V_S^{(0)} = v^{(0)}$, and the scalar perturbations of the metric become simply

$$\delta g_{00} = -2a^2\Psi Q^{(0)} \qquad \delta g_{ij} = 2a^2\Phi Q^{(0)}\gamma_{ij}\,. \tag{3.56}$$

Concerning vector perturbations, one needs to impose only one condition on the perturbation amplitudes. The vector gauge corresponds to set $H_T^{(1)} = 0$, so that $\Sigma = B^{(1)}$, $V_S^{(1)} = v^{(1)}$, and the vector perturbations of the metric become

$$\delta g_{0i} = -a^2 B^{(1)} Q_i^{(1)} \qquad \delta g_{ij} = 0\,. \tag{3.57}$$

3.1.3 Evolution equations for the gauge invariant variables

The evolution equations for the gauge invariant variables follow from the perturbation of Einstein's equations $\delta G_{\alpha\beta} = \delta T_{\alpha\beta}$, and of the conservation equations for the fluid, $\delta(T^{\alpha\beta}{}_{;\beta}) = 0$. The standard derivation is explained in details for example in reference [100]. Equivalently, the perturbation equations could also be derived by linearising the conservation and dynamic equations presented in the first chapter about a FRW universe [98], and then connecting the covariant perturbation variables with Bardeen's ones, as explained in reference [15]. The result is four independent equations for the scalar gauge invariant quantities, two for the vector quantities, and one for the tensor ones. Starting with scalar perturbations, one has two formulae relating the gauge invariant amplitudes of the metric perturbations with the matter ones:

$$2(k^2 - 3\kappa)\Phi = a^2\,\bar\rho\,\epsilon_m \tag{3.58}$$

$$-k^2(\Phi + \Psi) = a^2\,\bar p\,\pi_T^{(0)}\,, \tag{3.59}$$

where the second equation can be written in the same form as the Newtonian Poisson equation, if the spatial curvature κ and the anisotropic stress are neglected [100]. Moreover, one has the momentum conservation equation

$$V_S^{(0)\prime} + \frac{a'}{a} V_S^{(0)} = k\Psi + \frac{k}{1+w}({c_s}^2 \epsilon_m + w\Gamma) - \frac{2}{3}\frac{kw}{1+w}\left(1 - \frac{3\,\kappa}{k^2}\right)\pi_T^{(0)} \,, \tag{3.60}$$

and the energy conservation equation

$$\epsilon_m' - 3w\frac{a'}{a}\epsilon_m = -k(1+w)\left(1 - \frac{3\kappa}{k^2}\right)V_S^{(0)} - 2w\frac{a'}{a}\left(1 - \frac{3\kappa}{k^2}\right)\pi_T^{(0)} \,. \tag{3.61}$$

The equations for vector perturbations are a constraint equation

$$(k^2 - 2\kappa)\Sigma = 2a^2(\bar\rho + \bar p)V_C \,, \tag{3.62}$$

and an evolution equation for the matter

$$V_C' + (1 - 3{c_S}^2)\frac{a'}{a}V_C = -\frac{w}{1+w}\frac{k^2 - 2\kappa}{2k}\pi_T^{(1)} \,, \tag{3.63}$$

which shows that the vorticity of matter is generated by a vector type anisotropic stress perturbation. The tensor perturbations evolution is given by a wave-type equation

$$H_T^{(2)\prime\prime} + 2\frac{a'}{a}H_T^{(2)\prime} + (k^2 + 2\kappa)H_T^{(2)} = a^2\,\bar p\,\pi_T^{(2)} \,, \tag{3.64}$$

which represents the evolution of the amplitude of a gravitational wave.

It is possible to find solutions for the above systems of equations in some simple cases. We concentrate here on scalar perturbations, since the solution of the vector and tensor perturbation equations will be discussed respectively in chapter 5 and 4. If we assume a *perfect dust fluid* $w = {c_s}^2 = \Gamma = \pi_{ij} = 0$ in a flat universe, the system of equations given by (3.58-3.61) has the simple solution (where Ψ_0 is a constant)

$$\begin{cases} \Psi = \Psi_0 \\ \epsilon_m = -\frac{1}{6}\Psi_0 x^2 \\ V_S^{(0)} = \frac{1}{3}\Psi_0 x \,, \end{cases} \tag{3.65}$$

with $x = k\eta$, and where we have neglected the decaying mode in ϵ_m and $V_S^{(0)}$. The perturbations are always given by the contribution of the largest gauge invariant perturbation variable [96]. Therefore, one has that on super-horizon scales $x \ll 1$, perturbations are constant: $\Psi = \Psi_0$, and $\epsilon_m \ll V_s^{(0)} \ll \Psi$. On sub-horizon scales $x \gg 1$, however, the matter density perturbations grow like the scale factor for a matter dominated universe, $\epsilon_m \propto a$. This growth is very important in the linear regime in order to amplify primordial fluctuations once they have entered the horizon. In order to form structure by gravitational instability, one needs initial fluctuations of the order of at least 10^{-5}; the required initial spectrum of density perturbation may be given by inflation (*cf.* chapter 6).

Another important case in which the perturbation equations are solvable is the *perfect radiation fluid*, with $w = {c_s}^2 = 1/3$, $\Gamma = \pi_{ij} = 0$. In this case one finds oscillatory solutions,

$$\begin{cases} \Psi = -\epsilon_m/(2x^2) \\ \epsilon_m = \epsilon_0\left[(\sin x)/x - \cos x\right] \\ V_S^{(0)} = -\sqrt{3}/4\left(\frac{d\epsilon_m}{dx} - \frac{1}{x}\epsilon_m\right) \,, \end{cases} \tag{3.66}$$

where we set $x = {c_s}^2 k\eta$, corresponding to the acoustic horizon. In the super-horizon regime $x \ll 1$, perturbations are again constant, with $\Psi = \epsilon_0/2$ and $\epsilon_m \ll V_s^{(0)} \ll \Psi$; once they enter the horizon they start to collapse, but the fluid pressure resists the gravitational force and the fluid oscillates at constant amplitude: $\epsilon_m = -\epsilon_0 \cos x$, $V_s^{(0)} = \sqrt{3}/4\epsilon_0 \sin x$. The perturbations in the gravitational potential oscillate and decay like a^2: $\Psi = (\epsilon_0 \cos x)/(2x^2)$, and $a \propto \eta$ in a radiation dominated universe.

Another relevant case is the *two-component fluid*. We assume a mixture of matter and radiation, coupled only by gravity (therefore, a dark matter component). The energy of the fluid is given by the sum of the energy of matter and radiation, while the pressure is given by radiation alone; therefore, the perturbations are

$$\delta\rho = \delta\rho_{\rm rad} + \delta\rho_{\rm mat} \tag{3.67}$$

$$\delta p = \delta\rho_{\rm rad}/3 \,, \tag{3.68}$$

and one finds

$$w = \frac{1}{3}\left(1 + \frac{\rho_{\rm mat}}{\rho_{\rm rad}}\right)^{-1} , \qquad {c_s}^2 = \frac{1}{3}\left(1 + \frac{3}{4}\frac{\rho_{\rm mat}}{\rho_{\rm rad}}\right)^{-1} , \tag{3.69}$$

and therefore

$$\Gamma = 3{c_s}^2 \frac{\rho_{\rm mat}}{\rho_{\rm rad}} \left[\frac{3}{4} \frac{\delta\rho_{\rm rad}}{\rho_{\rm rad}} - \frac{\delta\rho_{\rm mat}}{\rho_{\rm mat}} \right] . \tag{3.70}$$

The requirement that the entropy perturbation vanish, so that the matter and radiation perturbations are initially in perfect thermal equilibrium, corresponds to $\delta\rho_{\rm rad}/\rho_{\rm rad} = (4/3)\delta\rho_{\rm mat}/\rho_{\rm mat}$: this is referred to as the assumption of *adiabatic initial conditions.* We proceed with the solution of the perturbation equations (3.58-3.61) under this assumption, but using the density variable Δ_g instead of ϵ_m, which with $\Gamma = 0$ satisfies the conservation equation [96]

$$\Delta_g' + 3({c_s}^2 - w)\frac{a'}{a}\Delta_g + (1+w)kV_S^{(0)} = 0 . \tag{3.71}$$

The adiabatic initial conditions then translate into

$$\lim_{x\to 0} \left(\frac{3}{4}\Delta_g^{\rm rad} - \Delta_g^{\rm mat} \right) = 0 , \qquad \lim_{x\to 0} \left(V_S^{(0)\rm rad} - V_S^{(0)\rm mat} \right) = 0 , \tag{3.72}$$

with $x = k\eta$, so that the velocity fields must also agree, as a consequence of energy conservation. In order to account for the situation which is relevant in a cosmological context, we want to find the solution for the radiation density perturbations after matter radiation equality. One has therefore $\Psi = \Psi_0$, dominated by the matter contribution. After imposing the aforementioned initial conditions, one obtains

$$\Delta_g^{\rm rad} = \frac{4}{3}\Psi_0 \cos\left(\frac{x}{\sqrt{3}}\right) - 8\Psi_0 \tag{3.73}$$

$$V_S^{(0)\rm rad} = \frac{1}{\sqrt{3}}\Psi_0 \sin\left(\frac{x}{\sqrt{3}}\right) \tag{3.74}$$

$$\Delta_g^{\rm mat} = -\Psi_0(5 + \frac{1}{6}x^2) \tag{3.75}$$

$$V_S^{(0)\rm mat} = \frac{1}{3}\Psi_0 x . \tag{3.76}$$

This result is very important, because it determines some of the characteristics of the angular power spectrum of the CMB anisotropies (through Eq. (3.114) derived in the next section). On super-horizon scales $x \ll 1$, the solution takes the form $\Delta_g^{\rm rad} \sim (4/3)\Delta_g^{\rm mat} \sim -(20/3)\Psi_0$: if one considers a Harrison-Zel'dovich initial power spectrum for the gravitation field $k^3|\Psi|^2 =$ *const*, this translates into the plateau of the CMB anisotropies at large scales, measured by the COBE satellite. On sub-horizon scales instead, the fluid oscillates as $\cos(c_s x)$: this behaviour translates into peaks in the CMB angular power spectrum. Imposing adiabatic initial conditions determines the cosine solution, and therefore the position of the acoustic peaks. We proceed now with a review on the formalism describing the CMB anisotropies and polarisation.

3.2 CMB anisotropies and polarisation

As discussed in section 1.3.3, after recombination the photons of the primordial fluid cease to interact with protons and electrons and propagate freely. Their distribution function therefore satisfies the Liouville equation, which in an unperturbed universe takes the form (where p denotes the physical photon momentum)

$$\partial_\eta f - \frac{a'}{a} p\, \partial_p f = 0\,, \tag{3.77}$$

so that $f = \bar{f}(ap)$, and the original black body distribution is maintained if there is no new injection of energy:

$$\bar{f}(ap) = \frac{1}{\exp{(p/T)} - 1}\,. \tag{3.78}$$

However, the universe is not perfectly FRW, but is characterised by small metric and matter perturbations as analysed in the previous section. The primordial perturbations imprint as small fluctuations in the temperature of the CMB black body distribution. Here we present a concise analysis of the formation of the CMB temperature anisotropies and polarisation, concentrating on the *primary anisotropies*: those which are formed at the last scattering surface, and are later solely modified by gravitational effects.

Most of the physics of the CMB perturbation evolution is already contained in the previous section. However, one should account for the fact that the interaction between the photon fluid and the matter is not only gravitational: photons exchange energy and momentum with the electrons through Thomson scattering. The evolution of the photon distribution function is given by a Boltzmann equation, which accounts for the collisions and for the fact that photons propagate along the perturbed geodesics. Moreover, the CMB observable properties are not the energy density and velocity perturbations but the higher order angular distribution of the CMB temperature and polarisation. The formation of temperature anisotropies and polarisation in the CMB from the gravitational perturbations is presented in a complete way in references [95,102], where Hu *et al.* develop the total angular momentum representation. This is useful for the following of this work because it provides a comprehensive description of the effects not only of scalar, but also of vector and tensor perturbations, on a equal footing: we will make use of the total angular momentum formalism in both chapters 4 and 5. The formalism consists in isolating the total angular dependence of the modes of the CMB fluctuations, as well as of the metric and matter perturbations, by combining their intrinsic angular structure with that of the plane wave spatial dependence. It therefore provides a common description for the CMB fluctuations and the metric and matter perturbations.

The temperature and polarisation distribution of the CMB radiation is a function of the spatial position $\mathbf{x}$ and the propagation direction $\hat{\mathbf{n}}$ of the light rays. In a flat universe one has simply $\mathbf{x} = -(\eta_0 - \eta)\hat{\mathbf{n}} = -r\hat{\mathbf{n}}$. The *angular modes* of the fluctuations ($\hat{\mathbf{n}}$ dependence) are isolated by a decomposition in spherical harmonics. The CMB temperature anisotropy is a scalar, spin-0 field on the sky, and therefore can be decomposed in terms of spherical harmonics $Y_\ell^m(\theta,\phi)$. The polarisation instead is a spin-2 field, and can be decomposed using the basis ${}_{\pm2}Y_\ell^m(\theta,\phi)\mathbf{M}_\pm$, where ${}_{\pm2}Y_\ell^m$ are the spin-weighted spherical harmonics, and $\mathbf{M}_\pm$ are tensors given by

$$\mathbf{M}_\pm = \frac{1}{2}(\hat{\mathbf{e}}_\theta \mp i\hat{\mathbf{e}}_\phi) \otimes (\hat{\mathbf{e}}_\theta \mp i\hat{\mathbf{e}}_\phi)\,, \tag{3.79}$$

and $(\hat{\mathbf{e}}_r, \hat{\mathbf{e}}_\phi, \hat{\mathbf{e}}_\theta)$ form an orthonormal basis. The spin-weighted spherical harmonics are not eigenstates of parity, but transform as ${}_sY_\ell^m \to (-1)^\ell{}_{-s}Y_\ell^m$; parity eigenstates can be constructed as

$$\frac{1}{2}[{}_2Y_\ell^m\mathbf{M}_+ \pm {}_{-2}Y_\ell^m\mathbf{M}_-]\,, \tag{3.80}$$

which have respectively "electric" $(-1)^\ell$ and "magnetic" $(-1)^{\ell+1}$ type parity.

The *radial modes* are given by the decomposition of the $\mathbf{x}$ dependence in plane waves. We choose a fixed orthonormal basis on the sky with $\hat{\mathbf{e}}_3 = \hat{\mathbf{k}}$, like in section 2.5.1. In conclusion, a complete basis for the temperature is

$$G_\ell^m = (-i)^\ell\sqrt{\frac{4\pi}{2\ell+1}}\,Y_\ell^m(\hat{\mathbf{n}})\exp(i\mathbf{k}\cdot\mathbf{x})\,, \tag{3.81}$$

and for the polarisation

$$ {}_{\pm 2}G_\ell^m = (-i)^\ell \sqrt{\frac{4\pi}{2\ell+1}}\, {}_{\pm 2}Y_\ell^m(\hat{\mathbf{n}}) \exp(i\mathbf{k}\cdot\mathbf{x}) \,. \tag{3.82} $$

Now one has that the plane wave also carries angular dependence, and in particular an orbital angular momentum:

$$ \exp(i\mathbf{k}\cdot\mathbf{x}) = \sum_\ell (-i)^\ell \sqrt{4\pi(2\ell+1)}\, j_\ell(kr) Y_\ell^0(\hat{\mathbf{n}}) \,, \tag{3.83} $$

where $j_\ell(kr)$ are the spherical Bessel functions [103]. One can now add the angular momenta of the plane wave Y_ℓ^0 and the spherical harmonics $Y_{\ell'}^m$, and isolate the total angular dependence of the basis functions (3.81) and (3.82). This is performed using the Clebsch-Gordan coefficients, and generally couples the states between $|\ell-\ell'|$ and $|\ell+\ell'|$ (*cf.* ref. [95] for the details). The radial dependence (in r) of a state of total ℓ' will be given by a weighted sum of $j_{|\ell-\ell'|}$ to $j_{|\ell+\ell'|}$, which can be re-expressed in terms of j_ℓ and its derivatives, using the recursion relations of spherical Bessel functions (B.14, B.15). In [95] it is shown that the new temperature basis becomes

$$ G_{\ell'}^m = \sum_\ell (-i)^\ell \sqrt{4\pi(2\ell+1)}\, j_\ell^{(\ell'\,m)}(kr) Y_\ell^m(\hat{\mathbf{n}}) \,, \tag{3.84} $$

where the new radial functions, for the lowest values of $(\ell'\,m)$ are

$$ \begin{aligned} &j_\ell^{(0\,0)}(x) = j_\ell(x) \quad j_\ell^{(1\,0)}(x) = j_\ell'(x) \qquad && j_\ell^{(2\,0)}(x) = \tfrac{1}{2}[3j_\ell''(x) + j_\ell(x)] \\ &\qquad j_\ell^{(1\,1)}(x) = \sqrt{\tfrac{\ell(\ell+1)}{2}}\tfrac{j_\ell(x)}{x} && j_\ell^{(2\,1)}(x) = \sqrt{\tfrac{3\ell(\ell+1)}{2}}\left(\tfrac{j_\ell(x)}{x}\right)' \\ & && j_\ell^{(2\,2)}(x) = \sqrt{\tfrac{3(\ell+2)!}{8(\ell-2)!}}\tfrac{j_\ell(x)}{x^2} \,. \end{aligned} \tag{3.85} $$

Here $\ell' = 0, 1, 2$ corresponds to the monopole, dipole and quadrupole anisotropy, while $m = 0, 1, 2$ corresponds to scalar, vector and tensor modes; $x = kr$, and $'$ exceptionally denotes derivatives with respect to x. The new polarisation basis, also found in [95] takes the form

$$ {}_{\pm 2}G_2^m = \sum_\ell (-i)^\ell \sqrt{4\pi(2\ell+1)}[\epsilon_\ell^{(m)}(kr) \pm i\beta_\ell^{(m)}(kr)]\, {}_{\pm 2}Y_\ell^m(\hat{\mathbf{n}}) \,, \tag{3.86} $$

where the radial functions, corresponding to scalar, vector and tensor modes, are given by

$$\begin{aligned}
\epsilon_\ell^{(0)}(x) &= \sqrt{\tfrac{3(\ell+2)!}{8(\ell-2)!}}\tfrac{j_\ell(x)}{x^2} & \beta_\ell^{(0)}(x) &= 0 \\
\epsilon_\ell^{(1)}(x) &= \tfrac{1}{2}\sqrt{(\ell-1)(\ell+2)}\left[\tfrac{j_\ell(x)}{x^2}+\tfrac{j'_\ell(x)}{x}\right] & \beta_\ell^{(1)}(x) &= \tfrac{1}{2}\sqrt{(\ell-1)(\ell+2)}\tfrac{j_\ell(x)}{x} \\
\epsilon_\ell^{(2)}(x) &= \tfrac{1}{4}\left[-j_\ell(x)+j''_\ell(x)+2\tfrac{j_\ell(x)}{x^2}+4\tfrac{j'_\ell(x)}{x}\right] & \beta_\ell^{(2)}(x) &= \tfrac{1}{2}\left[j'_\ell(x)+2\tfrac{j_\ell(x)}{x}\right].
\end{aligned} \tag{3.87}$$

$\epsilon_\ell^{(m)}$ represents the amplitude of an electric (E) parity state, and $\beta_\ell^{(m)}$ of a magnetic (B) one. In fact, a state of electric parity (like the source for polarisation from Thomson scattering, *cf.* Eq. (3.109)) is written as

$$\begin{aligned}
{}_2G_2^m\mathbf{M}_+ + {}_{-2}G_2^m\mathbf{M}_- &= \sum_\ell(-i)^\ell\sqrt{4\pi(2\ell+1)}\Big\{\epsilon_\ell^{(m)}[{}_2Y_\ell^{(m)}\mathbf{M}_+ + {}_{-2}Y_\ell^{(m)}\mathbf{M}_-] \\
&+ \; i\beta_\ell^{(m)}[{}_2Y_\ell^{(m)}\mathbf{M}_+ - {}_{-2}Y_\ell^{(m)}\mathbf{M}_-]\Big\}.
\end{aligned} \tag{3.88}$$

Recalling definition (3.80), one sees that the addition of angular momentum of the plane wave generates, out of a E type parity source, E type parity of amplitude $\epsilon_\ell^{(m)}$ but also B type parity $\beta_\ell^{(m)}$. For negative m, one has $\epsilon_\ell^{(-m)} = \epsilon_\ell^{(m)}$, but $\beta_\ell^{(-m)} = -\beta_\ell^{(m)}$: therefore in the following we will keep the notation $\pm m$ (which was neglected in section 3.1.1) to account for B type polarisation.

The important point is that the functions (3.84) and (3.86) constitute a basis also for the metric and matter perturbations. Relating the normal modes of the metric perturbations to those of the CMB fluctuations, one finds that the $m = 0, \pm1, \pm2$ modes of the radiation couple to scalar, vector and tensor modes of the metric. If one considers the decomposition in section 3.1.1, one can find that for scalar perturbations, $Q^{(0)} = \exp(i\mathbf{k}\cdot\mathbf{x}) = G_0^0$, $n^iQ^{(0)}{}_i = G_1^0$, and $n^in^jQ^{(0)}{}_{ij} \propto G_2^0$. Therefore scalars generate only $m = 0$ fluctuations in the radiation. For vectors, one has that

$$Q^{(\pm1)}{}_i = -\frac{i}{\sqrt{2}}(\hat{\mathbf{e}}_1 \pm i\hat{\mathbf{e}}_2)_i\exp(i\mathbf{k}\cdot\mathbf{x}), \tag{3.89}$$

so that $n^iQ^{(\pm1)}{}_i = G_1^{\pm1}$ and $n^in^jQ^{(\pm1)}{}_{ij} \propto G_2^{\pm1}$: they generate the $m = \pm1$ modes in the radiation. Tensors instead couple to the $m = \pm2$ modes, with

$$Q^{(\pm2)}{}_{ij} = -\sqrt{\frac{3}{8}}(\hat{\mathbf{e}}_1 \pm i\hat{\mathbf{e}}_2)_i \otimes (\hat{\mathbf{e}}_1 \pm i\hat{\mathbf{e}}_2)_j\exp(i\mathbf{k}\cdot\mathbf{x}), \tag{3.90}$$

and $n^i n^j Q^{(\pm 2)}{}_{ij} = G_2^{\pm 2}$.

We now proceed with an analysis of the generation of temperature and polarisation anisotropies from the gravitational and scattering sources. In agreement with references [95, 102], we define the metric perturbation $\delta g_{\alpha\beta} = a^2 h_{\alpha\beta}$ and pick the longitudinal gauge of Eqs. (3.56, 3.57).

3.2.1 Radiation transport

In order to represent the propagation of CMB radiation, one considers radiation propagating radially toward an observer, $\mathbf{E} \perp \hat{e}_r$, characterised by an intensity matrix existing on the subspace $\hat{\mathbf{e}}_\theta \otimes \hat{\mathbf{e}}_\phi$. Since one is describing the CMB anisotropies, it is convenient to represent the intensity matrix in units of temperature fluctuations rather than radiation intensity. The matrix can be decomposed in terms of the Pauli matrices,

$$\mathbf{T} = \Theta \mathbf{1} + Q\sigma_3 + U\sigma_1 + V\sigma_2 \,. \tag{3.91}$$

Here $\Theta = \Delta T/T$ represents the temperature perturbation summed over the polarisation states; Q represents the difference in temperature fluctuations polarised along the major axis $\hat{\mathbf{e}}_\theta$ and $\hat{\mathbf{e}}_\phi$; U is the difference along axis rotated of $45°$, $(\hat{\mathbf{e}}_\theta \pm \hat{\mathbf{e}}_\phi)/\sqrt{2}$; V is that between the circularly polarised states $(\hat{\mathbf{e}}_\theta \pm i\hat{\mathbf{e}}_\phi)/\sqrt{2}$. A more convenient representation, in which the coefficients are invariant under a general axis rotation, turns out to be (from the transformation properties of Pauli matrices under rotation) [95]

$$\mathbf{T} = \Theta \mathbf{1} + V\sigma_2 + (Q + iU)\mathbf{M}_+ + (Q - iU)\mathbf{M}_- \,, \tag{3.92}$$

with $\mathbf{M}_\pm = (\sigma_3 \mp i\sigma_1)/2$.

The Boltzmann equation describes the transport of photons under Thomson scattering by the electrons. Since circular polarisation cannot be generated by Thomson scattering, one can neglect V and rearrange the relevant components of the intensity matrix in a vector

$$\vec{T} = (\Theta, Q + iU, Q - iU) \,, \tag{3.93}$$

in terms of which the Boltzmann equation can be written

$$\frac{d}{d\eta}\vec{T}(\eta, \mathbf{x}, \hat{\mathbf{n}}) = \partial_\eta \vec{T} + n^i \vec{T}_{|i} = \vec{C}[\vec{T}] + \vec{G}[h_{\alpha\beta}] \tag{3.94}$$

(one has that $x_i' = n_i$). $\vec{C}[\vec{T}]$ and $\vec{G}[h_{\alpha\beta}]$ account respectively for the collisions between photons and electrons, and for the gravitational redshift. The gravitational term can be evaluated from the perturbed geodesic equation for photons, and in the $\vec{T}$ notation takes the form [95]

$$\vec{G}[h_{\alpha\beta}] = \left(\frac{1}{2} n^i n^j \dot{h}_{ij} + n^i \dot{h}_{0i} + \frac{1}{2} n^i h_{00|i}, 0, 0\right) , \tag{3.95}$$

since it affects the different polarisation states alike. The derivation of the scattering term is more involved. One starts by considering the process of Thomson scattering in the reference frame of electrons, in a coordinate basis fixed by the scattering plane, spanned by incoming and outgoing directional vectors $-\hat{\mathbf{n}}' \cdot \hat{\mathbf{n}} = \cos\beta$. The differential cross-section for Thomson scattering is given by

$$\frac{d\sigma}{d\Omega} = \frac{3}{8\pi} \sigma_T |\hat{\mathbf{E}}' \cdot \hat{\mathbf{E}}|^2 , \tag{3.96}$$

where $\hat{\mathbf{E}}'$ and $\hat{\mathbf{E}}$ denote the directions of the incoming and outgoing electric fields. Radiation polarised perpendicularly to the scattering plane scatters isotropically, while that polarised in the scattering plane picks up a factor $\cos^2\beta$. Within this setting, it is possible to derive the transfer properties of the Stokes parameters $(\Theta, Q \pm iU)$ arranged in the vector $\vec{T}$, as a function of the scattering angle β (*cf.* Eq. (47) of [95]). The next step is to convert the quantities from the scattering frame to the fixed basis on the sky $(\hat{\mathbf{e}}_1, \hat{\mathbf{e}}_2, \hat{\mathbf{k}})$. The full collision term involves the difference of scattering out of and into a given angle, and an integral over incoming angles. In terms of the vector $\vec{T}$, it takes the final form

$$\vec{C}[\vec{T}] = -\dot{\tau}\left[\vec{T}(\hat{\mathbf{n}}) - \left(\int \frac{d\hat{\mathbf{n}}'}{4\pi}\Theta' + \hat{\mathbf{n}} \cdot \mathbf{v}_B, 0, 0\right)\right] + \frac{1}{10}\dot{\tau} \int d\hat{\mathbf{n}}' \sum_{m=-2}^{2} \mathbf{P}^{(m)}(\mathbf{n}, \mathbf{n}')\vec{T}(\mathbf{n}') . \tag{3.97}$$

$\dot{\tau} = n_e \sigma_T a$ is the differential optical depth in conformal time, with n_e the free electron density. The term in brackets describes the isotropic effect of scattering on the temperature anisotropies, and the Doppler shift induced by transforming from the electron rest frame to the background one ($\mathbf{v}_B$ is the baryon velocity). The last term accounts for the anisotropic nature of Thomson scattering, and includes therefore the angular and polarisation dependence. As before, the index m corresponds to the contributions from scalar, vector and tensor scattering terms, and the matrix $\mathbf{P}^{(m)}$ expresses the rotation from the scattering to the background frame. It is expressed in terms of scalar and spin-weighted spherical harmonics as [95]

$$\mathbf{P}^{(m)} = \begin{pmatrix} Y_2^{m*}(\hat{\mathbf{n}}')Y_2^m(\hat{\mathbf{n}}) & -\sqrt{3/2}\,{}_2Y_2^{m*}(\hat{\mathbf{n}}')_2Y_2^m(\hat{\mathbf{n}}) & -\sqrt{3/2}\,{}_{-2}Y_2^{m*}(\hat{\mathbf{n}}')_2Y_2^m(\hat{\mathbf{n}}) \\ -\sqrt{6}\,Y_2^{m*}(\hat{\mathbf{n}}')_2Y_2^m(\hat{\mathbf{n}}) & 3\,{}_2Y_2^{m*}(\hat{\mathbf{n}}')_2Y_2^m(\hat{\mathbf{n}}) & 3\,{}_{-2}Y_2^{m*}(\hat{\mathbf{n}}')_2Y_2^m(\hat{\mathbf{n}}) \\ -\sqrt{6}\,Y_2^{m*}(\hat{\mathbf{n}}')_{-2}Y_2^m(\hat{\mathbf{n}}) & 3\,{}_2Y_2^{m*}(\hat{\mathbf{n}}')_{-2}Y_2^m(\hat{\mathbf{n}}) & 3\,{}_{-2}Y_2^{m*}(\hat{\mathbf{n}}')_{-2}Y_2^m(\hat{\mathbf{n}}) \end{pmatrix};$$

it appears that polarisation is generated through quadrupole ($\ell = 2$) anisotropies in the radiation, and vice versa. We now proceed to rewrite the Boltzmann equation as the evolution equation for the amplitudes of the normal modes of the temperature and polarisation.

3.2.2 Evolution equations

The temperature and polarisation fluctuations are expanded in the basis functions (3.81) and (3.82):

$$\Theta(\eta, \mathbf{x}, \hat{\mathbf{n}}) = \int \frac{d^3k}{(2\pi)^3} \sum_\ell \sum_{m=-2}^{2} \Theta_\ell^{(m)} G_\ell^m\,, \tag{3.98}$$

$$(Q \pm iU)(\eta, \mathbf{x}, \hat{\mathbf{n}}) = \int \frac{d^3k}{(2\pi)^3} \sum_\ell \sum_{m=-2}^{2} (E_\ell^{(m)} \pm iB_\ell^{(m)})\,{}_{\pm 2}G_\ell^m\,, \tag{3.99}$$

where $E_\ell^{(m)}$ represent polarisation with electric parity $(-1)^\ell$, and $B_\ell^{(m)}$ with magnetic parity $(-1)^{\ell+1}$. One can substitute these expressions in the Boltzmann equation (3.94), and find the evolution equations for the components $\vec{T}_\ell^{(m)} = (\Theta_\ell^{(m)}, E_\ell^{(m)}, B_\ell^{(m)})$. Special care should be taken when considering the gradient term on the left-hand-side of (3.94). This term represents the fact that as the radiation free-streams, spatial gradients in the distribution of temperature and polarisation produce anisotropies, and reflect in the observed angular distribution. One has in fact

$$n_i \frac{\partial}{\partial x^i} \to i\hat{\mathbf{n}} \cdot \mathbf{k} = i\sqrt{\frac{4\pi}{3}}\, k\, Y_1^0(\hat{\mathbf{n}})\,, \tag{3.100}$$

which multiplies the angular dependence of Eqs. (3.98, 3.99), generating a coupling between the ℓ and $\ell \pm 1$ moments of the distribution from the addition of angular momenta. The result of the free-streaming effect is therefore an infinite hierarchy of coupled ℓ moments that transfers power from the sources, at low multipoles, up to the high multipoles as time progress. The Boltzmann equations for temperature and polarisation become, with ${}_s\kappa^\ell_m = \sqrt{(\ell^2 - m^2)(\ell^2 - s^2)/\ell^2}$ [95],

$$\dot{\Theta}_\ell^{(m)} = k\left[\frac{{}_0\kappa_\ell^m}{2\ell-1}\Theta_{\ell-1}^{(m)} - \frac{{}_0\kappa_{\ell+1}^m}{2\ell+3}\Theta_{\ell+1}^{(m)}\right] - \dot{\tau}\Theta_\ell^{(m)} + S_\ell^{(m)} \tag{3.101}$$

$$\dot{E}_\ell^{(m)} = k\left[\frac{{}_2\kappa_\ell^m}{2\ell-1}E_{\ell-1}^{(m)} - \frac{2m}{\ell(\ell+1)}B_\ell^{(m)} - \frac{{}_2\kappa_{\ell+1}^m}{2\ell+3}E_{\ell+1}^{(m)}\right] - \dot{\tau}[E_\ell^{(m)} + \sqrt{6}P^{(m)}\delta_\ell^2] \tag{3.102}$$

$$\dot{B}_\ell^{(m)} = k\left[\frac{{}_2\kappa_\ell^m}{2\ell-1}B_{\ell-1}^{(m)} + \frac{2m}{\ell(\ell+1)}E_\ell^{(m)} - \frac{{}_2\kappa_{\ell+1}^m}{2\ell+3}B_{\ell+1}^{(m)}\right] - \dot{\tau}B_\ell^{(m)}\,. \tag{3.103}$$

The terms in the square bracket represent the free-streaming effect that couples the ℓ modes, and also couples the two parity polarisation states E and B (*cf.* Eq. (3.88)); except, however, for scalar perturbations, for which one has $B_\ell^{(0)} = 0$ (*cf.* Eqs. (3.87)). The first terms after the square bracket account for the isotropic effect of scattering, and the remaining terms, $S_\ell^{(m)}$ and $\dot{\tau}\sqrt{6}P^{(m)}$, account for the gravitational and the residual scattering effects:

$$\begin{aligned} S_0^{(0)} &= \dot{\tau}\Theta_0^{(0)} - \dot{\Phi}\,, \quad S_1^{(0)} = \dot{\tau}v_B^{(0)} + k\Psi\,, \quad S_2^{(0)} = \dot{\tau}P^{(0)}\,, \\ & \qquad\qquad\qquad\quad S_1^{(1)} = \dot{\tau}v_B^{(1)} + \dot{B}^{(1)}\,, \quad S_2^{(1)} = \dot{\tau}P^{(1)}\,, \\ & \qquad\qquad\qquad\qquad\qquad\qquad\qquad\quad S_2^{(2)} = \dot{\tau}P^{(2)} - \dot{H}_T^{(2)}\,. \end{aligned} \tag{3.104}$$

The term $\Theta_0^{(0)}$ cancels the scattering term in the equation describing the isotropic temperature fluctuation $\ell = m = 0$. The baryon velocity $\mathbf{v}_B$ enters the dipole equation $\ell = 1$, and represents the Doppler effect. The anisotropic part of Thomson scattering enters the quadrupole equations $\ell = 2$ for the temperature and E polarisation distributions; it is given by

$$P^{(m)} = \frac{1}{10}\left[\Theta_2^{(m)} - \sqrt{6}E_2^{(m)}\right]\,, \tag{3.105}$$

and does not source the equation for B polarisation, due to the opposite parity of B_2 and Θ_2, E_2.

The Boltzmann evolution equations are completed by the evolution equations for the perturbations, given in section 3.1.3. In this notation, the photon density perturbation corresponds to $\delta_\gamma = 4\Theta_0^{(0)}$, the photon velocity perturbation to $v_\gamma^{(m)} = \Theta_1^{(m)}$, and the anisotropic stress is $\pi_{T\gamma}^{(m)} \propto \Theta_2^{(m)}$. This result is obtained by writing Eq. (3.101) for the lowest multipoles $\ell = 0, 1, 2$ in the tight coupling limit $\dot{\tau} \to \infty$, and comparing it with the perturbation Eqs. (3.58-3.64) for each perturbation mode m. Note that, since we are using the longitudinal gauge, $\delta_\gamma = \epsilon_g^\gamma$. The solutions found in section 3.1.3 for the pure radiation fluid and for the mixture of dark matter and radiation can be directly re-expressed in terms of $\Theta_0^{(0)}$ and $\Theta_1^{(0)}$, and are valid in the tight coupling approximation. In order to analyse the behaviour of the coupled baryon-photon fluid when tight coupling breaks down, the Boltzmann equation (3.101) must be complemented with the scalar baryon equation

$$\dot{v}_B^{(0)} + \frac{a'}{a} v_B^{(0)} = k\Psi + \dot{\tau}\frac{4\rho_\gamma}{3\rho_B}(\Theta_1^{(0)} - v_B^{(0)})\,. \tag{3.106}$$

In the work presented in chapters 4 and 5 we will not need to go beyond the tight coupling approximation. Using Boltzmann equations (3.101), (3.102) we can derive a result which will be used in chapter 4. In section 4.4 we will need to evaluate the temperature anisotropies and polarisation sourced by the tensor perturbations induced by a primordial magnetic field. From Eq. (3.102), in the limit $\dot{\tau} \to \infty$, one derives $E_2^{(m)} = -\frac{\sqrt{6}}{4}\Theta_2^{(m)}$, and therefore $P^{(m)} = \frac{1}{4}\Theta_2^{(m)}$. Consequently, Eq. (3.101) for tensor perturbations at the lowest order takes the form

$$\dot{\Theta}_2^{(2)} = -\frac{3}{4}\dot{\tau}\Theta_2^{(2)} - \dot{H}_T^{(2)}\,, \tag{3.107}$$

which in the tight coupling limit implies simply

$$P^{(2)} = -\frac{1}{3}\frac{\dot{H}_T^{(2)}}{\dot{\tau}}\,. \tag{3.108}$$

In chapter 4, we will substitute this expression in Eqs. (3.110-3.112) to find the temperature anisotropy and polarisation components sourced by tensor perturbations.

3.2.3 Integral solutions and power spectra

The Boltzmann equations (3.101-3.103) describe how the sources $S_\ell^{(m)} G_\ell^{(m)}$ and

$$-\dot{\tau}\sqrt{6}P^{(m)}[{}_2G_\ell^{(m)}\mathbf{M}_+ + {}_{-2}G_\ell^{(m)}\mathbf{M}_-] \tag{3.109}$$

project as temperature anisotropies and polarisation on the sky. The projection is obtained by extracting the total angular dependence of the mode, from its decomposition in radial functions and spherical harmonics. The full solution then follows by integrating the projected source over the radial coordinate [95],

$$\frac{\Theta_\ell^{(m)}(\eta_0,k)}{2\ell+1} = \int_0^{\eta_0} d\eta\, e^{-\tau} \sum_{\ell'} S_{\ell'}^{(m)}(\eta)\, j_\ell^{(\ell' m)}(k(\eta_0-\eta))\,, \tag{3.110}$$

$$\frac{E_\ell^{(m)}(\eta_0,k)}{2\ell+1} = -\sqrt{6}\int_0^{\eta_0} d\eta\, \dot{\tau} e^{-\tau} P^{(m)}(\eta)\epsilon_\ell^{(m)}(k(\eta_0-\eta))\,, \tag{3.111}$$

$$\frac{B_\ell^{(m)}(\eta_0,k)}{2\ell+1} = -\sqrt{6}\int_0^{\eta_0} d\eta\, \dot{\tau} e^{-\tau} P^{(m)}(\eta)\beta_\ell^{(m)}(k(\eta_0-\eta))\,. \tag{3.112}$$

Here

$$\tau(\eta) = \int_\eta^{\eta_0} \dot{\tau}(\eta')d\eta' \tag{3.113}$$

is the optical depth between the epoch η and today; the combination $\dot{\tau}e^{\tau}$ is the visibility function, and expresses the probability that a photon last scattered between η and $\eta + d\eta$: therefore, it is sharply peaked at $\eta_{\rm dec}$. The difference between the integral solutions (3.110-3.112) and the differential form (3.101-3.103) is that in the former case the coupling between the modes is performed in one step, from the source at time η and distance $\eta_0 - \eta$ to the present; in the latter case, the power is steadily transferred to higher ℓ as the time advances. The integral solutions are useful for example to find approximate, analytical expressions for the CMB anisotropies in the tight coupling regime, as will be done in the next chapters. It is useful to rewrite the solution for the amplitude of the temperature anisotropy in a more familiar form, showing explicitly the contribution from the scalar, vector and tensor sources:

$$\frac{\Theta_\ell^{(0)}(\eta_0,k)}{2\ell+1} = \int_0^{\eta_0} d\eta\, e^{-\tau}\left[(\dot{\tau}\Theta_0^{(0)} + \dot{\tau}\Psi + \dot{\Psi} - \dot{\Phi})j_\ell^{(00)} + \dot{\tau}v_B^{(0)}j_\ell^{(10)} + \dot{\tau}P^{(0)}j_\ell^{(20)}\right] \tag{3.114}$$

$$\frac{\Theta_\ell^{(1)}(\eta_0,k)}{2\ell+1} = \int_0^{\eta_0} d\eta\, e^{-\tau}\left[\dot{\tau}(v_B^{(1)} - B^{(1)})j_\ell^{(11)} + (\dot{\tau}P^{(1)} + \frac{1}{\sqrt{3}}kB^{(1)})j_\ell^{(21)}\right]\,, \tag{3.115}$$

$$\frac{\Theta_\ell^{(2)}(\eta_0,k)}{2\ell+1} = \int_0^{\eta_0} d\eta\, e^{-\tau}\left[\dot{\tau}P^{(2)} - \dot{H}_T^{(2)}\right]j_\ell^{(22)}\,. \tag{3.116}$$

The last step in calculating the CMB fluctuations is the integration over the k modes. The two point statistics of the temperature and polarisation fields, and of the cross-correlations, are described by the power spectra $C_\ell^{\mathcal{X}\tilde{\mathcal{X}}}$, where $\mathcal{X}$ stands for each of the functions Θ, E,

B. They are defined as $\langle a_{\ell m} a^*_{\ell' m'} \rangle = C_\ell \, \delta_\ell^{\ell'} \delta_m^{m'}$, with $\Theta(\mathbf{x}_0, \hat{\mathbf{n}}, \eta_0) = \sum_{\ell m} a_{\ell m}(\mathbf{x}_0) Y_\ell^m(\hat{\mathbf{n}})$, and similar expressions in terms of spin-weighted harmonics for the polarisation field. Under the assumption of homogeneity and isotropy, the power spectrum depends neither on x_0, the observer's position, nor on m. The scalar, vector and tensor contributions are uncorrelated, so that, in terms of the moments defined in the total angular momentum formalism, one has

$$C_\ell^{\mathcal{X}\tilde{\mathcal{X}}} = \frac{2}{\pi} \frac{1}{(2\ell+1)^2} \int dk \, k^2 \sum_{m=-2}^{2} \mathcal{X}_\ell^{(m)}(\eta_0, k) \tilde{\mathcal{X}}_\ell^{(m)*}(\eta_0, k) \,, \tag{3.117}$$

where now m denotes the scalar, vector and tensor modes.

3.3 Effects of primordial magnetic fields on the CMB

As observed already in section 1.2.4, the presence of a primordial magnetic field affects the space-time geometry of the universe. The energy momentum tensor of the field takes the form (1.39) with zero electric field; the components are given by (*cf.* Eqs. (1.40-1.43))

$$\rho_B = \frac{B^2}{2} \,, \qquad p_B = \frac{B^2}{6} \,, \qquad q_B^\alpha = 0 \,, \qquad \pi_B^{\alpha\beta} = \frac{B^2}{3} h^{\alpha\beta} - B^\alpha B^\beta \,. \tag{3.118}$$

In order not to alter the background cosmology, one assumes that the magnetic energy density is a first order perturbation in linear perturbation theory. Magnetic energy density acts as a source in the Poisson equation (3.58), and by decomposing the magnetic anisotropic stress tensor $\pi_B^{\alpha\beta}$ into scalar, vector and tensor modes, one obtains the magnetic influence on the perturbation evolution equations (3.59-3.64). This is done for example in reference [104]; the form of a general projection to extract any mode, scalar, vector or tensor, from a generic tensorial perturbation, can be found in [105]. The magnetic field itself can be modelled in two ways: either as a small, homogeneous background component, the approach adopted for example in references [90], [91]; or as a stochastic field, 1/2 order in perturbation theory, described in the previous chapter and analysed for example in references [106], [107].

A fully general-relativistic treatment of the effects of a homogeneous magnetic field on the space-time metric is performed in references [90,91,108]. These works do not concentrate specifically on the imprint of a primordial magnetic field in the CMB anisotropies, but outline the basic equations and its main effects as a source of metric perturbations. In references

[90, 108], Tsagas and Barrow used the Ellis-Bruni covariant and gauge invariant formalism, and derived the exact non-linear equations, which account for the influence of the magnetic field on the conservation and dynamic equations presented in the general case in sections 1.2.3 and 1.2.5. Then they performed linearisation about a FRW universe, and concentrated on the magnetic effects on the growth of density inhomogeneities during both the matter and radiation dominated eras. Their results are improved and generalised in reference [91], where Tsagas and Maartens treated both scalar and vector effects of a weak homogeneous field. They included all the couplings between the fluid, the field and the curvature, and identified the following main results. The magneto-curvature coupling causes an enhancement of the adiabatic growing mode of density perturbations on super-horizon scales, during the radiation era. On sub-horizon scales, the magnetic field induces magnetosonic waves [12], and a consequent change in the sound velocity which can leave an imprint in the CMB. The field is also a source of vorticity, which may also lead to an observable effect in the CMB through the formation of Alfvén waves [12]. In the matter dominated era, the presence of a magnetic field can have effects on the linear growth of structures. The adiabatic growing mode of density perturbations on sub-horizon scales is slightly damped by the presence of the field, and the field can generate density fluctuations in a homogeneous medium by itself. Moreover, the authors investigate the magnetic effects on the shape distortion in the density distribution, which can have potentially important implications for structure formation.

We now turn to a brief review of previous articles which analysed more specifically the influence of a primordial magnetic field on CMB anisotropies and polarisation. First of all, one can ask the simple question of which order of magnitude of the field amplitude one might expect to leave an observable imprint in the CMB. This can be answered by a simple estimate [18, 107]. A stochastic magnetic field affects the amplitude of the fluctuations in the FRW background quadratically (*cf.* Eqs. (3.118), so that one has

$$\frac{\rho_B}{\rho_\gamma} \simeq 10^{-5}\left(\frac{B}{10^{-8}\,\mathrm{Gauss}}\right)^2 , \tag{3.119}$$

where ρ_γ is the photon energy density today, and B the field amplitude today. Since $\mathcal{O}(\Delta T/T) = 10^{-5}$, the largest field amplitude which is still compatible with homogeneity and isotropy, and leaves a detectable signal in the CMB, is of the order of 10^{-8} Gauss. One should now compare this value with the limits derived in section 2.5.2. If the magnetic field is causally created, one should account for the fact that the CMB probes very large scales: one has to estimate the field amplitude on scales of the order of 100 Mpc, which corresponds to a harmonic of about $\ell \sim 400$ (here we have used the angular diameter distance to the last scattering surface, $d_A \simeq 13700$ Mpc, from WMAP [5]). Using the scaling behaviour derived in section 2.5.2, and starting from the maximal values obtained for $\lambda = 1$ Mpc, one can infer residual fields of at best $B_{100\text{ Mpc}} \simeq 10^{-42}$ Gauss, and helicity of $\mathcal{B}_{100\text{ Mpc}} \sim 10^{-46}$ Gauss. Therefore, the amplitude of the induced fluctuations in the CMB is typically of the order of $\Delta T/T \sim (\rho_{B|100\text{Mpc}})/\rho_\gamma \ll 10^{-5}$. In conclusion, a causally created magnetic field does not lead to observable traces in the anisotropies or polarisation of the CMB, since its effect is to small to be distinguished among the other sources of fluctuations [18]. In order to obtain observable effects, one needs to require an inflationary created magnetic field, with negative spectral indices $-3 < n_S < n_A < -2$: in this case, the constraints on the amplitude are much weaker, and a field of the order of nanoGauss is allowed (as derived in reference [80]).

3.3.1 Effects on temperature anisotropies

The study of the imprint of a magnetic field in the CMB fluctuations has been motivated by two different aims: as a way to detect the possible presence of a primordial magnetic field, and as a way to constrain its amplitude (and in turn, the generation process). In reference [88], Barrow *et al.* find a constraint on the amplitude of a homogeneous magnetic field, evaluating the shear anisotropy induced by it and comparing it with the value allowed by the isotropy measurement of the COBE satellite. In agreement with the previous order of magnitude estimate, the maximal amplitude for the field is found to be $3.4 \times 10^{-9}(\Omega h_{50}^2)^{1/2}$ Gauss, where Ω is the cosmological density parameter and h_{50} the present value of the Hubble constant in units of $50\,\text{km}\,\text{sec}^{-1}$ Mpc^{-1}. This is still the strongest constraint to date for a primordial homogeneous field.

As already mentioned, on sub-horizon scales the magnetic field affects the acoustic oscillations of the baryon-photon fluid, generating magnetohydrodynamic waves (*cf.* also section 2.4.4). The *fast and slow magnetosonic waves* are compressional waves, and involve both density and velocity fluctuations [12]. Their velocity is bigger than the speed of sound, ${c_s}^2 \longrightarrow {c_s}^2 + {V_A}^2 \sin^2\theta$, where V_A is the Alfvén speed and θ the angle between $\mathbf{B}$ and the direction of propagation of the wave. This modification translates in a reduction of the amplitude of the first peak, as a consequence of the magnetic pressure which opposes the in-fall of the photon-baryon fluid in the potential well of the fluctuation. This effect has first been studied in reference [109], where Adams *et al.* considered a homogeneous magnetic field; it has been included also in reference [110], where Koh and Lee analysed both temperature and polarisation signals induced by scalar perturbations from a stochastic magnetic field.

The third kind of magnetohydrodynamic waves, *Alfvén waves*, is instead purely rotational, therefore does not involve scalar but vector perturbations [12]. The vector mode perturbations induced by a homogeneous magnetic field have been first studied in reference [111]; they induce temperature CMB anisotropies via a Doppler effect, and the main effect is the creation of correlations between multipoles $\ell \pm 1$ (a homogeneous magnetic field breaks statistical isotropy). This effect has been applied recently to the WMAP satellite data: in reference [112], Chen *et al.* used the new data to constrain the amplitude of the magnetic field, and found $B \lesssim 10^{-9}$ Gauss; in [113], Naselsky *et al.* observed that this effect is not the source of the detected non-Gaussianity from the WMAP data. Vector modes induced by a stochastic magnetic field have been extensively studied also in references [106, 114]: in these references, Subramanian and Barrow pointed out that the Alfvén mode can be over-damped and survives Silk damping on much smaller scales than the compressional mode [73], and can produce significant small angular scale temperature anisotropies through the Doppler effect, for $\ell = 1000 - 3000$. In order for this signal to be observable, the magnetic field amplitude should be of the order of nanoGauss, and the spectrum almost scale-invariant.

The tensor mode temperature fluctuations due to a stochastic magnetic field have been computed in reference [107], and the resulting power spectrum, evaluated analytically, is used to induce a bound on the magnetic field amplitude which depends on the spectral index, but is again of the order of nanoGauss. Analytical approximations for the tensor spectra are given, more recently, also in [115]: this work includes also the effect from the vector modes, and evaluates analytically both the temperature and polarisation signals from a stochastic magnetic field. The interplay between a primordial magnetic field and gravitational waves has been extensively studied, beside the effects on the CMB. For example, in reference [116], Maartens *et al.* considered a homogeneous magnetic field, and found that it can both generate gravitational waves on large scales, and damp preexisting waves. Reference [117] presents an interesting process of amplification of an inflationary created magnetic field, which arises from the interaction of the field with the spectrum of gravitational waves also generated during inflation. The mechanism is particularly efficient at super-horizon scales, and can amplify the original fields to values suitable for being seeds for the dynamo mechanism.

3.3.2 Effects on polarisation

The presence of a magnetic field at the epoch of last scattering can affect CMB polarisation by causing Faraday rotation of the linear polarisation direction. The effect was first studied in reference [118], for a magnetic field uniform on the scales of the width of the last scattering surface, 5 Mpc today, and concentrating on scalar perturbations. The magnetic field introduces a mixing term in the radiative transport equations (3.102-3.103), between E and B type polarisation. The Faraday rotation angle is given by $\frac{d\phi}{ad\eta} \propto n_e \lambda^2 (\mathbf{B} \cdot \hat{\mathbf{n}})$ (*cf.* Eq. (2.3)): since it depends on the wavelength, Kosowsky and Loeb proposed to estimate this effect by comparing the polarisation vector on a given direction at two different frequencies. A more direct single-frequency measurement is also possible, as pointed out in reference [89]. Scalar modes result in polarisation which is normally purely of the E sort (*cf.* section 3.2). A homogeneous magnetic field, however, will create B polarisation which correlates with the scalar temperature spectrum, since the E mode gets rotated into B mode by Faraday rotation. This parity-odd signal is specific to the presence of a large scale magnetic field. Reference [119] analyses the depolarisation effects consequent to Faraday rotation. All these effects are in principle detectable, for a homogeneous field amplitude of the order of nanoGauss; they have been recently revised in reference [120], in which Scoccola *et al.* observed that a nanoGauss homogeneous magnetic field generates B mode polarisation with an amplitude comparable to that due to weak gravitational lensing, at a frequency of 30 Ghz; however, the magnetic field signal is distinguishable since it depends on frequency, as stated before. The effect of Faraday rotation by a stochastic field has been analysed in [121], where it is found that a CMB Faraday rotation map cannot give any information about a possible helical component of the magnetic field. Distinctive signatures of a helical component in the CMB polarisation, not connected to Faraday rotation effects, will be analysed in the next chapter.

A primordial magnetic field can affect CMB polarisation not only by Faraday rotation, but also simply through the production of metric perturbations. Vorticity induced by the field in the photon-baryon fluid gives rise to B mode polarisation [122], and also to a minor extent to pure E polarisation and Θ–E cross-correlation [123]. The generation of B type polarisation makes it easier to separate the magnetic contribution from more conventional sources, like inflation-generated scalar modes, which only give rise to E polarisation. The above mentioned references claim that a scale-invariant spectrum of stochastic field with nanoGauss amplitude produces B type polarisation detectable in the high range $\ell \sim 1000 - 5000$. All the polarisation contributions both from vector and tensor modes have been investigated semi-analytically in reference [115]; a more detailed numerical analysis of the full linearised equations is performed in reference [124]. In this reference, Lewis considered an almost scale-invariant spectrum, and amplitude of the order of nanoGauss, and found observable contributions to B type polarisation, assuming idealised observations; he pointed out that foregrounds, such as weak lensing, and systematics may pose problems to the detection. He included a full analysis of the processes occurring at recombination, of neutrinos effects and of reionisation effects, and found a potentially important compensation to the tensor mode on super-horizon scales by neutrinos anisotropic stresses, which have been necessarily neglected in semi-analytical works.

We finally mention the generation of parity-odd cross-correlations Θ–B and E–B by the presence of helical magnetic fields or helical velocity flows, investigated for the first time in reference [93], and which is the subject of the next chapter.

Chapter 4

The CMB and helical magnetic fields: the tensor mode

This chapter contains the work done in reference [92], in which we studied the effect of a helicity component of a primordial stochastic magnetic field on the tensor part of the CMB temperature anisotropies and polarisation. We find analytical approximations for the tensor contributions induced by helicity, discussing their amplitude and spectral index in dependence of the power spectrum of the primordial magnetic field. We obtain that a helical magnetic field creates a parity-odd component of gravity waves, inducing parity-odd polarisation signals. However, only if the magnetic field is close to scale-invariant and if its helical part is close to maximal, the effect is sufficiently large to be observable.

In this chapter we use CGS electromagnetic units, so that the magnetic energy density is $B^2/8\pi$; we also explicitly show the $8\pi G$ factors. Moreover, in order to avoid the presence of too many upper indices, the derivative with respect to conformal time is now denoted by a dot $\dot{} = \frac{d}{d\eta}$, instead of $'$.

4.1 Introduction

In section 2.5, we have analysed the characteristics of a stochastic magnetic field, introducing the helicity term in the magnetic field spectrum. Extended studies have already investigated the effects of stochastic magnetic fields with vanishing helicity on the CMB, as reviewed in the previous chapter. In a seminal paper [93], Pogosian and collaborators have investigated the possibility that a helical magnetic field induced correlations between the temperature anisotropy and the B mode CMB polarisation. In this chapter we go beyond that work, and determine all the effects on the CMB fluctuations generated by a helical magnetic field. We shall show that, contrary to the statement of reference [93], a helical component also induces pure CMB anisotropies and polarisation. But of course its most remarkable effect is the above mentioned correlation of temperature anisotropy and B polarisation. We shall show that also a correlation between E and B polarisation is generated. We discuss only the tensor mode, gravitational waves, since the calculations for this case are simplest. Even if the resulting observational effects are small and may not be detectable, they are still interesting, being completely new and containing several surprising elements. Furthermore, a fluid vorticity field or non-parity-invariant initial spectrum of gravitational waves produced during inflation could induce very similar effects; in that sense our results are more generic than their derivation.

We refer to section 2.5 for the definitions of the magnetic field spectrum and its symmetric and helical contributions. In the next section, we compute the tensor component of the magnetic field energy momentum tensor which acts as a source for gravity waves; in section 4.3 we determine the induced gravity wave spectrum, which also shows a symmetric and a helical contribution. The induced CMB temperature anisotropy and polarisation spectra, as well as the above mentioned correlations, are computed in section 4.4 and 4.5; finally, we discuss our results and draw some conclusions.

4.2 Magnetic source term for tensor metric perturbations

The anisotropic stresses which act as source for metric perturbations are given by the magnetic field stress tensor [12]

$$\tau_{ij}(\mathbf{k}) = \frac{1}{(2\pi)^3}\frac{1}{4\pi}\int d^3p\,[B_i(\mathbf{p})B_j^*(\mathbf{p}-\mathbf{k}) - \frac{1}{2}B_l(\mathbf{p})B_l^*(\mathbf{p}-\mathbf{k})\delta_{ij}]\,. \tag{4.1}$$

We are interested in the generation of gravitational waves, and consequently we need to extract the transverse and traceless part of τ_{ij}. We make use of the tensor projector $T_{ijlm} = P_{il}P_{jm} - \frac{1}{2}P_{ij}P_{lm}$, with $P_{il} = \delta_{il} - \hat{k}_i\hat{k}_l$ [105, 107], so the tensor contribution to τ_{lm} is given by

$$\Pi_{ij} = (P_{il}P_{jm} - \frac{1}{2}P_{ij}P_{lm})\tau_{lm} \,. \tag{4.2}$$

Moreover, since the magnetic field is a stochastic variable, we need to calculate the two point correlation function of $\tau_{ij}(\mathbf{k})$, which takes the form

$$\langle\tau_{ij}(\mathbf{k})\tau^*_{lm}(\mathbf{k}')\rangle = \frac{1}{4(2\pi)^8}\int d^3p \int d^3q \,[\langle B_i(\mathbf{p})B_j(\mathbf{k}-\mathbf{p})B_l(-\mathbf{q})B_m(\mathbf{q}-\mathbf{k}')\rangle + \cdots\delta_{ij} + \cdots\delta_{lm}] \,, \tag{4.3}$$

and we are not interested in terms proportional to δ_{ij} and δ_{lm} , which after being projected out will not contribute to the final result for the tensor perturbation $\langle\Pi_{ij}\Pi_{lm}\rangle$ (*cf.* appendix B of [80]). Before applying the tensor projection, we can simplify the right hand side of (4.3) using Wick's theorem, expressing the four point correlators in terms of the two point ones,

$$\begin{aligned}
\langle B_i(\mathbf{k}_i)B_j(\mathbf{k}_j)B_l(\mathbf{k}_l)B_m(\mathbf{k}_m)\rangle &= \langle B_i(\mathbf{k}_i)B_j(\mathbf{k}_j)\rangle\langle B_l(\mathbf{k}_l)B_m(\mathbf{k}_m)\rangle \\
&+ \langle B_i(\mathbf{k}_i)B_l(\mathbf{k}_l)\rangle\langle B_j(\mathbf{k}_j)B_m(\mathbf{k}_m)\rangle \\
&+ \langle B_i(\mathbf{k}_i)B_m(\mathbf{k}_m)\rangle\langle B_j(\mathbf{k}_j)B_l(\mathbf{k}_l)\rangle \,.
\end{aligned} \tag{4.4}$$

Since the two point correlation function given in Eq. (2.41) is not symmetric, we are not allowed to change the order of indices i, j, l, m inside an expectation value. With Eq. (2.41) we can then compute the correlation function (4.3), which consists of a purely symmetric part proportional to $\int d^3p\, S(p)S(|\mathbf{k}-\mathbf{p}|)$, a purely helical part proportional to $\int d^3p\, A(p)A(|\mathbf{k}-\mathbf{p}|)$, and mixed terms, $i\int d^3p\, S(p)A(|\mathbf{k}-\mathbf{p}|)$: after a longish but simple calculation we obtain

$$\begin{aligned}
\langle\tau_{ij}(\mathbf{k})\tau^*_{lm}(\mathbf{k}')\rangle &= \frac{\delta(\mathbf{k}-\mathbf{k}')}{4(4\pi)^2}\int d^3p\,\{\, S(p)S(|\mathbf{k}-\mathbf{p}|)[(\delta_{il}-\hat{p}_i\hat{p}_l)(\delta_{jm}-(\widehat{\mathbf{k}-\mathbf{p}})_j(\widehat{\mathbf{k}-\mathbf{p}})_m) \\
&+ (\delta_{im}-\hat{p}_i\hat{p}_m)(\delta_{jl}-(\widehat{\mathbf{k}-\mathbf{p}})_j(\widehat{\mathbf{k}-\mathbf{p}})_l)] \\
&- A(p)A(|\mathbf{k}-\mathbf{p}|)[\epsilon_{ilt}\epsilon_{jmr}\hat{p}_t(\widehat{\mathbf{k}-\mathbf{p}})_r + \epsilon_{imf}\epsilon_{jlg}\hat{p}_f(\widehat{\mathbf{k}-\mathbf{p}})_g] \\
&+ iS(p)A(|\mathbf{k}-\mathbf{p}|)[\epsilon_{jmr}(\delta_{il}-\hat{p}_i\hat{p}_l)(\widehat{\mathbf{k}-\mathbf{p}})_r + \epsilon_{jlg}(\delta_{im}-\hat{p}_i\hat{p}_m)(\widehat{\mathbf{k}-\mathbf{p}})_g] \\
&+ iA(p)S(|\mathbf{k}-\mathbf{p}|)[\epsilon_{ilt}(\delta_{jm}-(\widehat{\mathbf{k}-\mathbf{p}})_j(\widehat{\mathbf{k}-\mathbf{p}})_m)\hat{p}_t + \epsilon_{imf}(\delta_{jl}-(\widehat{\mathbf{k}-\mathbf{p}})_j(\widehat{\mathbf{k}-\mathbf{p}})_l)\hat{p}_f] \\
&+ \cdots\delta_{ij} + \cdots\delta_{lm}\,\} \,.
\end{aligned} \tag{4.5}$$

The first two terms of the integrand will contribute to the symmetric part of the two point correlation function of the tensor source, while the second two terms give rise to a helical contribution. To express them we now introduce the two point correlation function for the tensor source, which can be modelled as

$$\langle \Pi_{ij}(\mathbf{k})\Pi^*_{lm}(\mathbf{k}')\rangle \equiv \frac{(2\pi)^3}{4}\left[\mathcal{M}_{ijlm}f(k) + i\mathcal{A}_{ijlm}g(k)\right]\delta(\mathbf{k}-\mathbf{k}')\,, \tag{4.6}$$

where the tensors $\mathcal{M}_{ijlm}$ and $\mathcal{A}_{ijlm}$ are given by

$$\mathcal{M}_{ijlm} \equiv P_{il}P_{jm} + P_{im}P_{jl} - P_{ij}P_{lm}\,, \tag{4.7}$$

$$\mathcal{A}_{ijlm} \equiv \frac{\hat{k}_q}{2}(P_{jm}\epsilon_{ilq} + P_{il}\epsilon_{jmq} + P_{im}\epsilon_{jlq} + P_{jl}\epsilon_{imq})\,. \tag{4.8}$$

Clearly, both $\mathcal{M}_{ijlm}$ and $\mathcal{A}_{ijlm}$ are symmetric in the first and second pair of indices. $\mathcal{M}_{ijlm}$ is also symmetric under the exchange of ij with lm while $\mathcal{A}_{ijlm}$ is anti-symmetric under this permutation. We shall often use simple properties like

$$\mathcal{M}_{ijij} = 4\,, \qquad \mathcal{M}_{iilm} = \mathcal{M}_{ijll} = 0 \tag{4.9}$$

$$P_{qi}\mathcal{M}_{ijlm} = \mathcal{M}_{qjlm}\,, \qquad P_{qi}\mathcal{A}_{ijlm} = \mathcal{A}_{qjlm} \tag{4.10}$$

$$\mathcal{M}_{ijlm}\mathcal{M}_{ijlm} = \mathcal{A}_{ijlm}\mathcal{A}_{ijlm} = 8 \tag{4.11}$$

$$\mathcal{A}_{ijlm}\mathcal{M}_{ijlm} = 0\,, \qquad \mathcal{A}_{ijij} = \mathcal{A}_{iijl} = \mathcal{A}_{ijll} = 0\,. \tag{4.12}$$

According to Eq. (4.2), we have now to act on $\langle\tau_{ab}(\mathbf{k})\tau^*_{cd}(\mathbf{k}')\rangle$ with the tensor projector

$$\mathcal{P}^{abcd}_{ijlm}(\hat{\mathbf{k}},\hat{\mathbf{k}}') = (P_{ia}P_{jb} - \frac{1}{2}P_{ij}P_{ab})(\hat{\mathbf{k}})(P_{lc}P_{md} - \frac{1}{2}P_{lm}P_{cd})(\hat{\mathbf{k}}')\,. \tag{4.13}$$

In these calculations we do not need to care about the position (up or down) of Latin indices as they are always contracted by a Kronecker δ. The symmetric and antisymmetric parts of Eq. (4.6) are invariant under the application of the projector (4.13), so that it is easy to separate the symmetric and helical parts of the source spectrum, $f(k)$ and $g(k)$:

$$2(2\pi)^3\delta(\mathbf{k}-\mathbf{k}')f(k) = \mathcal{M}_{abcd}\langle\tau_{ab}(\mathbf{k})\tau^*_{cd}(\mathbf{k}')\rangle \tag{4.14}$$

$$2(2\pi)^3\delta(\mathbf{k}-\mathbf{k}')g(k) = -i\mathcal{A}_{abcd}\langle\tau_{ab}(\mathbf{k})\tau^*_{cd}(\mathbf{k}')\rangle\,. \tag{4.15}$$

We can now apply the tensor $\mathcal{M}_{ijlm}$ to Eq. (4.5), and obtain (the first term of this has already been computed in references [80, 107, 115])

$$f(k) = \frac{2}{(4\pi)^5}\int d^3p\,[\,S(p)S(|\mathbf{k}-\mathbf{p}|)(1+\gamma^2)(1+\beta^2) + 4A(p)A(|\mathbf{k}-\mathbf{p}|)(\gamma\beta)\,]\,, \qquad (4.16)$$

where $\gamma = \hat{\mathbf{k}}\cdot\hat{\mathbf{p}}$ and $\beta = \hat{\mathbf{k}}\cdot(\widehat{\mathbf{k}-\mathbf{p}})$. Note that the square of the helical part of the magnetic field spectrum (2.41) contributes to the symmetric part of the source spectrum. This is not surprising, since the product of two quantities with odd parity has even parity. The antisymmetric part of the tensor source spectrum is obtained by acting with $\mathcal{A}_{ijlm}$ on Eq. (4.5), and is given by the mixed term

$$g(k) = \frac{8}{(4\pi)^5}\int d^3p\, S(p)A(|\mathbf{k}-\mathbf{p}|)(1+\gamma^2)\beta\,. \qquad (4.17)$$

We can also express the correlator (4.6) in terms of the tensor basis introduced in Eq. (3.90),

$$e^{\pm}_{ij} = -\sqrt{\frac{3}{8}}(\mathbf{e}_1 \pm i\mathbf{e}_2)_i \otimes (\mathbf{e}_1 \pm i\mathbf{e}_2)_j\,, \qquad (4.18)$$

which is a basis for tensor perturbations, satisfying the transverse-traceless condition $\delta_{ij}e^{\pm}_{ij} = 0$, $\hat{k}_i e^{\pm}_{ij} = 0$ and $e^{\pm}_{ij}e^{\mp}_{ij} = 3/2$ (see also section 3.1.1). Positive circularly polarised gravity waves are proportional to e^{+}_{ij}, while negative circularly polarised gravity waves are given by the coefficient of e^{-}_{ij}. In this basis Π_{ij} is expressed as

$$\Pi_{ij}(\mathbf{k}) \equiv e^{+}_{ij}\Pi^{+}(\mathbf{k}) + e^{-}_{ij}\Pi^{-}(\mathbf{k})\,. \qquad (4.19)$$

We can rewrite $f(k)$ and $g(k)$ in terms of the components $\Pi^{\pm}$ as

$$2(2\pi)^3\delta(\mathbf{k}-\mathbf{k}')\,f(k) = 3\langle\Pi^{+}(\mathbf{k})\Pi^{+*}(\mathbf{k}') + \Pi^{-}(\mathbf{k})\Pi^{-*}(\mathbf{k}')\rangle\,, \qquad (4.20)$$

$$2(2\pi)^3\delta(\mathbf{k}-\mathbf{k}')\,g(k) = -3\langle\Pi^{+}(\mathbf{k})\Pi^{+*}(\mathbf{k}') - \Pi^{-}(\mathbf{k})\Pi^{-*}(\mathbf{k}')\rangle\,, \qquad (4.21)$$

where we have used the form of $\mathcal{M}_{ijlm}$ and $\mathcal{A}_{ijlm}$ in this basis,

$$\begin{aligned}\mathcal{M}_{ijlm} &= \frac{4}{3}\left[e^{+}_{ij}\otimes e^{-}_{lm} + e^{-}_{ij}\otimes e^{+}_{lm}\right]\\ \mathcal{A}_{ijlm} &= \frac{4i}{3}\left[e^{+}_{ij}\otimes e^{-}_{lm} - e^{-}_{ij}\otimes e^{+}_{lm}\right]\,,\end{aligned}$$

and the simple properties of $\mathcal{M}_{ijlm}$ and $\mathcal{A}_{ijlm}$ mentioned above (4.9-4.12). Similarly, defining the usual linear polarisation basis for gravitational waves

$$\begin{aligned} e^T_{ij} &= (\mathbf{e}_1 \otimes \mathbf{e}_1 - \mathbf{e}_2 \otimes \mathbf{e}_2)_{ij} \\ e^\times_{ij} &= (\mathbf{e}_1 \otimes \mathbf{e}_2 + \mathbf{e}_2 \otimes \mathbf{e}_1)_{ij} \,, \end{aligned} \tag{4.22}$$

and the components of Π with respect to this basis,

$$\Pi_{ij} = \Pi^T e^T_{ij} + \Pi^\times e^\times_{ij} \,, \tag{4.23}$$

we obtain also

$$\langle \Pi^T(\mathbf{k})\Pi^{T*}(\mathbf{k}') + \Pi^\times(\mathbf{k})\Pi^{\times*}(\mathbf{k}')\rangle = (2\pi)^3\delta(\mathbf{k}-\mathbf{k}')\, f(k) \tag{4.24}$$

$$\langle \Pi^\times(\mathbf{k})\Pi^{T*}(\mathbf{k}') - \Pi^T(\mathbf{k})\Pi^{\times*}(\mathbf{k}')\rangle = i(2\pi)^3\delta(\mathbf{k}-\mathbf{k}')\, g(k)\,. \tag{4.25}$$

Using Eqs. (4.16), (4.17), and the expressions for the spectra (2.49-2.52), it is possible to calculate $f(k)$ and $g(k)$. The details of the calculations are given in appendix A. The integrals cannot be computed analytically, but a good approximation gives, for $k < k_D$ (see also [107,115]):

$$f(k) \simeq \mathcal{A}_S \left((\lambda k_D)^{2n_S+3} + \frac{n_S}{n_S+3}(\lambda k)^{2n_S+3} \right) - \mathcal{A}_A \left((\lambda k_D)^{2n_A+3} + \frac{n_A-1}{n_A+4}(\lambda k)^{2n_A+3} \right) \tag{4.26}$$

$$g(k) \simeq \mathcal{C}\, (\lambda k_D)^{n_S+n_A+2}\, (\lambda k) \left[1 + \frac{n_A-1}{n_S+3}\left(\frac{k}{k_D}\right)^{n_S+n_A+2} \right] , \tag{4.27}$$

where $\mathcal{A}_S$, $\mathcal{A}_A$ and $\mathcal{C}$ are positive constants given in Eqs. (A.11-A.13) of appendix A. They depend on the spectral indices n_S and n_A of the magnetic field and on its amplitudes, which are given in terms of B^2_λ, $\mathcal{B}^2_\lambda$, and λ.

Note that the contribution of magnetic field helicity to the symmetric part of the source $f(k)$ is negative. However, Eq. (2.63) insures that it never dominates, hence $f(k) \geq 0$. For $n_S, n_A > -3/2$, the two terms proportional to the upper cutoff $k_D^{2n_{S,A}+3}$ dominate in $f(k)$, which consequently depends only on the cutoff frequency and behaves like a white noise source [107]. For $n_S < -3/2$ or also $n_A < -3/2$, the dominating terms go like k^{2n_S+3} and k^{2n_A+3} respectively. On the contrary, the antisymmetric source $g(k)$ never shows a white noise behavior. For $n_S + n_A > -2$ the dominant term is proportional to $k\, k_D^{n_S+n_A+2}$; for $n_S + n_A < -2$, $g(k)$ does not depend on the upper cutoff, but is proportional to $k^{n_S+n_A+3}$. The singularities in the pre-factors $\mathcal{A}_S$, $\mathcal{A}_A$ and $\mathcal{C}$ which appear at $n_S = -3$ and $n_A = -4$ are the usual logarithmic singularities of scale-invariant spectra; however, as demonstrated in section 2.5.2, the helical contribution must obey $n_A \geq n_S > -3$. The apparent singularities in the pre-factors at $n_{S,A} = -3/2$ and at $n_S + n_A = -2$ are removable when multiplied with the k-dependent parts in Eqs. (4.26) and (4.27). In the integrals over k which we shall perform to calculate the C_ℓ's we only take into account the dominant terms of $f(k)$ and $g(k)$.

If the magnetic field is causal, we expect $n_S = 2$ and $n_A = 3$ (*cf.* section 2.5.2), so that

$$f(k) \simeq \mathcal{A}_S(k_D\lambda)^7 - \mathcal{A}_A(k_D\lambda)^9 \tag{4.28}$$

$$g(k) \simeq \mathcal{C}k\lambda(k_D\lambda)^7 . \tag{4.29}$$

Comparing the limit given in Eq. (2.67) with the expressions for $\mathcal{A}_S$ and $\mathcal{A}_A$ derived in the appendix A, one can see that $f(k)$ always remains positive.

The analysis of the evolution of a non-helical magnetic field interacting with the primordial plasma, and the derivation of the appropriate damping scale k_D, has been discussed in section 2.4.4, where we presented the results of references [73, 79]. In [73], Subramanian and Barrow considered a magnetic field with a tangled component superimposed on a homogeneous field. We assume that the latter can be obtained by smoothing our stochastic field on a scale which is larger than the damping scale (for details, see [80, 107]). The damping scale for the tensor mode is obtained taking into account that the source of gravitational radiation after equality becomes sub-dominant (*cf.* next section), so that the relevant tensor damping scale is the Alfvén wave damping scale from the time of the creation of the magnetic field up to equality [80]. Since we are interested here in the imprint of the magnetic field on the CMB, we need not to care about the time evolution of the damping scale, the relevant scales for the CMB tensor anisotropies being those which are greater or equal to the horizon at equality. Therefore, the relevant cutoff scale is given by the Alfvén wave damping scale at equality [73] $k_D^{-1} \simeq v_A l_\gamma(T_{\rm eq})$, where $l_\gamma(T_{\rm eq}) \simeq 0.35\,{\rm Mpc}$ is the comoving diffusion length of photons at equality (here we have used that $l_\gamma^{\rm phys}(T) \simeq 10^{22}{\rm cm}(T/T_{\rm dec})^{-3}$, from [73], as well as $z_{\rm eq} \simeq 3454$ and $z_{\rm dec} = 1088$ from the WMAP results [5]). The Alfvén speed is at most of order 10^{-3} (section 2.4.4), so that the damping scale is of the order of kpc or smaller.

Even if considering a helical component in the magnetic field, we set all the power to zero on scales smaller than k_D^{-1}. This is not really correct, since we are not accounting for a possible inverse cascade, and consequent modification of the primordial magnetic spectrum [83,84]. In particular, simulations show that the spectrum should decay like a power law with index of the order of -4 on small scales, $k > k_D$. However, as we shall see, for $n_{S,A} < -3/2$ the induced C_ℓ are dominated by the contribution at the largest scales, k_D^{-1}, for the $n_{S,A} \sim -4$ part of the spectrum: one has in fact $C_\ell \propto (\ell/k_D\eta_0)^{2n_A+6}$, with $\ell \ll k_D\eta_0$. Therefore, we do not lose much by neglecting the contribution from the scales smaller than k_D^{-1}.

4.3 Tensor metric perturbations induced by the magnetic field

A stochastic magnetic field can act as a source for Einstein's equations and therefore generate gravitational waves [80, 107, 115]. The tensor modes are the simplest case of metric perturbations, and in the transverse and traceless gauge they are fully described by the tensor $h_{ij}(\mathbf{x}, \eta)$, satisfying

$$h_{ij} = h_{ji}, \qquad h_{ii} = 0, \qquad h_{ij}\hat{k}^j = 0\,. \tag{4.30}$$

The linear evolution equation for gravitational waves, given by Eq. (3.64), is rewritten in this case as

$$\ddot{h}_{ij}(\mathbf{k},\eta) + 2\frac{\dot{a}}{a}\dot{h}_{ij}(\mathbf{k},\eta) + k^2 h_{ij}(\mathbf{k},\eta) = \frac{8\pi G}{a^2(\eta)}\Pi_{ij}(\mathbf{k}), \tag{4.31}$$

where $\Pi_{ij}(\mathbf{k})$ is now the source tensor given in (4.2), and we have accounted for the time dependence $a^{-2}(\eta)$, which comes from the fact that the magnetic field is frozen in the plasma. Therefore, $\Pi_{ij}(\mathbf{k},\eta)$ is a coherent source, in the sense that each mode undergoes the same time evolution [80]. We neglect other possible anisotropic stresses of the plasma, like collisionless hot dark matter particles, or massless neutrinos.

We want to compute the induced CMB anisotropies and polarisation, which can be expressed in terms of the two-point correlation spectrum $\langle \dot{h}_{ij}(\mathbf{k})\dot{h}_{lm}(\mathbf{k}')\rangle$, taking the form:

$$\langle \dot{h}_{ij}(\mathbf{k},\eta)\dot{h}^*_{lm}(\mathbf{k}',\eta)\rangle = \frac{(2\pi)^3}{4}\left[\mathcal{M}_{ijlm}H(k,\eta) + i\mathcal{A}_{ijlm}\mathcal{H}(k,\eta)\right]\delta(\mathbf{k}-\mathbf{k}')\,. \tag{4.32}$$

Here $(2\pi)^3 H(k,\eta)\delta(\mathbf{k}-\mathbf{k}') = \langle \dot{h}_{ij}(\mathbf{k})\dot{h}^*_{ij}(\mathbf{k}')\rangle$ is the usual isotropic part of the gravitational wave spectrum which is sourced by $f(k)$, and $\mathcal{H}(k,\eta)$ describes the helical part, sourced by $g(k)$.

The perturbation tensor h_{ij} can also be expressed in terms of the basis $e^{\pm}_{ij}$ defined in Eq. (4.18):

$$h_{ij}(\mathbf{k},\eta) = h^+(\mathbf{k},\eta)e^+_{ij} + h^-(\mathbf{k},\eta)e^-_{ij}\,. \tag{4.33}$$

Just like for the anisotropic stress power spectra, one has that

$$2(2\pi)^3\delta(\mathbf{k}-\mathbf{k}')\ H(k,\eta) \equiv 3\langle \dot{h}^+(\mathbf{k},\eta)\dot{h}^{+*}(\mathbf{k}',\eta) + \dot{h}^-(\mathbf{k},\eta)\dot{h}^{-*}(\mathbf{k}',\eta)\rangle\,, \tag{4.34}$$

$$2(2\pi)^3\delta(\mathbf{k}-\mathbf{k}')\ \mathcal{H}(k,\eta) \equiv -3\langle \dot{h}^+(\mathbf{k},\eta)\dot{h}^{+*}(\mathbf{k}',\eta) - \dot{h}^-(\mathbf{k},\eta)\dot{h}^{-*}(\mathbf{k}',\eta)\rangle\,. \tag{4.35}$$

In terms of h^T and $h^\times$, defined like in Eq. (4.23), $\mathcal{H}$ accounts for the correlation between h^T and $h^\times$,

$$\langle \dot{h}^\times(\mathbf{k})\dot{h}^{T*}(\mathbf{k}') - \dot{h}^T(\mathbf{k})\dot{h}^{\times *}(\mathbf{k}')\rangle = i(2\pi)^3\delta(\mathbf{k}-\mathbf{k}')\ \mathcal{H}(k)\,. \tag{4.36}$$

The evolution equation for the components $h^{\pm}(\mathbf{k},\eta)$ is simply

$$\ddot{h}^{\pm}(\mathbf{k},\eta) + 2\frac{\dot{a}}{a}\dot{h}^{\pm}(\mathbf{k},\eta) + k^2h^{\pm}(\mathbf{k},\eta) = \frac{8\pi G}{a^2(\eta)}\Pi^{\pm}(\mathbf{k})\,. \tag{4.37}$$

In order to compute the CMB fluctuations, we need to determine the functions $\dot{h}^{\pm}(\mathbf{k},\eta)$ (see Eq. (4.43)). An approximate solution to the above differential equation can be found in [80], [107]. The important point is that, because of the rapid falloff of the magnetic field source in the matter dominated era, perturbations created after equality are sub-dominant, so that one obtains, for the dominant contribution at $\eta > \eta_{\rm eq}$:

$$\dot{h}^{\pm}(\mathbf{k},\eta) \simeq \frac{16\pi G}{H_0^2\Omega_{\rm rad}}\ln\left(\frac{z_{\rm in}}{z_{\rm eq}}\right)\Pi^{\pm}(\mathbf{k})\,\frac{j_2(k\eta)}{\eta}\,, \tag{4.38}$$

where $\Omega_{\rm rad}$ is the radiation density parameter today and $z_{\rm in,eq}$ corresponds to the redshift at the moment of creation of the magnetic field and at matter-radiation equality respectively. The function j_2 is the spherical Bessel function [103]. The term $\ln(z_{\rm in}/z_{\rm eq})$ accounts for the logarithmic build up of gravity waves from $z_{\rm in}$ to $z_{\rm eq}$. For the spectra (4.34) and (4.35) we then obtain

$$H(k,\eta) \simeq \left[\frac{16\pi G}{H_0^2\Omega_r}\ln\left(\frac{z_{\rm in}}{z_{\rm eq}}\right)\frac{j_2(k\eta)}{\eta}\right]^2 f(k)\,, \tag{4.39}$$

$$\mathcal{H}(k,\eta) \simeq \left[\frac{16\pi G}{H_0^2\Omega_{\rm rad}}\ln\left(\frac{z_{\rm in}}{z_{\rm eq}}\right)\frac{j_2(k\eta)}{\eta}\right]^2 g(k)\,. \tag{4.40}$$

The gravity wave power spectra H and $\mathcal{H}$ are constant on large scales, $k\eta \ll 1$ and decay and oscillate inside the horizon.

Our first result is that a helical magnetic field induces a parity-odd gravity wave component. From Eq. (4.37) it is clear that such a component appears whenever there are parity-odd anisotropic stresses. It could in principle also be detected directly, via gravity wave background detection experiments. We do not discuss this very hypothetical idea any further, but calculate the effect of such a component on CMB anisotropies and polarisation.

4.4 CMB fluctuations

Magnetic fields in the universe lead to all types of metric perturbations: scalar, vector and tensor, as analysed in section 3.3. In [115] it is shown that vector and tensor perturbations from a magnetic field induce CMB anisotropies of the same order of magnitude. In the following we estimate the CMB fluctuations due to gravitational waves induced by the stochastic magnetic field, the spectrum of which contains a helicity component, $A(k) \neq 0$. Since the CMB signature of stochastic magnetic fields with isotropic spectrum is given in details in references [107,115], here we concentrate on the effects from the helical part of the magnetic field spectrum, and discuss the corrections which it induces to the previous results.

To compute the CMB fluctuations power spectra we use the total angular momentum method of Hu and White [95], introduced in section 3.2. The angular power spectrum of CMB fluctuations is given by Eq. (3.117)

$$C_\ell^{\mathcal{X}\tilde{\mathcal{X}}} = \frac{2}{\pi}\frac{1}{(2\ell+1)^2}\int dk\, k^2 \sum_{m=-2}^{2} \mathcal{X}_\ell^{(m)}(\eta_0,k)\tilde{\mathcal{X}}_\ell^{(m)*}(\eta_0,k)\,, \tag{4.41}$$

where $\mathcal{X}$ takes the values of Θ, temperature fluctuation, E, polarisation with positive parity, and B, polarisation with negative parity, for each perturbation mode. For tensor modes, one has that $m = \pm 2$. Since we only consider tensor modes in this work, we suppress the index 2 and just denote the two states by $+$ and $-$ in what follows. Reference [115] applies the total angular momentum method to parity-even magnetic field spectra: in this case, according to parity conservation the sum over $\pm$ can be replaced by a factor 2. In our case instead, we always need to sum over both states.

From the form of $f(k)$ (4.26), the parity-even CMB fluctuation correlators can be expressed as:

$$C_\ell^{\mathcal{X}\tilde{\mathcal{X}}} = C_{(S)\ell}^{\mathcal{X}\tilde{\mathcal{X}}} - C_{(A)\ell}^{\mathcal{X}\tilde{\mathcal{X}}}, \tag{4.42}$$

where $C_{(A)\ell}^{\mathcal{X}\tilde{\mathcal{X}}}$ is the power spectrum induced by the purely helical part of the source term, proportional to $A(p)A(|\mathbf{k}-\mathbf{p}|)$. The contribution of this helical part to the parity-even CMB power spectra is always negative, but, as we shall see, condition (2.63) insures that $C_{(A)\ell}^{\mathcal{X}\mathcal{X}} < C_{(S)\ell}^{\mathcal{X}\mathcal{X}}$ so that the power spectra do not become negative.

The new effect is that the helical part of the magnetic field induces parity-odd CMB correlators, $C_\ell^{\Theta B}$ and C_ℓ^{EB} (see also [93]). These are expressed in terms of the helical magnetic source $g(k)$ which is proportional to the convolution of $A(k)$ with $S(k)$ (see Eq. (4.17)).

We now derive the CMB fluctuations $\Theta_\ell^{\pm}(\eta_0, k)$, $E_\ell^{\pm}(\eta_0, k)$, $B_\ell^{\pm}(\eta_0, k)$ and then perform the integral (4.41). Rather than a numerical study, we present analytical approximations for our results. These are not very accurate, but allow a discussion of the dependence of the correlators on n_S and n_A. We will also be able to determine the spectral index of the CMB correlators (dependence on ℓ) as a function of n_S and n_A. At the present stage, we think this scaling information is more interesting than accurate numerical results. These can then follow for specific, interesting values of the spectral indices in future work. The details of the analytical approximations are presented in appendix B.

Below, we shall always work in the approximation of instant recombination. Moreover, in our approximations we did not take into account the decay of gravity waves for modes which entered the horizon before decoupling. Our results therefore will be reasonable approximations (within a factor of two or so) only for $\ell \lesssim 60$, where the tensor CMB signal is largest. Even though this may seem poor accuracy, here we only want to obtain estimates of the correct order of magnitude of this anyway small effect. This will enable use to judge for which cases a more involved numerical study is justified.

4.4.1 CMB temperature anisotropies

Within the instant recombination approximation, gravitational waves simply cause CMB photons to propagate along perturbed geodesics from the last scattering surface to us. The induced CMB temperature anisotropies are given by

$$\frac{\Theta_\ell^{\pm}(\mathbf{k},\eta_0)}{2\ell+1} = -\frac{4}{3}\int_{\eta_{\rm dec}}^{\eta_0} d\eta\, \dot{h}^{\pm}(\mathbf{k},\eta) j_\ell^{\pm}[k(\eta_0-\eta)]\,, \tag{4.43}$$

where we have used Eqs. (3.110) and (3.108); $j_\ell^{\pm}$ are the tensor temperature radial functions of the two different parities, both given by (*cf.* Eqs. (3.85))

$$j_\ell^{\pm}(x) = \sqrt{\frac{3}{8}\frac{(\ell+2)!}{(\ell-2)!}}\,\frac{j_\ell(x)}{x^2}\,. \tag{4.44}$$

Using the solution (4.38) for $\dot{h}^{\pm}(\mathbf{k},\eta)$, we obtain

$$\begin{aligned}\frac{\Theta_\ell^{\pm}(\mathbf{k},\eta_0)}{2\ell+1} &\simeq -\sqrt{\frac{3}{8}\frac{(\ell+2)!}{(\ell-2)!}}\left[\frac{8}{\rho_c\Omega_{\rm rad}}\ln\left(\frac{z_{\rm in}}{z_{\rm eq}}\right)\right]\Pi^{\pm}(\mathbf{k})\int_{x_{\rm dec}}^{x_0} dx\,\frac{j_2(x)}{x}\frac{j_\ell(x_0-x)}{(x_0-x)^2} \\ &\simeq \frac{-2}{\rho_c\Omega_{\rm rad}}\ln\left(\frac{z_{\rm in}}{z_{\rm eq}}\right)\Pi^{\pm}(\mathbf{k})\frac{J_{\ell+3}(x_0)}{x_0^3}\,\ell^{5/2}\,,\end{aligned} \tag{4.45}$$

where we have set $x \equiv k\eta$ and $x_0 \equiv k\eta_0$. For the second $\simeq$ sign we have used the approximation (B.5) given in appendix B for the integral over x. This approximation is valid only for $x_{\rm dec} = k\eta_{\rm dec} \lesssim 1$.

The general expression (4.41) for the temperature anisotropy power spectrum now gives

$$C_\ell^{\Theta\Theta} \simeq \frac{16}{3\pi}\left[\frac{1}{\rho_c\Omega_{\rm rad}}\ln\left(\frac{z_{\rm in}}{z_{\rm eq}}\right)\right]^2\frac{\ell^5}{\eta_0^3}\int_0^{k_D\eta_0} dx_0\,\frac{J_{\ell+3}^2(x_0)}{x_0^4}\,f\left(\frac{x_0}{\eta_0}\right)\,. \tag{4.46}$$

A good approximation for the function $f(k)$ is given in appendix A, Eq. (A.9). The first term of (A.9) comes entirely from the non-helical component B_λ, and has already been determined in references [107, 115]; the second term comes instead from the helical component, and its influence on the C_ℓ is new. We denote it by $C_{(A)\ell}^{\Theta\Theta}$. Then, splitting the induced temperature anisotropy power spectrum as

$$C_\ell^{\Theta\Theta} = C_{(S)\ell}^{\Theta\Theta} - C_{(A)\ell}^{\Theta\Theta}\,, \tag{4.47}$$

we obtain (now x_0 is renamed x)

$$C^{\Theta\Theta}_{(A)\ell} \simeq \frac{2^9\pi}{9} \frac{\left[\frac{\Omega_A}{\Omega_{\rm rad}}\ln\left(\frac{z_{\rm in}}{z_{\rm eq}}\right)\right]^2}{(2n_A+3)\Gamma^2\left(\frac{n_A+4}{2}\right)} \frac{\ell^5}{(\eta_0 k_D)^3} \times \int_0^{x_D} dx\, \frac{J^2_{\ell+3}(x)}{x^4}\left[1+\frac{n_A-1}{n_A+4}\left(\frac{x}{x_D}\right)^{2n_A+3}\right], \tag{4.48}$$

where we have set $x_D = k_D\eta_0$. We have introduced the 'helicity density parameter' Ω_A defined by

$$\Omega_A \equiv \frac{\mathcal{B}^2_\lambda}{8\pi\rho_c}(k_D\lambda)^{n_A+3} \simeq \frac{1}{\rho_c}\int_0^{k_D}\frac{dk}{k}\frac{d\rho_{\mathcal{B}}(k)}{d\ln k} \simeq \frac{\mathcal{B}^2_{k_D}}{8\pi\rho_c}, \tag{4.49}$$

and analogously we will use

$$\Omega_S \equiv \frac{B^2_\lambda}{8\pi\rho_c}(k_D\lambda)^{n_S+3} \simeq \frac{1}{\rho_c}\int_0^{k_D}\frac{dk}{k}\frac{d\rho_B(k)}{d\ln k} \simeq \frac{B^2_{k_D}}{8\pi\rho_c}, \tag{4.50}$$

where we have introduced $\mathcal{B}^2_{k_D} = \mathcal{B}^2_\lambda(k_D\lambda)^{n_A+3}$, the field strength at the cutoff scale $1/k_D$, and correspondingly for B_{k_D}. With these definitions the results will be expressed entirely in terms of physical quantities and the reference scale λ does no longer enter. Remember also that $(2\pi)^4(\mathcal{B}^2_\lambda\lambda^{n_A+3})^2/\Gamma^2\left(\frac{n_A+4}{2}\right) = |A_0|^2$, where $|A_0|$ is the normalisation of the helical component of the magnetic power spectrum (2.50). The integral (4.46) is dominated at $x_0 \simeq \ell$. With $x_0/x_{\rm dec} = \eta_0/\eta_{\rm dec} \simeq 60$, this means that our approximation is valid for $\ell \lesssim 60$ (see appendix B).

If $n_A > -3/2$, the first term in the square bracket in Eq. (4.48) dominates. Since the integral converges and is maximal around $k \simeq \ell/\eta_0 \ll k_D$, we can replace it by the integral to infinity and use Eq. (B.7) of appendix B. This gives

$$\ell^2 C^{\Theta\Theta}_{(A)\ell} \simeq \frac{2^{10}}{27}\frac{\left[\frac{\Omega_A}{\Omega_{\rm rad}}\ln\left(\frac{z_{\rm in}}{z_{\rm eq}}\right)\right]^2}{(2n_A+3)\Gamma^2\left(\frac{n_A+4}{2}\right)}\left(\frac{\ell}{k_D\eta_0}\right)^3 \qquad \text{for } n_A > -3/2\,. \tag{4.51}$$

The temperature power spectrum has the well known behavior of C_ℓ's induced by white noise gravity waves, $C_\ell \propto \ell$.

If $n_A < -3/2$, the second term in the square bracket of Eq. (4.48) dominates, and we find

$$\ell^2 C^{\Theta\Theta}_{(A)\ell} \simeq \frac{2^8\sqrt{\pi}}{9} \frac{\left[\frac{\Omega_A}{\Omega_{\rm rad}} \ln\left(\frac{z_{\rm in}}{z_{\rm eq}}\right)\right]^2}{(2n_A+3)\Gamma^2\left(\frac{n_A+4}{2}\right)} \frac{\Gamma\left(\frac{1}{2}-n_A\right)}{\Gamma(1-n_A)} \frac{n_A-1}{n_A+4} \left(\frac{\ell}{k_D\eta_0}\right)^{2n_A+6} \qquad \text{for } -3 < n_A < -3/2\,. \tag{4.52}$$

Like for the symmetric contribution given in references [107, 115], we get a scale-invariant spectrum for $n_A = -3$. The expressions for $\ell^2 C^{\Theta\Theta}_{(S)\ell}$ are obtained from those given above upon replacing Ω_A by Ω_S, n_A by n_S and $\Gamma^2\left(\frac{n_A+4}{2}\right)$ by $\Gamma^2\left(\frac{n_S+3}{2}\right)$. For $-3 < n_S < -3/2$, one also has to replace the factor $(n_A-1)/(n_A+4)$ by $n_S/(n_S+3)$. We do not repeat these formulas here since they can be found in reference [115] (up to some factors of order unity which are of no relevance for this discussion).

This is in principle the final result for temperature anisotropies. Let us check that $C^{\Theta\Theta}_{(A)\ell}$ is indeed never larger than $C^{\Theta\Theta}_{(S)\ell}$ so that

$$C^{\Theta\Theta}_{\ell} = C^{\Theta\Theta}_{(S)\ell} - C^{\Theta\Theta}_{(A)\ell} \geq 0\,.$$

We first consider $n_A \geq n_S > -3/2$. Then

$$\frac{C^{\Theta\Theta}_{(A)\ell}}{C^{\Theta\Theta}_{(S)\ell}} = \frac{\mathcal{B}^4_\lambda\,\Gamma^2(\frac{n_S+3}{2})\,(2n_S+3)\,(k_D\lambda)^{2(n_A-n_S)}}{B^4_\lambda\,\Gamma^2(\frac{n_A+4}{2})\,(2n_A+3)} = \frac{|A_0|^2}{S_0^2\,k_D^{2(n_S-n_A)}} \frac{2n_S+3}{2n_A+3} \leq 1\,. \tag{4.53}$$

In the first equality we have inserted the definitions of Ω_A and Ω_S and the last inequality comes from Eqs. (2.67) and (2.65). If instead $n_S \leq n_A < -3/2$, we find

$$\frac{C^{\Theta\Theta}_{(A)\ell}}{C^{\Theta\Theta}_{(S)\ell}} = N(n_A, n_S) \frac{|A_0|^2}{S_0^2\,k_D^{2(n_S-n_A)}} \left(\frac{\ell}{k_D\eta_0}\right)^{2(n_A-n_S)}, \tag{4.54}$$

where $N(n_A, n_S)$ is a function of the spectral indices n_S and n_A. It is of order unity in the allowed range, $-3 < n_A \leq n_S < -3/2$. Now $k_D\eta_0 \gg \ell$ for all values of ℓ for which our result applies. Hence again

$$\frac{C^{\Theta\Theta}_{(A)\ell}}{C^{\Theta\Theta}_{(S)\ell}} \leq 1\,. \tag{4.55}$$

Finally, we consider the case $-3 < n_S < -3/2 < n_A$, so that we have to apply the result (4.51) for $C^{\Theta\Theta}_{(A)\ell}$ and (4.52) with the mentioned modifications for $C^{\Theta\Theta}_{(S)\ell}$. A short calculation gives

$$\frac{C^{\Theta\Theta}_{(A)\ell}}{C^{\Theta\Theta}_{(S)\ell}} \simeq \frac{|A_0|^2}{S_0^2\, k_D^{2(n_S-n_A)}} \left(\frac{k_D\eta_0}{\ell}\right)^{2n_S+3} \leq 1\,, \tag{4.56}$$

since the first factor is less than one due to Eq. (2.67) and $k_D \gg \ell/\eta_0$ with $n_S < -3/2$.

Clearly, the helical component is maximal for $n_A \simeq n_S$, where we may have $|A_0| \simeq S_0$.

4.4.2 The induced CMB polarisation

Tensor perturbations induce both E polarisation with positive parity, and B polarisation with negative parity. CMB polarisation induced by gravity waves has been studied for example in references [95, 125, 126]; possible contributions from a magnetic field have been discussed in section 3.3.2. Our aim is to estimate the effect on the polarisation signal from the helical component of the magnetic field. Like for the temperature anisotropies, we use the angular momentum method developed in reference [95].

E type polarisation

The integral solution for E type polarisation from gravity waves is given in section 3.2.3. Again, we will work in the instant recombination approximation. The order of magnitude of our result is reasonable for $\ell \lesssim 60$, since in this case also we restrict ourselves to the evaluation of the super-horizon scales spectrum. In our approximation we have (*cf.* Eq. (3.111))

$$\frac{E_\ell^{\pm}(\mathbf{k},\eta_0)}{2\ell+1} = \sqrt{\frac{2}{3}}\int_{\eta_{\rm dec}}^{\eta_0} d\eta\, \dot{h}^{\pm}(\mathbf{k},\eta)\epsilon_\ell^{\pm}[k(\eta_0-\eta)]\,, \tag{4.57}$$

here

$$\epsilon_\ell^{\pm}(x) = \frac{1}{4}\left[-j_\ell(x) + j_\ell''(x) + 2\frac{j_\ell(x)}{x^2} + 4\frac{j_\ell'(x)}{x}\right] \simeq \frac{1}{4}\left[\frac{\ell^2}{x^2}j_\ell - 2j_\ell(x)\right] \quad \text{for } \ell \gg 1 \tag{4.58}$$

is the E-type polarisation radial function for the tensor mode (3.87), and for the last equality we have used the recurrence relations for spherical Bessel functions (B.14, B.15).

We now use our solution (4.38) to express $\dot{h}^{\pm}(\mathbf{k},\eta)$ in terms of $\Pi^{\pm}(\mathbf{k})$. With this, Eq. (4.57) becomes

$$\begin{aligned}\frac{E_\ell^{\pm}(\mathbf{k},\eta_0)}{2\ell+1} &\simeq \sqrt{\frac{3}{2}}\left[\frac{1}{\rho_c\Omega_{\rm rad}}\ln\left(\frac{z_{\rm in}}{z_{\rm eq}}\right)\right]\Pi^{\pm}(\mathbf{k})\int_{x_{\rm dec}}^{x_0}dx\,\frac{j_2(x)}{x}\left[-2+\frac{\ell^2}{(x_0-x)^2}\right]j_\ell(x_0-x)\\ &\simeq -\frac{1}{2}\left[\frac{1}{\rho_c\Omega_{\rm rad}}\ln\left(\frac{z_{\rm in}}{z_{\rm eq}}\right)\right]\frac{J_{\ell+3}(x_0)}{\sqrt{x_0}}\,\Pi^{\pm}(\mathbf{k})\,,\end{aligned} \tag{4.59}$$

where again $x \equiv k\eta$ and $x_0 \equiv k\eta_0$, and we have evaluated the time integral using approximation (B.9). Here we have also neglected a term of the order of $(\ell^2/x_0^2)J_{\ell+3}(x_0)$, which in principle is of the same order in the above expression, but is always subdominant once we perform the integral over k. Since the power spectra for the E polarisation are parity-even, only the parity-even part of the $\Pi^{\pm}$ auto-correlator (4.20) contributes to the expression for C_ℓ^{EE} derivable from Eq. (4.41). Again we present here only the effect coming from the helical part of the magnetic field; using Eq. (A.9) we find (x_0 is renamed x)

$$C_{(A)\ell}^{EE} \simeq \frac{2^5\pi}{9}\frac{\left[\frac{\Omega_A}{\Omega_{\rm rad}}\ln\left(\frac{z_{\rm in}}{z_{\rm eq}}\right)\right]^2}{(2n_A+3)\Gamma^2\left(\frac{n_A+4}{2}\right)}\frac{1}{(k_D\eta_0)^3}\int_0^{x_D}dx\,x\,J_{\ell+3}^2(x)\left[1+\frac{n_A-1}{n_A+4}\left(\frac{x}{x_D}\right)^{2n_A+3}\right] \tag{4.60}$$

The corresponding equation for $C_{(S)\ell}^{EE}$ can be found in reference [115]. There, a somewhat different approximation than ours has been used for the time integral.

For $n_A \geq -2$, the integral over x is dominated by the upper cutoff, $x_D = k_D\eta_0$. Using the approximation (B.10), we obtain

$$\ell^2 C_{(A)\ell}^{EE} \simeq \frac{2^5}{9}\frac{\left[\frac{\Omega_A}{\Omega_{\rm rad}}\ln\left(\frac{z_{\rm in}}{z_{\rm eq}}\right)\right]^2}{(2n_A+3)\Gamma^2\left(\frac{n_A+4}{2}\right)}\left(\frac{\ell}{k_D\eta_0}\right)^2 \times \begin{cases} 1 & \text{for } n_A > -3/2 \\ \frac{n_A-1}{(n_A+4)(2n_A+4)} & \text{for } -2 < n_A < -3/2 \\ -\frac{3}{2}\ln\left(\frac{k_D\eta_0}{\ell^2}\right) & \text{for } n_A = -2 \end{cases}$$

The result for $C_{(S)\ell}^{EE}$ is obtained upon replacing n_A by n_S and Ω_A by Ω_S (more precisely the factor $\Gamma^2(\frac{n_A+4}{2})$ has to be replaced by $\Gamma^2(\frac{n_S+3}{2})$ and the factor $(n_A-1)/(n_A+4)$ by $n_S/(n_S+3)$). For $-3 < n_A < -2$, using (B.7), we obtain

$$\ell^2 C_{(A)\ell}^{EE} \simeq \frac{2^4\sqrt{\pi}}{9}\frac{\left[\frac{\Omega_A}{\Omega_{\rm rad}}\ln\left(\frac{z_{\rm in}}{z_{\rm eq}}\right)\right]^2}{(2n_A+3)\Gamma^2\left(\frac{n_A+4}{2}\right)}\frac{\Gamma(-n_A-2)}{\Gamma(-n_A-\frac{3}{2})}\frac{n_A-1}{n_A+4}\left(\frac{\ell}{k_D\eta_0}\right)^{2n_A+6} \quad \text{for } -3 < n_A < -2\,. \tag{4.61}$$

Again the E polarisation power spectrum from the symmetric part of the magnetic field spectrum is obtained upon replacement of n_A by n_S and Ω_A by Ω_S. Similar evaluations like the ones presented in the previous paragraph show that

$$C_\ell^{EE} = C_{(S)\ell}^{EE} - C_{(A)\ell}^{EE} \geq 0 \,. \tag{4.62}$$

B type polarisation

Like for E polarisation, the integral solutions for B polarisation in the case of tensor perturbations are given in section 3.2.3. In the approximation of instant recombination we have

$$\frac{B_\ell^\pm(\mathbf{k},\eta_0)}{2\ell+1} = \sqrt{\frac{2}{3}}\int_{\eta_{\rm dec}}^{\eta_0} d\eta\, \dot{h}^\pm(\mathbf{k},\eta)\beta_\ell^\pm[k(\eta_0-\eta)]\,, \tag{4.63}$$

where

$$\beta_\ell^\pm(x) = \pm\frac{1}{2}\left[j_\ell'(x) + 2\frac{j_\ell(x)}{x}\right] \simeq \pm\frac{1}{2}\left[\frac{\ell}{x}j_\ell(x) - j_{\ell+1}(x)\right] \quad \text{for } \ell \gg 1\,. \tag{4.64}$$

With Eq. (4.38) we can write the above integral in terms of the tensor sources $\Pi^\pm(\mathbf{k})$:

$$\begin{aligned}\frac{B_\ell^\pm(\mathbf{k},\eta_0)}{2\ell+1} &\simeq \frac{\pm\sqrt{6}}{\rho_c\Omega_{\rm rad}}\ln\left(\frac{z_{\rm in}}{z_{\rm eq}}\right)\Pi^\pm(\mathbf{k})\int_{x_{\rm dec}}^{x_0} dx\,\frac{j_2(x)}{x}\left[\frac{\ell}{x_0-x}j_\ell(x_0-x) - j_{\ell+1}(x_0-x)\right]\\ &\simeq \frac{\mp 1}{2\rho_c\Omega_{\rm rad}}\ln\left(\frac{z_{\rm in}}{z_{\rm eq}}\right)\frac{J_{\ell+4}(x_0)}{\sqrt{x_0}}\Pi^\pm(\mathbf{k})\,,\end{aligned} \tag{4.65}$$

where we have again used approximation (B.9). Like for the E polarisation, in this case also it is the parity-even part of the magnetic source, $f(k)$, which contributes to the C_ℓ. Eq. (4.41) takes the form

$$C_{(A)\ell}^{BB} \simeq \frac{2^5\pi}{9}\frac{\left[\frac{\Omega_A}{\Omega_{\rm rad}}\ln\left(\frac{z_{\rm in}}{z_{\rm eq}}\right)\right]^2}{(2n_A+3)\Gamma^2\left(\frac{n_A+4}{2}\right)}\frac{1}{(k_D\eta_0)^3}\int_0^{x_D} dx\, x\, J_{\ell+4}^2(x)\left[1+\frac{n_A-1}{n_A+4}\left(\frac{x}{x_D}\right)^{2n_A+3}\right] \tag{4.66}$$

Note that within our approximation, for $\ell \gg 1$, $C_{(A)\ell}^{BB} \simeq C_{(A)\ell}^{EE}$. This is also the case for $C_{(S)\ell}^{BB}$ and $C_{(S)\ell}^{EE}$, see [115]. Evaluating the integral using expressions (B.10) and (B.7), for the different ranges of the spectral index n_A, we obtain

$$\ell^2 C^{BB}_{(A)\ell} \simeq \frac{2^5}{9}\frac{\left[\frac{\Omega_A}{\Omega_{\rm rad}}\ln\left(\frac{z_{\rm in}}{z_{\rm eq}}\right)\right]^2}{(2n_A+3)\Gamma^2\left(\frac{n_A+4}{2}\right)}\left(\frac{\ell}{k_D\eta_0}\right)^2 \times \begin{cases} 1 & \text{for } n_A > -3/2 \\ \frac{n_A-1}{(n_A+4)(2n_A+4)} & \text{for } -2 < n_A < -3/2 \\ -\frac{3}{2}\ln\left(\frac{k_D\eta_0}{\ell^2}\right) & \text{for } n_A = -2 \end{cases}$$

$$\ell^2 C^{BB}_{(A)\ell} \simeq \frac{2^4\sqrt{\pi}}{9}\frac{\left[\frac{\Omega_A}{\Omega_{\rm rad}}\ln\left(\frac{z_{\rm in}}{z_{\rm eq}}\right)\right]^2}{(2n_A+3)\Gamma^2\left(\frac{n_A+4}{2}\right)}\frac{\Gamma(-n_A-2)}{\Gamma(-n_A-3/2)}\left(\frac{\ell}{k_D\eta_0}\right)^{2n_A+6} \quad \text{for } n_A < -2\,. \quad (4.67)$$

Again, the contributions from the symmetric part are obtained by replacing Ω_A by Ω_S and n_A by n_S, up to factors of order unity, and we find

$$C^{BB}_\ell = C^{BB}_{(S)\ell} - C^{BB}_{(A)\ell} \geq 0\,.$$

Within our approximation, we have $C^{BB}_\ell \simeq C^{EE}_\ell$. From ordinary inflationary perturbations one expects $C^{BB}_\ell \simeq \frac{8}{13}C^{EE}_\ell$ for gravity waves, which is comparable to our findings.

Temperature and E polarisation cross-correlation

The symmetric part of the source term, $f(k)$, can only induce parity-even CMB correlators. Besides the power spectra for temperature anisotropies and E and B type polarisations analysed in the previous sub-sections, it can also source the cross-correlation between temperature anisotropy and E polarisation. In order to evaluate this contribution, we have to substitute into Eq. (4.41) the integral solutions for the tensor mode Eqs. (4.45) and (4.59), to obtain:

$$C^{\Theta E}_{(A)\ell} \simeq \frac{2^5\pi}{9}\frac{\left[\frac{\Omega_A}{\Omega_{\rm rad}}\ln\left(\frac{z_{\rm in}}{z_{\rm eq}}\right)\right]^2}{(2n_A+3)\Gamma^2\left(\frac{n_A+4}{2}\right)}\frac{\ell^{5/2}}{(k_D\eta_0)^3}\int_0^{x_D} dx\,\frac{J^2_{\ell+3}(x)}{x^{3/2}}\left[1+\frac{n_A-1}{n_A+4}\left(\frac{x}{x_D}\right)^{2n_A+3}\right] \quad (4.68)$$

We can evaluate this integral using (B.7), and we find,

$$\ell^2 C^{\Theta E}_{(A)\ell} \simeq \frac{2^4\sqrt{\pi}}{9}\frac{\left[\frac{\Omega_A}{\Omega_{\rm rad}}\ln\left(\frac{z_{\rm in}}{z_{\rm eq}}\right)\right]^2}{(2n_A+3)\Gamma^2\left(\frac{n_A+4}{2}\right)}\frac{\Gamma(\frac{3}{4})}{\Gamma(\frac{5}{4})}\left(\frac{\ell}{k_D\eta_0}\right)^3 \quad \text{for } n_A > -3/2 \quad (4.69)$$

and

$$\ell^2 C^{\Theta E}_{(A)\ell} \simeq \frac{2^4\sqrt{\pi}}{9} \frac{\left[\frac{\Omega_A}{\Omega_{\rm rad}} \ln\left(\frac{z_{\rm in}}{z_{\rm eq}}\right)\right]^2}{(2n_A+3)\Gamma^2\left(\frac{n_A+4}{2}\right)} \frac{\Gamma(-\frac{3}{4}-n_A)}{\Gamma(-\frac{1}{4}-n_A)} \frac{n_A-1}{n_A+4} \left(\frac{\ell}{k_D\eta_0}\right)^{2n_A+6} \text{for } -3 < n_A < -3/2 \,. \tag{4.70}$$

In this case also, the contribution from the symmetric part of the magnetic field spectrum to the Θ–E correlator is always larger than this helical part.

4.5 CMB correlators caused by magnetic field helicity

If the source (or the initial conditions) have no helical component, $\langle \Pi^+(\mathbf{k})\Pi^{+*}(\mathbf{k}')\rangle = \langle \Pi^-(\mathbf{k})\Pi^{-*}(\mathbf{k}')\rangle$, the above correlators are the only non-vanishing ones. However, as soon as the tensor magnetic source spectrum has a helical contribution

$$(2\pi)^3 g(k) \equiv -\frac{3}{2}\langle \Pi^+(\mathbf{k})\Pi^{+*}(\mathbf{k}) - \Pi^-(\mathbf{k})\Pi^{-*}(\mathbf{k})\rangle \neq 0\,,$$

the parity-odd CMB power spectra are non zero. This has been observed first in [93], where the vector contributions have been calculated. Here we compute the gravity wave contributions. We need again to evaluate Eq. (4.41). Taking into account that the gravity waves components $\dot{h}^{\pm}(\mathbf{k})$ are directly proportional to the source components (Eq. (4.38)), and considering the parity of the radial functions

$$j_\ell^+(x) = j_\ell^-(x), \qquad \epsilon_\ell^+(x) = \epsilon_\ell^-(x), \qquad \beta_\ell^+(x) = -\beta_\ell^-(x), \tag{4.71}$$

it is clear that cross-correlations between temperature and B polarisations $C_\ell^{\Theta B}$, and between E and B polarisation C_ℓ^{EB}, cannot vanish, since they are given by momentum integrals of $g(k)$. Using the expressions of the tensor integral solutions $\Theta_\ell^{\pm}$ (4.45), $E_\ell^{\pm}$ (4.59) and $B_\ell^{\pm}$ (4.65), we can calculate the power spectra $C_\ell^{\Theta B}$ and C_ℓ^{EB}.

4.5.1 Temperature and B polarisation cross-correlation

For temperature and B polarisation cross-correlation we obtain, after integrating over time,

$$C_\ell^{\Theta B} \simeq \frac{2}{\pi}\left[\frac{\ln\left(\frac{z_{\rm in}}{z_{\rm eq}}\right)}{\rho_c\Omega_{\rm rad}}\right]^2 \ell^{5/2}\int_0^{k_D} dk\, k^2\, \frac{J_{\ell+3}(x)J_{\ell+4}(x)}{x^{\frac{7}{2}}}\langle \Pi^+(k)\Pi^{+*}(k) - \Pi^-(k)\Pi^{-*}(k)\rangle\,. \tag{4.72}$$

The anti-symmetric source function $g(k)$ is given in Eq. (4.27), and the integral over k can be calculated using (B.7). Note that $g(k)$ depends on both spectral indices n_A and n_S, and we will have to evaluate the integral dividing the two cases $n_A + n_S \lessgtr -2$. We finally arrive at

$$
\begin{aligned}
C_\ell^{\Theta B} &\simeq -\frac{2^8\pi}{9}\frac{\Omega_S\Omega_A \ln^2\left(\frac{z_{\rm in}}{z_{\rm eq}}\right)}{\Omega_{\rm rad}^2(n_A+n_S+2)\Gamma(\frac{n_A+4}{2})\Gamma(\frac{n_S+3}{2})}\left(k_D\eta_0\right)^{-4}\,\ell^{5/2} \\
&\times \int_0^{x_D} dx\, \frac{J_{\ell+3}(x)J_{\ell+4}(x)}{\sqrt{x}}\left[1+\frac{n_A-1}{n_S+3}\left(\frac{x}{x_D}\right)^{n_A+n_S+2}\right]
\end{aligned}
$$

$$
\ell^2 C_\ell^{\Theta B} \simeq \begin{cases} -\frac{8\pi\sqrt{\pi/2}\,\Omega_S\Omega_A\ln^2\left(\frac{z_{\rm in}}{z_{\rm eq}}\right)}{\Omega_{\rm rad}^2(n_A+n_S+2)\Gamma(\frac{n_A+4}{2})\Gamma(\frac{n_S+3}{2})}\left(\frac{\ell}{k_D\eta_0}\right)^4 & \text{for } n_S+n_A>-2 \\ -\frac{2^7\sqrt{\pi}\Omega_S\Omega_A\ln^2\left(\frac{z_{\rm in}}{z_{\rm eq}}\right)}{9\,\Omega_{\rm rad}^2(n_A+n_S+2)\Gamma(\frac{n_A+4}{2})\Gamma(\frac{n_S+3}{2})}\frac{\Gamma\left(-\frac{n_A}{2}-\frac{n_S}{2}-\frac{1}{4}\right)}{\Gamma\left(-\frac{n_A}{2}-\frac{n_S}{2}+\frac{1}{4}\right)}\frac{n_A-1}{n_S+3}\left(\frac{\ell}{k_D\eta_0}\right)^{n_A+n_S+6} & \\ & \text{for } -6<n_S+n_A<-2 \end{cases}
$$

Independently on the spectral indices, $\ell^2 C_\ell^{\Theta B}$ is always negative for positive A_0. In this case of temperature and B polarisation cross-correlation, we have also computed the spectra numerically, in order to test the reliability of our analytical estimation. The amplitude of the numerical result is bigger than the analytic one by a factor of two or less, so within the error we estimated for our approximations (see appendix B). We expect this to be one of the worst approximations due to the relatively slow convergence of $\int dx J_{\ell+3}(x)J_{\ell+4}(x)/\sqrt{x}$.

4.5.2 E and B polarisation cross-correlation

Following the same procedure as in the previous paragraph, we can evaluate the E and B polarisation cross-correlation created by the helical part of the magnetic field. Using formula (4.41), we get:

$$
\begin{aligned}
C_\ell^{EB} &\simeq -\frac{2^6\pi}{9}\frac{\Omega_S\Omega_A \ln^2\left(\frac{z_{\rm in}}{z_{\rm eq}}\right)}{\Omega_{\rm rad}^2(n_A+n_S+2)\Gamma(\frac{n_A+4}{2})\Gamma(\frac{n_S+3}{2})}\left(k_D\eta_0\right)^{-4} \\
&\times \int_0^{x_D} dx\, x^2 J_{\ell+3}(x)J_{\ell+4}(x)\left[1+\frac{n_A-1}{n_S+3}\left(\frac{x}{x_D}\right)^{n_A+n_S+2}\right]. \qquad (4.73)
\end{aligned}
$$

In the case $n_A + n_S > -2$, the integral in $x = k\eta_0$ is divergent, and we need to evaluate it using approximation (B.12), which gives:

$$\ell^2 C_\ell^{EB} \simeq \frac{2^5}{9} \frac{\Omega_S \Omega_A \ln^2\left(\frac{z_{\text{in}}}{z_{\text{eq}}}\right)}{\Omega_{\text{rad}}^2 (n_A + n_S + 2)\Gamma(\frac{n_A+4}{2})\Gamma(\frac{n_S+3}{2})} \frac{(-1)^\ell}{k_D \eta_0} \sin(2x_D) \left(\frac{\ell}{k_D \eta_0}\right)^2 \qquad (4.74)$$

$$\text{for } n_S + n_A > -2.$$

It is not possible to assign a precise value to the variable $x_D = \eta_0 k_D$, because of the unavoidable incertitude in the estimation of the magnetic field damping scale, which depends on the amplitude of the magnetic field and is therefore smeared out over a certain range of scales. Therefore, we expect that the presence of the term $\sin(2x_D)$ most probably leads to a considerable suppression in the amplitude of the E–B cross-correlation term.

For $n_A + n_S < -2$, the momentum integral in Eq. (4.73) is dominated by the second term in the square brackets, and in order to perform the integration, we need to distinguish two different cases: For $-4 \leq n_A + n_S < -2$, the exponent of x is still positive, so that we have to use the approximation given in Eq. (B.12). A further distinction is therefore necessary, since the dominant term in approximation (B.12) depends on whether the exponent is above or below 1 as discussed in the appendix:

$$\ell^2 C_\ell^{EB} \simeq \frac{2^5}{9} \frac{\Omega_S \Omega_A \ln^2\left(\frac{z_{\text{in}}}{z_{\text{eq}}}\right)}{\Omega_{\text{rad}}^2 (n_A + n_S + 2)\Gamma(\frac{n_A+4}{2})\Gamma(\frac{n_S+3}{2})} \frac{n_A - 1}{n_S + 3} \frac{(-1)^\ell}{k_D \eta_0} \sin(2x_D) \left(\frac{\ell}{k_D \eta_0}\right)^2 ,$$

$$\text{for } -3 < n_A + n_S < -2;$$

$$\ell^2 C_\ell^{EB} \simeq \frac{2^5}{9} \frac{\Omega_S \Omega_A \ln^2\left(\frac{z_{\text{in}}}{z_{\text{eq}}}\right)}{\Omega_{\text{rad}}^2 (n_A + n_S + 2)\Gamma(\frac{n_A+4}{2})\Gamma(\frac{n_S+3}{2})} \frac{n_A - 1}{n_S + 3} \frac{(-1)^{\ell+1}}{(k_D \eta_0)^2} \sin(2\ell^2) \left(\frac{\ell^2}{k_D \eta_0}\right)^{n_A+n_S+4}$$

$$\text{for } -4 < n_A + n_S < -3.$$

Both contributions are suppressed by the presence of the two terms $\sin(2\ell^2)$ and $\sin(2x_D)$ since usually one averages over band powers in ℓ (for the second case), and again x_D is not a very sharp cutoff but has a certain width (for the first case).

If $-6 < n_A + n_S < -4$, the second term in the integrand of Eq. (4.73) still dominates, but since the exponent of x is now negative, the integral converges and we can make use of approximation (B.7).

$$\ell^2 C_\ell^{EB} \simeq -\frac{2^5\sqrt{\pi}}{9}\frac{\Omega_S\Omega_A \ln^2\left(\frac{z_{\rm in}}{z_{\rm eq}}\right)}{\Omega_{\rm rad}^2(n_A+n_S+2)\Gamma(\frac{n_A+4}{2})\Gamma(\frac{n_S+3}{2})}\frac{\Gamma\big(-\frac{n_A}{2}-\frac{n_S}{2}-\frac{3}{2}\big)}{\Gamma\big(-\frac{n_A}{2}-\frac{n_S}{2}-1\big)}\frac{n_A-1}{n_S+3}\left(\frac{\ell}{k_D\eta_0}\right)^{n_A+n_S+6}$$
$$\text{for } -6 < n_A+n_S < -4.$$

This result is not suppressed by oscillations.

4.6 Discussion

In this chapter we have computed CMB anisotropies due to gravity waves induced by a primordial magnetic field. We have mainly concentrated on the effects of a possible helical component of the field. Magnetic fields induce scalar, vector and tensor perturbations which are typically of the same order. In this sense the tensor contribution can be regarded as an order of magnitude estimate for the full contribution.

As it has already been found in references [107, 115], the C_ℓ's are proportional to

$$\ell^2 C_\ell \propto \left(\frac{\Omega_B}{\Omega_{\rm rad}}\right)^2 \ln^2\left(\frac{z_{\rm in}}{z_{\rm eq}}\right). \tag{4.75}$$

The first term of the right hand side is $\left(\frac{\Omega_B}{\Omega_{\rm rad}}\right)^2 \simeq 10^{-10}\left(B/10^{-8}\text{Gauss}\right)^4$ (see Eq. (3.119)), hence for a primordial magnetic field of the order of $B \simeq 10^{-9}$ to 10^{-8} Gauss we would expect to detect its effects in the CMB anisotropy and polarisation spectrum. Here $B = B_{k_D} = B_\lambda(\lambda k_D)^{n+3}$ is the maximum value of the magnetic field, which is the field at the upper cutoff scale $1/k_D$. In Eq. (4.75) Ω_B stands for Ω_S or Ω_A, and in the above expression for B_{k_D}, n stands for n_A or n_S depending on which contribution we are considering. The second term in Eq. (4.75) represents the logarithmic build up of gravity waves, $\ln^2(z_{\rm in}/z_{\rm eq}) \simeq 660$ to 3100. Here the first value corresponds to magnetic field generation at the electroweak phase transition, $T_{\rm in} = 200$ GeV and the second value represents a possible inflationary generation at $T_{\rm in} \simeq 10^{15}$ GeV. For scale-invariant spectra, $n_A = n_S \simeq -3$, the right hand side of Eq. (4.75) gives roughly the amplitude of the induced CMB perturbations. Taking into account the pre-factor $2^8\sqrt{\pi}/9$, scale invariant magnetic fields produced at some GUT scale, $T \simeq 10^{15}$ GeV have to be of the order of $B \simeq \mathcal{B} \simeq 10^{-10}$ Gauss to contribute a signal on the level of about 1% to the CMB temperature anisotropies and polarisation.

If the initial magnetic field is not scale-invariant, the scales k_D and η_0 suppress the results by factors of $1/(k_D\eta_0)$ and $\ell/(k_D\eta_0)$ which are much smaller than unity. As already discussed, the damping scale k_D is given by $k_D^{-1} \simeq v_A l_\gamma(T_{\rm eq}) \simeq v_A \times 0.35$ Mpc, and v_A is the Alfvén velocity, $v_A^2 = \langle B\rangle^2/(4\pi(\rho+p))$ for the magnetic field averaged over a scale larger than the damping scale. Clearly, $v_A \lesssim 10^{-3}$ so that B does not induce density perturbations larger than 10^{-5}. Therefore, the damping scale is of the order of 1 kpc or less. The latter value is reached for maximal magnetic fields which are of the order of $\langle B\rangle \sim 10^{-9}$Gauss. On the other hand $a_0(\eta_0 - \eta_{\rm dec}) \simeq \eta_0$ is simply the angular diameter distance to the last scattering surface, which has been very accurately measured with the WMAP satellite [5], $\eta_0 = d_A = 13.7 \pm 0.5$ Gpc. So that $k_D\eta_0 \sim 10^7$ or even larger, depending on the magnetic field amplitude.

Our results differ somewhat, but not in a very significant way, from the results obtained in reference [115]. Since our magnetic field spectra are either scale-invariant or blue, the induced spectra $\ell^2 C_\ell$ are also either scale-invariant or blue. They grow towards large ℓ. It is therefore an advantage to choose ℓ as large as possible. However, in our calculations we have not taken into account the decay of gravity waves which enter the horizon before decoupling. Our results are therfore correct only for $\ell < \eta_0/\eta_{\rm dec} \sim 60$. To be on the safe side, we choose $\ell = 50$ in our graphics. In Fig. 4.1, we show $\ell^2 C^{XY}_{(A)\ell}$ at $\ell = 50$ for the different quantities (temperature anisotropy, E and B polarisation and correlators) as a function of n_A with n_S fixed to 2 and -2.99. We show the absolute value of the correlator in units of

$$\left(\frac{\Omega_A}{\Omega_{\rm rad}}\right)^2 \ln^2\left(\frac{z_{\rm in}}{z_{\rm eq}}\right) \simeq 10^{-10}\left(\frac{\mathcal{B}_{k_D}}{10^{-9}\text{Gauss}}\right)^4 ,$$

and

$$\frac{\Omega_A\Omega_S}{\Omega_{\rm rad}^2} \ln^2\left(\frac{z_{\rm in}}{z_{\rm eq}}\right) \simeq 10^{-10}\left(\frac{\mathcal{B}_{k_D}}{10^{-9}\text{Gauss}}\right)^2 \left(\frac{B_{k_D}}{10^{-9}\text{Gauss}}\right)^2 .$$

Note that the parity even spectra $C^{XY}_{(A)\ell}$ are always negative and have to be subtracted from $C^{XY}_{(S)\ell}$ which is of the same order of magnitude or larger since $\Omega_S \geq \Omega_A$ and $n_S \leq n_A$. For the limiting case, $\Omega_S \simeq \Omega_A$ and $n_S \simeq n_A$, the presence of a helical component in the magnetic field spectrum can in principle cancel the effect of the symmetric part on the CMB. In that very particular case, the signature of the presence of a magnetic field will appear only through the parity-odd correlators.

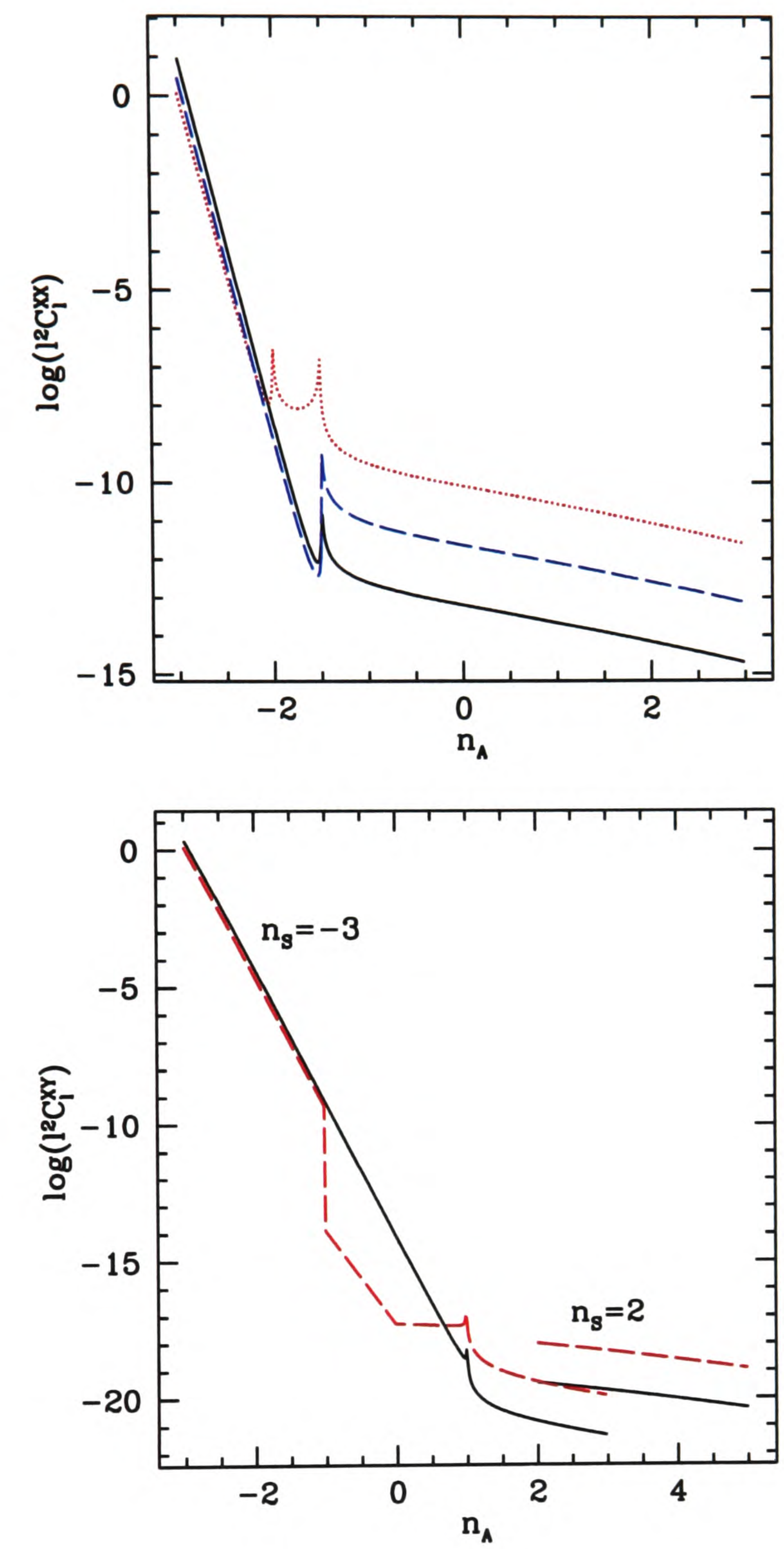

Figure 4.1: On the top panel we show the amplitudes of the parity-even correlators, $\ell^2 C^{\Theta\Theta}_{(A)\ell}$ (solid, black), $\ell^2 C^{EE}_{(A)\ell}$ (dotted, red) and $\ell^2 C^{\Theta E}_{(A)\ell}$ (dashed, blue) as a function of the spectral index n_A for $\ell = 50$. The logarithm of the absolute value of $\ell^2 C^{XY}_{(A)\ell}$ is shown in units of $(\Omega_A/\Omega_{\rm rad})^2 \ln^2(z_{\rm in}/z_{\rm eq})$. We do not plot $\ell^2 C^{BB}_{(A)\ell}$ which equals $\ell^2 C^{EE}_{(A)\ell}$ within our approximation. The spikes at $n_A = -2$ for $\ell^2 C^{EE}_{\ell}$ and at $n_A = -3/2$ are not real, but artefacts due to the break-down of our approximations at these values. On the bottom panel we show the corresponding parity-odd correlators, $\ell^2 C^{\Theta B}_{(A)\ell}$ (solid, black), $\ell^2 C^{EB}_{(A)\ell}$ (dashed, red) in units of $(\Omega_A \Omega_S/\Omega^2_{\rm rad}) \ln^2(z_{\rm in}/z_{\rm eq})$ for $n_S = -2.99$ and $n_S = 2$. In this last case, only the allowed range $n_A \geq n_S = 2$ is plotted. Again the spike at $n_A = 1$ for $n_S = -2.99$ and the precipitous drop at $n_A = -1$ in $\ell^2 C^{EB}_{(A)\ell}$ are due to the limitation of our approximation close to the transition indices.

From Fig. 4.1 it is clear that only for $n_{A,S} \lesssim -2$ and $\Omega_A \simeq \Omega_S \sim 10^{-5}$, the effect on the CMB will be of the order of a percent or more. In reference [80] it has been shown that for $n_S > -2$, magnetic fields with $B_\lambda \gtrsim 10^{-10}$ Gauss, $\lambda \sim 1$ Mpc, produce gravity waves on small scales incompatible with the nucleosynthesis bound. Here we require $B_{k_D} \lesssim 10^{-8}$ Gauss so that Ω_B remains a small fraction of the radiation density throughout. Then $B_\lambda = B_{k_D}(\lambda k_D)^{-(n+3)} \ll B_{k_D}$ for $n > -2$. Therefore, by keeping B_{k_D} sufficiently small, we automatically satisfy the bound derived in reference [80]. The result is most interesting for the window of $-3 < n_S \lesssim n_A \lesssim -2$ and $\Omega_A \simeq \Omega_S \sim 10^{-5}$, which requires $\mathcal{B}_{k_D} \simeq B_{k_D} \sim 10^{-10}$Gauss. If magnetic field helicity is causally produced, which implies $n_S = 2$ and $n_A = 3$, this effect cannot be observed in the CMB since the parity violating terms are suppressed by about 15 orders of magnitude (see lines in the lower right corner of the bottom panel of Fig. 4.1).

In Fig. 4.2 we show the ratio $C^{\Theta B}_{(A)\ell}/C^{\Theta E}_{(A)\ell}$ for $n_S = -3$ as function of n_A. Again, we are mainly interested in the part of the graph with $-3 < n_A < -2$, where this ratio raises from the order unity to about 10^5. Consequently, if a close to maximal helical magnetic field, with a spectrum not too far from scale-invariant, $-3 < n_S < n_A < -2$ is produced in the early universe, it is more promising to search for its parity violating terms than for the parity even contributions.

We can conclude that helical magnetic fields with a spectrum close to the scale-invariant value, $-3 < n_S \simeq n_A \lesssim -2$ and close to maximal amplitudes on small scales, $B_{k_D} \gtrsim 10^{-10}$ Gauss, can lead to observable parity violating terms $C^{\Theta B}_\ell$ and C^{EB}_ℓ in the CMB. Such magnetic fields might in principle be produced during an inflationary epoch where the photon is not minimally coupled or via its coupling to the dilaton (see section 2.3.3 for various proposal of magnetic field production during an inflationary phase). However, so far no concrete proposal has led to $n_{S,A} \simeq -3$, nor to the creation of a helical term. As we have shown, the effect is largely suppressed and clearly unobservable for causal magnetic fields, produced during the electroweak phase transition or even later.

Nevertheless, our calculation also shows the possible effect of parity violating processes during inflation, which may lead to a non-vanishing helical component of gravity waves $\mathcal{H} \neq 0$ (Eq. (4.35)). In this case the above calculation can be trivially repeated and will result in non-vanishing parity violating CMB correlators, $C^{\Theta B}_\ell \neq 0$ and $C^{EB}_\ell \neq 0$. We think

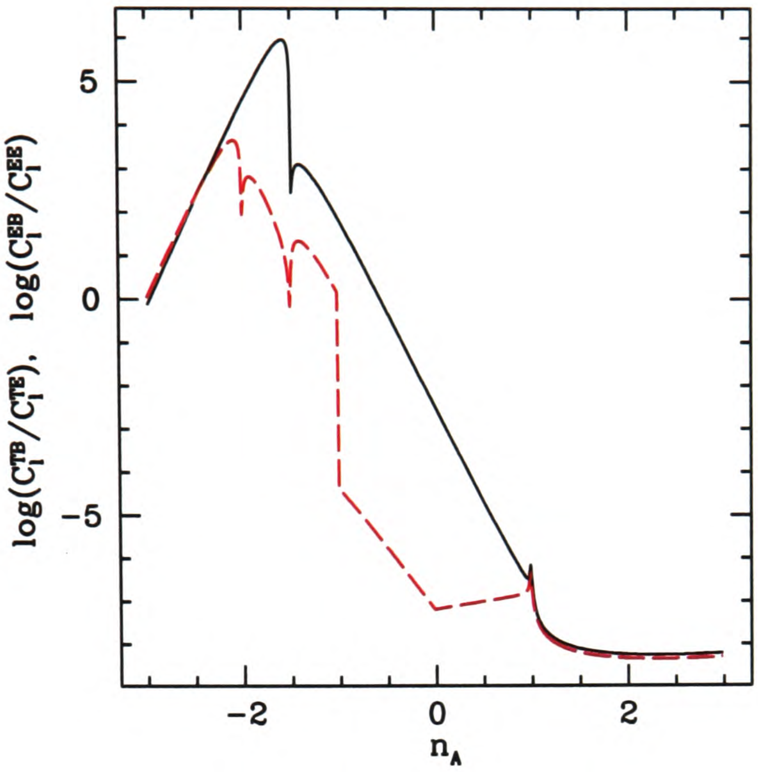

Figure 4.2: We show the ratio of the correlators, $C_\ell^{\Theta B}/C_\ell^{\Theta E}$ (solid, black), and C_ℓ^{EB}/C_ℓ^{EE} (dashed, red) for $n_S = -3$ as functions of the spectral index n_A for $\ell = 50$. The logarithm of the absolute value is shown in units of $\Omega_A/\Omega_S \leq 1$. The spikes visible at certain values of the spectral index n_A are mainly due to our relatively crude approximations.

that already this remark, together with our knowledge that at least at low energies, nature does violate parity, should be a sufficient motivation to derive experimental limits on these correlators.

Chapter 5

Charge asymmetry of the universe

The aim of this chapter is to place a cosmological constraint on the presence of an electrical charge asymmetry in the universe. Using the covariant formalism introduced in the first chapter to model the charged universe, we find that, in the magnetohydrodynamic limit, the effect of a non-zero charge is to induce a magnetic field and vorticity in the metric. We then use the isotropy of the CMB to place stringent constraints on the possible electrical charge asymmetry. We find the net excess charge per baryon to be $q_B < 10^{-26}e$ in the case of a uniform distribution of charge, where e is the charge of the electron. If the charge asymmetry is inhomogeneous, the constraints will depend on the spectral index, n, of the induced magnetic field and range from $q_B < 10^{-20}e$ $(n = -2)$, to limits of $q_B < 5 \times 10^{-26}e$ $(n \geq 2)$. If one could further assume that the charge asymmetries of individual particle species are not anti-correlated so as to cancel, this would imply, for photons, $q_\gamma < 10^{-35}e$; for neutrinos, $q_\nu < 4 \times 10^{-35}e$; and for heavy (light) dark matter particles $q_{\rm dm} < 4 \times 10^{-24}e$ $(q_{\rm dm} < 4 \times 10^{-30}e)$.

In this chapter we go back to the definitions and formalism presented in chapter 1. In particular, $\Theta = 3\dot{a}/a$ denotes the volume expansion and not the CMB temperature anisotropy as in chapter 3.

5.1 Introduction

Charge conservation is a consequence of the invariance of electrodynamics under a gauge transformation. If one considers the Lagrangian density of a system of electromagnetic fields interacting with charged particles $\mathcal{L} = -\frac{1}{4}F_{\alpha\beta}F^{\alpha\beta} - j^\alpha A_\alpha$, where A_α is the vector potential and $F_{\alpha\beta} = A_{\beta;\alpha} - A_{\alpha;\beta}$ the electromagnetic field tensor, then under a gauge transformation $A_\alpha \to A_\alpha + \Lambda_{;\alpha}$ the Lagrangian changes like $\mathcal{L} \to \mathcal{L} - j^\alpha \Lambda_{;\alpha}$. Consequently, the action changes like

$$\mathcal{S} \to \mathcal{S} - \int_D (j^\alpha \Lambda)_{;\alpha} \sqrt{-g}\, d^4x + \int_D j^\alpha{}_{;\alpha} \Lambda \sqrt{-g}\, d^4x\,. \tag{5.1}$$

The first term is a surface term and can be set to zero; in order for the action to be invariant, one has then that $j^\alpha{}_{;\alpha} = 0$. Therefore, if violation of gauge invariance occurs in some epoch of the evolution of the universe, this can lead to the presence of a charge asymmetry. There has been many propositions in the past of different ways to achieve charge non-conservation, and create an overall charge imbalance in the universe. The first cosmological analysis of a charged universe undertaken was in the context of the steady state model of the universe by Lyttleton and Bondi [127], where an attempt was made to explain the recession of galaxies through electromagnetic repulsion. The authors first performed a simple Newtonian analysis. They assumed that the charge of the proton and the electron were different by a small amount $q_P = -(1+\varepsilon)e$, and evaluated the electrostatic repulsion felt by a charged hydrogen atom situated on the boundary of a sphere of charged atoms. The ratio of electrostatic repulsion to gravitational attraction is found to be $\mu = \varepsilon e/(\sqrt{G}m_P) = 10^{18}\varepsilon$, where m_P is the proton mass, so that if $\varepsilon > 10^{-18}$, electrostatic repulsion overcomes gravitational attraction. The bound on ε at that time was given by the Millikan experiment as $\varepsilon < 10^{-17}$. The repulsive force takes the form $F = Gm_P(\mu - 1)\rho R$, where ρ is the density of atoms in the sphere, and R the radius: this leads to a linear velocity-distance law, and they thought they could recover Hubble expansion. Since in this picture the density would diminish in time, and the expansion decreases, in order to account for their steady state model they postulated creation of charge (and therefore of matter) at a rate $\mathcal{Q}$ everywhere in space: they modified Maxwell's equations to include a direct coupling to the vector potential $F^{\alpha\beta}{}_{;\beta} = j^\alpha - \chi A^\alpha$, violating gauge invariance, and leading to a non-continuity equation $j^\alpha{}_{;\alpha} = \mathcal{Q}$. They estimated that the creation rate required in order to maintain the universe in the actual conditions should be of one hydrogen atom per second in a cube of edge 250 km. This model seems acceptable in the Newtonian context. However, they attempted a relativistic generalisation of it in the context of a De Sitter space-time which was wrong, as pointed out by Swann [128]. The reason is strictly connected with the topic of this chapter. In order to preserve the space-time homogeneity and isotropy required by the De Sitter metric element, they derived a solution for their model with electromagnetic fields $F^{\alpha\beta} = 0$ and spatial current $J^{\alpha} = 0$: therefore, removing the mechanism by which the steady state was realised. They still found that in their model space-time was expanding, but this was no longer given by electrostatic repulsion, but implicit in the assumption of a De Sitter metric.

A similar model, using the Proca theory of electromagnetism, was analysed in details by Barnes [129]. Here again the author made use of the fact that the breaking of gauge symmetry in the context of the Proca theory allows the presence of a non-zero, uniform charge density, with zero electric and magnetic fields: therefore, preserving the homogeneity and isotropy of the background cosmology. In his analysis the author did not impose the steady state condition, avoiding the error of Lyttleton and Bondi. He calculated a general relativistic model of cosmological expansion dominated by the charged background, and found that the energy density associated with the charge would decay like $\rho_q \propto a^{-6}(\eta)$, so that the energy due to the charge must have been dominant at some early stages of the universe's evolution. Present dominance of the charged background would mean that the very early expansion would have been more rapid than in the conventional FRW model, too rapid for nucleosynthesis or thermalisation of the background radiation to occur.

More recently, other articles have proposed models of charge non-conservation. The spontaneous breaking of gauge symmetry, and the subsequent development of a charge imbalance, was considered by Ignatiev *et al.* [130], and Dolgov and Silk [131] used it as a mechanism of creation of primordial magnetic fields. An implementation of a homogeneous and isotropic charge density was proposed in the context of massive electrodynamics [132], and the possibility of charge non-conservation has been analysed in brane world models [133, 134], and in varying speed of light theories [135].

5.2 Current experimental constraints

In principle, a potential charge asymmetry could be carried by a number of different, stable components in the universe. These can include photons, neutrinos, dark matter, or a difference in the electron and proton charges. There already are experimental constraints on all these components. Experimental constraints on the charge of photons come simply by measuring whether light gets deflected by a magnetic field. Semertzidis *et al.* [136] estimated the deflection of a laser beam in an alternating magnetic field, and derived a bound on the photon charge of $q_\gamma < 8 \times 10^{-17}e$. A tighter bound, $q_\gamma < 5 \times 10^{-30}e$, has been derived from the lack of dispersion of the radio pulses coming from the pulsar PSR 1937+21, as they pass through the galactic magnetic field [137]. The charge of neutrinos has been constrained in the same way, observing the emission of the supernova 1987A; however, a tighter constraint for all flavours comes from the analysis of red giant luminosity evolution in globular clusters, and results in $q_\nu < 2 \times 10^{-14}e$ [138]. The difference in electron and proton charges is constrained with laboratory measurements of two different kind: electro-acoustic techniques, in which an alternating electric field is applied to an acoustic cavity containing gas, and one measures the generation of sound waves at the field frequency [139]; or Millikan-type experiments, using levitating steel balls [140]. They both limit the electron-proton charge difference to be $q_{e-p} < 10^{-21}e$. No direct constraints are available for dark matter particles, of course, but constraints have been established on the fraction of dark matter due to charged heavy particles, with mass between 10^4 and 10^7 GeV. The constraint is of the order of 10^{-5}, and has has been achieved by searching for super-heavy isotopes of hydrogen in sea water [141, 142].

In this chapter we obtain a cosmological constraint on a possible charge asymmetry in the universe, characterised by a uniform or a stochastic distribution, placing the potential contribution of the aforementioned individual components in context. The premise will be that the small charge imbalance was generated by a mechanism violating charge conservation at some very early time of the evolution of the universe, but that charge is conserved in the period in which we are establishing the constraints. This allows us to use the standard formulation of electrodynamics in curved space-time, introduced in chapter 1.

5.3 Model of a charged universe

We consider a model of the universe filled with a charged perfect fluid, which could be matter or radiation, characterised by the energy-momentum tensor $T_F^{\alpha\beta} = \rho u^\alpha u^\beta + p h^{\alpha\beta}$; the charge will give rise to an electromagnetic field, with $T_{EM}^{\alpha\beta} = F^\alpha{}_\gamma F^{\beta\gamma} - \frac{1}{4} g^{\alpha\beta} F_{\gamma\delta} F^{\gamma\delta}$. The energy-momentum conservation equation accounts for the interaction between the fluid and the field, so that [12]

$$T_F^{\alpha\beta}{}_{;\beta} = F^{\alpha\beta} j_\beta \,. \tag{5.2}$$

Using the splitting of the four-current introduced in section 1.2.4, $u_\alpha j^\alpha = -q$, $J^\alpha = h^\alpha{}_\beta j^\beta$, and the form of the electromagnetic field tensor (1.10), the coupling term can be rewritten as

$$F^{\alpha\beta} j_\beta = qE^\alpha + F^{\alpha\beta} J_\beta = qE^\alpha + u^\alpha E^\beta J_\beta + \epsilon^{\alpha\beta\gamma} J_\beta B_\gamma \,. \tag{5.3}$$

We further assume the usual equation of state for a perfect fluid $p = w\rho$; then, the energy conservation equation for the fluid, $u_\alpha T_F^{\alpha\beta}{}_{;\beta} = u_\alpha F^{\alpha\beta} j_\beta$, takes the form

$$\dot\rho + (1+w)\Theta\rho = -E^\beta J_\beta \,, \tag{5.4}$$

and the momentum conservation equation $h_{\alpha\beta} T_F^{\beta\gamma}{}_{;\gamma} = h_{\alpha\beta} F^{\beta\gamma} j_\gamma$ takes the form

$$(1+w)\rho\,\dot u_\alpha + w D_\alpha \rho = qE_\alpha + \epsilon_{\alpha\beta\gamma} J^\beta B^\gamma \,. \tag{5.5}$$

If the charged fluid is composed by non-relativistic matter, one has $q = \varepsilon\, e\, n_{\rm mat} = \frac{\varepsilon\, e}{m}\rho_{\rm mat}$, where $\varepsilon\, e$ and $n_{\rm mat}$ represent respectively the charge and the number density of the fluid particles, and m is their mass; if instead the radiation component is charged, one has $q = \varepsilon\, e\, n_{\rm rad} \propto \rho_{\rm rad}^{3/4}$, with similar definitions. It appears from this picture that the introduction of a charged fluid breaks the isotropy of the universe, through the creation of currents and electromagnetic fields. Therefore, it is in principle possible to use the CMB as a measure of the isotropy of the universe to constrain the presence of an overall charge asymmetry.

We must further consider the fact that the universe has a very high conductivity, during all the phases of its evolution, as discussed in section 2.4.2. Therefore, we perform our analysis in the ideal magnetohydrodynamics limit, for which the conductivity goes to infinity while the current remains finite [12]. In the reference frame of comoving observers, corresponding to the reference frame of the fluid in this picture, Ohm's law takes the form $J_\alpha = \sigma E_\alpha$ (*cf.* section 1.2.4). Consequently, applying the magnetohydrodynamic limit one finds that the electric field (but not the magnetic field) must go to zero [90]. This assures that the spatial current remains finite, avoiding the possibility of an instantaneous response of the fluid to the electromagnetic fields. Note that this is valid because our analysis is performed in the reference frame of observers comoving with the fluid, characterised by the four-velocity u^α; in a reference frame with four-velocity $\tilde u^\alpha = u^\alpha + v^\alpha$, the magnetohydrodynamic limit implies the presence of an electric field $\tilde{E}_\alpha = -\epsilon_{\alpha\beta\gamma} v^\beta B^\gamma$.

Another way of rephrasing the magnetohydrodynamic limit is found by considering the time evolution of the electric and magnetic fields given by Maxwell's equations (1.34) and (1.35) of section 1.2.4. As explained in section 3.3, the presence of a primordial, uniform magnetic field in a FRW universe is accounted for by assuming that the energy density of the field is a first order quantity in perturbation theory, and that the field itself is a small background component. We introduce the presence also of an electric field with the same characteristics. Then, the evolution of the fields at the lowest order is given by

$$\dot{B}_\alpha = -\frac{2}{3}\Theta B_\alpha \,, \tag{5.6}$$

$$\dot{E}_\alpha = -J_\alpha - \frac{2}{3}\Theta E_\alpha \,. \tag{5.7}$$

The first of these equations suggests that the magnetic field varies on an approximative time-scale given by the Hubble time Θ^{-1}. By substituting with Ohm's law $J_\alpha = \sigma E_\alpha$ in the second equation, one finds that the time-scale of variation of the electric field is instead of the order $(\sigma + (2/3)\Theta)^{-1}$. One further has that, for all the epochs of the evolution of the universe, $\sigma/\Theta \gg 1$ (for example, $\sigma/\Theta \sim 10^{28}$ today, *cf.* section 2.4.2). Therefore, while the magnetic field varies on a time-scale comparable to the Hubble time, the electric field varies on a much smaller time-scale, given by σ^{-1}, and gets dissipated much quicker. The infinite conductivity limit provides an explanation of the reason why large scale magnetic fields, and not electric fields, are observed in the universe.

In the case of a charged cosmic fluid which we are analysing, and in the reference frame of comoving observers, adopting the infinite conductivity limit reduces the form of the relevant equations to

$$\dot{\rho} + (1+w)\Theta\rho = 0 \,, \tag{5.8}$$

$$(1+w)\rho\,\dot{u}_\alpha + wD_\alpha\rho = \epsilon_{\alpha\beta\gamma} J^\beta B^\gamma \,, \tag{5.9}$$

for the energy and momentum conservation, and

$$
\begin{aligned}
2\,\omega_\alpha B^\alpha &= q && (5.10)\\
D_\alpha B^\alpha &= 0 && (5.11)\\
\epsilon_{\alpha\beta\gamma} D^\beta B^\gamma &= J_\alpha - \epsilon_{\alpha\beta\gamma}\dot{u}^\beta B^\gamma && (5.12)\\
h_{\alpha\beta}\dot{B}^\beta &= (\omega_{\alpha\beta} + \sigma_{\alpha\beta} - \frac{2}{3}\Theta h_{\alpha\beta})B^\beta\,, && (5.13)
\end{aligned}
$$

for Maxwell's equations. We have defined the charge density as $q = \varepsilon\, e\, n$, both in the case of charged non-relativistic matter and radiation; therefore, using $\rho_{\rm mat} \propto n_{\rm mat}$ and $\rho_{\rm rad} \propto n_{\rm rad}^{4/3}$, Eq. (5.8) implies the charge evolution $\dot{q} + \Theta q = 0$. Equation (5.10) shows that in a universe with infinite conductivity, the presence of a charge density implies the presence of a magnetic field, and induces vorticity in the metric. Therefore, the analysis in a non-perturbative framework should be carried on in the context of tilted Bianchi universes, *i.e.* homogeneous and anisotropic universes in which the surfaces of homogeneity are not orthogonal to the matter flow. In this case the equations given above are complemented by the propagation equations for the kinematic quantities given in section 1.2.5: Raychaudhuri's equation, the evolution equations for the vorticity and the shear, and the constraints equations coming from the space projection of the Ricci identities.

However, the goal of this analysis is to constrain the presence of charge in the universe by using the isotropy of the CMB. Consequently, the charge has to be considered a small perturbation, $\varepsilon \to 0$, and we want to use linear perturbation theory on a FRW universe. The relevant equation at this purpose is (5.10): a constraint on the charge density can be derived from constraints on the magnetic field and the vorticity induced by it. The charge density q is a first order variable in perturbation theory; so are the magnetic energy density B^2, the vorticity ω_α, the acceleration $\dot{u}_\alpha$, the spatial current J_α, the shear $\sigma_{\alpha\beta}$ and the density inhomogeneities $D_\alpha\rho$. Since we want to constrain the charge density by constraining magnetic field and vorticity, we need to evaluate the time evolution of these two quantities. At the lowest order, the magnetic field evolution is

$$\dot{B}_\alpha + \frac{2}{3}\Theta B_\alpha = 0\,, \tag{5.14}$$

and the vorticity evolution is (*cf.* Eq. (1.49))

$$\dot{\omega}_\alpha + \frac{2}{3}\Theta\,\omega_\alpha = -\frac{1}{2}\epsilon_{\alpha\beta\gamma}D^\beta\dot{u}^\gamma\,; \tag{5.15}$$

note that this equation is the same as (3.63), once one performs the substitution $\omega_{ij} = a\,V_C\,Q^{(1)}{}_{[i|j]}$ (*cf.* (3.49)) and changes from proper to conformal time [15]. Substituting with the momentum conservation equation (5.9), and using the identity $\epsilon_{\alpha\beta\gamma}D^\beta D^\gamma f = -2\dot{f}\omega_\alpha$ [91], equation 5.15 becomes

$$\dot{\omega}_\alpha + \left(\frac{2}{3} - w\right)\Theta\,\omega_\alpha = -\frac{1}{2\rho(1+w)}\epsilon_{\alpha\beta\gamma}D^\beta\epsilon^\gamma{}_{\delta\mu}J^\delta B^\mu\,. \tag{5.16}$$

The magnetic field evolution equation gives the usual scaling behaviour $B_\alpha = B_{0\alpha}/a^2$, where B_0 denotes the field amplitude today. The evolution for the vorticity is more involved, since it is sourced by the charge through the magnetic field and the current. We know however that the charge density evolves like the number density of particles, $\dot{q}+\Theta q = 0$: this equation can give us insight on the behaviour of vorticity. By deriving Eq. (5.10), and imposing the charge scaling, $2\dot{\omega}_\alpha B^\alpha + 2\omega_\alpha \dot{B}^\alpha = -\Theta q$, we find, from the magnetic field evolution

$$B^\alpha\dot{\omega}_\alpha = -\frac{1}{3}\Theta B^\alpha\omega_\alpha\,. \tag{5.17}$$

This identity is satisfied in the two cases $(a\omega_\alpha)^\cdot = 0$, and $(a\boldsymbol{\omega})^\cdot \perp \mathbf{B}$. In the first case, the evolution of the vorticity is such that $\dot{\omega}_\alpha + \frac{\dot{a}}{a}\omega_\alpha = 0$; in the second case, one has that only the component parallel to the magnetic field satisfies $\dot{\omega}_\parallel + \frac{\dot{a}}{a}\omega_\parallel = 0$. In the following, we will always assume that $\omega_\alpha \propto a^{-1}$. Given that we want to constrain the charge using Eq. (5.10), we are in fact interested only in $\omega_\parallel$. However, in the following we will set constraints on the vorticity vector independently, through the induced CMB anisotropies: our assumption, therefore, corresponds to postulating that the entire vorticity contribution to CMB anisotropies comes only from the $\omega_\parallel$ component. It is customary to do so, when one is aiming to establish constraints on non-standard CMB anisotropies sources: for example, we did the same assumption when analysing the gravity wave signal from the helical magnetic field, in chapter 4. In this case, our premise that $\omega_\alpha = \omega_{0\alpha}/a$ is conservative, in the sense that it makes the final limit on the charge less tight.

We now proceed to evaluate the bounds on the charge in two different configurations: uniformly and stochastically distributed charge. Note that the strategy of limiting the charge asymmetry of the universe by using the observed isotropy of the FRW space-time has already been adopted in two previous works: Orito and Yoshimura [143] also used the measurement of CMB temperature fluctuations, instead Masso and Rota [144] derived a bound using nucleosynthesis. In both these references, however, it is claimed that the presence of a non-zero charge density would generate a large scale electric field in the universe: they modelled the universe as an insulating medium rather that a highly conducting one. Our work differs from both of them in this, we believe, crucial aspect.

5.4 Uniform distribution of charge

Let us first focus on a uniform charge distribution. We assume the vorticity and the magnetic field to be uniform vector fields. In this case, the anisotropic expansion of the universe caused by them will leave an imprint on the propagation of light rays from the last-scattering surface until today. In [8, 88] tight constraints were derived on both ω and B respectively, for a general class of homogeneous and anisotropic models. It was found that

$$B_0 \;<\; 3\times 10^{-9}\Omega^{1/2}\,h\,\mathrm{Gauss}\,, \tag{5.18}$$

$$\omega_0 \;<\; 10^{-7}\,H_0\,, \tag{5.19}$$

where $H_0 = 100\,h\,\mathrm{km\,sec^{-1}Mpc^{-1}}$ is the Hubble constant today, and $1-\Omega$ is the curvature. The bound in Eq. (5.19) was found assuming the usual scaling for the vorticity in the matter era in the absence of sources: $\omega_\alpha = \omega_{0\alpha}/a^2$, as can be derived from Eq. (5.16). Therefore, we have to correct this bound accounting for our assumption for the evolution of vorticity sourced by the charge, $\omega_\alpha = \omega_{0\alpha}/a$. This simply changes the limit by a factor of $1/a(\eta_{\rm rec}) \simeq 10^3$: $\omega_0 < 10^{-4}\,H_0$. With the above constraints we obtain a limit on the charge asymmetry today, using the Schwarz inequality on Eq. (5.10),

$$q_0 \leq 2|\omega_0||B_0| \leq 2.4\times 10^{-74}\;h^2\;\Omega^{1/2}\mathrm{GeV}^3\,. \tag{5.20}$$

It may be that the charge asymmetries corresponding to individual particle species are such as to cancel to some extent, yielding to a universe which is more neutral overall. However, should this not be the case, this last equation implies a maximal allowed charge $q_X = q/n_X$ for each different constituent X, where n_X is the number density of charged particles. For a flat universe ($\Omega = 1$), and assuming that the charge asymmetric matter is baryonic ($\Omega_B h^2 = 0.02$), we find that the maximal allowed charge excess per baryon is

$$q_B \lesssim 10^{-26} e\,. \tag{5.21}$$

If the charged particles are instead dominated by the dark matter constituents ($\Omega_{\rm dm} = 0.26$), we get $q_{\rm dm} \lesssim 4 \times 10^{-27} e\; m_{\rm dm}\; {\rm GeV}^{-1}$. For example, a conservative limit comes from neutralinos of mass of 1 TeV, $q_{\rm dm} \lesssim 4 \times 10^{-24} e$; considering instead a light dark matter particle with $m_{\rm dm} \sim 10$ MeV [145, 146], one gets $q_{\rm dm} \lesssim 4 \times 10^{-30} e$. If we assume that the charge imbalance is predominantly caused by photons, with $n_\gamma = 421.84\ {\rm cm}^{-3}$, we obtain $q_\gamma \lesssim 10^{-35} e$; for each species of neutrinos we obtain instead $q_\nu \lesssim 0.4 \times 10^{-34} e$, from $n_\nu = 115.05\ {\rm cm}^{-3}$. All these constraints are orders of magnitude more restrictive than the limits from laboratory experiments or astrophysical observations mentioned in section 5.2, subject to the assumption that any charge asymmetries between species are not anti-correlated.

5.5 Stochastic distribution of charge

One might expect that any mechanism of charge creation will be local, possibly a result of local violation of gauge invariance arising at some phase transition, or due to the escape of charge into extra dimensions. It would then be more appropriate to consider a stochastic distribution of charge asymmetry with, or without, a net imbalance in charge. The simplest assumption we can make, is that the magnetic field and the vorticity created by the charge density are two independent stochastic variables, with gaussian distribution. The requirement of background homogeneity and isotropy forces the first moments of the distributions to be zero, otherwise we recover the case of the uniform distribution; this in turns imply by the independence assumption that $\langle q \rangle = 0$. We further assume that the magnetic field and vorticity induced have power law power spectra, respectively $S(k) = S_0\, k^n$ and $\Omega(k) = \Omega_0\, k^m$, where the two spectral indices are different consequently to the independence assumption. We have then that:

$$\begin{aligned}\langle B_i(\mathbf{k})B_j^*(\mathbf{q})\rangle &= \frac{(2\pi)^3}{2}\delta(\mathbf{k}-\mathbf{q})(\delta_{ij}-\hat{k}_i\hat{k}_j)\,S(k)\,, \quad k<k_D \\ \langle \omega_i(\mathbf{k})\omega_j^*(\mathbf{q})\rangle &= \frac{(2\pi)^3}{2}\delta(\mathbf{k}-\mathbf{q})(\delta_{ij}-\hat{k}_i\hat{k}_j)\,\Omega(k)\,,\end{aligned}$$

where we have introduced the upper cutoff frequency k_D in the magnetic field power spectrum, which accounts for the interaction of the magnetic field with the cosmic plasma at small scales (*cf.* section 2.4.4). At recombination, one has $k_D(\eta_{\rm rec}) \simeq (V_A L_S(\eta_{\rm rec}))^{-1} \simeq 10\,{\rm Mpc}^{-1}$, from [73]. The factors $(\delta_{ij}-\hat{k}_i\hat{k}_j)$ in the power spectra come from the divergence-less property of both the magnetic field and the vorticity (*cf.* Eq. (1.53)). As usual, we define

$$B_\lambda^2 = \langle B^i(\mathbf{x})B_i(\mathbf{x})\rangle|_\lambda = \frac{S_0}{(2\pi)^2}\frac{\Gamma\left(\frac{n+3}{2}\right)}{\lambda^{n+3}}\,, \tag{5.22}$$

$$\omega_\lambda^2 = \langle \omega^i(\mathbf{x})\omega_i(\mathbf{x})\rangle|_\lambda = \frac{\Omega_0}{(2\pi)^2}\frac{\Gamma\left(\frac{m+3}{2}\right)}{\lambda^{m+3}}\,, \tag{5.23}$$

to be the energy densities of the magnetic field and the vorticity in a region of size λ.

We wish to estimate the mean fluctuation of charge in a region of size λ:

$$\langle\, q_\lambda^2\,\rangle = \frac{1}{V_\lambda^2}\int d^3r_1 d^3r_2\, e^{-\frac{r_1^2}{2\lambda^2}}\, e^{-\frac{r_2^2}{2\lambda^2}}\,\langle q(\mathbf{r}_1+\mathbf{x})q(\mathbf{r}_2+\mathbf{x})\rangle\,. \tag{5.24}$$

From Eq. (5.10) one has

$$q(\mathbf{k}) = \frac{2}{(2\pi)^3}\int d^3p\,\omega_i(\mathbf{k}-\mathbf{p})B^i(\mathbf{p})\,, \tag{5.25}$$

so the charge density power spectrum is

$$\langle q(\mathbf{k})q^*(\mathbf{h})\rangle = \Omega_0\,S_0\,\delta^3(\mathbf{k}-\mathbf{h})\int d^3p\,|\mathbf{k}-\mathbf{p}|^m\,p^n[1+(\widehat{\mathbf{k}-\mathbf{p}}\cdot\hat{\mathbf{p}})^2]\,, \tag{5.26}$$

where $0<p<k_D$, since it is the magnetic field wave vector. The angular part of this integral is computed using Eqs. (A.4) and (A.5) of appendix A. We need now to substitute Eq. (5.26) in Eq. (5.24); the integral can be evaluated approximatively using the technique

described in appendix A, and after a long calculation we finally obtain

$$\langle q_\lambda^2 \rangle \simeq \frac{4\, B_\lambda^2\, \omega_\lambda^2}{\Gamma(\frac{n+3}{2})\,\Gamma(\frac{m+3}{2})}\, f(n,m,\lambda,k_D)\,, \tag{5.27}$$

with

$$\begin{aligned} f \;=\; & \frac{2\,(\lambda k_D)^{n+3}}{3\,(n+3)}\,\Gamma\left(\frac{m+3}{2},(\lambda k_D)^2\right)+\frac{(\lambda k_D)^{n+m+3}}{n+m+3}\left[\Gamma\left(\frac{3}{2}\right)-\Gamma\left(\frac{3}{2},(\lambda k_D)^2\right)\right]+ \\ & \frac{2m-n-3}{3(n+3)(n+m+3)}\left[\Gamma\left(\frac{n+m+6}{2}\right)-\Gamma\left(\frac{n+m+6}{2},(\lambda k_D)^2\right)\right]\,, \end{aligned} \tag{5.28}$$

where $\Gamma(a,x)$ denotes the incomplete gamma function (6.5.3 of [103]).

Eq. (5.27) provides a limit for the charge asymmetry parameter $q_X = \sqrt{\langle q_\lambda^2 \rangle}/n_X$ today, as a function of the parameters characterising the magnetic field and the vorticity: amplitudes, spectral indices, cutoff frequency and coherence scale.

As already presented in the previous chapters of this thesis, the amplitude B_λ of a cosmic magnetic field must satisfy stringent constraints, which have been estimated in several articles using completely independent methods. The most direct constraint on the magnetic field intensity comes from the observation of Faraday rotation in radio sources, as mentioned in section 2.2: for example in [147] it is shown that, for a cluster magnetic field, $B_\lambda \lesssim 10^{-6}$Gauss on scales $\lambda \simeq 1$ kpc. If the charge imbalance, and consequently the magnetic field, was created before recombination, we can apply the limits which come from CMB observations. We will use the limit derived in [107], by considering the CMB anisotropies induced by gravitational waves created by the anisotropic stresses of the primordial magnetic field. Eq. (28) of [107] states, for $\lambda = 0.1h^{-1}$Mpc,

$$B_\lambda < 7.9\times 10^{-6}\exp(2.99n)\ \text{Gauss}, \qquad \text{for } n < -\tfrac{3}{2}, \tag{5.29}$$

$$B_\lambda < 9.5\times 10^{-8}\exp(0.37n)\ \text{Gauss}, \qquad \text{for } n > -\tfrac{3}{2}. \tag{5.30}$$

We also use the constraint derived in [80], by imposing the nucleosynthesis bound on the energy density of the gravitational waves induced again by the field: Eq. (33) of [80] gives, also for $\lambda = 0.1h^{-1}$ Mpc,

$$B_\lambda < 700h\times 10^{-9}\left(\frac{\eta_{\rm in}}{\lambda}\right)^{\frac{n+3}{2}}\ \text{Gauss}\,. \tag{5.31}$$

In this work, in order to be conservative, we have chosen for the epoch of creation of the magnetic field the nucleosynthesis epoch, $\eta_{\rm in} = \eta_{\rm nuc} \simeq 0.1$ MeV $\simeq 10^{11}$ sec.

In order to constrain (5.27), we next need to find an upper bound for ω_λ, which is not present in the literature. Again, it can be found using the isotropy of the CMB. We need to evaluate the vector contribution to the CMB temperature anisotropy, given in Eq. (3.115). As already mentioned, the vorticity variable $\omega_i = \frac{1}{2}\epsilon_{ijk}\omega^{jk}$ is related to the vector gauge invariant variable V_C through relation (3.49) $\omega_{ij} = a\, V_C\, Q^{(1)}{}_{[i|j]}$. Remembering the definition $V_C = v^{(1)} - B^{(1)}$, where $v^{(1)}$ is the vector part of the fluid velocity perturbation and $B^{(1)}$ the vector metric perturbation, we finally find

$$\omega_i = \frac{k}{2}(v^{(1)} - B^{(1)})Q_i^{(1)}\,. \tag{5.32}$$

For the purposes of this analysis, we neglect the finite thickness of the last scattering surface and work in the tight coupling limit, for which $v^{(1)} = v_\gamma = v_B$. In this limit, the dominant effect of vector perturbations is the creation of a dipole in the temperature anisotropy. From the general expression for the CMB power spectrum Eq. (3.117), substituting with the vector source (3.115), we finally find

$$C_\ell = \frac{8}{\pi}\frac{\ell(\ell+1)}{a^2(\eta_{\rm rec})}\int_0^\infty dk\,\Omega(k)\frac{j_\ell^2(k\eta_*)}{(k\eta_*)^2}\,, \tag{5.33}$$

where $\eta_* = \eta_0 - \eta_{\rm rec}$, and the factor $a^{-2}(\eta_{\rm rec})$ accounts for the vorticity time evolution. This integral can be evaluated analytically using (B.7), to find

$$\frac{\ell^2 C_\ell}{2\pi} \simeq 4\sqrt{\pi}\frac{\Gamma(\frac{3-m}{2})}{\Gamma(\frac{m+3}{2})\Gamma(\frac{4-m}{2})}\, z_{\rm rec}^2\,\omega_\lambda^2\,\frac{\lambda^{m+3}}{{\eta_*}^{m+1}}\,\ell^{m+1}\,. \tag{5.34}$$

The maximum value for the CMB temperature anisotropy is $\ell^2 C_\ell/(2\pi) \simeq 10^{-10}$, and in order to constrain ω_λ we fix the ℓ dependence by considering the two extreme values $\ell = 4$, if $m < -1$, and $\ell = 200$, if $m > -1$.

We can finally evaluate Eq. (5.27), and obtain an upper bound on the charge density in a region of size λ, by applying the aforementioned constraints on B_λ and the limit on ω_λ just derived. The bounds are represented in Fig. 5.1, as a function of the spectral index n of the magnetic field. For every value of n, we have maximised (5.27) with respect to the vorticity

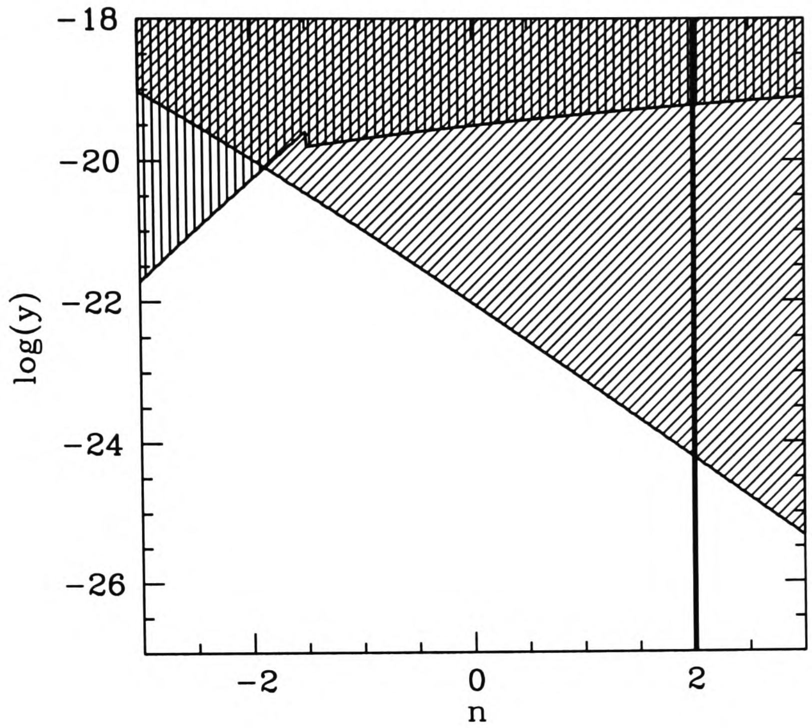

Figure 5.1: This figure shows the limits on the charge fraction parameter y which apply to a stochastic distribution of charge, as a function of the spectral index of the induced magnetic field, for $\lambda = 0.1h^{-1}$Mpc. The diagonally-shaded region represents the exclusion region derived from nucleosynthesis constraints [80]; the vertically-shaded region is excluded by CMB anisotropies [107]. Magnetic field constraints from clusters [147] give a less restrictive bound, which is not shown in the figure. If the process generating the charge is causal, then $n \geq 2$.

spectral index m, on which we have no theoretical prediction. Note that the quantity shown in the y-axis,

$$y = \frac{q_X}{e}\left(\frac{\Omega_X}{\Omega_B}\frac{m_P}{m_X}\right) \tag{5.35}$$

is the charge fraction parameter "normalised" to the case of baryonic charge asymmetric matter. If the process generating the charge and the magnetic field is causal, *e.g.* it takes place during a phase of standard Friedmann expansion, then the spectral index must satisfy $n \geq 2$ [18]. In this case, the limits on q_X are more stringent than in the case in which the generation occurs during inflation.

5.6 Discussion

In this chapter we have derived a cosmological constraint on the presence of a non-zero electric charge in the universe. A conservation law associated with a long range force, such as charge conservation with the electromagnetic force, is usually believed to be exact as a result of gauge invariance. Conservation of charge appears to hold in all particle decays, and, as discussed in section 5.2, there are strong experimental constraints on the charge of particles which are predicted to be neutral by the standard model of particle physics. However, even though electric charge conservation is well established on Earth, this may not imply directly the overall neutrality of the universe: to be able to draw this conclusion, one would have to assume in addition that charge has to be conserved on all scales and during the entire evolution of the universe. This may not be the case; one can invoke a resemblance with the fact that particle physics experiments have never observed any process violating baryon number, although the universe does contain a baryon asymmetry. Given these premises, the determination of a *cosmological* constraint on the charge asymmetry of the universe is of conceptual importance.

We have mentioned some of the current propositions for mechanisms that lead to the generation of a charge asymmetry in the universe. In the context of brane world scenarios, charge non-conservation arises in the form of charge leakage into extra dimensions; in varying speed of light theories, it can be a consequence of the variation of the fine structure constant; allowing for some modification of the standard model, it can arise if the gauge symmetry is temporarily broken during a phase transition taking place in the early universe, or if one imposes a small, non-zero mass to the photon. In our analysis, we did not consider a complete model in which the charge asymmetry originates: by doing so, our constraints gain in generality (although perhaps loosing in motivation). The assumption we made, that charge is conserved in the period in which our constraint is established, points toward a model in which the charge is created during a primordial phase transition leading to a transitory breaking of the electromagnetic gauge symmetry. Including a specific mechanism of charge creation could be a possible extension and improvement of this work.

We have obtained our constraints on the overall charge imbalance of the universe in two different cases: a uniform distribution of charge, and a distribution characterised by stochastic fluctuations. In order to derive our results, we made the assumptions that the universe is a good conductor, and that the charge is a first order perturbation in a background FRW model; moreover, we generalised the scaling of the charge-induced vorticity as the inverse of the scale factor. These are the only assumptions which affect the uniform distribution limit: in the case of the stochastic distribution, we further assumed that vorticity and magnetic field are two independent, gaussian stochastic variables. A further, interesting extension of our analysis would be to go beyond the linear calculation, and evaluate the full effect that the presence of a non-zero charge has on the background dynamics of the space-time.

In the case of a uniform distribution of charge, it is remarkable that our cosmological limit, once translated in terms of constraints for the single charge carriers, gives results which are orders of magnitude stronger than the ones derived by terrestrial experiments or astrophysical observations. If the charge is distributed stochastically, the limits are less stringent: this is a consequence of the fact that the CMB bound on stochastic vorticity is less tight than in the uniform case, and in addition we have maximised it with respect to the vorticity spectral index m. However, we still find interesting constraints for high values of the magnetic field spectral index: these would apply, in the case of a causally created charge asymmetry, for example during a phase transition.

Chapter 6

Observational constraint on the fourth derivative of the inflaton potential

This chapter deals with a rather different subject than the rest of the work presented in this thesis. We have seen how the observed properties of the CMB can be used to place constraints on the presence of different components in the universe, if they act as a source of perturbation in the background metric. We have analysed the effect on the CMB induced by a primordial helical magnetic field in the universe, or by a hypothetical charged background fluid. Here we will consider the most important source of CMB temperature fluctuations: the density perturbations created during inflation. We present a work done in collaboration with Dr. Steen Hansen and Dr. Martin Kunz, in which we have used the flow equations for the slow-roll inflationary parameters n_S (scalar spectral index), r (tensor to scalar ratio), and $dn_S/d\ln k$ (running of the spectral index), and combined their result with the observational constraints from the CMB temperature anisotropy spectrum, to place a lower limit on the fourth derivative of the inflaton potential [148].

In this chapter, a prime denotes derivative with respect to the inflaton field $' = \frac{d}{d\phi}$, and a dot denotes derivative with respect to physical time $\dot{} = \frac{d}{dt}$. Again, we use units such that $c = 8\pi G = \frac{8\pi}{m_{\rm Pl}^2} = 1$, where $m_{\rm Pl}$ denotes the Planck mass.

6.1 Inflation and the slow roll approximation

We re-examine here in more details the description of the inflationary scenario started in the end of section 1.3.3. This section and the following are based on references [4, 149, 150].

An inflationary phase in the evolution of the universe is a phase of accelerated expansion, in which the strong energy condition $\rho + 3p > 0$ is violated. This is realised if the universe is dominated by the vacuum energy of a scalar field ϕ which drives the expansion. Therefore, one has to consider the dynamics of a scalar field in an expanding FRW background. One further makes the assumption that the scalar field is homogeneous, at least on a scale comparable to H^{-1}, and initially displaced by the global, zero-energy minimum of its self-interacting potential $V(\phi)$. At first, one neglects the quantum fluctuations in the scalar field, and only considers its classical evolution. The energy momentum tensor for the field is

$$T_{\alpha\beta} = \partial_\alpha \phi \partial_\beta \phi - \frac{1}{2} g_{\alpha\beta} \partial_\gamma \phi \partial^\gamma \phi + g_{\alpha\beta} V(\phi) , \tag{6.1}$$

and given that ϕ is homogeneous, it takes the form of a perfect fluid, with

$$\rho = \frac{1}{2}\dot{\phi}^2 + V(\phi) , \tag{6.2}$$

$$p = \frac{1}{2}\dot{\phi}^2 - V(\phi) . \tag{6.3}$$

The evolution equations for an expanding universe containing a homogeneous scalar field are obtained by substituting the above expressions for the energy and the pressure in the Friedmann equations (1.68), (1.66) (setting the curvature and the cosmological constant to zero):

$$3H^2 = V(\phi) + \frac{1}{2}\dot{\phi}^2 , \tag{6.4}$$

$$\ddot{\phi} + 3H\dot{\phi} = -V'(\phi) . \tag{6.5}$$

The last equation is analogous to the equation of a particle rolling down a hill, with friction term $3H\dot{\phi}$ given by the expansion of the universe. From Raychaudhuri's equation (1.67) one deduces that the condition for having an inflationary phase is

$$\ddot{a} > 0 \quad \longleftrightarrow \quad \rho + 3p < 0 \quad \longleftrightarrow \quad V(\phi) > \dot{\phi}^2 . \tag{6.6}$$

so that the potential energy of the field must dominate the kinetic energy. This is possible provided that the potential is flat enough, so that the scalar field is expected to roll slowly toward the minimum of the potential. This is the "slow roll" regime of the field dynamics. Once the minimum is reached, the inflationary phase terminates, and the field undergoes rapid oscillations, entering the "reheating" phase. In the following analysis we will only need to consider a simplified picture in which the field is in the slow roll regime. We will ignore the reheating phase, assuming that inflation ends with the end of slow roll, and the transition to the radiation dominated era is instantaneous.

The *slow roll approximation* consists in neglecting the kinetic energy term and the acceleration $\ddot{\phi}$, so that the system of equations (6.4-6.5) takes the simpler form

$$3H^2 \simeq V(\phi)\,, \tag{6.7}$$

$$3H\dot{\phi} \simeq -V'(\phi)\,. \tag{6.8}$$

Note that dropping the kinetic energy term in Eq. (6.4) can follow from the requirement of having an inflationary phase, while dropping the acceleration term in Eq. (6.5) is an additional demand of the slow roll approximation: one assumes that the acceleration due to the slope of the potential is balanced by the friction due to the expansion of the universe. The consistency condition for neglecting the kinetic energy term with respect to the potential can be translated into a condition on the first derivative of the potential [151]: using (6.7-6.8), one finds $V'/V < \sqrt{6}$. Equivalently, the consistency condition for neglecting the acceleration term with respect to the first derivative of the potential can be stated as $V''/V < 3$. These two conditions are necessary for the slow roll approximation of the field dynamics, and when they are violated, the slow roll phase terminates. In the context of the slow roll approximation, one normally defines a hierarchy of *slow roll parameters*

$$\epsilon \equiv \frac{1}{2}\left(\frac{V'}{V}\right)^2, \qquad \eta \equiv \frac{V''}{V}, \qquad \xi^2 \equiv \frac{V'V'''}{V^2}, \tag{6.9}$$

where the first measures the slope of the potential and the second the curvature, and the following ones are related to higher order derivatives. The condition that the potential is flat requires ϵ, $|\eta| < 1$, and so on.

The inflationary phase should last long enough to solve the size/flatness/entropy problem and the horizon problem. The amount of inflation is usually specified by the *number of e-folds* N, given by

$$N = \ln\left(\frac{a(t_{\rm end})}{a(t_{\rm in})}\right) = \int_{t_{\rm in}}^{t_{\rm end}} H(t)dt \simeq -\int_{\phi_{\rm in}}^{\phi_{\rm end}} \frac{V}{V'}d\phi\,, \tag{6.10}$$

where the last inequality holds in the context of the slow roll approximation. From this definition, one sees that evaluating the amount of inflation does not require the solution of the equations of motion. At first order in the slow roll approximation, one can rewrite $dN/d\phi \simeq -(2\epsilon)^{-1/2}$.

6.2 Density perturbations and gravitational waves

In chapter 3, we have assumed the presence of initial fluctuations in the FRW metric on all scales: inflation provides the means to produce these fluctuations. The initial fluctuations are causally generated, on scales well inside the Hubble radius; therefore, a first requirement of an inflationary model is that the observable universe is within it at the beginning of inflation. However, since the Hubble radius is nearly constant during inflation, at some point a given scale will cross outside it. Before dealing with the mechanism of creation of the fluctuations, we evaluate here the epoch of horizon-crossing [150]. For a given comoving scale k_*, this happens when $k_* = a(t_*)H(t_*)$; one has therefore

$$\frac{k_*}{a_0 H_0} = \frac{a_*}{a_{\rm end}}\frac{a_{\rm end}}{a_{\rm reh}}\frac{a_{\rm reh}}{a_{\rm eq}}\frac{a_{\rm eq}}{a_0}\frac{H_*}{H_0}\,, \tag{6.11}$$

where we have indicated the relevant stages of the evolution of the universe. We want to rewrite this expression in terms of energy densities. We use the relations $3H^2 = \rho$ and $\rho^0_{\rm rad} = \rho(t_{\rm eq})a^4(t_{\rm eq})$; we also assume matter domination between the end of inflation and the reheating phase, and making use of definition (6.10), we finally have

$$\frac{k_*}{a_0 H_0} = e^{-N_*}\left(\frac{\rho_{\rm reh}}{\rho_{\rm end}}\right)^{\frac{1}{3}}\left(\frac{\rho^0_{\rm rad}}{\rho_{\rm reh}}\right)^{\frac{1}{4}}\left(\frac{\rho_*}{\rho_0}\right)^{\frac{1}{2}}. \tag{6.12}$$

Considering that $\rho \simeq V$ during slow roll, it follows that the number of e-folds from the end of inflation back to when the scale crossed the horizon is given by

$$N_* = 62 - \ln \frac{k_*}{a_0 H_0} - \ln \frac{10^{16}\ \text{GeV}}{V_{\text{end}}^{1/4}} - \frac{1}{3} \ln \frac{V_{\text{end}}^{1/4}}{\rho_{\text{reh}}^{1/4}}\,, \tag{6.13}$$

where the normalisation 10^{16} GeV is chosen because it is the energy scale of inflation calculated from the COBE measurement (as will appear later on). The biggest scale observable is the horizon $2H_0^{-1} \simeq 6000$ Mpc, and a scale of 1 Mpc crossed outside the horizon about 9 e-folds afterwards. If one assumes that reheating is prompt, one can conclude that the observable universe leaves the horizon 50 to 60 e-folds before the end of inflation. Therefore, inflation has to last at least 60 e-folds in order to solve the horizon problem. Since the scale leaving the horizon at a given epoch is directly related to the number of e-folds, using Eqs. (6.10) and (6.13) one can also relate each scale with the corresponding value the inflaton field had at the time of horizon-crossing. At first order in slow roll, $d\phi/d\ln k \simeq \sqrt{2\epsilon}$.

We now revise briefly the mechanism of creation of the primordial fluctuations. A spectrum of adiabatic density perturbations arises from the vacuum fluctuations of the inflaton field. In the context of the slow roll approximation, one can neglect the back reaction of the metric perturbation on the scalar field[1]. The evolution equation for the Fourier component of the field perturbation can be obtained perturbing Eq. (6.5),

$$\delta\ddot{\phi}_{\mathbf{k}} + 3H\delta\dot{\phi}_{\mathbf{k}} + \left[\left(\frac{k}{a}\right)^2 + V''\right]\delta\phi_{\mathbf{k}} = 0\,. \tag{6.14}$$

Since in the slow roll approximation the potential is almost flat, one can drop V'', until at least a few Hubble times after horizon-exit: the slow roll condition on the second derivative of the potential takes the form $V'' < H^2$. Well before horizon-exit, the wavenumber $k/a \gg H$, so one can assume flat space-time and quantise the field $\delta\phi_{\mathbf{k}}$ in the conventional way. The fundamental assumption one has to make in this picture is that the inflaton field is in the vacuum state. Without going in the details of the calculation, we just state that the vacuum expectation value a few Hubble times after horizon-crossing, when the vacuum fluctuations

[1] At linear order, including the metric perturbation would add to equation (6.14) a term $(\delta\Box)\bar{\phi}$ with $\Box = (-g)^{-1/2}\partial_\alpha(-g)^{1/2}g^{\alpha\beta}\partial_\beta$. The background field is position-independent, and time-independent in the limit in which the slow roll approximation becomes exact: in this limit, the effect of the metric perturbation would exactly vanish. Ignoring the metric perturbation if the field is sufficiently slowly varying gives an error of the same order of the slow roll approximation [150].

can be regarded as classical, is given by $\langle|\delta\phi_{\mathbf{k}}|^2\rangle = H^2/(2k^3)$; this leads to the power spectrum $\mathcal{P}_\phi(k) = (H_*/2\pi)^2$. Since the Hubble constant is slowly varying, the spectrum is evaluated at the epoch of horizon-crossing, denoted by H_*. Given this result, one still has to relate the field perturbation to the metric perturbation; what one is ultimately interested in, is the power spectrum of the curvature perturbation generated by the scalar field: $\mathcal{R} = (H/\dot{\phi})\delta\phi$, where this expression is valid in linear perturbation theory, independently of slow roll [150]. One has that $\mathcal{P}_{\mathcal{R}}^{1/2} = (H/\dot{\phi})\mathcal{P}_\phi^{1/2}$, so that the power spectrum a few Hubble times after horizon-exit is given by

$$\mathcal{P}_{\mathcal{R}} = \left(\frac{H_*^2}{2\pi\dot{\phi}_*}\right)^2 \simeq \frac{1}{24\pi^2}\frac{V_*}{\epsilon_*}, \tag{6.15}$$

where for the second equality we have used the slow roll equations (6.7), (6.8), and the first of definitions (6.9). The important point is that the curvature perturbation (and therefore its power spectrum) is time-independent while k is well outside the horizon. Therefore, the amplitude of the observable density perturbation, when the relevant scales have entered back the horizon long after inflation, is still related to the properties of the inflaton potential at the time the scales crossed outside the horizon during inflation. The CMB temperature anisotropy observed by the COBE satellite can be used to determine the value of the primordial spectrum on a scale corresponding roughly to the horizon today, provided that the density perturbation is adiabatic and dominates the anisotropy. The measurement gives $\delta_H(k = a_0H_0) \simeq 2\times10^{-5}$; in the case of a universe without cosmological constant, one has that $\delta_H = (2/5)\mathcal{P}_{\mathcal{R}}^{1/2}$ [149]. After multiplying the above expression for the spectrum by $m_{\rm Pl}^2/8\pi$ in order to get the correct dimensions, one obtains the "energy scale of inflation"

$$V^{1/4} \simeq \epsilon^{1/4}10^{16}\ \mathrm{GeV}, \tag{6.16}$$

which in particular gives the maximum value of the potential when the observable universe leaves the horizon. The standard approximation used to describe the spectrum (6.15) is the power law approximation, which is usually valid because only a limited range of scales are observable. The spectral index is defined as

$$n_S - 1 = \frac{d\ln\mathcal{P}_{\mathcal{R}}}{d\ln k}. \tag{6.17}$$

Inflation also generates a background of gravitational waves. The evolution equation for gravitational waves stated in chapter 3 is the same as (6.14) when the mass term V'' is set to zero. It follows that each mode of the gravitational wave can be treated as a massless scalar field, $\psi = (m_{\rm Pl}^2/16\pi)^2 h_{+,\times}$, and the spectrum is given again by

$$\mathcal{P}_G = 8\left(\frac{H_*}{2\pi}\right)^2 \simeq \frac{2}{3\pi^2}V_* \,. \tag{6.18}$$

In this case also, we define the spectral index

$$n_T = \frac{d\ln\mathcal{P}_G}{d\ln k} \,. \tag{6.19}$$

We have defined each spectrum by its amplitude and spectral index, however, the overall amplitude is a free parameter, determined by the normalisation of the potential. The relevant observable quantity is the relative amplitude of the two spectra; this is normally defined in terms of the ratio between the tensor and scalar CMB spectra, $r = C_\ell^T/C_\ell^S$. One can demonstrate that this quantity is related to the tensor spectral index through a factor $r = -\kappa n_T$, which depends on the given cosmology [152, 153], in particular on the value of Ω_Λ and Ω_M. In the following analysis we have used the value $\kappa = 5$, corresponding to $\Omega_\Lambda = 0.65$ and $\Omega_M = 0.35$ [154].

The form of the curvature and gravity waves spectra given above is valid at first order in the slow roll expansion, and one can see that the tensor power spectrum is connected to the potential itself, while the curvature power spectrum involves also the first derivative of the potential, and therefore the first slow roll parameter ϵ. Each observable quantity can be associated with a slow roll parameter; in particular, every time one takes a derivative in $d\ln k$, one goes one step further in the slow roll expansion. In fact, using the lowest order relation $d\phi/d\ln k = \sqrt{2\epsilon}$, one has that the spectral indices can be written as

$$\begin{aligned} n_S - 1 &= 2\eta - 6\epsilon + O(\xi^2)\,, && (6.20)\\ n_T &= -\frac{r}{\kappa} = -2\epsilon + O(\xi^2)\,, && (6.21) \end{aligned}$$

where $\xi^2 \equiv \frac{V'V'''}{V^2}$, and we neglect it here to remain consistent at the lowest order in slow roll. However, if we want to parametrise the running of the spectral index $\partial_{\ln k} \equiv \frac{dn_S}{d\ln k}$, we have

$$\partial_{\ln k} = -2\xi^2 - 24\epsilon^2 + 16\epsilon\eta + O(\sigma^3)\,, \tag{6.22}$$

with the definition

$$\sigma^3 = \frac{V'^2 V''''}{V^3}\,.$$

The first two expressions (6.20), (6.21) are truncated at order ξ^2, ignoring errors that are quadratic in ϵ and η, and requiring that $|\xi^2| \ll \max(\epsilon, |\eta|)$ [149]. In order to derive the third expression (6.22), we need to take the derivative of n_S, and every time we take the derivative of a slow roll parameter we get a quantity which is one order higher in slow roll; therefore, we need to introduce the new parameter $|\sigma^3| \ll \max(\epsilon^2, \epsilon|\eta|, |\xi^2|)$.

6.3 The flow equations

From the set of equations (6.20-6.22), using the recursive form of the slow roll expansion, one can derive a system of differential equations which describes the evolution of n_S and r as the inflaton rolls down its potential. Taking $\frac{d\phi}{d\ln k} = \sqrt{2\epsilon}$, one gets [155,156]

$$\frac{dn_S}{d\ln k} = 4\frac{r}{\kappa}\left[(n_S - 1) + \frac{3}{2}\frac{r}{\kappa}\right] - 2\xi^2\,, \tag{6.23}$$

$$\frac{dn_T}{d\ln k} = \frac{r}{\kappa}\left[(n_S - 1) + \frac{r}{\kappa}\right]. \tag{6.24}$$

These equations were first analysed by Hoffman and Turner in [154], and later on by Hansen and Kunz in [157]; in order to close the system, one has to assume that the parameter ξ^2, corresponding to the third derivative of the potential, is constant.

In our attempt to find a constraint on the quantity V''''/V, we will make the assumption that either σ^3 or V''''/V is constant (see below), so we will not need to require a better accuracy than the one given in the set of equations (6.20-6.22), and in the corresponding first order relation $\frac{d\phi}{d\ln k} = \sqrt{2\epsilon}$. The second derivative of the scalar spectral index takes the form

$$\frac{d^2 n_S}{d\ln k^2} = 2\sigma^3 + 2\xi^2\eta - 24\xi^2\epsilon - 192\epsilon^3 + 192\epsilon^2\eta - 32\epsilon\eta^2 + O(\tau)\,. \tag{6.25}$$

with $\tau \propto \frac{d\sigma^3}{d\ln k}$, which in our approximation is negligible or zero. By using the definitions in

Eqs. (6.20-6.22), we get the new system of flow equations

$$\begin{aligned}
\frac{dn_S}{dN} &= -\partial_{\ln k} && (6.26)\\
\frac{dr}{dN} &= -\frac{r}{\kappa}\left[(n_S-1)+\frac{r}{\kappa}\right] && (6.27)\\
\frac{d\partial_{\ln k}}{dN} &= -2\sigma^3 - \frac{1}{2}\partial_{\ln k}\left(9\frac{r}{\kappa}-(n_S-1)\right)+ && (6.28)\\
& \quad 2(n_S-1)^2\frac{r}{\kappa}+15(n_S-1)\left(\frac{r}{\kappa}\right)^2+15\left(\frac{r}{\kappa}\right)^3,
\end{aligned}$$

where we have used the first order expression $d\ln k = -dN$, consistent with our assumptions in Eqs. (6.20-6.22). The parameter σ^3 is related to the fourth derivative of the potential trough $\sigma^3 = rV''''/5V$. In order to close this set of equations, we need to assume that either σ^3 or V''''/V can be treated as a constant throughout inflation. The choice between these two assumptions is arbitrary, but will affect the behaviour of the flow in the parameter space.

The observational bounds which we use are the ones obtained in [158] (for similar results see [159–162])

$$0.8 < n_S < 1.0\,, \qquad (6.29)$$

$$0 < r < 0.3\,, \qquad (6.30)$$

$$-0.05 < \partial_{\ln k} < 0.02\,. \qquad (6.31)$$

Such observations can be inverted to give constraints on the inflationary potential and its derivatives. As already showed, the COBE experiment [163] gave the first constraint on the first derivative of the inflaton potential,

$$\frac{V^{3/2}}{m_{\rm Pl}^3 V'} \simeq 0.4\times10^{-5}\,, \qquad (6.32)$$

and the bounds above, Eqs. (6.29-6.31), provide constraints on the first and second derivatives of the potential: $|V'/V| < 0.25$, $|V''/V| < 0.1$. Hansen and Kunz [157] found $V'''/V > -0.2$.

We study the flow in the three dimensional parameter space $(n_S, r, \partial_{\ln k})$, and by also making use of the observational constraints (6.29-6.31), we will be able to induce a limit on the fourth derivative of the potential, V''''/V.

6.4 Discussion

As discussed before, in slow roll inflation, the scales relevant for structure formation exited the horizon roughly 50 e-folds before the end of inflation, and it is at this time that the experimental bounds on the observable parameters in Eqs. (6.29-6.31) apply. We are going to consider only the case of single field inflation, which will end when the slow roll conditions $V'/V < \sqrt{6}$ and $V''/V < 3$ are violated. In terms of the value of the parameters n_S and r, these conditions translate into the slow roll "validity-region" [4, 154]

$$\frac{r}{\kappa} < 6 \quad \text{or} \quad \left|(n_S - 1) + 3\frac{r}{\kappa}\right| < 6\,. \tag{6.33}$$

Using the evolution equations (6.26-6.28), we let all the points of the boundary (6.33) flow back 50 e-folds (we take the value $\kappa = 5$). This is done for different fixed values of the parameter σ^3 (or V''''/V). We can then induce a constraint on this latter by demanding that, at $N = 50$, at least some of the points of the boundary land inside that region in the $(n_S, r, \partial_{\ln k})$ space which is allowed by observations, Eqs. (6.29-6.31). If no points land inside the space allowed by observations, then we can deduce that we took an unrealistic value for the parameter σ^3 or V''''/V.

To follow the flow backward in time, the slow roll conditions (6.33) provide us with the initial values for the two variables n_S and r. As initial condition for the variable $\partial_{\ln k}$ we will take Eq. (6.23), with the extra assumption that $\xi^2 = 0$. We verified that the position of the points after 50 e-fold is virtually independent on the initial conditions chosen, and therefore this assumption does not affect our results. Moreover, with these initial conditions and in the case $\sigma^3 = 0$, all the points of the boundary flow into the validity region. For other cases (e.g. $\sigma^3 \neq 0$) we exclude numerically the possibility that a point could first flow outside this validity region and then later re-enter the region.

In the case where σ^3 is treated as a constant during the last 50 e-folds, we find that for $\sigma^3 < -3.5 \times 10^{-4}$ there are no final points in agreement with observations. This is easily seen in Fig. 6.1, in which the dashed line which corresponds to the value $\sigma^3 = -3 \times 10^{-4}$ is about to exit from the region given by the observational limits, Eq. (6.29). On the other hand, we are not able to induce any limit on the parameter σ^3 in the case $\sigma^3 > 0$, because for sufficiently small value of r there will always be points in the allowed region.

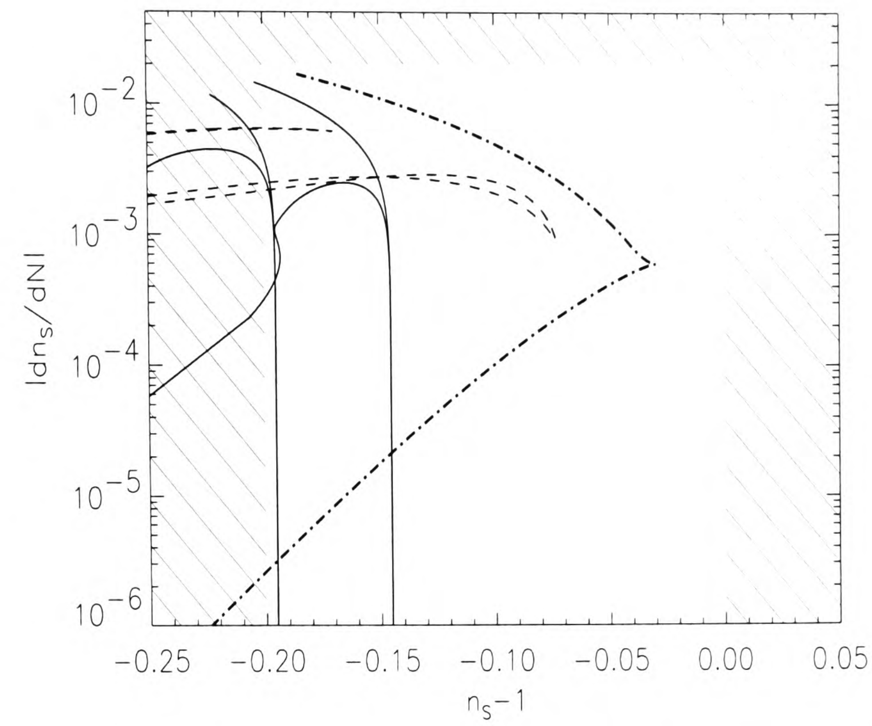

Figure 6.1: The slow roll validity region flown back 50 e-folds, for different fixed values of the parameters σ^3 and V''''/V. The dot-dashed line shows the case $\sigma^3 = 0$ (identical to $V''''/V = 0$); the two dashed lines show, from right to left, the two cases $\sigma^3 = -10^{-4}$ and $\sigma^3 = -3 \times 10^{-4}$; the solid lines instead represent the case in which V''''/V is kept constant, and the values are, again from right to left, $V''''/V = -10^{-2}$ and $V''''/V = -1.8 \times 10^{-2}$. The hatched region is excluded by observations. It is clear from the figure, that a slightly larger negative value of the parameter σ^3 (or V''''/V) will not be acceptable because it doesn't satisfy the observational constraint.

If one instead assumes that V''''/V can be treated as a constant during inflation, the curve which represent the evolved validity region exceeds the observational boundary if $V''''/V < -0.02$. Also in this case there will always be acceptable points if V''''/V takes positive values, however, also in this case only for very small r.

In conclusion, we have shown that the combination of the slow roll equations (6.26-6.28) and the observational results (6.29-6.31) can lead to a lower bound $V''''/V > -0.02$, for single field models which end inflation by breaking the slow roll conditions (6.33). With a larger number of e-folds this bound becomes slightly stronger.

As already mentioned, the inflationary flow equations (6.23-6.24) were first introduced by Hoffman and Turner [154]. Hansen and Kunz used them to place a constraint on the third derivative of the potential [157]; the work presented here is the direct continuation of their work, and uses the same procedure, with the difference of adding to consideration the equation for the evolution of the running of the scalar spectral index. Kinney [164] generalised the form of the flow equations to arbitrary order in slow roll, using the version

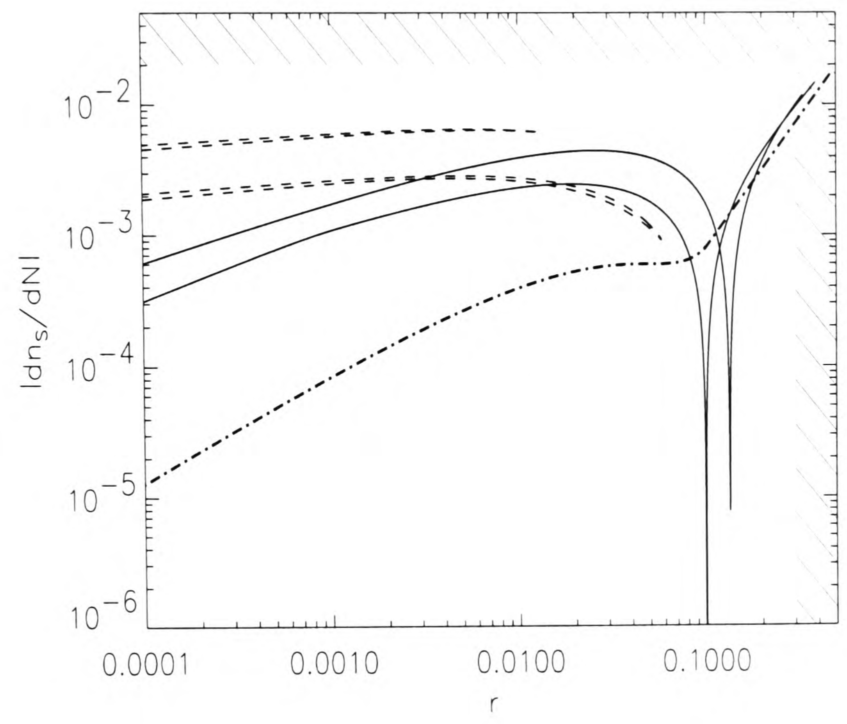

Figure 6.2: Same as Fig. 6.1, but for r and dn_S/dN.

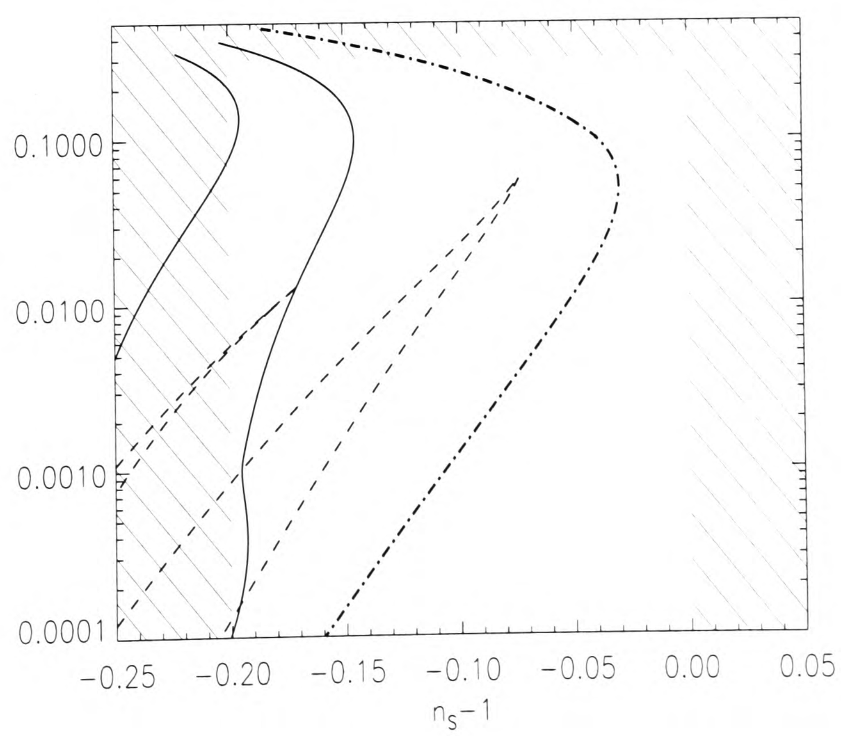

Figure 6.3: Same as Fig. 6.1, but for r and n_S.

of the slow roll expansion based on the Hamilton-Jacobi formulation of inflation [165]. In this case, one defines the slow roll parameters as derivatives of the Hubble constant instead of the inflationary potential. In terms of these parameters, one can write down a hierarchy of flow equations which is exact, beyond the slow roll approximation. Kinney used it as a way to reconstruct the inflaton potential starting from observations [166, 167]. However, the legitimacy of using the results of Kinney's flow equations to reconstruct the potential has been contested by Liddle [168]: he argued that the flow equations given in terms of the Hubble slow roll parameters do not relate at all with the inflationary dynamics. This questions the possibility of connecting the outcome of the flow equations with specific models of inflation. It is not yet clear, however, if the results of [168] also apply to the flow equations written in terms of the inflationary observables n_S and r, first introduced by Hoffman and Turner. The reason being that the connection between the spectral indices and the slow roll parameters makes use of the dynamical equation (6.8), through the expression for the spectrum (6.15). Further investigation is still needed to solve this matter.

Chapter 7

Conclusions

The research presented in this thesis is based on four separate works. The thesis contains a detailed exposition of each work, together with a review of the basic concepts and theoretical framework pertaining them.

A great part of the thesis deals with cosmic magnetic fields. In the second chapter we have attempted to give a comprehensive presentation of the characteristics of such fields, and to outline the principal reasons that motivate their study. We have briefly summarised the experimental evidence for the presence of magnetic fields in astrophysical objects: galaxies, clusters of galaxies and high redshift objects. The main point is the appearance, in all these different structures, of magnetic fields with intensity of the same order of magnitude: about $0.1 - 10\,\mu$G. The problem of the origin of these fields is to date unsolved; the current picture is that they come from seed fields created before the formation of the structures in which they are observed, and subsequently amplified during the gravitational collapse. In the last twenty years, there have been many proposals on different methods to generate the seeds for the observed magnetic fields. Section 2.3 contains a list of them, principally of the primordial ones, being of more relevance for our research. Without going into the details of each mechanism, the purpose of this summary is to show that the primordial generation mechanisms often rely on interesting but conjectural new ideas in theoretical physics; consequently, the resulting amplitudes for the seed fields are frequently model dependent. As a matter of fact, to date there is no preferred model for the generation of the primordial seed fields, although the general claim of each of the proposed mechanisms is that they give rise to seeds which are strong enough to be at the origin of the fields observed in galaxies and clusters.

Causal generation mechanisms are a bit more predictive than inflationary ones; nevertheless, they produce seeds at very small scales, if compared to those at which the magnetic fields are observed today: at best, at the scale of the horizon at the epoch of creation, occurring during a primordial phase transition. Therefore, a fundamental issue is how to extrapolate the correct amplitudes of the causally generated fields at the required galactic and cluster scales. Connected to this, is the analysis of the time evolution of the magnetic seeds subsequently to their generation, particularly if they are characterised by non-zero helicity. We have shown that, as a consequence of the very high conductivity of the universe, the field is frozen in the primordial fluid, and on large scales simply redshifts with the expansion. At smaller scales, one distinguish two cases: later than the e^+e^- annihilation, the field simply dissipates energy because of radiation viscosity; prior to the e^+e^- annihilation the fluid is turbulent, and if the field is characterised by a helical component then a process of "inverse cascade" may occur, that can enhance the coherence length of the field. However, as pointed out in section 2.4.4, the time evolution of primordial helical fields remains an open issue, and no real agreement has been reached in the literature between theoretical results and numerical simulations. Assuming flux freezing for the non-helical component, and a specific model for the evolution of the coherence length of the helical component, in section 2.5.2 we have worked out the correct way of extrapolating the amplitude of causally generated fields at galactic and cluster scales [18]. This work was motivated by the fact that many authors used a too optimistic scaling law, first proposed by Hogan [47]; the use of this scaling law in some cases led to the conclusion that the proposed mechanism gave an acceptable amplitude for seeding astrophysical magnetic fields. Starting from the property of divergence-less of a magnetic field, we have derived the correct scaling law, and found that *a magnetic field which has evolved on large scales simply via flux conservation from its creation at the electroweak phase transition until today is not sufficient to have seeded the large scale magnetic fields observed in clusters, even if it underwent dynamo amplification. The same conclusion can be drawn for the helical component, if it evolves according to the specific model assumed.* This work complements the result of a previous one [80], which found the strongest constraints up to date on the amplitude of a primordial magnetic field, applying also to the case of non-causally-generated seeds.

The fact that the intensity of a primordial magnetic field must obey very stringent constraints, as found in references [18,80], reflects on the amplitude of the signal it can induce on the CMB. Section 3.3 presents a summary of some of the effects a primordial magnetic field can have on CMB temperature anisotropies and polarisation: they have been extensively studied in the last decade, considering magnetic fields with vanishing helicity. However, the presence of a helical component in the magnetic field spectrum can have interesting consequences on the CMB signal, as first pointed out by Pogosian and collaborators [93]. Indeed, in chapter 4 we have analysed the effect of a helical magnetic field on the tensor mode temperature anisotropies and polarisation, and found that it induces parity-odd cross-correlations in the polarisation signal [92]. The gravitational waves sourced by the helical component of the magnetic field show an asymmetry in the amplitude of the two polarisation states: the difference between the expectation values of the right- versus left-handed polarisation is non-zero, and acts as a source for parity-odd polarisation spectra in the CMB. We have evaluated analytically the CMB spectra for the temperature, E and B polarisations, and parity-even as well as parity-odd cross-correlations. The choice of evaluating the spectra analytically forced us to make some assumptions: we have postulated instant recombination, and our spectra are valid only for $\ell < 60$. However, these approximations are reasonable, given that we are analysing the tensor mode signal. Moreover, all the parameters in the analysis are left free, and we are able to show how the CMB spectra vary as a function of the intensity, spectral index, and upper cutoff scale of the stochastic field. Our analysis reached the conclusion that *only helical magnetic fields with a spectrum close to scale-invariant lead to observable parity-violating terms in the CMB polarisation power spectra: Θ-B and E-B cross-correlations.* This is connected to the fact that primordial magnetic fields with scale-invariant spectra, generated at the epoch of inflation, can in principle have amplitudes as high as 10^{-9} Gauss: the limits of reference [80] are the least restrictive in this case.

The upper bounds on the intensity of a primordial magnetic field can be used also to place a constraint on a hypothetical electric charge asymmetry in the universe. In chapter 5, we have postulated that the universe possesses an overall non-zero electric charge, arising from an unspecified mechanism which breaks charge conservation (and therefore gauge invariance) in the early phases of the universe's evolution. Because of the fact that the universe is a very good conductor, the presence of a non-zero charge in the cosmic fluid manifests itself through the generation of a magnetic field and vorticity in the metric: the electric field can be set to zero in the context of the magnetohydrodynamic limit. Magnetic fields and vorticity are both sources of CMB anisotropies, and their amplitude can be quite severely constrained simply using the results from the COBE satellite measurement. From the upper limits on the amplitude of the magnetic field and the vorticity, we have derived an upper limit on the charge density of the universe. We have analysed two different configurations for the charge: uniformly and stochastically distributed; in the second case, the limit depends on the spectral index of the induced magnetic field. We stress the importance of the fact that we derived a cosmological constraint on the charge density, which can be significant on its own about the neutrality of the universe, despite charge conservation being well established on Earth. The cosmological limit on the charge density can be translated into upper bounds on the charge of different particles, if one postulates that the overall charge imbalance is due only to a single particle species at a time. We have assumed that the charge can be due to charged photons, neutrinos, dark matter particles, or to a difference between the charges of the proton and the electron. *From the bound derived in the case of a uniformly distributed charge, we obtain upper limits on the charge of single particles which are orders of magnitude stronger than the ones given by laboratory experiments or astrophysical observations. If the charge is distributed stochastically, the upper bounds are still interesting in the case in which the charge is generated at a primordial phase transition.*

The last work presented in this thesis, in chapter 6, concerns the theory of inflation. Inflation provides the creation of scalar and tensor perturbations in the metric; the scalar ones may be at the origin of the formation of large scale structure, and the tensor ones give rise to a stochastic background of gravitational waves. It is possible to extract information about the features of the spectra of these primordial perturbations from observations of the CMB anisotropies. The observable variables are the power spectral indices of the density and tensor perturbations, and the overall amplitude of these; each observable quantity can be related to the parameters defined in the slow roll expansion. The evolution of the observables during inflation can be followed by the flow-equations. These were first analysed in [154], and were used in [157] to obtain a constraint on the value of the third derivative of the inflaton potential, by combining their results with the observational bounds from CMB observations. The work presented in chapter 6 is the direct continuation of the one of reference [157]: we show that *a combination of the higher order flow-equations and the observational bound on* *the inflationary parameters allows one to put a non-trivial constraint on the fourth derivative of the inflaton potential.*

Appendix A

The magnetic source for gravity waves

This appendix refers to the work presented in chapter 4. We give here the details on how to compute the gravity waves source functions $f(k)$ and $g(k)$. The isotropic tensor spectrum in the case of a magnetic field without helicity term is derived in [107]. Here we concentrate on the source terms which account for the helical part of the magnetic field spectrum. By acting with the tensor projector on (4.5), we find expressions (4.16) and (4.17) for the symmetric and helical parts of the source spectrum. Taking into account that the angle $\beta = \hat{\mathbf{k}} \cdot (\widehat{\mathbf{k}-\mathbf{p}}) = \frac{k-p\gamma}{\sqrt{k^2-2kp\gamma+p^2}}$, we can rewrite the two expressions which contain $A(k)$ in the form

$$f^A(k) = \frac{8}{(4\pi)^5} \int d^3p A(p) A(|\mathbf{k}-\mathbf{p}|) \frac{\gamma \cdot (k-p\gamma)}{\sqrt{k^2-2kp\gamma+p^2}} \tag{A.1}$$

$$\begin{aligned} g(k) &= \frac{4}{(4\pi)^5} \int d^3p \left[S(p) A(|\mathbf{k}-\mathbf{p}|) \frac{(k-p\gamma)(1+\gamma^2)}{\sqrt{k^2-2kp\gamma+p^2}} \right. \\ &\left. + A(p) S(|\mathbf{k}-\mathbf{p}|) \left(2\gamma - \frac{\gamma p^2 (1-\gamma^2)}{k^2-2kp\gamma+p^2} \right) \right] . \end{aligned} \tag{A.2}$$

The contribution to $f(k)$ from $S(k)$ alone is computed in reference [107]. There one finds

$$f^S(k) = \frac{2}{(4\pi)^5} \int d^3p S(p) S(|\mathbf{k}-\mathbf{p}|)(1+\gamma^2) \left(1 + \frac{(k-p\gamma)^2}{k^2-2kp\gamma+p^2} \right) . \tag{A.3}$$

We can now substitute the power law Ansatz (2.49), (2.50) for $S(k)$ and $A(k)$ in these expressions and try to calculate the integrals. The integration over $\gamma = \hat{\mathbf{k}} \cdot \hat{\mathbf{p}}$ is elementary, using

$$\int d\gamma \, (k^2 + p^2 - 2kp\gamma)^{\frac{\alpha}{2}} = -\frac{1}{kp(\alpha+2)}(k^2+p^2-2kp\gamma)^{\frac{\alpha+2}{2}} \tag{A.4}$$

$$\begin{aligned}\int d\gamma \, \gamma^m \, (k^2 + p^2 - 2kp\gamma)^{\frac{\alpha}{2}} &= -\frac{\gamma^m}{kp(\alpha+2)}(k^2+p^2-2kp\gamma)^{\frac{\alpha+2}{2}} \\ &\quad + \frac{m}{kp(\alpha+2)} \int d\gamma \, \gamma^{m-1} \, (k^2+p^2-2kp\gamma)^{\frac{\alpha+2}{2}} \, .\end{aligned} \tag{A.5}$$

This last integration by parts has to be performed in the worst cases three times, reducing the power m of γ from 3 down to 0. Since we are integrating γ over the interval $[-1, 1]$, we get a series of $m+1$ terms of the form

$$\frac{(k+p)^{\alpha+2n} \pm |k-p|^{\alpha+2n}}{(k\,p)^n} \, , \tag{A.6}$$

with $n = 1, 2, ...(m+1)$. To evaluate the integral over p, we can expand these terms using the binomial decomposition $(1+x)^\alpha = 1 + \alpha x + \alpha(\alpha-1)x^2 + \cdots$. Since, in general, the value of the exponent α is not an integer, we need to truncate the series somewhere, which is well justified only if $x \ll 1$. To achieve this, we split the integral into two contributions, $\int_0^{k_D} = \int_0^k + \int_k^{k_D}$. In the first term $p/k < 1$, while in the second $k/p < 1$, which allows us to approximate Eq. (A.6) truncating the binomial series at the second term,

$$(k+p)^\alpha - |k-p|^\alpha \simeq \begin{cases} 2\alpha k^{\alpha-1} p + \frac{1}{3}\alpha(\alpha-1)(\alpha-2)k^{\alpha-3}p^3 & p < k \\ 2\alpha p^{\alpha-1} k + \frac{1}{3}\alpha(\alpha-1)(\alpha-2)p^{\alpha-3}k^3 & p > k \end{cases} \tag{A.7}$$

and

$$(k+p)^\alpha + |k-p|^\alpha \simeq \begin{cases} 2k^\alpha + \alpha(\alpha-1)k^{\alpha-2}p^2 & p < k \\ 2p^\alpha + \alpha(\alpha-1)p^{\alpha-2}k^2 & p > k \, . \end{cases} \tag{A.8}$$

We then perform the integration over p. For each contribution we keep only the terms which, depending on the value of the spectral index, may dominate the result. So, we finally obtain, for $k < k_D$

$$\begin{aligned} f(k) &\simeq \frac{\lambda^3}{8(2n_S+3)}\left[\frac{B_\lambda^2}{\Gamma\left(\frac{n_S+3}{2}\right)}\right]^2\left((\lambda k)_D^{2n_S+3}+\frac{n_S}{n_S+3}(\lambda k)^{2n_S+3}\right)- \\ &\quad -\frac{\lambda^3}{6(2n_A+3)}\left[\frac{\mathcal{B}_\lambda^2}{\Gamma\left(\frac{n_A+4}{2}\right)}\right]^2\left((\lambda k)_D^{2n_A+3}+\frac{n_A-1}{n_A+4}(\lambda k)^{2n_A+3}\right) \qquad \text{(A.9)} \\ &= \mathcal{A}_S\lambda^{2n_S+3}\left(k_D^{2n_S+3}+\frac{n_S}{n_S+3}k^{2n_S+3}\right)-\mathcal{A}_A\lambda^{2n_A+3}\left(k_D^{2n_A+3}+\frac{n_A-1}{n_A+4}k^{2n_A+3}\right) \\ g(k) &\simeq \frac{\lambda^4 k}{3(n_S+n_A+2)}\left[\frac{B_\lambda^2}{\Gamma\left(\frac{n_S+3}{2}\right)}\right]\left[\frac{\mathcal{B}_\lambda^2}{\Gamma\left(\frac{n_A+4}{2}\right)}\right]\left((\lambda k_D)^{n_S+n_A+2}+\frac{n_A-1}{n_S+3}(\lambda k)^{n_S+n_A+2}\right) \\ &= \mathcal{C}k\lambda\,(\lambda k_D)^{n_S+n_A+2}\left[1+\frac{n_A-1}{n_S+3}\left(\frac{k}{k_D}\right)^{n_S+n_A+2}\right], \qquad \text{(A.10)} \end{aligned}$$

where the coefficients are given by the magnetic field amplitudes at scale λ:

$$\mathcal{A}_S \simeq \frac{\lambda^3}{8(2n_S+3)}\left[\frac{B_\lambda^2}{\Gamma\left(\frac{n_S+3}{2}\right)}\right]^2 \qquad \text{(A.11)}$$

$$\mathcal{A}_A \simeq \frac{\lambda^3}{6(2n_A+3)}\left[\frac{\mathcal{B}_\lambda^2}{\Gamma\left(\frac{n_A+4}{2}\right)}\right]^2 \qquad \text{(A.12)}$$

$$\mathcal{C} \simeq \frac{\lambda^3}{3(n_S+n_A+2)}\left[\frac{B_\lambda^2}{\Gamma\left(\frac{n_S+3}{2}\right)}\right]\left[\frac{\mathcal{B}_\lambda^2}{\Gamma\left(\frac{n_A+4}{2}\right)}\right]. \qquad \text{(A.13)}$$

The singularities at n_S, $n_A = -3/2$ respectively and at $n_S + n_A = -2$ are removable.

Appendix B

Useful mathematical relations

As appendix A, this appendix also refers to the topic of chapter 4. We present here the mathematical tools used to evaluate the magnetic helicity induced CMB power spectra, given in sections 4.4 and 4.5.

B.1 Integrals of Bessel functions

In sections 4.4 and 4.5 we use approximate solutions for the three integrals

$$\int_{x_{\rm dec}}^{x_0} dx\, \frac{j_2(x)}{x} \frac{j_\ell(x_0-x)}{(x_0-x)^2}\,, \qquad \int_{x_{\rm dec}}^{x_0} dx\, \frac{j_2(x)}{x} \frac{j_\ell(x_0-x)}{(x_0-x)}\,, \qquad \int_{x_{\rm dec}}^{x_0} dx\, \frac{j_2(x)}{x} j_\ell(x_0-x)\,. \quad \text{(B.1)}$$

These integrals are solvable only by numerical method. However, the aim of this analysis is to give an approximate analytic result. In this appendix we therefore derive and test analytic approximations to the above integrals. To achieve this, we first modify them slightly, in order to make them solvable analytically. Then, we adjust the result obtained in this way by comparing it with the exact numerical integration.

Let us concentrate, as an example, on the first integral. We first perform a variable transform to $y = x_0 - x$. The integration boundaries then become 0 and $x_0 - x_{\rm dec}$. Below, we derive an approximation for

$$\int_0^{x_0} \frac{j_2(x_0-y)}{x_0-y} \frac{j_\ell(y)}{y^n} dy\,.$$

Since Bessel functions change on a scale $\Delta y \sim 1$, this approximation is good for the integrals in Eq. (B.1) if $x_{\rm dec} < 1$. In order to find the CMB spectra, after the integration over x in Eq. (B.1) we have to perform an integration over k. For ℓ fixed, this integral is either dominated by the contribution at $k\eta_0 = x_0 \sim \ell$ or at the upper cutoff, k_D. For the integrals which are dominated at $x_0 = k\eta_0 \sim \ell$, the inequality $x_{\rm dec} < 1$ is equivalent to $\ell \simeq x_0 \simeq 60x_{\rm dec} \lesssim 60$. In some cases, however, our integral over k is dominated at the upper cutoff k_D with $\eta_{\rm dec}k_D \gg 60$ and of course also $\eta_0 k_D \gg 60$. Since for $\ell \simeq 60$, the dominant contribution to the integral comes from $y \lesssim 60$, our inaccuracy of the boundary will not invalidate the approximation also for this case.

The approximation in the upper boundary of the integral, $x_0 - x_{\rm dec} \simeq x_0$ makes us miss the characteristic decay of fluctuations on angular scales corresponding to $\ell \gtrsim 60$.

To make the first integral in Eq. (B.1) solvable analytically, we now modify the powers of y and $x_0 - y$. Taking into account that the spherical Bessel function $j_\nu(x)$ has its maximum value at $x \simeq \nu$, we make the attempt:

$$
\begin{aligned}
\int_0^{x_0} dx\, \frac{j_2(x)}{x}\frac{j_\ell(x_0-x)}{(x_0-x)^2} &= \frac{\pi}{2}\int_0^{x_0} dx\, \frac{J_{5/2}(x)}{x^{3/2}}\frac{J_{\ell+\frac{1}{2}}(x_0-x)}{(x_0-x)^{5/2}} \\
&\simeq \frac{\pi}{2}\sqrt{\frac{2}{5\,\ell}}\int_0^{x_0} dx\, \frac{J_{5/2}(x_0-y)}{x_0-y}\frac{J_{\ell+\frac{1}{2}}(y)}{y^2}\,. && \text{(B.2)}\\
&\simeq \frac{\pi}{5}\sqrt{\frac{2}{5\,\ell}}\frac{J_{\ell+3}(x_0)}{x_0^2}\,. && \text{(B.3)}
\end{aligned}
$$

For the last equality, we have used 6.581.2 of [169],

$$
\begin{aligned}
\int_0^a dx\, \frac{J_p(x)}{x^{1-b}}\frac{J_q(a-x)}{a-x} &= \frac{2^b}{aq}\sum_{m=0}^{\infty}\frac{(-1)^m\,\Gamma(b+p+m)\,\Gamma(b+m)}{m!\,\Gamma(b)\,\Gamma(p+m+1)}(b+p+q+2m) \\
&\quad\times J_{b+p+q+2m}(a)\,, \qquad (\mathrm{Re}\,(b+p)>0,\ \mathrm{Re}\,q>0) \qquad \text{(B.4)}
\end{aligned}
$$

and the recurrence relation $J_{\nu-1}(x) + J_{\nu+1}(x) = \frac{2\nu}{x}J_\nu$ (9.1.27 of [103]), keeping only the highest order terms in ℓ. We can now compare this approximated analytic result with an exact numerical integration. Since the analytic result is again a Bessel function divided by a power law, it has a maximum at $x_0 \simeq \ell$, and its envelope has a power law decay for $x_0 > \ell$. This two characteristics are very well reproduced by the numerical result, which however decays somewhat faster; it turns out that a better approximation is

$$
\int_0^{x_0} dx\, \frac{j_2(x)}{x}\frac{j_\ell(x_0-x)}{(x_0-x)^2} \simeq \frac{1}{3}\sqrt{\frac{3\,\ell}{2}}\frac{J_{\ell+3}(x_0)}{x_0^3}\,. \qquad \text{(B.5)}
$$

To estimate the goodness of our approximation, let us now take into account the integration over k, as in Eq. (4.41). What we are finally interested in is (Eq. (4.48))

$$\int_0^{x_D} dx_0\, x_0^2 \,\frac{J_{\ell+3}^2(x_0)}{x_0^6}\left[1+\frac{n_A-1}{n_A+4}\left(\frac{x_0}{x_D}\right)^{2n_A+3}\right]. \tag{B.6}$$

As already discussed in chapter 4, this integral is always convergent and dominated by the contribution around $x_0 \simeq \ell$: we should therefore make sure that our approximation is good around that value. We have that for $\ell = 30$, our approximation underestimates the numerical result by about factor of two; for $\ell = 40$, the error reduces to 15%.

Fig. B.1 shows the numerical result for the integral in (B.5) (green, dotted line), together with its analytical approximation (the right hand side of Eq. (B.5), blue and long dashed) and a numerical evaluation of the same integral when $x_{\rm dec}$ is not set to zero (red, solid). For small values of ℓ (in the upper panel of Fig. B.1, $\ell = 50$), Eq. (B.5) is a good approximation in the region $x_0 \simeq \ell$. However, if $\ell > 60$ setting $x_{\rm dec} \to 0$ causes a large overestimation of the result. In the lower panel of Fig. B.1 it is shown that, for $\ell = 200$, the difference between the integral with lower bound 0 and the one with lower bound $x_{\rm dec}$ is more than a factor of ten. Consequently, as already stated before, we can rely on all our approximations only for $\ell \lesssim 60$.

We proceed now to evaluate integral (B.6). Since $x_D = k_D\eta_0 \gtrsim 10^6$, for $\ell \lesssim 60$, integral (B.6) can be calculated in the limit $x_D \to \infty$, using formula 6.574.2 of [169]:

$$\begin{aligned}\int_0^{\infty} dx\, J_p(x) J_q(x) x^{-b} &= \frac{\Gamma(b)\Gamma\left(\frac{p+q-b+1}{2}\right)}{2^b\Gamma\left(\frac{-p+q+b+1}{2}\right)\Gamma\left(\frac{p+q+b+1}{2}\right)\Gamma\left(\frac{p-q+b+1}{2}\right)} \\ &\quad (\mathrm{Re}\,(p+q+1) > \mathrm{Re}\, b > 0)\,.\end{aligned} \tag{B.7}$$

This approximation is used for example in Eqs. (4.51, 4.52).

With the same procedure we can approximate the second integral of Eq. (B.1), for which we find ($\ell \lesssim 60$)

$$\int_{x_{\rm dec}}^{x_0} dx\, \frac{j_2(x)}{x}\frac{j_\ell(x_0-x)}{(x_0-x)} \simeq \frac{1}{3}\sqrt{\frac{3\,\ell}{2}}\frac{J_{\ell+3}(x_0)}{x_0^2}\,. \tag{B.8}$$

This approximation underestimates the numerical result with an error of about 40% for $\ell = 30$, which reduces to 20% at $\ell = 60$. In this case also, the integral over x_0 is convergent.

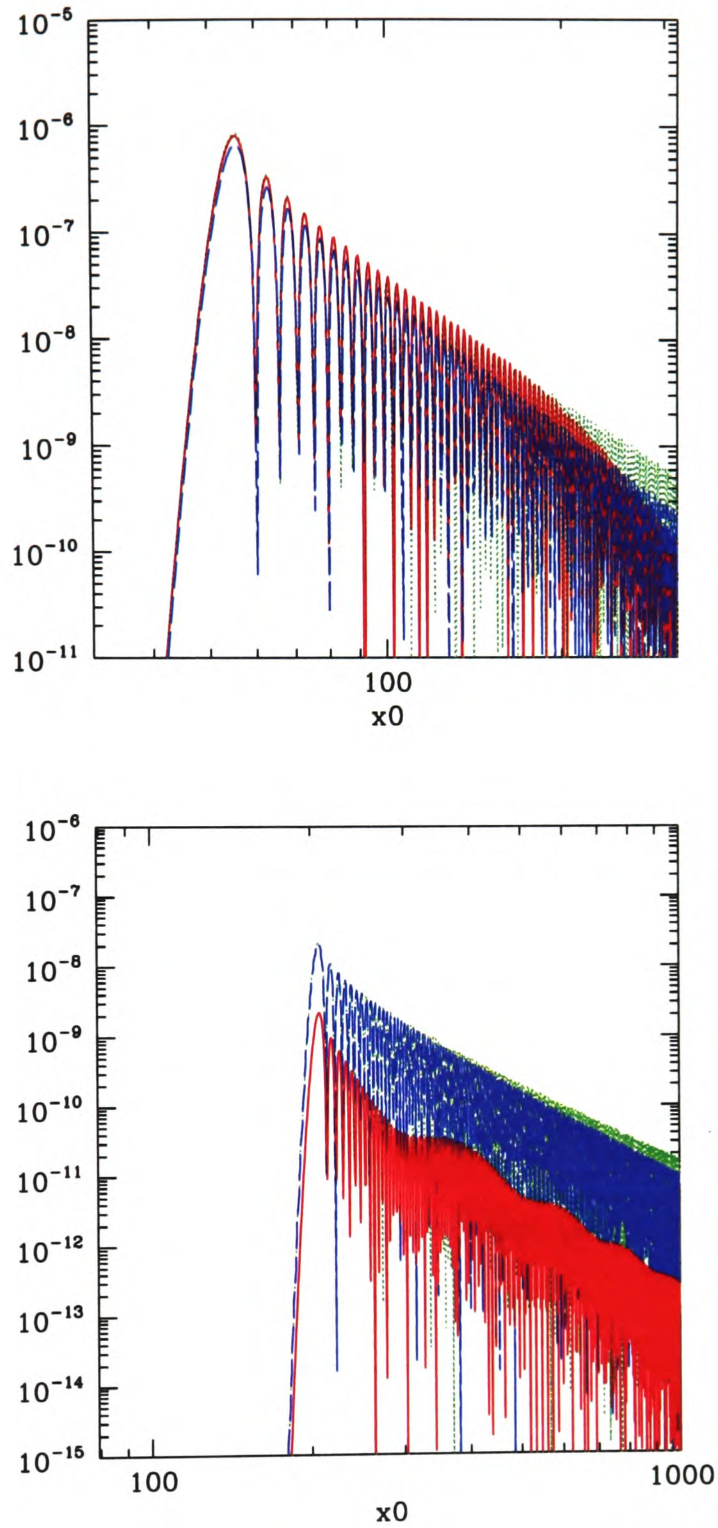

Figure B.1: In both panels, as a function of x_0: the green dotted line shows the numerical value of the integral in (B.5), the blue, long dashed line shows the analytic approximation (right hand side of Eq. (B.5)), and the red, solid line shows the numerical value of integral (B.5) if $x_{\rm dec}$ is not put to zero. All these functions are squared, and multiplied by x_0^3: this gives us an indication of the result, after the integration over x_0, as stated in Eq. (B.6). In the upper panel $\ell = 50$, in the lower panel $\ell = 200$. First of all, we note that it appears clearly that the value of the integrals is dominated at $x_0 \simeq \ell$, and that the function goes to zero quicker than x_0^{-3}, which justifies our approximation $x_D \rightarrow \infty$ and the use of formula B.7. Secondly, we note that for $\ell = 50$ and $x_0 \sim \ell$, our approximation (blue, long-dashed) is good for both the integrals. However, if $\ell = 200$, the approximation overestimates the correct numerical result by about a factor of ten.

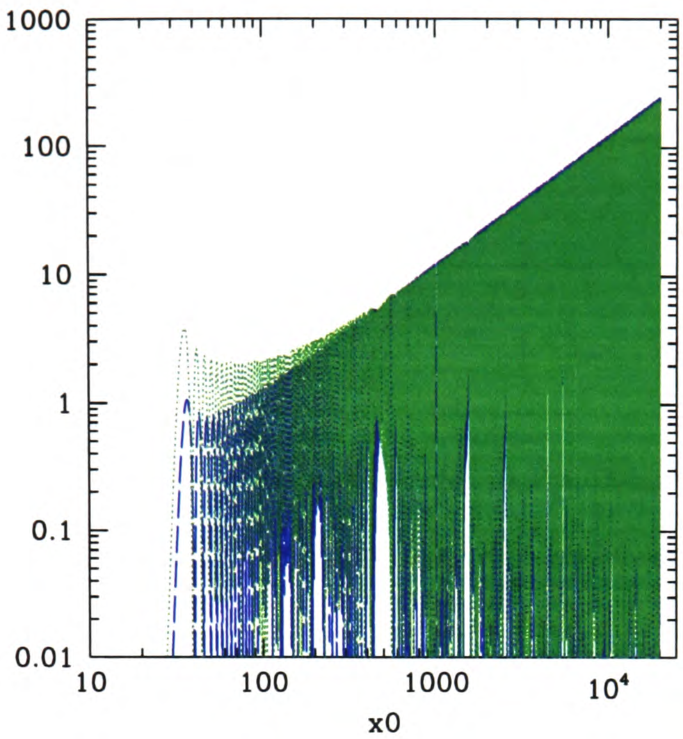

Figure B.2: We plot the value of integral (B.9) squared and multiplied by x_0^3 as function of x_0, for $\ell = 30$. The green, dotted line represents again the numerical result, and the blue, long dashed line is the analytic approximation. In this case the slope is positive, and hence the integral dx_0/x_0 of this function is dominated by the upper cutoff.

and we can proceed as before.

The situation is different for the third integral of Eq. (B.1). In this case, the numerical result is approximated by the following function ($\ell \lesssim 60$):

$$\int_{x_{\rm dec}}^{x_0} dx\, \frac{j_2(x)}{x} j_\ell(x_0 - x) \simeq \frac{1}{3}\sqrt{\frac{2}{5}}\, \frac{J_{\ell+3}(x_0)}{\sqrt{x_0}}\,. \tag{B.9}$$

It is clear that if we insert this function in an integral like (B.6) we cannot perform the limit $x_D \to \infty$ since this integral is dominated at the upper cutoff. Consequently, we need a good approximation for the behavior of the integral for large values of $x_0 \to x_D$. In this case, we no longer require our approximation to be accurate at $x_0 \simeq \ell$, but we concentrate on its behavior for high values of x_0, which will dominate in the integral over x_0. Fig. B.2 shows the approximation for $\ell = 30$, which overestimate the numerical result by an error within 1%.

We also have to evaluate the integral over $x_0^2\, dx_0$ of the square of (B.9), which we encounter in two different cases. The first (see section 4.4.2) is of the kind $\int_0^{x_D} dx\, x^p J_\ell^2(x)$. For $p < 0$ this integral converges and we may evaluate it in the limit $x_D \to \infty$, in which it is of the form (B.4). For $p > 0$ and $x_D \gg \ell^2$, the integral can be approximated using the asymptotic expansion of $J_\ell(x)$ for large arguments [103], $J_\ell(x) \sim \sqrt{2/(\pi x)}\cos[x - (2\ell+1)\pi/4]$. Approximating the oscillations by a factor of 1/2, we obtain

$$\int_0^{x_D} dx\, x^p J_\ell^2(x) \simeq \int_{\ell^2}^{x_D} dx\, x^p J_\ell^2(x) \simeq \begin{cases} \frac{x_D^p}{p\pi} & p > 0\,, \\ \frac{1}{\pi}\ln\left(\frac{x_D}{\ell^2}\right) & p = 0\,. \end{cases} \tag{B.10}$$

For the second case, $\int_0^{x_D} dx\, x^p J_\ell(x) J_{\ell+1}(x)$, which we encounter in Section 4.5, we use again the large argument approximation for the Bessel functions, for $x \gg \ell^2$,

$$\begin{aligned} J_\ell(x)J_{\ell+1}(x) &\simeq \frac{2}{\pi x}\cos\left(x - (2\ell+1)\frac{\pi}{4}\right)\cos\left(x - (2\ell+3)\frac{\pi}{4}\right) \\ &= \frac{2}{\pi x}\cos\left(x - (2\ell+1)\frac{\pi}{4}\right)\sin\left(x - (2\ell+1)\frac{\pi}{4}\right) \\ &= \frac{1}{\pi x}\sin\left(2x - \left(\ell + \frac{1}{2}\right)\pi\right) = \frac{(-1)^{\ell+1}}{\pi x}\cos(2x)\,, \end{aligned} \tag{B.11}$$

so that for $p > 0$

$$\begin{aligned} \int_0^{x_D} dx\, x^p J_\ell(x) J_{\ell+1}(x) &\simeq \frac{(-1)^{\ell+1}}{\pi}\int_{\ell^2}^{x_D} dx\, x^{p-1}\cos(2x) \\ &\simeq \frac{(-1)^{\ell+1}}{2\pi}\left(x_D^{p-1}\sin(2x_D) - \ell^{2p-2}\sin(2\ell^2)\right)\,. \end{aligned} \tag{B.12}$$

In the limits to which we have restricted ourselves, we always have $x_D \gg \ell^2$. Consequently, the dominant contribution in the last expression can be given either by the first term in the bracket, if $p > 1$, or by the second term, if $p < 1$. Numerical checks show that the approximation is good for $p > 1$, but it is rather poor in the second case, $p < 1$. Since we shall not be very much interested in this case, we do not go any further in this analysis.

When evaluating expression (B.7), we often also use

$$\begin{aligned} \Gamma(2x) &= \frac{2^{2x-1}}{\sqrt{\pi}}\Gamma(x)\Gamma\left(x + \frac{1}{2}\right) \\ \frac{\Gamma(x+a)}{\Gamma(x+b)} &\sim x^{a-b} + \mathcal{O}(x^{a-b-1}) \qquad \text{for } x \gg 1 \end{aligned} \tag{B.13}$$

(see Eqs. (6.1.18) and (6.1.47) of [103]).

B.2 Recurrent relations for spherical Bessel functions

We use several recurrence relations for spherical Bessel functions in our derivations, most notably

$$\frac{\ell+1}{x}j_\ell(x) + j_\ell'(x) = j_{\ell-1}(x) \tag{B.14}$$

and

$$\frac{\ell}{x}j_\ell(x) - j_\ell'(x) = j_{\ell+1}(x)\,. \tag{B.15}$$

Bibliography

[1] G.F.R. Ellis. Relativistic cosmology. In *Proceedings of the International School of Physics Enrico Fermi*, volume XLVII. Academic press, 1971.

[2] G.F.R. Ellis. Relativistic cosmology. In E. Schatzman, editor, *Cargèse Lectures in Physics*, volume 6. Gordon & Breach, 1973.

[3] G.F.R. Ellis and H. Van Elst. Cosmological models. In Marc Lachièze-Rey, editor, *Theoretical and Observational Cosmology.* Kluwer, 1999.

[4] E.W. Kolb and M.S. Turner. *The Early Universe.* Addison-Wesley, 1990.

[5] D.N. Spergel et al. *Astrophys. J. Suppl.*, 148:175, 2003.

[6] J.R. Mould et al. *Astrophys. J.*, 529:698, 2000.

[7] R.A. Knop et al. *Astrophys. J.*, 598:102, 2003.

[8] E.F. Bunn, P.G. Ferreira, and J. Silk. *Phys. Rev. Lett.*, 77:2883, 1996.

[9] J.D. Barrow, R. Juskiewicz, and D.H. Sonoda. *Mon. Not. Roy. Astron. Soc.*, 213:917, 1985.

[10] J.D. Barrow. *Phys. Rev. D*, 55:7451, 1997.

[11] C.B. Collins and S.W. Hawking. *Astrophys. J.*, 180:317, 1973.

[12] J.D. Jackson. *Classical Electrodynamics.* John Wiley & Sons, second edition, 1975.

[13] R. Maartens and B. Bassett. *Class. Quant. Grav.*, 15:705, 1998.

[14] R. Maartens, T. Gebbies, and G.F.R. Ellis. *Phys. Rev. D*, 59:83506, 1999.

[15] M. Bruni, P.K.S. Dunsby, and G.F.R. Ellis. *Astrophys. J.*, 395:34, 1992.

[16] R. Durrer. Cosmologie. Cosmology lectures, available at the personal webapge http://theory.physics.unige.ch/ durrer/home.html.

[17] M. Trodden and S.M. Carroll. Tasi lectures: Introduction to cosmology. Lectures delivered at the TASI-02 and TASI-03 summer schools at the University of Colorado at Boulder [astro-ph/0401547].

[18] R. Durrer and C. Caprini. *JCAP*, 11:010, 2003.

[19] L.D. Davis and J.L. Greenstein. *Astrophys. J.*, 114:206, 1951.

[20] P.P. Kronberg. *Rep. Prog. Phys.*, 57:325, 1994.

[21] E.G. Zweibel and C. Heiles. *Nature*, 385:131, 1997.

[22] D. Grasso and H.R. Rubinstein. *Phys. Rept.*, 348:163, 2001.

[23] M. Giovannini. *Int. J. Mod. Phys. D*, 13:391, 2004.

[24] C.L. Sarazin. *X-ray Emissions from Clusters of Galaxies.* Cambridge University Press, 1988.

[25] C.L. Carilli and G.B. Taylor. *Ann. Rev. Astron. Astrophys.*, 40:319, 2002.

[26] T.E. Clarke, P.P. Kronberg, and H. Bohringer. *Astrophys. J.*, 547:L111, 2001.

[27] K. Dolag, M. Bartelmann, and H. Lesch. *Astron. & Astrophys.*, 387:383, 2002.

[28] T. Kolatt. *Astrophys. J.*, 495:546, 1998.

[29] M. Murgia et al. Preprint arXiv astro-ph/0406225, 2004.

[30] K. Dolag, M. Bartelmann, and H. Lesch. *Astron. & Astrophys.*, 348:351, 1999.

[31] A.Z. Dolginov. *Phys. Rept.*, 162:337, 1988.

[32] D. Biskamp. *Nonlinear Magnetohydrodynamics.* Cambridge University Press, 1993.

[33] R.M. Kulsrud. *Annu. Rev. Astron. Astrophys.*, 37:37, 1999.

[34] G.B. Field. Is the dynamo theory of the galactic magnetic field wrong? In A. Ferrara et al., editors, *The Physics of the Interstellar Medium and Intergalactic Medium.* volume 80. Astronomical Society of the Pacific, 1995.

[35] R. Kulsrud et al. *Phys. Rept.*, 283:213, 1997.

[36] L. Biermann and A. Schluter. *Phys. Rev.*, 82:863, 1951.

[37] H. Lesch and M. Chiba. *Astron. & Astrophys.*, 297:305, 1995.

[38] R.M. Kulsrub et al. *Astrophys. J.*, 480:481, 1997.

[39] K. Subramanian, D. Narashima, and S.M. Chitre. *Mon. Not. Roy. Astron. Soc.*, 271:L15, 1994.

[40] M. Langer, J.L. Puget, and Aghanim N. *Phys. Rev. D*, 67:043505, 2003.

[41] E.R. Harrison. *Mon. Not. Roy. Astron. Soc.*, 147:279, 1970.

[42] E.R. Harrison. *Phys. Rev. Lett.*, 30:188, 1973.

[43] M.J. Rees. *Q. Jl. R. Astr. Soc.*, 28:197, 1987.

[44] T. Vachaspati and A. Vilenkin. *Phys. Rev. Lett.*, 67:1057, 1991.

[45] C.J. Hogan. arXiv `astro-ph/0005380`, 2000.

[46] Z. Berezhiani and A.D. Dolgov. *Astropart. Phys.*, 21:59, 2004.

[47] C.J. Hogan. *Phys. Rev. Lett.*, 51:1488, 1983.

[48] J.M. Quashnock, A. Loeb, and D.N. Spergel. *Astrophys. J.*, 344:L49, 1989.

[49] B. Cheng and A.V. Olinto. *Phys. Rev. D*, 50:2421, 1994.

[50] G. Sigl, A.V. Olinto, and K. Jedamzik. *Phys. Rev. D*, 55:4582, 1997.

[51] G. Baym, D. Bodeker, and L. McLerran. *Phys. Rev. D*, 53:662, 1996.

[52] D. Boyanovsky, H.J. de Vega, and M. Simionato. Primordial magnetic fields from cosmological phase transitions. In N. Sanchez and Y.N. Parijskij, editors, *Proceedings of the 9th. International School of Astrophysics 'Daniel Chalonge'*. Kluwer, 2003.

[53] O. Tornqvist. *Phys. Rev. D*, 58:43501, 1998.

[54] D. Grasso and A. Riotto. *Phys. Lett. B*, 418:258, 1998.

[55] J. Ahonen and K. Enqvist. *Phys. Rev. D*, 57:664, 1998.

[56] T. Vachaspati. *Phys. Lett. B*, 265:258, 1991.

[57] K. Enqvist and P. Olesen. *Phys. Lett. B*, 319:178, 1993.

[58] M. Hindmarsh and A. Everett. *Phys. Rev. D*, 58:103505, 1998.

[59] J.M. Cornwall. *Phys. Rev. D*, 56:6146, 1997.

[60] T. Vachaspati. *Phys. Rev. Lett.*, 87:251302, 2001.

[61] T. Vachaspati. Invited talk at International Workshop on Particle Physics and the Early Universe (COSMO-01), Rovaniemi, Finland, 30 Aug - 4 Sep 2001 [astro-ph/0111124], 2001.

[62] S.M. Carroll and G.B. Field. Talk given at 33rd Rencontres de Moriond: Fundamental Parameters in Cosmology, Les Arcs, France, 17-24 Jan 1998 [astro-ph/9807159], 1998.

[63] G.B. Field and S.M. Carroll. *Phys. Rev. D*, 62:103008, 2000.

[64] M. Joyce and M. Shaposhnikov. *Phys. Rev. Lett.*, 79:1193, 1997.

[65] M.S. Turner and L.M. Widrow. *Phys. Rev. D*, 37:2473, 1988.

[66] B. Ratra. *Astrophys. J.*, 391:L1, 1992.

[67] D. Lemoine and M. Lemoine. *Phys. Rev. D*, 52:1955, 1995.

[68] M. Gasperini, M. Giovannini, and G. Veneziano. *Phys. Rev. Lett.*, 75:3796, 1995.

[69] K. Bamba and J. Yokoyama. *Phys. Rev. D*, 69:43507, 2004.

[70] E.A. Calzetta, A. Kandus, and F.D. Mazzitelli. *Phys. Rev. D*, 57:7139, 1998.

[71] T. Prokopec, O. Tornqvist, and R. Woodard. *Phys. Rev. Lett.*, 89:101301, 2002.

[72] T. Prokopec and R. Woodard. *Am. J. Phys.*, 72:60, 2004.

[73] K. Subramanian and J.D. Barrow. *Phys. Rev. D*, 58:083502, 1998.

[74] M. Christensson and M. Hindmarsh. *Phys. Rev. D*, 60:063001, 1999.

[75] J. Ahonen and K. Enqvist. *Phys. Lett. B*, 382:40, 1996.

[76] G. Baym and H. Heiselberg. *Phys. Rev. D*, 56:5254, 1997.

[77] P. Olesen. Primordial magnetic fields and their development. In P.H. Damgaard and J. Jurkiewicz, editors, *NATO ASI SERIES, New Developments in Quantum Field Theory*, volume B366. PLENUM, 1998.

[78] M. Giovannini. *Phys. Rev. D*, 58:124027, 1998.

[79] K. Jedamzik, V. Katalinic, and A.V. Olinto. *Phys. Rev. D*, 57:3264, 1998.

[80] C. Caprini and R. Durrer. *Phys. Rev. D*, 65:23517, 2001.

[81] A. Pouquet et al. *J. Fluid. Mech.*, 77:321, 1976.

[82] D.T. Son. *Phys. Rev. D*, 59:63008, 1999.

[83] M. Christensson, M. Hindmarsh, and A. Brandenburg. *Phys. Rev. E*, 64:56405, 2001.

[84] M. Christensson, M. Hindmarsh, and A. Brandenburg. SUSX-TH-02-014 NORDITA 2002-43 AP [astro-ph/0111124], 2001.

[85] A. Brandenburg, K. Enqvist, and P. Olesen. *Phys. Rev. D*, 54:1291, 1996.

[86] G. Sigl. *Phys. Rev. D*, 66:123002, 2002.

[87] R. Banerjee and K. Jedamzik. *Phys. Rev. Lett.*, 91:251301, 2003.

[88] J.D. Barrow, P.G. Ferreira, and J. Silk. *Phys. Rev. Lett.*, 78:3610, 1997.

[89] E.S. Scannapieco and P.G. Ferreira. *Phys. Rev. D*, 56:7493, 1997.

[90] C. Tsagas and J.D. Barrow. *Class. Quant. Grav.*, 14:2539, 1997.

[91] C. Tsagas and R. Maartens. *Phys. Rev. D*, 61:83519, 2000.

[92] C. Caprini, R. Durrer, and T. Kahniashvili. *Phys. Rev. D*, 69:63006, 2004.

[93] L. Pogosian, T. Vachaspati, and S. Winitzki. *Phys. Rev. D*, 65:83502, 2002.

[94] A. Davis, M. Lilley, and O. Tornqvist. *Phys. Rev. D*, 60:21301, 1999.

[95] W. Hu and M. White. *Phys. Rev. D*, 56:596, 1997.

[96] R. Durrer. The theory of cmb anisotropies. Lectures given at the 'Mitteldeutsche Physik-COMBO', WS 2002/2003, available at the webpage http://theory.physics.unige.ch/ durrer/home.html.

[97] S.W. Hawking. *Astrophys. J.*, 145:544, 1966.

[98] G.F.R. Ellis and M. Bruni. *Phys. Rev. D*, 40:1804, 1989.

[99] J.M. Bardeen. *Phys. Rev. D*, 22:1882, 1980.

[100] H. Kodama and M. Sasaki. *Progr. Theor. Phys. Suppl.*, 78:1, 1984.

[101] R. Durrer. *Fund. Cosm. Phys.*, 15:209, 1994.

[102] W. Hu et al. *Phys. Rev. D*, 57:3290, 1998.

[103] M. Abramowitz and I. Stegun. *Handbook of mathematical functions.* Dover Publications, 1972.

[104] T. Kahniashvili et al. Cmb signatures of a primordial magnetic field. In R. Durrer, J. Garcia-Bellido, and M. Shaposhnikov, editors, *Cosmology and Particle Physics, CAPP 2000*, volume 555. American Institute of Physics, 2001.

[105] R. Durrer and M. Kunz. *Phys. Rev. D*, 57:3199, 1998.

[106] K. Subramanian and J.D. Barrow. *Phys. Rev. Lett.*, 81:3575, 1998.

[107] R. Durrer, P.G. Ferreira, and T. Kahniashvili. *Phys. Rev. D*, 61:43001, 2000.

[108] C. Tsagas and J.D. Barrow. *Class. Quant. Grav.*, 15:3523, 1998.

[109] J. Adams et al. *Phys. Lett. B*, 388:253, 1996.

[110] S. Koh and C.H. Lee. *Phys. Rev. D*, 62:83509, 2000.

[111] R. Durrer, T. Kahniashvili, and A. Yates. *Phys. Rev. D*, 58:123004, 1998.

[112] G. Chen et al. Preprint arXiv `astro-ph/0403695`, 2004.

[113] P.D. Naselsky et al. Preprint arXiv `astro-ph/0405181`, 2004.

[114] K. Subramanian and J.D. Barrow. *Mon. Not. Roy. Astron. Soc.*, 335:L57, 2002.

[115] A. Mack, T. Kahniashvili, and A. Kosowsky. *Phys. Rev. D*, 65:123004, 2002.

[116] R. Maartens, C.G. Tsagas, and C. Ungarelli. *Phys. Rev. D*, 63:123507, 2001.

[117] C.G. Tsagas, P.K.S. Dunsby, and M. Marklund. *Phys. Lett. B*, 561:17, 2003.

[118] A. Kosowsy and A. Loeb. *Astrophys. J.*, 469:1, 1996.

[119] D. Harari, J. Hayward, and M. Zaldarriaga. *Phys. Rev. D*, 55:1841, 1997.

[120] C. Scoccola, D Harari, and S. Mollerach. Preprint arXiv `astro-ph/0405396`, 2004.

[121] L. Campanelli et al. Preprint arXiv `astro-ph/0405420`, 2004.

[122] T.R. Seshadri and K. Subramanian. *Phys. Rev. Lett.*, 87:101301, 2001.

[123] K. Subramanian, T.R. Seshadri, and J.D. Barrow. *Mon. Not. Roy. Astron. Soc.*, 344:L31, 2003.

[124] A. Lewis. Preprint arXiv `astro-ph/0406096`, 2004.

[125] M. Zaldarriaga and U. Seljak. *Phys. Rev. D*, 55:1830, 1997.

[126] M. Kamionkowsy, A. Kosowsky, and A. Stebbins. *Phys. Rev. D*, 55:7368, 1997.

[127] R.A. Lyttleton and H. Bondi. *Proc. R. Soc. London*, A 252:313, 1959.

[128] W.F.G. Swann. *Astrophys. J.*, 133:738, 1961.

[129] A. Barnes. *Astrophys. J.*, 227:1, 1979.

[130] A.Y. Ignatiev, V.A. Kuzmin, and M.E. Shaposhnikov. *Phys. Lett. B*, 84:315, 1979.

[131] D. Dolgov and J. Silk. *Phys. Rev. D*, 47:3144, 1993.

[132] M. Brisudova, R.P. Woodard, and W.H. Kinney. *Class. Quant. Grav.*, 18:3929, 2001.

[133] S.L. Dubovsky, V.A. Rubakov, and P.G. Tinyakov. *JHEP*, 8:41, 2000.

[134] H.J. Mosquera-Cuesta, A. Penna-Firme, and A. Perez-Lorenzana. *Phys. Rev. D*, 67:87702, 2003.

[135] S. Landau, P. Sisterna, and H. Vucetich. *Phys. Rev. D*, 63:81303, 2001.

[136] Y.K. Semertzidis, G.T. Danby, and D.M. Lazarus. *Phys. Rev. D*, 67:17701, 2003.

[137] G.G. Raffelt. *Phys. Rev. D*, 50:7729, 1994.

[138] G.G. Raffelt. *Phys. Rept.*, 320:319, 1999.

[139] H.F. Dylla and J.G. King. *Phys. Rev. A*, 7:1224, 1973.

[140] M. Marinelli and G. Morpugo. *Phys. Lett. B*, 137:439, 1984.

[141] P. Verkerk et al. *Phys. Rev. Lett.*, 68:1116, 1992.

[142] A. Gould et al. *Phys. Lett. B*, 238:337, 1990.

[143] S. Orito and M. Yoshimura. *Phys. Rev. Lett.*, 54:2457, 1985.

[144] E. Masso and F. Rota. *Phys. Lett. B*, 545:221, 2002.

[145] C. Boehm, A. Djouadi, and M. Drees. *Phys. Rev. D*, 62:35012, 2000.

[146] C. Boehm and P. Fajet. *Nucl. Phys. B*, 683:219, 2004.

[147] L. Rudnick and K.M. Blundell. *Astrophys. J.*, 588:143, 2003.

[148] C. Caprini, S. Hansen, and M. Kunz. *Mon. Not. Roy. Astron. Soc.*, 588:143, 2003.

[149] D.H. Lyth and A. Riotto. *Phys. Rept.*, 314:1, 1999.

[150] A. Liddle and D.H. Lyth. *Phys. Rept.*, 231:1, 1993.

[151] P.J. Steinhardt and M.S. Turner. *Phys. Rev. D*, 29:2162, 1984.

[152] L. Knox. *Phys. Rev. D*, 52:4307, 1995.

[153] M.S. Turner and M. White. *Phys. Rev. D*, 53:6822, 1996.

[154] M.B. Hoffman and M.S. Turner. *Phys. Rev. D*, 64:23506, 2001.

[155] A. Liddle and D.H. Lyth. *Phys. Lett. B*, 291:391, 1992.

[156] A. Kosowsky and M.S. Turner. *Phys. Rev. D*, 52:1739, 1995.

[157] S.H. Hansen and M. Kunz. *Mon. Not. Roy. Astron. Soc.*, 336:1007, 2002.

[158] S. Hannestad et al. *Astropart.Phys.*, 17:375, 2002.

[159] W.H. Kinney, A. Melchiorri, and A. Riotto. *Phys. Rev. D*, 63:23505, 2001.

[160] S. Hannestad, S.H. Hansen, and F.L. Villante. *Astropart.Phys.*, 16:137, 2001.

[161] X. Wang, M. Tegmark, and M. Zaldarriaga. *Phys. Rev. D*, 65:123001, 2002.

[162] S. Leach and A. Liddle. *Mon. Not. Roy. Astron. Soc.*, 341:1151, 2003.

[163] E.F. Bunn, A. Liddle, and M. White. *Phys. Rev. D*, 54:5917, 1996.

[164] W.H. Kinney. *Phys. Rev. D*, 66:83508, 2002.

[165] A. Liddle, P. Parsons, and J.D. Barrow. *Phys. Rev. D*, 50:7222, 1994.

[166] R. Easther and W.H. Kinney. *Phys. Rev. D*, 67:43511, 2003.

[167] W.H. Kinney et al. *Phys. Rev. D*, 69:103516, 2004.

[168] A. Liddle. *Phys. Rev. D*, 68:103504, 2003.

[169] I.S. Gradshteyn and I.M. Ryzhik. *Tables of integrals, series and products.* Academic Press, 1965.